Finite Volume and Partial Quenching for Chiral Perturbation Theory and QCD-like Theories

Thesis for the Degree of Doctor of Philosophy in Theoretical Physics

Thomas Rössler

Department of Astronomy and Theoretical Physics, Lund University,
Sölvegatan 14A, SE 223-62 Lund, Sweden

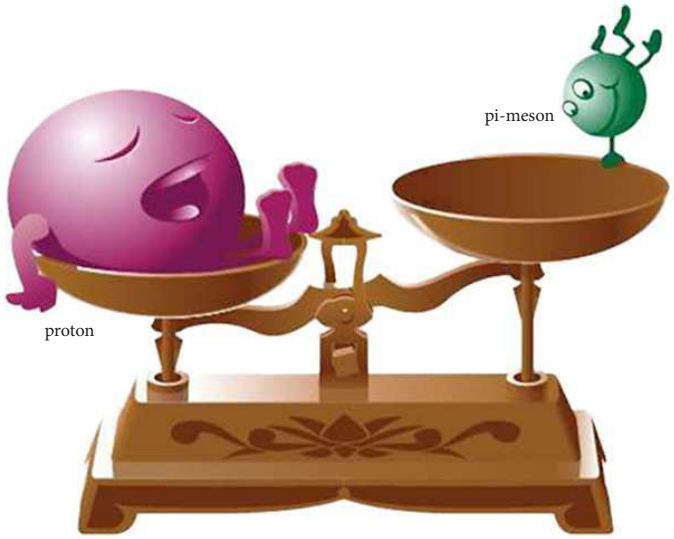

Thesis Advisor: Johan Bijnens
Faculty Opponent: Kim Splittorff

To be presented, with the permission of the Faculty of Science of Lund University, for public criticism in Lundmarksalen at the Department of Astronomy and Theoretical Physics on the 23rd of October 2015 at 13:00

DOKUMENTDATABLAD enl SIS 61 41 21

Organization
LUND UNIVERSITY
Department of Astronomy and Theoretical Physics
Sölvegatan 14A
SE–223 62 LUND, Sweden

Document name
DOCTORAL DISSERTATION

Date of issue
October 2015

Sponsoring organization

Author(s)
Thomas Rössler

Title and subtitle
Finite Volume and Partial Quenching for Chiral Perturbation Theory and QCD-like Theories

Abstract
Chiral Perturbation Theory (ChPT) is a powerful framework that allows to access the properties and dynamics of QCD in the low-energy regime where the naive perturbative approach of full QCD is no longer possible. Finite volume (FV) effects for Chiral Perturbation Theory are both of fundamental interest as well as high practical use: In Lattice QCD, a numerical Monte Carlo approach to low-energy quantities, the FV is inevitable. Thus, to obtain a powerful symbiosis between the two fields, it is necessary to have the FV effects well under control both qualitatively and quantitatively.

This thesis starts by pushing the frontier of the FV effects for mesonic ChPT to two-loop order or NNLO. The power of the results is then significantly extended by generalizing to the partially quenched case, the latter being an approximation which is highly advantageous to lattice computations and frequently used. The FV effects for Partially Quenched Chiral Perturbation Theory (PQChPT), being the effective field theory framework for Partially Quenched QCD (PQQCD), are computed for all possible different cases of potentially degenerate or non-degenerate masses.

As a supplement, we use our expertise to perform partially quenched FV calculations by applying it to Effective Field Theories (EFTs) for QCD-like theories. The resulting EFT frameworks are similar to ChPT, but heavily rely on the global chiral symmtry group and its breaking pattern in the underlying theory. Three different cases are studied in detail.

All corrections of interest throughout the thesis are calculated ab-initio. Analytical results are given, implemented into numerical programs and studied numerically. The analytical work heavily relies on the extensive use of computer algebra.

Key words:
Chiral Perturbation Theory, QCD, Finite Volume, Partially Quenched, Effective Field Theory, Symmetry Breaking

Classification system and/or index terms (if any):

Supplementary bibliographical information:

Language
English

ISSN and key title:

ISBN 978-91-7623-474-7 (print)
978-91-7623-475-4 (pdf)

Recipient's notes

Number of pages
166 (A4)

Price
priceless

Security classification

Distributor
Department of Astronomy and Theoretical Physics, Sölvegatan 14A, SE–223 62 Lund, Sweden

I, the undersigned, being the copyright owner of the abstract of the above-mentioned dissertation, hereby grant to all reference sources the permission to publish and disseminate the abstract of the above-mentioned dissertation.

Signature Thomas Rössler

Date 2015-09-17

Finite Volume and Partial Quenching for Chiral Perturbation Theory and QCD-like Theories

Thesis for the Degree of Doctor of Philosophy in Theoretical Physics

Thomas Rössler

Department of Astronomy and Theoretical Physics, Lund University,
Sölvegatan 14A, SE 223-62 Lund, Sweden

LUND
UNIVERSITY

Faculty of Science
Department of Astronomy and Theoretical Physics

Printed in Sweden by Media-Tryck, Lund, 2015

ISBN 978-91-7623-474-7 (print)
ISBN 978-91-7623-475-4 (pdf)

für die tote Materie.
Für das Lebendige aber gelten andere Gesetze.

(frei nach: Jürgen Neffe, "Einstein", S. 11)

There are two kinds of pain.
The sort of pain that makes you strong,
or useless pain,
the sort of pain that's only suffering.

I have no patience for useless things.

Moments like this require someone who will act.

Francis Underwood, House of Cards

Abstract/Summary

Chiral Perturbation Theory (ChPT) is a powerful framework that allows to access the properties and dynamics of QCD in the low-energy regime where the naive perturbative approach of full QCD is no longer possible. Finite volume (FV) effects for Chiral Perturbation Theory are both of fundamental interest as well as high practical use: In Lattice QCD, a numerical Monte Carlo approach to low-energy quantities, the FV is inevitable. Thus, to obtain a powerful symbiosis between the two fields, it is necessary to have the FV effects well under control both qualitatively and quantitatively.

This thesis starts by pushing the frontier of the FV effects for mesonic ChPT to two-loop order or NNLO. The power of the results is then significantly extended by generalizing to the partially quenched case, the latter being an approximation which is highly advantageous to lattice computations and frequently used. The FV effects for Partially Quenched Chiral Perturbation Theory (PQChPT), being the effective field theory framework for Partially Quenched QCD (PQQCD), are computed for all possible different cases of potentially degenerate or non-degenerate masses.

As a supplement, we use our expertise to perform partially quenched FV calculations by applying it to Effective Field Theories (EFTs) for QCD-like theories. The resulting EFT frameworks are similar to ChPT, but heavily rely on the global chiral symmtry group and its breaking pattern in the underlying theory. Three different cases are studied in detail.

All corrections of interest throughout the thesis are calculated ab-initio. Analytical results are given, implemented into numerical programs and studied numerically. The analytical work heavily relies on the extensive use of computer algebra.

Popular Science Summary

This thesis contains research in the area of theoretical particle physics. The field deals with describing the properties of the most fundamental constituents of matter and their interactions. Matter in general is composed of atoms which in turn are composed of electrons and nuclei. The nuclei are in turn composed of protons and neutrons. We know of one more layer of substructure. The protons and neutrons are essentially made of up and down quarks. The electron and up and down quarks have to our present knowledge no substructure. There are four quarks more than the up and down and five so-called leptons in addition to the electron. These form the matter part of the underlying theory called the Standard Model. There are four known forces, gravitational, electromagnetic, weak and strong. The latter three are included in the Standard Model while the former is well described by General Relativity. The forces are mediated by carrier particles called gauge bosons. The final constituent of the Standard Model is the Higgs boson which gives masses to the weak force gauge bosons and the quarks and leptons.

In the Standard Model, the weak interaction is a very short range interaction due to the mass of the gauge boson. The latter is understood via the Higgs mechanism. Paper I and paper IV are in the area of alternative ways to realize the Higgs mechanism beyond the simplest version that is part of the Standard Model.

Paper II and paper III are useful for precision determinations of a number of the parameters of the Standard Model. The particles involved in paper II and III are composed of quarks, anti-quarks and gluons, the gauge bosons for the strong interaction. The underlying technique used in paper II and III is called effective field theory. It comes into play when the underlying theory, like the theory of the strong force, is strongly interacting so the usual techniques cannot be employed. The effective field theory applied here uses only the symmetries of the fundamental theory to make as many predictions as possible. Paper IV uses the same technique for studying models where the Higgs boson might itself be a composite state.

Contents

This thesis is based on the following publications:

I Johan Rathsman, Thomas Rössler
Closing the Window on Light Charged Higgs Bosons in the NMSSM
Advances in High Energy Physics **2012** (2012) 853706 [arXiv:1206.1470].

II Johan Bijnens, Thomas Rössler
Finite Volume at Two-loops in Chiral Perturbation Theory
Journal of High Energy Physics **1501** (2015) 034 [arXiv:1411.6384].

III Johan Bijnens, Thomas Rössler
Finite Volume for Three-Flavour Partially Quenched Chiral Perturbation Theory through NNLO in the Meson Sector
Submitted to *Journal of High Energy Physics* (2015) [arXiv:1508.07238]

IV Johan Bijnens, Thomas Rössler
Finite Volume and Partially Quenched QCD-like Effective Field Theories
Submitted to *Journal of High Energy Physics* (2015) [arXiv:1509.04082]

Further authorship

A Thomas Rössler
Tutorial Note on Merging Matrix Elements with Parton Showers
[arXiv:1503.07916].

B Johan Bijnens, Thomas Rössler†
Finite volume for masses and decay constants
Proceedings of Science, SISSA (2015)
work in progress, based on talk given at the
8th International Workshop on Chiral Dynamics 2015

† speaker

Author's Contribution to the Papers

Paper I: I did the Monte Carlo analysis of the production process. Johan Rathsman did some parameter sampling of the SUSY model under discussion. We both have contributed to the manuscript by writing our respective parts. The reader will note that this paper considers a different topic than the other three papers as well as the thesis introduction.

Paper II: The paper considers finite volume corrections for masses and decay constants in Chiral Perturbation Theory to two-loop order. Johan (Hans) Bijnens and I derived the results independently. I wrote a Licenciate thesis about the same topic while Hans wrote the major part of the manuscript using an outline that I had created. I then contributed with smaller parts, modifications and corrections to the publication. Furthermore, I compared our results to those of earlier calculations [1, 2, 3, 4]. Due to a different notation and expansion (e. g. quantities vs. squared quantities), that translation was non-trivial, and could also only be done for certain parts.

Paper III: The paper generalizes the calculation of paper II to the partially quenched case, with all sea and valence quark masses being free. I derived all results independently, using a different method ("supersymmetric formulation") than Hans ("quarkflow"). I checked that our results agree analytically which is a non-trivial task due to the structure and size of the expressions. I also wrote numerical programs with which I pioneered the numerical studies. The main draft of the manuscript was written by me.

Paper IV: The paper uses methods from Chiral Perturbation Theory to explore Effective Field Theories for Lagrangians similar to QCD. The analytical results were again derived independently. In particular, I have derived the SO case with a different method than Hans. The manuscript was written in a collaborative action.

All articles are reprinted with kind permission of respective publishers. The author would like to thank the Nobel Foundation and the Royal Swedish Academy of Sciences for their kind permission to use the illustration on the cover and front page (Copyright: The Royal Swedish Academy of Sciences, Illustration by Typoform).

Introduction

1 Preamble

Symmetries and conservation laws have proven to be successful concepts in the description of physical systems. Their usage as "tools" has become indispensable. In many cases, it is possible to gain a qualitative, sometimes even quantitative, understanding of static properties as well as the dynamics by exploiting the power of symmetry arguments. This extremely far-reaching topic can barely be touched in a thesis introduction, but its fundamental role in the work that physicists do nowadays can hardly be overemphasized.

Fundamental theoretical physics - apart from being an art on its own - acquires its actual value and success only via tests against experiment. The real cornerstones of the field that have made history mostly have in common that *non-trivial* and *definite* predictions could be made based on the theory, together with an explicit or implicit prescription of how respective prognosis can be either verified or falsified experimentally. An example is the prediction of a fermion of opposite electric charge and the same mass when compared to the electron by Dirac - today referred to as the positron.

The application of symmetries and symmetry groups has been an essential ingredient for a large part of significant progress. It was often based on symmetry concepts that theorists could make quantitative and qualitative predictions, e. g. the existence of the Ω^- and its approximate mass in the baryon decuplet or the "November Revolution" of 1974 - predictions that lead to important discoveries and a better understanding of the fundamental laws of nature. Similarly, the introduction of gauge symmetries lead to a deeper understanding of particles and their interactions. Even broken and approximate symmetries - no matter if broken explicity, spontaneously, anomalously - remain useful concepts and physicists are eager to extract as much useful information as possible from their symmetry considerations.

The PhD thesis at hand consists of an introduction, followed by four scientific papers. The introduction successively introduces to different aspects of Chiral Perturbation Theory and related topics via several chapters. Essential features of Mesonic Chiral Perturbation Theory are covered in Chapters 2 and 3. Chapter 4 establishes a power counting scheme. I then go over to the actual calculation of quantum corrections using ChPT: Chapter 5 deals with one-loop or NLO, Chapter 6 with two-loop or NNLO computations. Chapter 7 contains some peculiarities when calculating mesonic decay constants. All of these chapters are purely introductive. The remainder then deals with the actual research topics of this thesis: Partial Quenching and Finite Volume Effects. The latter are introduced to in Chapter 8, equipping the reader with all potentially necessary prerequisites for a study of paper II. [1] Chapter 9 deals with two different approaches for obtaining partially quenched quantum corrections. It is tightly connected to paper III and IV. Together with Chapter 8, it provides the foundations for a study of paper III. Chapter 10 finally covers Effective Field Theories for QCD-like. This will set the stage for paper IV. In paper IV, the effective

[1] Paper II and parts of the introduction have also been published as a Licentiate thesis in December 2014, in full accordance with the study regulations at Lund University. Still, the introduction has undergone several modifications and extensions. The earlier publication does not change the fact that this PhD thesis can be read as a self-contained document.

field approach for QCD-like theories meets both finite volume corrections and the partially quenched approximation. Thus, in a way, all Chapters 8 - 10 will contribute important background information for its study. Three appendices provide further details and deeper background information about selected topics.

2 From QCD to ChPT

Quantum chromodynamics (QCD) is nowadays considered to be the theory describing the strong force. One of the problems that come with this non-abelian gauge theory is the energy range where it provides reliable perturbative predictions. The smallness of the coupling constant at high energies makes it possible to test and confirm the theory in highly energetic scattering processes and, since the theory is renormalizable to all orders, better and better perturbative predictions can be obtained, at least in principle. The growth of the coupling constant towards lower energy scales finally leads to a breakdown of perturbation theory and, in the low energy ranges (e. g. hadroformation), different methods have to be employed. One way is given by a numerical evaluation in the path-integral formalism (Lattice QCD, the only way for a non-perturbative ab initio treatment of QCD to date). Alternatively, one can perform calculations in an effective field theory (EFT) framework. Chiral Perturbation Theory (ChPT) [5, 6, 7] is an effective field theory for QCD, starting from the symmetries of QCD. As the relevant dynamical degrees of freedom, pseudoscalar mesons will replace the quarks[2] and gluons of QCD (in meson ChPT). At every perturbative order in the EFT, we will introduce new higher-dimensional operators (i.e. all which are consistent with the symmetry) - operators that spoil the all-order renormalizability of the theory - that embody the unknown effects from higher scales and bring them into the theory. The coefficients of these new operators, called Low Energy Constants (LECs), renormalize the theory and will have to be determined (usually by experiment) in order to evaluate predictions numerically. As I will elaborate upon further below, the relation between Lattice QCD and ChPT is highly symbiotic rather than purely competitive. For example, Lattice QCD can help ChPT in the determination of the LECs whereas ChPT plays an important role as a validity check for and to extrapolate lattice results, being able to correct e. g. for unphysical lattice effects such as unphysical quark masses, finite volume effects and lattice spacings. The calculations in this thesis have been performed to strengthen the synergy between the two fields by systematically adressing some of these unphysical lattice effects in the ChPT framework so that the possibilities given by a matching between lattice and ChPT results will be improved in the future.

[2]The background-interested reader might find the side remark exciting that George Zweig, who postulated the "quarks" of QCD independently, called them "aces", but Murray Gell-Mann and his "quarks" were more influential and his term prevailed.

3 Foundations of ChPT and Lowest Order

The Lagrangian of QCD with N out of six flavours massless

$$\mathcal{L}_{\mathrm{QCD}} = \sum_{\substack{i=1 \\ (u,d,s,c,b,t)}}^{6} \bar{\psi}_i(i\not{D} - m_i)\psi_i - \frac{1}{4}\mathcal{G}_{\mu\nu,a}\mathcal{G}_a^{\mu\nu} \qquad m_i = 0 \ \forall i \leq N \tag{1}$$

is symmetric under a chiral $\mathrm{SU(N)}_L \times \mathrm{SU(N)}_R \times \mathrm{U(1)}_L \times \mathrm{U(1)}_R$, or equivalently under $\mathrm{SU(N)}_L \times \mathrm{SU(N)}_R \times \mathrm{U(1)}_V \times \mathrm{U(1)}_A$. The $\mathrm{U(1)}_V$ is the conservation of the baryon number, thus leading to a classification of hadrons into baryons and mesons[3], whereas the $\mathrm{U(1)}_A$ is anomalous. The cases of interest in meson ChPT are $N = 2$ and $N = 3$. Specifying to the latter case, it is strongly believed[4] that a spontaneous breakdown of the $\mathrm{SU(3)}_L \times \mathrm{SU(3)}_R$ down to the diagonal subgroup $\mathrm{SU(3)}_V$ occurs via a scalar quark condensate of type

$$0 \neq \langle \bar{q}q \rangle \,, \tag{2}$$

thus producing an octet of pseudoscalar Goldstone bosons that can be identified with the eight lowest-mass mesons in the hadron spectrum. The matrix ϕ which is Hermitian and traceless parametrizes the broken part of the group by using the exponential representation as [5]

$$U(x) \;=\; \exp\left(i\frac{\sqrt{2}\phi(x)}{F_0}\right) \tag{3}$$

where ϕ itself transforms under $\mathrm{SU(3)}_V$ as an octet and contains the physical particles (without isospin breaking) as

$$\phi(x) \;=\; \begin{pmatrix} \frac{1}{\sqrt{2}}\pi^0 + \frac{1}{\sqrt{6}}\eta & \pi^+ & K^+ \\ \pi^- & -\frac{1}{\sqrt{2}}\pi^0 + \frac{1}{\sqrt{6}}\eta & K^0 \\ K^- & \bar{K}^0 & -\frac{2}{\sqrt{6}}\eta \end{pmatrix}. \tag{4}$$

By adding terms breaking the chiral symmetry of equation (1) explicitly, we can make the symmetry an approximate one, thus giving the mesons masses. The lowest order chiral SU(3) Lagrangian, i. e. the most general chiral Lagrangian consistent with parity, time-reversal, Lorentz symmetry of QCD, is given by

$$\mathcal{L}_2 = \frac{F_0^2}{4}\mathrm{Tr}[D_\mu U (D^\mu U)^\dagger] + \frac{F_0^2}{4}\mathrm{Tr}(\chi U^\dagger + U\chi^\dagger). \tag{5}$$

[3]To be precise, note that $\mathrm{U(1)}_V$ is also a symmetry in the massive case and $\mathrm{SU(N)}_V$ also in the case of degenerate masses, whereas the conservation of the axial-vector currents necessarily relies on the chiral limit.

[4]One argument is the absense of degenerate "parity partners" in the hadron spectrum. It should be noted that a scalar quark condensate provides a sufficient, but not a necessary condition for the spontaneous breakdown.

[5]Obviously, U itself is in SU(N), i.e. either SU(3) or SU(2) in the cases of interest.

where we have added the lowest-order symmetry-breaking terms. These are, again, the most general terms that break the chiral symmetry while still respecting the other (exact) symmetries of QCD mentioned above. Note that U transforms under the whole original symmetry group with elements denoted by (L, R) as[6]

$$U \mapsto RUL^\dagger \tag{6}$$

The symmetry-breaking mass matrix

$$\chi = 2B_0 \begin{pmatrix} \hat{m} & 0 & 0 \\ 0 & \hat{m} & 0 \\ 0 & 0 & m_s \end{pmatrix} \tag{7}$$

introduces the quark masses in the isospin limit[7], and B_0 is a LEC that parametrizes the amount of chiral symmetry breaking and in this function also dictates the vacuum expectation value $\langle \bar{q}q \rangle = -F_0^2 B_0$ to lowest order. Note that the Lagrangian (5) has the correct normalization of the kinetic term for the bosons and additionally contains terms suppressed by higher powers of the pion decay constant F_0. The Lagrangian in equation (5) is constructed so that it would be chirally invariant if also χ *would* transform in the same way as U. The lowest order masses for the pseudoscalar Pseudo-Goldstone bosons can be obtained by expansion of the exponential and are (in the isospin limit) given by

$$\begin{aligned} M_{\pi,2}^2 &= 2B_0 \hat{m}, \\ M_{K,2}^2 &= B_0(\hat{m} + m_s), \\ M_{\eta,2}^2 &= \frac{2}{3} B_0 \left(\hat{m} + 2m_s\right). \end{aligned} \tag{8}$$

They trivially fulfil the Gell-Mann Okubo relation

$$4M_K^2 = 3M_\eta^2 + M_\pi^2 \,. \tag{9}$$

The ChPT perturbative series is now a systematic expansion in momenta and masses, rather than one in a small dimensionless coupling.

4 Higher Orders: Power Counting in ChPT

At higher orders in ChPT, new contributions originate from two different sources: On the one hand, diagrams containing loops are going to contribute, thus making it necessary to

[6] U *transforms linearly* under chiral transformations. Still, the map defined in equation (6) is called a non-linear realization of the group since it does *not* operate on a vector space.

[7] Usually, $\chi = 2B_0(s + ip)$ in the external field formulation of ChPT, so the case of a constant mass matrix is contained in the more general description. In the general definition, it *indeed* behaves like U under chiral transformations. Here, even the extension of the formalism to local chiral transformations is possible (note the covariant derivatives in equation (5)).

expand the exponential in equation (3) to higher order in ϕ. At the same time, we can write down more new operators consistent with the exact symmetries of QCD - both ones which are consistent with chiral symmetry and others which break it explicitly. We thus have an expansion of our general Lagrangian

$$\mathcal{L} = \mathcal{L}_2 + \mathcal{L}_4 + \mathcal{L}_6 + ... \tag{10}$$

where the higher-order operators may contain more derivatives and/or higher powers of χ (cf. equation (7)). The new unknown constants multiplying the new operators that we have introduced in this scheme will have to be fixed primarily by experiment. The most general Lagrangian for a chiral SU(3) at order p^4, for example, can be written as (using the original choice of Gasser and Leutwyler)

$$\begin{aligned}
\mathcal{L}_4 = {} & L_1 \left\{ \mathrm{Tr}[D_\mu U (D^\mu U)^\dagger] \right\}^2 + L_2 \mathrm{Tr}\left[D_\mu U (D_\nu U)^\dagger \right] \mathrm{Tr}\left[D^\mu U (D^\nu U)^\dagger \right] \\
& + L_3 \mathrm{Tr}\left[D_\mu U (D^\mu U)^\dagger D_\nu U (D^\nu U)^\dagger \right] + L_4 \mathrm{Tr}\left[D_\mu U (D^\mu U)^\dagger \right] \mathrm{Tr}\left(\chi U^\dagger + U \chi^\dagger \right) \\
& + L_5 \mathrm{Tr}\left[D_\mu U (D^\mu U)^\dagger (\chi U^\dagger + U \chi^\dagger) \right] + L_6 \left[\mathrm{Tr}\left(\chi U^\dagger + U \chi^\dagger \right) \right]^2 \\
& + L_7 \left[\mathrm{Tr}\left(\chi U^\dagger - U \chi^\dagger \right) \right]^2 + L_8 \mathrm{Tr}\left(U \chi^\dagger U \chi^\dagger + \chi U^\dagger \chi U^\dagger \right) \\
& - i L_9 \mathrm{Tr}\left[f^R_{\mu\nu} D^\mu U (D^\nu U)^\dagger + f^L_{\mu\nu} (D^\mu U)^\dagger D^\nu U \right] + L_{10} \mathrm{Tr}\left(U f^L_{\mu\nu} U^\dagger f^{\mu\nu}_R \right) \\
& + H_1 \mathrm{Tr}\left(f^R_{\mu\nu} f^{\mu\nu}_R + f^L_{\mu\nu} f^{\mu\nu}_L \right) + H_2 \mathrm{Tr}\left(\chi \chi^\dagger \right)
\end{aligned} \tag{11}$$

where we have introduced LECs called L_i (apart from the so-called contact terms H_i[8]). The $f^{\mu\nu}$ are field-strength tensors related to the vector fields in the external field formalism of ChPT. In the SU(2) case, the Lagrangian instead reads

$$\begin{aligned}
\mathcal{L}_4 = {} & \frac{l_1}{4} \left\{ \mathrm{Tr}[D_\mu U (D^\mu U)^\dagger] \right\}^2 + \frac{l_2}{4} \mathrm{Tr}[D_\mu U (D_\nu U)^\dagger] \mathrm{Tr}[D^\mu U (D^\nu U)^\dagger] \\
& + \frac{l_3}{16} \left[\mathrm{Tr}(\chi U^\dagger + U \chi^\dagger) \right]^2 + \frac{l_4}{4} \mathrm{Tr}[D_\mu U (D^\mu \chi)^\dagger + D_\mu \chi (D^\mu U)^\dagger] \\
& + l_5 \left[\mathrm{Tr}(f^R_{\mu\nu} U f^{\mu\nu}_L U^\dagger) - \frac{1}{2} \mathrm{Tr}(f^L_{\mu\nu} f^{\mu\nu}_L + f^R_{\mu\nu} f^{\mu\nu}_R) \right] \\
& + i \frac{l_6}{2} \mathrm{Tr}[f^R_{\mu\nu} D^\mu U (D^\nu U)^\dagger + f^L_{\mu\nu} (D^\mu U)^\dagger D^\nu U] \\
& - \frac{l_7}{16} \left[\mathrm{Tr}(\chi U^\dagger - U \chi^\dagger) \right]^2 \\
& + \frac{h_1 + h_3}{4} \mathrm{Tr}(\chi \chi^\dagger) + \frac{h_1 - h_3}{16} \Big\{ \left[\mathrm{Tr}(\chi U^\dagger + U \chi^\dagger) \right]^2 \\
& + \left[\mathrm{Tr}(\chi U^\dagger - U \chi^\dagger) \right]^2 - 2 \mathrm{Tr}(\chi U^\dagger \chi U^\dagger + U \chi^\dagger U \chi^\dagger) \Big\} \\
& - 2 h_2 \mathrm{Tr}(f^L_{\mu\nu} f^{\mu\nu}_L + f^R_{\mu\nu} f^{\mu\nu}_R)
\end{aligned} \tag{12}$$

[8]The contact term coefficients cannot be measured directly in physical quantities involving mesons and are thus irrelevant for the calculations in this thesis.

with constants denoted by l_i (h_i). At order p^6, also called next-to-next-to-leading order (NNLO), new constants C_i respective c_i are introduced into the SU(3) respective SU(2) theory.

The ChPT expansion in masses and momenta necessitates a well-defined ordering criterion for the different contributions to an observable of interest. To close this section, I would like to shortly introduce to the so-called Weinberg power counting scheme [5] and how it works in practice. We follow closely the discussion in [8]. As can be best seen from the expressions for the lowest order meson masses (equation (8)), a quark *mass* will contribute as a meson *mass squared*, thus corresponding to a momentum squared or two derivatives in the Lagrangian. Generally speaking, a single vertex out of a Lagrangian $\mathcal{L}_{2n}$ will contribute with $2n$ in this power counting scheme. We introduce the chiral dimension D of a diagrammatic contribution as

$$D = 4N_L - 2N_I + \sum_{n=1}^{\infty} 2nN_{2n}, \tag{13}$$

where N_L denotes the number of loops, N_I the number of internal lines and N_{2n} denotes the number of vertices that originate from the Lagrangian $\mathcal{L}_{2n}$ (since besides the powers coming from the vertices, a Lorentz invariant integration measure provides four powers of momentum whereas a propagator provides two inverse powers).[9] Using the identity

$$N_L = N_I - (N_V - 1) \qquad N_V = \sum_n N_{2n} \tag{14}$$

one can also eliminate either N_L or N_I. In the latter case, we find

$$D = 2 + \sum_{n=1}^{\infty} 2(n-1)N_{2n} + 2N_L, \tag{15}$$

We can also see from this formula that the maximal number of loops contributing to a fixed chiral dimension is given by

$$N_L = \frac{D-2}{2}. \tag{16}$$

The practical estimation of the chiral dimension of a diagram can still best be done according to formula (13). Some examples are given in figure 1.

5 Quantum Corrections for Masses: A Simple p^4 Example

In this section, we rederive for instructive reasons the NLO corrections to the meson masses in chiral SU(3). We conventionally denote the sum of irreducible self-energy diagrams by

[9] Note that the authors of [8] missed a factor of 4 in front of N_L.

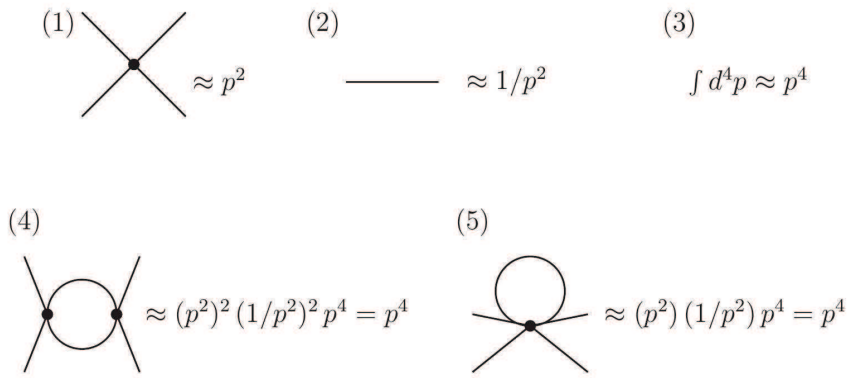

Figure 1: Illustration of the Weinberg power counting scheme according to equation (13). Upper row: (1) vertex of order p^2, (2) propagator, (3) p^4 contribution resulting from a loop integration. Lower row: Different one-loop contributions to $\pi\pi$ scattering. All vertices are of lowest order.

$-i\Sigma(p^2)$. The physical mass M can then be obtained from it by solving for the position of the propagator pole

$$M^2 - M_0^2 - \Sigma(M^2) = 0 \tag{17}$$

with M_0 denoting the mass to lowest order. At order p^4, this step is trivial, once $\Sigma_4(p^2)$ is known, since

$$M^2 = M_0^2 + \Sigma(M^2) = M_0^2 + \Sigma(M_0^2) + \mathcal{O}(p^6). \tag{18}$$

All self-energies at this order will have the form

$$\Sigma_4^\phi(p^2) = A_\phi + B_\phi p^2, \tag{19}$$

so the masses can be obtained via

$$M^2 = M_0^2 + A_\phi + B_\phi M_0^2 + \mathcal{O}(p^6). \tag{20}$$

To calculate $\Sigma_4(p^2)$, we need - as a first step - the expansion of the general Lagrangian (11) in terms of physical fields. Specifically, we need (cf. also discussion in section 4)

- the Lagrangian $\mathcal{L}_2$ with two meson fields, giving the lowest order masses, (equations(8))
- the Lagrangian $\mathcal{L}_2$ with four meson fields, for the loop contribution
- the Lagrangian $\mathcal{L}_4$ with two meson fields, for the contact contribution

Due to space restrictions, we only show the expansions (of the latter two) in terms of the matrix ϕ (and its derivative) with $\mathcal{M}$ denoting the mass matrix in equation (7).

$$\mathcal{L}_2^{4\phi} = \frac{1}{24F_0^2}\left\{\mathrm{Tr}([\phi,\partial_\mu\phi]\phi\partial^\mu\phi) + B_0\mathrm{Tr}(\mathcal{M}\phi^4)\right\}. \tag{21}$$

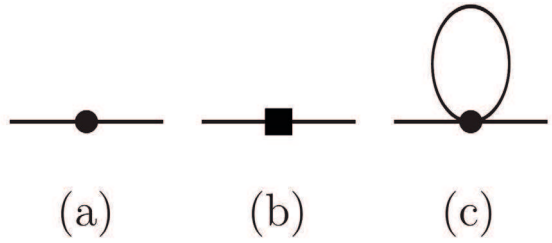

Figure 2: Diagrammatic contributions to the pseudoscalar self-energy, up to $\mathcal{O}(p^4)$. The circles in a) and c) are of $\mathcal{O}(p^2)$, the filled box in b) is of $\mathcal{O}(p^4)$.

$$\begin{aligned}\mathcal{L}_4^{2\phi} = \frac{1}{F_0^2}\Big\{ & L_4 \quad 8 \quad B_0\mathrm{Tr}(\partial_\mu\phi\partial^\mu\phi)\mathrm{Tr}(\mathcal{M}) \\ & +L_5 \quad 8 \quad B_0\mathrm{Tr}(\partial_\mu\phi\partial^\mu\phi\mathcal{M}) \\ & +L_6 \quad (-32) \quad B_0^2\mathrm{Tr}(\mathcal{M})\mathrm{Tr}(\mathcal{M}\phi^2) \\ & +L_7 \quad (-32) \quad B_0^2[\mathrm{Tr}(\mathcal{M}\phi)]^2 \\ & +L_8 \quad (-16) \quad B_0^2(\mathrm{Tr}(\phi\mathcal{M}\phi\mathcal{M}) + \mathrm{Tr}(\phi^2\mathcal{M}^2))\Big\}\end{aligned} \tag{22}$$

The expansion in terms of the eight pseudoscalars is similarly trivial. As a next step, we need to calculate how these operators contribute to the self-energy, thereby taking into account the different possibilities and combinatorics properly.[10] Figure 2 shows the three different types of diagrams that contribute to the two-point function to the desired order.

For the loop diagram, only two integrals are non-vanishing at this level, i. e.

$$A(m^2) = \frac{1}{i}\int \frac{d^dq}{(2\pi)^d}\frac{1}{q^2-m^2} \tag{23}$$

$$B(m^2) = \frac{1}{i}\int \frac{d^dq}{(2\pi)^d}\frac{q^2}{q^2-m^2} = m^2A(m^2) \tag{24}$$

which leaves only one integral to be solved:

$$A(m^2) = \frac{m^2}{16\pi^2}\Big\{\lambda_0 - \ln(m^2) + \mathcal{O}(\epsilon)\Big\} \tag{25}$$

[10]Using a computer-algebra system, this step can equally well be achieved by "brute-forcing" and summing over all possible combinatorical cases - even if they lead to the same contraction - and then multiplying by the proper symmetry factor of the diagram.

We choose a renormalization scheme which is a ChPT-specific variant of MSbar

$$\lambda_0 = \frac{1}{\bar{\epsilon}} = \frac{1}{\epsilon} + \ln(4\pi) + 1 - \gamma_E \tag{26}$$

The renormalization scale μ^2 will cancel out of all physical results since the LECs cancel by construction the μ^2 dependence of the loop part.

As example, I show the loops contributions to the pion and the kaon self-energy.

	ϕ^4 term	derivative term	sum of both
Pion loop	$\frac{B_0\hat{m}}{6F_0^2}10 = \frac{1}{6F_0^2}(5m_\pi^2)$	$\frac{1}{6F_0^2}(-4m_\pi^2 - 4p^2)$	$\frac{1}{6F_0^2}(m_\pi^2 - 4p^2)$
Kaon loop	$\frac{B_0(3\hat{m}+m_s)}{6F_0^2}2 = \frac{1}{6F_0^2}(2m_K^2 + 2m_\pi^2)$	$\frac{1}{6F_0^2}(-2m_K^2 - 2p^2)$	$\frac{1}{6F_0^2}(2m_\pi^2 - 2p^2)$
Eta loop	$\frac{B_0\hat{m}}{6F_0^2}2 = \frac{1}{6F_0^2}(m_\pi^2)$	-	$\frac{1}{6F_0^2}(m_\pi^2)$

Table 1: Coefficients of the one-loop diagram contribution to the self-energy $\Sigma_4(p^2)$ for the pion, split up according to which operator of $\mathcal{L}_2^{4\phi}$ contributes and which virtual particle occupies the loop, given in units of the divergent integral $A(m^2)$. Note that derivatives can come with the loop particles, thus introducing their masses into the result, as well as with the external particles, introducing their own squared momenta. Lowest order mass relations were applied to the symmetry-breaking terms. Observe also the cancellation of the kaon mass dependence: In an unbroken SU(2), the pion has to remain massless.

	ϕ^4 term	derivative term	sum of both
Pion loop	$\frac{B_0(3\hat{m}+m_s)}{6F_0^2}\frac{3}{2} = \frac{1}{6F_0^2}(\frac{3}{2}m_K^2 + \frac{3}{2}m_\pi^2)$	$\frac{1}{6F_0^2}(-\frac{3}{2}m_\pi^2 - \frac{3}{2}p^2)$	$\frac{1}{6F_0^2}(\frac{3}{2}m_K^2 - \frac{3}{2}p^2)$
Kaon loop	$\frac{B_0(\hat{m}+m_s)}{6F_0^2}6 = \frac{1}{6F_0^2}(6m_K^2)$	$\frac{1}{6F_0^2}(-3m_K^2 - 3p^2)$	$\frac{1}{6F_0^2}(3m_K^2 - 3p^2)$
Eta loop	$\frac{B_0(\hat{m}+3m_s)}{6F_0^2}\frac{1}{2} = \frac{1}{6F_0^2}(\frac{3}{2}m_\eta^2 - \frac{1}{2}m_K^2)$	$\frac{1}{6F_0^2}(-\frac{3}{2}m_\eta^2 - \frac{3}{2}p^2)$	$\frac{1}{6F_0^2}(-\frac{1}{2}m_K^2 - \frac{3}{2}p^2)$

Table 2: Coefficients of the one-loop diagram contribution to the self-energy $\Sigma_4(p^2)$ for the kaon, split up according to which operator of $\mathcal{L}_2^{4\phi}$ contributes and which virtual particle occupies the loop, given in units of the divergent integral $A(m^2)$. Note that derivatives can come with the loop particles, thus introducing their masses into the result, as well as with the external particles, introducing their own squared momenta. Lowest order mass relations were applied to the symmetry-breaking terms.

The operators of $\mathcal{L}_4^{2\phi}$ contribute similarly. The renormalization of the LECs cancels the loop infinities by construction, thus producing finite quantum corrections to the masses. It was checked that the results agree with [7, 8] who obtained

$$M_{\pi,4}^2 \;=\; M_{\pi,2}^2\left\{1 + \frac{M_{\pi,2}^2}{32\pi^2F_0^2}\ln\left(\frac{M_{\pi,2}^2}{\mu^2}\right) - \frac{M_{\eta,2}^2}{96\pi^2F_0^2}\ln\left(\frac{M_{\eta,2}^2}{\mu^2}\right)\right.$$

$$+\frac{16}{F_0^2}\left[(2m+m_s)B_0(2L_6^r-L_4^r)+mB_0(2L_8^r-L_5^r)\right]\Bigg\}, \tag{27}$$

$$\begin{aligned} M_{K,4}^2 &= M_{K,2}^2\Bigg\{1+\frac{M_{\eta,2}^2}{48\pi^2F_0^2}\ln\left(\frac{M_{\eta,2}^2}{\mu^2}\right) \\ &\quad +\frac{16}{F_0^2}\left[(2m+m_s)B_0(2L_6^r-L_4^r)+\frac{1}{2}(m+m_s)B_0(2L_8^r-L_5^r)\right]\Bigg\}, \end{aligned} \tag{28}$$

$$\begin{aligned} M_{\eta,4}^2 &= M_{\eta,2}^2\left[1+\frac{M_{K,2}^2}{16\pi^2F_0^2}\ln\left(\frac{M_{K,2}^2}{\mu^2}\right)-\frac{M_{\eta,2}^2}{24\pi^2F_0^2}\ln\left(\frac{M_{\eta,2}^2}{\mu^2}\right)\right. \\ &\quad \left.+\frac{16}{F_0^2}(2m+m_s)B_0(2L_6^r-L_4^r)+8\frac{M_{\eta,2}^2}{F_0^2}(2L_8^r-L_5^r)\right] \\ &\quad +M_{\pi,2}^2\left[\frac{M_{\eta,2}^2}{96\pi^2F_0^2}\ln\left(\frac{M_{\eta,2}^2}{\mu^2}\right)-\frac{M_{\pi,2}^2}{32\pi^2F_0^2}\ln\left(\frac{M_{\pi,2}^2}{\mu^2}\right)\right. \\ &\quad \left.+\frac{M_{K,2}^2}{48\pi^2F_0^2}\ln\left(\frac{M_{K,2}^2}{\mu^2}\right)\right] \\ &\quad +\frac{128}{9}\frac{B_0^2(m-m_s)^2}{F_0^2}(3L_7^r+L_8^r). \end{aligned} \tag{29}$$

The LECs renormalize as

$$L_i \equiv (\mu c)^{-2\epsilon}\left(\frac{-1}{32\pi^2\epsilon}\Gamma_i+L_i^r(\mu)\right)=(\mu)^{-2\epsilon}\left(\frac{-1}{32\pi^2}\Gamma_i\lambda_0+L_i^r(\mu)+\mathcal{O}(\epsilon)\right) \tag{30}$$

with coefficients Γ_i, and $\ln c = -1/2(\ln(4\pi)-\gamma+1)$ specifying the finite part in our renormalization conventions. The L_i^r thus acquire the already mentioned scale dependence

$$L_i^r(\mu_2)=L_i^r(\mu_1)+\frac{\Gamma_i}{16\pi^2}\ln\left(\frac{\mu_1}{\mu_2}\right). \tag{31}$$

The l_i in the SU(2) case renormalize in a similar manner, and authors usually quote the μ-independent $\bar{l}_i$ which are defined as

$$\bar{l}_i=\frac{32\pi^2}{\gamma_i}l_i^r(\mu)-\ln\frac{M_\pi^2}{\mu^2}. \tag{32}$$

For the numerical evaluation of the mass corrections Δm_4, one can promote the lowest order masses in the p^4 terms on the right hand side of equation (27) to physical masses. Since the induced difference is of higher order, the formal accuracy is maintained. It should be noted that the elimination of the lowest order parameters in favour of the physical ones is not unique due to the Gell-Mann Okubo degeneracy. This plays a particular importance if the complete mass expansion is done to higher order since a part of the higher order

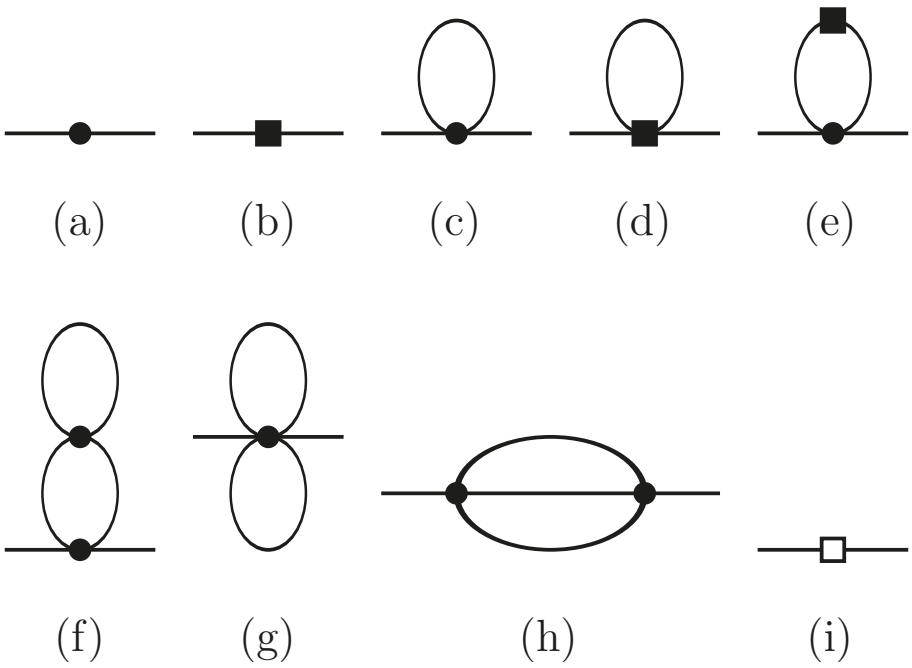

Figure 3: Diagrammatic contributions to the pseudoscalar self-energy, up to $\mathcal{O}(p^6)$. Circular vertices are of $\mathcal{O}(p^2)$, the filled boxes are of $\mathcal{O}(p^4)$, the open box is of $\mathcal{O}(p^6)$.

terms will evidently acquire an explicit dependence on the specific choice for the elimination procedure in the lower orders. The inverse pion decay constant can be promoted to its physical value due to a similar argument.

6 Anatomy of the p^6 Calculation

The NNLO corrections to the pseudoscalar self-energy are, according to the power counting scheme established in section 4, given by diagram contributions with up to two loops [9]. All relevant diagrams can be seen in figure 3. These are all tadpole[11] integrals except for the sunset diagram in figure 3h).

For the evaluation of the two-loop integrals, mainly two complications arise compared to the NLO case. By considering figure 3, note that a new one-loop integral with a squared propagator arises. Two of the three two-loop diagrams, i. e. diagrams f) and g), yield simple products of one-loop integrals. This is very convenient, but note that expansions as in equation (25) are no longer sufficient, and the terms linear in ϵ play a crucial role in order to calculate the NNLO mass correction up to $\mathcal{O}(1)$ in the ϵ expansion.[12] The other

[11]The term "tadpole" was introduced by Sidney Coleman. The background-interested reader might find it amusing that the editor of the respective publication did not appreciate the terminology at first, but caved in, once Sidney proposed "lollypop" and "spermion" as alternatives.

[12]In the infinite volume case of the mass correction, only $A(m^2)$ has to be known up to $\mathcal{O}(\epsilon)$, known

major complication is given by the sunset diagram, figure 3h). Apart from its property of irreducibility to products of one-loop integrals, its momentum flow leads to an explicit dependence on p^2.[13] For the time being, the evaluation of the three integrals[14]

$$\begin{aligned} H(m_1^2,m_2^2,m_3^2;p^2) &= \langle\langle 1\rangle\rangle\,, \\ H_\mu(m_1^2,m_2^2,m_3^2;p^2) &= \langle\langle q_\mu\rangle\rangle = p_\mu H_1(m_1^2,m_2^2,m_3^2;p^2)\,, \\ H_{\mu\nu}(m_1^2,m_2^2,m_3^2;p^2) &= \langle\langle q_\mu q_\nu\rangle\rangle \\ &= p_\mu p_\nu H_{21}(m_1^2,m_2^2,m_3^2;p^2) + g_{\mu\nu} H_{22}(m_1^2,m_2^2,m_3^2;p^2)\,, \end{aligned} \tag{33}$$

will be sufficient, where we have used the notation of [11]

$$\langle\langle X\rangle\rangle = \frac{1}{i^2}\int \frac{d^dq}{(2\pi)^d}\frac{d^dr}{(2\pi)^d}\frac{X}{(q^2-m_1^2)\,(r^2-m_2^2)\,((q+r-p)^2-m_3^2)}\,. \tag{34}$$

With the exception of the simple one-loop calculation in section 5, all computations have been carried out with the help of FORM [12]. This includes the generation of all contributions to a diagram of given topology as well as all successive manipulations in order to simplify the expressions.

We apply Passarino-Veltman type identities to reduce the occuring integrals to a minimal set. For the one-loop integrals, only the two scalar integrals (with one and two powers of the propagator) serve as a basis set, i. e. in addition to $A(m^2)$ (see equation (23)) we need the two-propagator integral with zero momentum flow

$$B_0(m^2) = \frac{1}{i}\int \frac{d^dq}{(2\pi)^d}\frac{1}{(q^2-m^2)^2}. \tag{35}$$

For the sunsets, we can apply different kinds of symmetry identities to make further cancellations work out. Whereas H is symmetric in all three mass arguments, only the second and third argument can be interchanged in the other two integrals. The relation between H_1 and H

$$H_1(m_1^2,m_2^2,m_3^2;p^2) + H_1(m_2^2,m_1^2,m_3^2;p^2) + H_1(m_3^2,m_1^2,m_2^2;p^2) = H(m_1^2,m_2^2,m_3^2;p^2) \tag{36}$$

can be applied and trivially implies also

$$H_1(m^2,m^2,m^2;p^2) = 1/3\; H(m^2,m^2,m^2;p^2). \tag{37}$$

from e. g. [10].

[13] Note also that whenever derivatives with respect to p^2 play a role, the explicit dependence of integrals on the external momentum will evidently lead to derivatives of these, thus making it necessary to evaluate several more integrals explicitly, cf. section 7.

[14] We count three integrals since e. g. H_{22} can be reduced to the three remaining ones and products of one-loop integrals. Similarly, the sunset integrals with both loop momenta standing in the numerator - which are omitted in equation (33) - can be reduced to the aforementioned. A more complete view over the Passarino-Veltman type reduction procedure used thoughout this thesis and the resulting identities interrelating the intergrals can be found in section 8.

The evaluation of the NNLO mass correction requires, apart from the NNLO corrections to the self-energy, again a self-consistent solution to the pole equation (cf. equation (17)). In addition to the new diagrammatic contributions, new NNLO terms also arise from the NLO self-energy since the latter is now supposed to be evaluated at the NLO mass and inverse decay constant in order to maintain formal p^6 accuracy.[15] In this way, also the specific choice of meson masses in the NLO terms of the self-energy enters explicitly at $\mathcal{O}(p^6)$: Mass expressions that were degenerate at $\mathcal{O}(p^4)$ due to the lowest order relations will generate different terms in the higher orders.[16] In a rather sketchy way, we thus generally evaluate

$$M^2 - M_0^2 \underbrace{-\Sigma_4(M_0^2)}_{\mathcal{O}(p^4)} \underbrace{-\Sigma_4(M_4^2) + \Sigma_4(M_0^2)}_{\mathcal{O}(p^6)} \underbrace{-\Sigma_6(M_0^2)}_{\mathcal{O}(p^6)} = \mathcal{O}(p^8). \tag{38}$$

Equation (38) has to be understood in the way that $\Sigma_4(M_4^2)$ will be obtained by insertion of the analytical expression for the NLO mass expansion. After cancellations, the difference to $\Sigma_4(M_0^2)$ will then be of $\mathcal{O}(p^6)$. We only implicitly require a consistent choice for the elimination in terms of the pseudoscalar masses in Σ_4 in order to have a consistent perturbative series up to $\mathcal{O}(p^6)$.

The very instructive equation (38) oversimplifies the actual procedure. If we want to evaluate the mass correction by using physical meson masses as input, additional terms in the higher orders will of course be generated. One generally finds for the mass correction fulfilling all necessary features

$$\begin{array}{ll}
\left\{ -\Sigma_4(M_0^2 \to M_{phys}^2; p^2 \to M_{phys}^2) \right\} & \mathcal{O}(p^4) \\
-\Sigma_4(M_0^2; p^2 = M_4^2 = M_0^2 + \Delta m_4^2) & \\
+\Sigma_4(M_0^2 \to M_{phys}^2 = M_0^2 + \Delta m_4^2; p^2 \to M_{phys}^2 = M_0^2 + \Delta m_4^2) & \mathcal{O}(p^6) \\
\left. -\Sigma_6(M_0^2; p^2 = M_0^2) \right\} \Big|_{M_0^2 \to M_{phys}^2} & \mathcal{O}(p^6)
\end{array} \tag{39}$$

Here the first argument represents the lowest order parameters $\hat{m}$ and m_s that naturally emerge in the calculation, together with a choice of their elimination in favour of the lowest order meson masses, whereas the second argument represents the genuine p^2 dependence.

By following this recipe, apart from the "infinite renormalization" that makes the $\mathcal{O}(p^6)$ finite, an additional "finite renormalization" occurs that depends on the (different kinds of) specific choices at $\mathcal{O}(p^4)$. Obviously, the new p^6 terms coming from the self-energy

[15] It is worth to note that neither the new diagrammatic pieces nor the "renormalization" terms from the NLO self-energy are finite in four dimensions when taken alone, but only their sum.

[16] Both effects, on the one hand the effect of the evaluation of the self-energy at NLO corrected masses and inverse decay constant and on the other hand the choice regarding degenerate expressions, are evidently entangled and can - in a practical calculation - be taken into account in one go.

itself can - if overall p^6 accuracy is sought - easily be expressed in terms of (any convenient choice of) physical masses. These are again all formally equivalent.

Via diagrams i) from figure 3, the new LECs C_i enter the calculation. They renormalize via

$$C_i \equiv (\mu c)^{-4\epsilon}\left(\frac{\gamma_{2i}}{\epsilon^2}+\frac{\gamma_{1i}}{\epsilon}+C_i^r(\mu)\right)=\mu^{-4\epsilon}\left(\gamma_{2i}\lambda_2+\gamma_{1i}\lambda_1+C_i^r(\mu)+\mathcal{O}(\epsilon)\right)\ . \qquad (40)$$

Just to give one explicit example, I show the NLO and NNLO kaon mass correction in infinite volume coming out of our calculation as a byproduct. All our results in infinite volume for the masses and decay constants have been checked against the known results [10].

$$\begin{aligned} F_\pi^4\Delta m_K^{2(4)} &= +\overline{A}(m_\eta^2)\left(-1/4\,m_\eta^2-1/12\,m_\pi^2\right)\\ &\quad +8\Big(2L_6^r-L_4^r\Big)\Big(2m_K^2+m_\pi^2\Big)-8m_K^4\Big(L_5^r-2L_8^r\Big) \end{aligned} \qquad (41)$$

$$\begin{aligned} F_\pi^4\Delta m_K^{2(6)} &= +64\,m_K^6\,C_{32}^r+32\,m_K^6\,C_{31}^r+192\,m_K^6\,C_{21}^r+128\,m_K^6\,C_{20}^r+96\,m_K^6\,C_{19}^r-64\,m_K^6\,C_{16}^r\\ &\quad -32\,m_K^6\,C_{15}^r-32\,m_K^6\,C_{14}^r-64\,m_K^6\,C_{13}^r-32\,m_K^6\,C_{12}^r+32\,m_\pi^2\,m_K^4\,C_{32}^r+192\,m_\pi^2\,m_K^4\,C_{21}^r\\ &\quad -32\,m_\pi^2\,m_K^4\,C_{20}^r-96\,m_\pi^2\,m_K^4\,C_{19}^r-32\,m_\pi^2\,m_K^4\,C_{17}^r+64\,m_\pi^2\,m_K^4\,C_{16}^r-16\,m_\pi^2\,m_K^4\,C_{15}^r\\ &\quad +32\,m_\pi^2\,m_K^4\,C_{14}^r-32\,m_\pi^2\,m_K^4\,C_{13}^r+48\,m_\pi^4\,m_K^2\,C_{21}^r+48\,m_\pi^4\,m_K^2\,C_{20}^r+48\,m_\pi^4\,m_K^2\,C_{19}^r\\ &\quad +16\,m_\pi^4\,m_K^2\,C_{17}^r-48\,m_\pi^4\,m_K^2\,C_{16}^r-16\,m_\pi^4\,m_K^2\,C_{14}^r\\ &\quad -512\,(L_8^r)^2\,m_K^6-2048\,L_6^rL_8^rm_K^6-768\,L_6^rL_8^rm_\pi^2\,m_K^4-256\,L_6^rL_8^rm_\pi^4\,m_K^2-2048\,(L_6^r)^2\,m_K^6\\ &\quad -2048\,(L_6^r)^2\,m_\pi^2\,m_K^4-512\,(L_6^r)^2\,m_\pi^4\,m_K^2+384\,L_5^rL_8^rm_K^6+128\,L_5^rL_8^rm_\pi^2\,m_K^4+768\,L_5^rL_6^rm_K^6\\ &\quad +512\,L_5^rL_6^rm_\pi^2\,m_K^4+256\,L_5^rL_6^rm_\pi^4\,m_K^2-64\,(L_5^r)^2\,m_K^6-64\,(L_5^r)^2\,m_\pi^2\,m_K^4+1024\,L_4^rL_8^rm_K^6\\ &\quad +384\,L_4^rL_8^rm_\pi^2\,m_K^4+128\,L_4^rL_8^rm_\pi^4\,m_K^2+2048\,L_4^rL_6^rm_K^6+2048\,L_4^rL_6^rm_\pi^2\,m_K^4+512\,L_4^rL_6^rm_\pi^4\,m_K^2\\ &\quad -384\,L_4^rL_5^rm_K^6-256\,L_4^rL_5^rm_\pi^2\,m_K^4-128\,L_4^rL_5^rm_\pi^4\,m_K^2-512\,(L_4^r)^2\,m_K^6-512\,(L_4^r)^2\,m_\pi^2\,m_K^4\\ &\quad -128\,(L_4^r)^2\,m_\pi^4\,m_K^2+89/27\,\frac{1}{16\pi^2}\,L_3^rm_K^6-4/27\,\frac{1}{16\pi^2}\,L_3^rm_\pi^2\,m_K^4+41/27\,\frac{1}{16\pi^2}\,L_3^rm_\pi^4\,m_K^2\\ &\quad +122/9\,\frac{1}{16\pi^2}\,L_2^rm_K^6-16/9\,\frac{1}{16\pi^2}\,L_2^rm_\pi^2\,m_K^4+56/9\,\frac{1}{16\pi^2}\,L_2^rm_\pi^4\,m_K^2+4\,\frac{1}{16\pi^2}\,L_1^rm_K^6\\ &\quad \left(\frac{1}{16\pi^2}\right)^2\Big(-4709/1728\,m_K^6-19/108\,m_\pi^2\,m_K^4-13/24\,m_\pi^4\,m_K^2\\ &\quad -763/1296\,\pi^2\,m_K^6-73/648\,\pi^2\,m_\pi^2\,m_K^4-1/8\,\pi^2\,m_\pi^4\,m_K^2\Big)\\ &\quad +\overline{A}(m_\pi^2)^2\left(-1/2\,m_\pi^{-2}\,m_K^4-27/32\,m_K^2\right)+\overline{A}(m_\pi^2)\,\overline{A}(m_K^2)\left(-3/4\,m_K^2\right)\\ &\quad +\overline{A}(m_\pi^2)\,\overline{A}(m_\eta^2)\left(-41/48\,m_K^2+1/12\,m_\pi^2\right)\\ &\quad +\overline{A}(m_\pi^2)\Big(+32\,L_8^rm_K^4+24\,L_8^rm_\pi^2\,m_K^2+64\,L_6^rm_K^4+88\,L_6^rm_\pi^2\,m_K^2-16\,L_5^rm_K^4-12\,L_5^rm_\pi^2\,m_K^2 \end{aligned}$$

$$
\begin{aligned}
&-32\,L_4^r m_K^4 - 68\,L_4^r m_\pi^2\,m_K^2 + 15\,L_3^r m_\pi^2\,m_K^2 + 12\,L_2^r m_\pi^2\,m_K^2 + 48\,L_1^r m_\pi^2\,m_K^2 + 3/4\,\frac{1}{16\pi^2}\,m_K^4\Big) \\
&+\overline{A}(m_K^2)^2\,\Big(-251/72\,m_K^2 - 3/8\,m_\pi^2\Big) + \overline{A}(m_K^2)\,\overline{A}(m_\eta^2)\,\Big(-2/3\,m_K^2\Big) \\
&+\overline{A}(m_K^2)\,\Big(+64\,L_8^r m_K^4 + 128\,L_6^r m_K^4 + 16\,L_6^r m_\pi^2\,m_K^2 - 32\,L_5^r m_K^4 - 80\,L_4^r m_K^4 - 8\,L_4^r m_\pi^2\,m_K^2 \\
&+30\,L_3^r m_K^4 + 36\,L_2^r m_K^4 + 72\,L_1^r m_K^4 + 3/4\,\frac{1}{16\pi^2}\,m_K^4 + 3/4\,\frac{1}{16\pi^2}\,m_\pi^2\,m_K^2\Big) \\
&+\overline{A}(m_\eta^2)^2\,\Big(-5/36\,m_K^2 - 25/128\,m_\pi^2 - 43/1152\,m_\pi^4\,m_\eta^{-2}\Big) \\
&+\overline{A}(m_\eta^2)\,\Big(+32\,L_8^r m_K^4 - 56/3\,L_8^r m_\pi^2\,m_K^2 + 16/3\,L_8^r m_\pi^4 + 64/3\,L_7^r m_K^4 - 32\,L_7^r m_\pi^2\,m_K^2 + 32/3\,L_7^r m_\pi^4 \\
&+128/3\,L_6^r m_K^4 - 8/3\,L_6^r m_\pi^2\,m_K^2 - 112/9\,L_5^r m_K^4 + 4/3\,L_5^r m_\pi^2\,m_K^2 - 8/9\,L_5^r m_\pi^4 - 32\,L_4^r m_K^4 \\
&+4\,L_4^r m_\pi^2\,m_K^2 + 28/3\,L_3^r m_K^4 - 7/3\,L_3^r m_\pi^2\,m_K^2 + 16/3\,L_2^r m_K^4 - 4/3\,L_2^r m_\pi^2\,m_K^2 + 64/3\,L_1^r m_K^4 \\
&-16/3\,L_1^r m_\pi^2\,m_K^2 + 1/2\,\frac{1}{16\pi^2}\,m_K^4 + 1/4\,\frac{1}{16\pi^2}\,m_\pi^2\,m_K^2\Big) \\
&-15/32\,H(m_\pi^2,m_\pi^2,m_K^2,m_K^2)\,m_K^4 + 3/4\,H(m_\pi^2,m_\pi^2,m_K^2,m_K^2)\,m_\pi^2\,m_K^2 \\
&+29/16\,H(m_\pi^2,m_K^2,m_\eta^2,m_K^2)\,m_K^4 + 3/4\,H(m_K^2,m_K^2,m_K^2,m_K^2)\,m_K^4 \\
&+181/288\,H(m_K^2,m_\eta^2,m_\eta^2,m_K^2)\,m_K^4 - H_1(m_\pi^2,m_K^2,m_\eta^2,m_K^2)\,m_K^4 \\
&+3/4\,H_1(m_K^2,m_\pi^2,m_\pi^2,m_K^2)\,m_K^4 - 5/2\,H_1(m_K^2,m_\pi^2,m_\eta^2,m_K^2)\,m_K^4 \\
&-5/4\,H_1(m_K^2,m_\eta^2,m_\eta^2,m_K^2)\,m_K^4 - H_1(m_\eta^2,m_\pi^2,m_K^2,m_K^2)\,m_K^4 \\
&+9/4\,H_{21}(m_\pi^2,m_\pi^2,m_K^2,m_K^2)\,m_K^4 - 9/32\,H_{21}(m_K^2,m_\pi^2,m_\pi^2,m_K^2)\,m_K^4 \\
&+27/16\,H_{21}(m_K^2,m_\pi^2,m_\eta^2,m_K^2)\,m_K^4 + 9/4\,H_{21}(m_K^2,m_K^2,m_K^2,m_K^2)\,m_K^4 \\
&+27/32\,H_{21}(m_K^2,m_\eta^2,m_\eta^2,m_K^2)\,m_K^4
\end{aligned}
\tag{42}
$$

We have used the notation $\overline{A}(m^2)$ to denote the $\mathcal{O}(1)$ term in the ϵ expansion of the integral $A(m^2)$.

7 Corrections to the Decay Constants

The (physical) pion decay constant is defined by the coupling of the axial-vector current to the pion,

$$
\langle 0|A_\mu(0)|\pi^-(p)\rangle = i\sqrt{2}p_\mu F_\pi\,; \qquad A_\mu = \bar{u}\gamma_\mu\gamma_5 d\,. \tag{43}
$$

Amongst other things, it dictates the rate of leptonic charged pion decays as

$$
\Gamma^{(0)}(\pi\to\ell\nu) = \frac{G_F^2|V_{ud}|^2F_\pi^2}{4\pi}m_\pi m_\ell^2\left(1-\frac{m_\ell^2}{m_\pi^2}\right)^2 \tag{44}
$$

Its physical value in this convention is $F_\pi = 92.2$ MeV.[17] We also encounter its inverse powers in the chiral expansions, e. g. of the pseudoscalar masses.[18]

The remaining two decay constants can be defined in a way similar to equation (43), but for definiteness we will keep the example of the pion in the remainder of this section.

One way to calculate the chiral expansion of F_π is via the axial-vector pseudoscalar two-point function. The diagrams up to order p^6 can be seen in figure 4. Their structural similarity to the mass diagrams (cf. figure 3) facilitates their calculation. In addition to these, the wavefunction renormalization of the external pion state has to be taken into account. In its most general way, this can be seen from the LSZ theorem. Originally used for scattering amplitudes, the argument holds for any kind of physical quantity. There are different equivalent formulations (e. g. that differ if they use truncated Green's functions or not), so we only consider the easiest for our purpose. According to

$$ {}_{out}\langle\phi_1 ... \phi_i | \phi_i ... \phi_n\rangle_{in} = \langle\phi_1 ... \phi_n\rangle = Z^{-\frac{n}{2}} G_{trunc}(\phi_1, ..., \phi_n)\,, \tag{45}$$

an S-matrix element (or any other amplitude) can be calculated given the corresponding truncated Green's function and the wavefunction renormalization factors $\sqrt{Z}$ of the external fields. Each field thereby contributes with its own $1/\sqrt{Z}$.

The underlying reason is that the propagator pole of the bare two-point function acquires under resummation a residue Z^{-1} with $Z = 1 + \frac{d\Sigma}{dp^2}|_{p^2=M^2_{phys}}$. This residue is absorbed into a rescaling of the respective field $\phi \to \phi' = \sqrt{Z}\phi$.[19] The effect of the rescaling then enters explicitly for all n-point functions (with $n \neq 2$). In the case of our two-point function which involves one external pion field, one power of the wavefunction renormalization has to be divided out.[20] Schematically, since

$$\begin{aligned} \langle\phi\phi\rangle &\simeq \frac{i}{Z(p^2 - M_{phys})^2} + \text{non-pole terms} \\ \langle\phi'\phi'\rangle &\simeq \frac{i}{(p^2 - M_{phys})^2} + \text{non-pole terms}, \end{aligned} \tag{46}$$

we find for the amplitudes that involve only one scalar field

$$\begin{aligned} \langle\phi a^\mu\rangle &\simeq \frac{i}{Z(p^2 - M_{phys})^2} i\Pi + \text{non-pole terms} \\ \langle\phi' a^\mu\rangle &\simeq \frac{i}{\sqrt{Z}(p^2 - M^2_{phys})} i\Pi + \text{non-pole terms} \end{aligned} \tag{47}$$

[17] There are several conventions that differ by different powers of $\sqrt{2}$.

[18] It formally enters as the lowest order parameter and will then be substituted for the physical one in our calculations, cf. section 6.

[19] Note that Z as defined here is sometimes denoted by Z^{-1}, in particular in the traditional renormalization literature, i. e. $\phi_{bare} = \sqrt{Z}\phi_r$ with ϕ_r being the renormalized field. The bare propagator residue is correspondingly Z.

[20] In an n-point function, these would be n powers of $\sqrt{Z}$ to be divided out. Each external leg gets a resummation factor $1/Z$ (when expressed in terms of the *truncated* Green's function) that is only partially cancelled by the wavefunction renormalization $\sqrt{Z}$.

with $i\Pi$ being the diagrammatic contribution. The fields ϕ' are then normalized to single particle states and the physical amplitudes resulting from the calculation are finite.

As formal input for an expression for F_π to $\mathcal{O}(p^6)$, apart from the axial-vector pseudoscalar two-point function, we need again the pseudoscalar two-point function $\Sigma(p^2)$, all to the same order.[21]

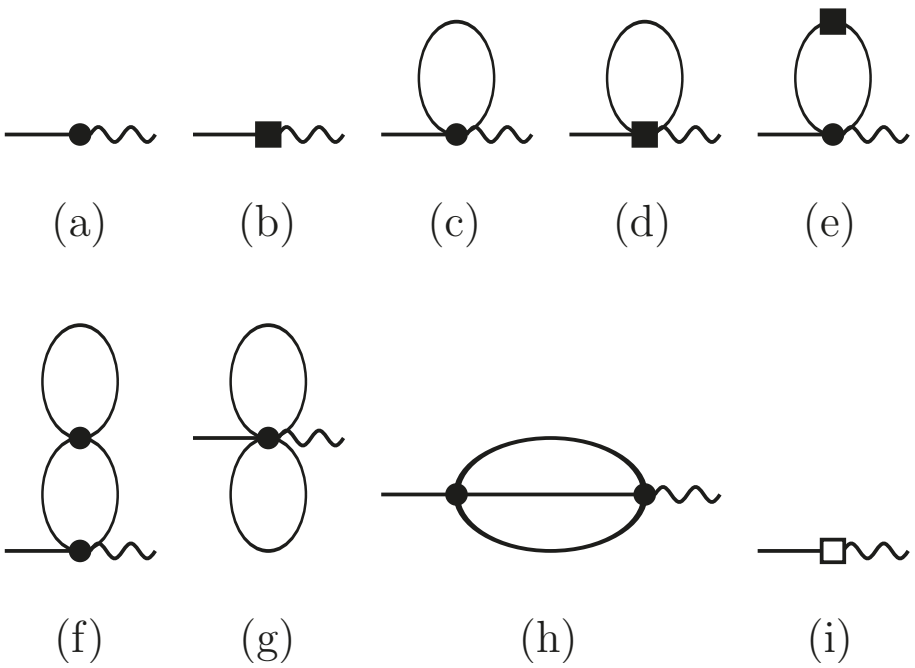

Figure 4: Diagrammatic contributions to the pseudoscalar decay constants, up to $\mathcal{O}(p^6)$. Circular vertices are of $\mathcal{O}(p^2)$, the filled boxes are of $\mathcal{O}(p^4)$, the open box is of $\mathcal{O}(p^6)$. The wiggly lines denote the external source field that is coupled to the desired current. Note the necessity for the wavefunction renormalization of the external pseudoscalar to obtain the physical decay constants, as discussed in the text.

8 Finite Volume Effects

It is inevitably the nature of any lattice calculation that it is performed in a finite volume. In order to perform a proper matching between a Lattice QCD calculation and ChPT, a good control over the additional quantum corrections to physical quantities which emerge due to the finiteness of the volume is required. Only then, ChPT can serve as a reliable

[21] Formally, $\Sigma(p^2)$ up to $\mathcal{O}(p^6)$ will yield $\frac{d\Sigma}{dp^2}$ up to $\mathcal{O}(p^4)$, to be multiplied by the lowest order expression for the axial-vector pseudoscalar two-point function that starts at $\mathcal{O}(p^2)$. (The order counting here is done in terms of masses and momenta in the numerators, not in terms of the suppression via pion decay constants.)

validity check for the lattice calculation, or LECs can be properly extracted from the lattice result.

ChPT in a finite volume [13, 14, 15] was introduced already shortly after the introduction of the theory itself. Conceptually, a finite volume is introduced that restricts the size of the Euclidean 3-dimensional space. The "time" dimension is assumed to be much larger. This treatment self-evidently breaks Lorentz invariance. A Passarino-Veltman type integral reduction can still be performed, provided that additional projections obeying the remaining symmetry are allowed and explicitly taken into account.

The introduction of a finite volume with periodic boundary conditions naturally restricts and discretizes the set of allowed momenta to propagate, thus promoting momentum integrals to sums. Our calculations are done in the "p–regime" defined by $M_\pi L \gg 1$, i. e. where the system is distorted mildly and the only change with respect to the continuous case is the modification of the propagators of the meson fields due to the periodic boundary conditions.

$$\int \frac{dp}{2\pi} F(p) \to \frac{1}{L} \sum_{n \in \mathbf{Z}} F(p_n) \equiv \int_V \frac{dp}{2\pi} F(p), \tag{48}$$

With the help of a Poisson summation formula, these can be moved back to a sum of integrals

$$\frac{1}{L} \sum_{n \in \mathbf{Z}} F(p_n) = \sum_{l_p} \int \frac{dp}{2\pi} e^{i l_p p} F(p), \tag{49}$$

where the summation over l_p runs over the set of vectors of length nL and separation of the $l_p = 0$ term allows to elegantly perform a well-defined decomposition of an arbitrary integral into an infinite volume (IV) and a finite volume (FV) part

$$I = I^\infty + I^V. \tag{50}$$

The tensor reduction and the notation used for our integrals will be shown for the case of a Euclidean space-time. They can be similarly obtained for a Minkowski space-time by simple replacements and small adaptations. Regarding the transition and translation of expressions between Euclidean and Minkowski space-time, the reader may consult section C.

Regarding the Passarino-Veltman reduction, the four-vector

$$t_\mu \equiv (1, 0, 0, 0) \tag{51}$$

is additionally allowed as projector in the FV case and sufficient to provide a reduction to scalar components in the center-of-mass (cms) frame.[22] We furthermore introduce the purely spatial part of the metric as

$$t_{\mu\nu} \equiv \delta_{\mu\nu} - t_\mu t_\nu = \mathrm{diag}(0, 1, 1, 1) \tag{52}$$

[22] In this frame, $p \cdot l_p = 0$.

as a convenient abbreviation.[23]

The remainder of this section has the aim to properly set up a notation for the integrals. Since the structure of the FV integrals contains the (simpler) structure of the IV integrals, we only show notation and reductions of the former. We use the integral notation introduced in [11], i. e. we write the basic one-loop one-propagator integrals as

$$\lfloor X \rfloor = \int_V \frac{d^d r}{(2\pi)^d} \, \frac{X}{(r^2+m^2)^n} \,, \tag{53}$$

the one-loop two-propagator integrals as

$$\langle X \rangle = \int_V \frac{d^d r}{(2\pi)^d} \, \frac{X}{(r^2+m_1^2)^{n_1}((r-p)^2+m_2^2)^{n_2}} \,, \tag{54}$$

and finally for the sunsets

$$\langle\langle X \rangle\rangle \equiv \int_V \frac{d^d r}{(2\pi)^d} \frac{d^d s}{(2\pi)^d} \, \frac{X}{(r^2+m_1^2)^{n_1}(s^2+m_2^2)^{n_2}((r+s-p)^2+m_3^2)^{n_3}} \,. \tag{55}$$

The reduction of the one-loop one-propagator integrals reads

$$\begin{aligned}
\lfloor 1 \rfloor^V &= A^V, \\
\lfloor r_\mu \rfloor^V &= 0, \\
\lfloor r_\mu r_\nu \rfloor^V &= \delta_{\mu\nu} A_{22}^V + t_{\mu\nu} A_{23}^V, \\
\lfloor r_\mu r_\nu r_\alpha \rfloor^V &= 0.
\end{aligned} \tag{56}$$

The general two-propagator case allows for momentum flow, the full reduction can only be performed in the cms frame as[24]

$$\begin{aligned}
\langle 1 \rangle^V \big|_{\text{cms}} &= B^V, \\
\langle r_\mu \rangle^V \big|_{\text{cms}} &= p_\mu B_1^V, \\
\langle r_\mu r_\nu \rangle^V \big|_{\text{cms}} &= p_\mu p_\nu B_{21}^V + \delta_{\mu\nu} B_{22}^V + B_{23}^V t_{\mu\nu}, \\
\langle r_\mu r_\nu r_\alpha \rangle^V \big|_{\text{cms}} &= p_\mu p_\nu p_\alpha B_{31}^V + (\delta_{\mu\nu} p_\alpha + \delta_{\mu\alpha} p_\nu + \delta_{\nu\alpha} p_\mu) \, B_{32}^V \\
&\quad + (t_{\mu\nu} p_\alpha + t_{\mu\alpha} p_\nu + t_{\nu\alpha} p_\mu) \, B_{33}^V,
\end{aligned} \tag{57}$$

[23]Note that the FV effect has to be distinguished from other lattice effects, in particular also from the introduction of a lattice spacing, although both of these effects have in common that they generally break the three-dimensional Euclidean rotational symmetry down to a discrete cubic symmetry group. Note also that this does *not* imply that the quantities that are evaluated cannot still be invariant under larger symmetries. This is particularly obvious for our evaluation of quantities involving a single particle in its cms frame with periodic boundary conditions: The quantities do not feel the cubic shape of the volume at all, i. e. the volume is solely *parametrized* by a cubic length L via $V = L^3$.

[24]The integral B_0 that appears in the masses and decay constants can either be considered the general integral B with zero momentum flow or alternatively as the one-propagator integral A with the propagator squared, cf. equation (53) with $n = 2$. The same reduction as for A with $n = 1$ applies, obviously without necessity to specify to the cms frame.

The same holds for the sunset integrals. Here, the case with non-vanishing momentum flow is necessary for our calculation (cf. figure 3 h). Since in an arbitrary frame only a partial reduction

$$\begin{aligned}
\langle\langle 1\rangle\rangle^V &\equiv H^V, \\
\langle\langle r_\mu\rangle\rangle^V &\equiv H_1^V\, p_\mu + H_{3\mu}^V, \\
\langle\langle s_\mu\rangle\rangle^V &\equiv H_2^V\, p_\mu + H_{4\mu}^V, \\
\langle\langle r_\mu r_\nu\rangle\rangle^V &\equiv H_{21}^V\, p_\mu p_\nu + H_{22}^V\, \delta_{\mu\nu} + H_{27\mu\nu}^V, \\
\langle\langle r_\mu s_\nu\rangle\rangle^V &\equiv H_{23}^V\, p_\mu p_\nu + H_{24}^V\, \delta_{\mu\nu} + H_{28\mu\nu}^V, \\
\langle\langle s_\mu s_\nu\rangle\rangle^V &\equiv H_{25}^V\, p_\mu p_\nu + H_{26}^V\, \delta_{\mu\nu} + H_{29\mu\nu}^V,
\end{aligned} \tag{58}$$

is possible, we specify to the cms frame where we can write

$$\begin{aligned}
\langle\langle 1\rangle\rangle^V &\equiv H^V, \\
\langle\langle r_\mu\rangle\rangle^V &\equiv H_1^V\, p_\mu, \\
\langle\langle s_\mu\rangle\rangle^V &\equiv H_2^V\, p_\mu, \\
\langle\langle r_\mu r_\nu\rangle\rangle^V &\equiv H_{21}^V\, p_\mu p_\nu + H_{22}^V\, \delta_{\mu\nu} + H_{27}^V\, t_{\mu\nu}, \\
\langle\langle r_\mu s_\nu\rangle\rangle^V &\equiv H_{23}^V\, p_\mu p_\nu + H_{24}^V\, \delta_{\mu\nu} + H_{28}^V\, t_{\mu\nu}, \\
\langle\langle s_\mu s_\nu\rangle\rangle^V &\equiv H_{25}^V\, p_\mu p_\nu + H_{26}^V\, \delta_{\mu\nu} + H_{29}^V\, t_{\mu\nu}.
\end{aligned} \tag{59}$$

Relations between these integrals follow immediately from the reduction procedure by taking Lorentz contractions. In our calculations, we use

$$p^2 H_{21} + d H_{22} + 3 H_{27} + m_1^2 H = A(m_2^2) A(m_3^2) \tag{60}$$

to eliminate H_{22} and

$$d A_{22}(m^2) + 3 A_{23}(m^2) + m^2 A(m^2) = 0\,. \tag{61}$$

to eliminate A_{22} as traditionally done in the IV computations.[25]

An important comment has to be made about the finite volume sunset integrals. Whereas the one-loop finite volume integrals are purely finite, the corrections to the H^V come with a single pole in ϵ. Note that these poles are obviously necessary to properly cancel the divergences in the final result.[26] We calculated the coefficients with the help of the partial result in [11] and found

[25] A similar relation between the B_0 type integrals was not needed since the integrals did not occur in the calculation.

[26] In the one-loop reducible part of the two-loop terms, products of IV one-loop integrals with FV one-loop integrals will emerge, i. e. FV integrals multiplied by a pole.

$$
\begin{aligned}
\tilde{H}^V &= \frac{\lambda_0}{16\pi^2}\left(A^V(m_1^2)+A^V(m_2^2)+A^V(m_3^2)\right)+\frac{1}{16\pi^2}\left(A^{V\epsilon}(m_1^2)+A^{V\epsilon}(m_2^2)+A^{V\epsilon}(m_3^2)\right)\\
&\quad +H^V\,,\\
\tilde{H}_1^V &= \frac{\lambda_0}{16\pi^2}\frac{1}{2}\left(A^V(m_2^2)+A^V(m_3^2)\right)+\frac{1}{16\pi^2}\frac{1}{2}\left(A^{V\epsilon}(m_2^2)+A^{V\epsilon}(m_3^2)\right)+H_1^V\,,\\
\tilde{H}_{21}^V &= \frac{\lambda_0}{16\pi^2}\frac{1}{3}\left(A^V(m_2^2)+A^V(m_3^2)\right)+\frac{1}{16\pi^2}\frac{1}{3}\left(A^{V\epsilon}(m_2^2)+A^{V\epsilon}(m_3^2)\right)+H_{21}^V\,,\\
\tilde{H}_{27}^V &= \frac{\lambda_0}{16\pi^2}\left(A_{23}^V(m_1^2)+\frac{1}{3}A_{23}(m_2^2))+\frac{1}{3}A_{23}^V(m_3^2)\right)\\
&\quad +\frac{1}{16\pi^2}\left(A_{23}^{V\epsilon}(m_1^2)+\frac{1}{3}A_{23}^{V\epsilon}(m_2^2+\frac{1}{3}A_{23}^{V\epsilon}(m_3^2))\right)+H_{27}^V\,.
\end{aligned}
\tag{62}
$$

For the finite part of the sunsets, we also separated the corresponding one-loop FV terms $A^{V\epsilon}$ as it was implicitly done in [11]. All terms containing $A^{V\epsilon}$ then cancelled as expected in the expressions for the masses and decay costants calculated in this thesis.

Regarding our numerical evaluation of the FV correction to a physical quantity, it should be noted that we use physical IV masses as input for our numerical evaluation. Additional terms will emerge in the p^6 expression due to that choice. The generalization of equation (39) therefore is

$$
\begin{aligned}
&\Big\{ -\Sigma_4(M_0^2\to M_{phys,IV}^2;p^2\to M_{phys,IV}^2) && \Big\}\mathcal{O}(p^4)\\
&-\Sigma_4(M_0^2;p^2=M_4^2=M_0^2+\Delta m_{4,full}^2) && \Big\}\\
&+\Sigma_4(M_0^2\to M_{phys,IV}^2=M_0^2+\Delta m_{4,IV}^2;p^2\to M_{phys,IV}^2=M_0^2+\Delta m_{4,IV}^2) && \Big\}\mathcal{O}(p^6)\\
&-\Sigma_6(M_0^2;p^2=M_0^2)\Big\}\Big|_{M_0^2\to M_{phys,IV}^2} && \Big\}\mathcal{O}(p^6)
\end{aligned}
\tag{63}
$$

9 Partial Quenching

Calculations in Lattice QCD are often performed in the partially quenched approximation. As opposed to the (fully) quenched case where the effect of sea quark loops is neglected completely, the partially quenched result is obtained by including them with a set of masses different from the ones used in the valence sector. These sea quark masses are usually chosen larger, decreasing the computational cost of the calculation, and allowing for an independent variation of valence quark masses without necessitating expensive reevaluations of fermion determinants. The underlying theory is referred to as Partially Quenched QCD (PQQCD). The partial quenching can also be introduced into ChPT. [16] It has been argued in the literature [17, 18, 19] that the resulting theory, Partially Quenched ChPT (PQChPT), is indeed the effective theory for PQQCD. The Lagrangian density is structurally very similar to the Lagrangian of Chiral Perturbation Theory for genenic N_F flavours.[27] Since the dynamical fields are no longer parametrized by $N \times N$ matrices, but are collected into ones of higher dimension, there is no operator reduction resulting from Cayley-Hamilton relations. In fact, the only formal modification of the Lagrangian that is needed is a generalization of the ordinary traces to so-called supertraces over the extended Goldstone manifold. A definition will be given further below. An important advantage to the use of partially quenched field theories is, as opposed to fully quenched calculations where the sea contribution is neglected completely, that it is connected to the physical "unquenched" underlying theory by a *continuous* transformation, i. e. a continuous deformation of parameters. This does not only further extrapolations in the different masses due to the explicit dependence, but allows even for a *direct* extraction of physical results from unphysical simulations. By matching a PQQCD calculation from the lattice to a PQChPT perturbative expansion, the LECs of ChPT can be determined, without accounting for the partial quenching explicitly.[28]

9.1 The Supersymmetric Formulation

In the supersymmetric formulation [16], loops of bosonic ghost quarks cancel exactly the valence loop contribution. The masses of the ghosts are fixed to the set of masses in the valence sector. The resulting quenched result is then supplemented with virtual quantum corrections originating from an additional set of sea quarks whose masses are different.

[27] This can be shown in different ways, e. g. the formal equivalence of the resulting equations of motion or alternatively the replica method [20].

[28] Although it has been argued that the LECs of ChPT and its partially quenched version coincide, one has to account for changes in the operator basis when one wishes to express the results in the classical two- or three-flavour Gasser-Leutwyler notation. For the three-flavour case, this is discussed in section 2.1 of paper III. Note also the curious fact that L_0 - being inaccessible both for unquenched simulations and experiments - can only be extracted from partially quenched simulations.

The procedure is being accomplished by parametrizing the Goldstone fields as

$$\Phi = \begin{pmatrix} \left[\ q_V\bar{q}_V\ \right] & \left[\ q_V\bar{q}_S\ \right] & \left[\ q_V\bar{q}_B\ \right] \\ \left[\ q_S\bar{q}_V\ \right] & \left[\ q_S\bar{q}_S\ \right] & \left[\ q_S\bar{q}_B\ \right] \\ \left[\ q_B\bar{q}_V\ \right] & \left[\ q_B\bar{q}_S\ \right] & \left[\ q_B\bar{q}_B\ \right] \end{pmatrix} . \tag{64}$$

where the index V stands for valence, S stands for sea and B stands for boson.[29] The Lagrangian structure

$$\begin{aligned} \mathcal{L}_4 &= \sum_{i=0}^{12} \hat{L}_i X_i + \text{contact terms} \\ &= \hat{L}_0 \langle u^\mu u^\nu u_\mu u_\nu \rangle + \hat{L}_1 \langle u^\mu u_\mu \rangle^2 + \hat{L}_2 \langle u^\mu u^\nu \rangle \langle u_\mu u_\nu \rangle \\ &+ \hat{L}_3 \langle (u^\mu u_\mu)^2 \rangle + \hat{L}_4 \langle u^\mu u_\mu \rangle \langle \chi_+ \rangle + \hat{L}_5 \langle u^\mu u_\mu \chi_+ \rangle \\ &+ \hat{L}_6 \langle \chi_+ \rangle^2 + \hat{L}_7 \langle \chi_- \rangle^2 + \frac{\hat{L}_8}{2} \langle \chi_+^2 + \chi_-^2 \rangle \\ &- i\hat{L}_9 \langle f_+^{\mu\nu} u_\mu u_\nu \rangle + \frac{\hat{L}_{10}}{4} \langle f_+^2 - f_-^2 \rangle \\ &+ i\hat{L}_{11} \left\langle \hat{\chi}_- \left(\nabla^\mu u_\mu - \frac{i}{2} \hat{\chi}_- \right) \right\rangle \\ &+ \hat{L}_{12} \left\langle \left(\nabla^\mu u_\mu - \frac{i}{2} \hat{\chi}_- \right)^2 \right\rangle \\ &+ \hat{H}_1 \langle F_L^2 + F_R^2 \rangle + \hat{H}_2 \langle \chi \chi^\dagger \rangle, \end{aligned} \tag{65}$$

is similar to the case of standard ChPT, but due to the additional complexity of the field, no Cayley-Hamilton relations are applied. Here, $\langle\ \rangle$ denote supertraces, defined in terms of ordinary ones by

$$\mathrm{Str} \begin{pmatrix} A & B \\ C & D \end{pmatrix} = \mathrm{Tr}\, A - \mathrm{Tr}\, D \tag{66}$$

where B and C denote the fermionic blocks in the matrix. The supersinglet Φ_0, generalizing the η', is integrated out to account for the axial anomaly as in standard ChPT. That implies the additional condition

$$\langle \Phi \rangle = \mathrm{Str}\,(\Phi) = 0\,. \tag{67}$$

[29] We use the terms boson/fermion as referring to the statistics obeyed by the fields. The ghost quarks are spin 1/2 particles, but with bosonic statistics. Note that meson fields consisting of a boson and a fermion obey fermionic statistics.

This has important implications, in particular on the neutral propagator. The derivation and a detailed discussion of this can be found in [17, 18]. The resulting structure of the neutral propagator, a proper setup of all notation and both technical and non-technical details regarding the calculation, the reader can find in paper III.

9.2 The Quarkflow Method

An alternative approach does not make use of ghost quarks, but "follows the quark lines" explicitly. The matrix Φ is written in terms of generic fields ϕ_{ij} throughout the calculation.[30] The construction of the Feynman diagrams is performed using these purely symbolic indices.

Only afterwards, fields which connect to the external states are replaced by their proper valence quarks fields. The remaining symbolic indices are now sea quark indices. They are, in a last step, replaced by an explicit sum over all flavours of the desired sea quark sector.

The results in paper III have been derived using both the quarkflow method [21] and the supersymmetric formulation [16]. This serves, together with other consistency checks, as an important cross-check for the correctness and reliability of the lengthy analytical expressions.

10 QCD-like Theories

For field theories which are similar to QCD, but with quark fields transforming according to different representations of the gauge group, the effective field theory framework can be extended beyond Chiral Perturbation Theory. We refer to the underlying field theories as "QCD-like", and classify them according to their breaking pattern of the global chiral symmetry [22, 23]. Independently of the specific gauge group employed, but depending on whether the quark fields transform as a complex, real or pseudo-real representation, a different effective field theory framework is necessary.[31]

Methods from Chiral Perturbation Theory can be used to calculate masses, decay constants and vacuum expectation values also for QCD-like EFTs. Obvious computational differences come from the various different unbroken subgroups and from the different associated parametrizations of the Goldstone manifolds. The general assumption of symmetry breaking via a scalar quark condensate is kept.

The three different cases are discussed in more detail below. We have calculated masses, decay constants and vacuum expectation values (VEVs). Our two-loop results include again

[30] This implies, obviously, the Lagrangian.

[31] Whereas the first case is a given a by generalization of the ChPT result to N_f quark flavours, the real and pseudo-real case start from an extended global symmetry and are in the remainder also referred to as the "adjoint" respective "two color" case since the fundamental representation of SU(2) is pseudo-real and the adjoint representation of a matrix Lie group is real.

simultaneous partial quenching and finite volume effects and thus provide higher precision on both of these frontiers.[32]

10.1 Complex Representation: QCD/ChPT for general N_F

This section generalizes the discussion of section 3 of standard ChPT to N_F flavours. The repetition of essential features also serves to set up a consistent notation for later use and will furthermore allow the reader to easily compare the structure to the other two cases.[33] The relevant part of the global chiral symmetry for QCD/ChPT with N_F flavours reads $SU(N_F)_L \times SU(N_F)_R$. Its spontaneous breakdown generates a VEV

$$\langle \overline{q}_{Lj} q_{Ri} \rangle = \frac{1}{2} \langle \overline{q} q \rangle \delta_{ij} \tag{68}$$

that transforms under the broken part, but is left invariant under the vector subgroup $SU(N_F)_V$.

The QCD Lagrangian with helicity-reduced spinors and with external fields included is given by

$$\begin{aligned} \mathcal{L} &= \overline{q}_{Li} i\gamma^\mu D_\mu q_{Li} + \overline{q}_{Ri} i\gamma^\mu D_\mu q_{Ri} + \overline{q}_{Li} \gamma^\mu l_{\mu ij} q_{Lj} + \overline{q}_{Ri} \gamma^\mu r_{\mu ij} q_{Rj} \\ &\quad - \overline{q}_{Ri} \mathcal{M}_{ij} q_{Lj} - \overline{q}_{Li} \mathcal{M}^\dagger_{ij} q_{Rj} \,. \end{aligned} \tag{69}$$

where i is a flavour index, q_L and q_R are column vectors and the external fields l_μ, r_μ and $\mathcal{M} = s - ip$ matrices (in flavour), and $D_\mu q = \partial_\mu q - iG_\mu q$ is the covariant derivative associated with the gauge group. The different quantities transform under the chiral group as

$$\begin{aligned} q_L &\to g_L q_L, \qquad q_R \to g_R q_R, \qquad \mathcal{M} \to g_R \mathcal{M} g_L^\dagger \,, \\ l_\mu &\to g_L l_\mu g_L^\dagger + i g_L \partial_\mu g_L^\dagger, \qquad r_\mu \to g_R r_\mu g_L^\dagger + i g_R \partial_\mu g_R^\dagger \,. \end{aligned} \tag{70}$$

Defining, mainly for later use, a $2N_F$-dimensional column vector

$$\hat{q} = \begin{pmatrix} q_R \\ q_L \end{pmatrix} \tag{71}$$

and introducing the large $2N_F \times 2N_F$ matrices

$$\hat{V}_\mu = \begin{pmatrix} r_\mu & 0 \\ 0 & l_\mu \end{pmatrix}, \qquad \hat{\mathcal{M}} = \begin{pmatrix} 0 & \mathcal{M} \\ \mathcal{M}^\dagger & 0 \end{pmatrix}, \qquad \hat{g} = \begin{pmatrix} g_R & 0 \\ 0 & g_L \end{pmatrix}, \tag{72}$$

the symmetry transformation (70) becomes

$$\hat{q} \to \hat{g}\hat{q} \,, \qquad \hat{V}_\mu \to \hat{g}\hat{V}_\mu \hat{g}^\dagger + i\hat{g}\partial_\mu \hat{g}^\dagger \,, \qquad \hat{\mathcal{M}} \to \hat{g}\hat{\mathcal{M}}\hat{g}^\dagger \,. \tag{73}$$

As indicated above, the VEV $\langle \overline{q} q \rangle = \langle \overline{q}_R q_L \rangle$ + h.c. then leaves an invariance under $SU(N_F)_V$.

[32] For the model calculations, we restrict the partial quenching to the easiest case with two mass scales only, i. e. $d_{\text{val}} = d_{\text{sea}} = 1$, although the extension is again straightforward (yielding more lengthy formulae). The quarkflow method is employed for all computations.

[33] We use a notation with helicity-reduced Dirac spinors. Despite the labels L and R, a confusion with Weyl spinors should be avoided. We rewrite the theories in terms on $2N_F$-dimensional vectors of (helicity-reduced) spinors, following the arguments in [24].

10.2 Real Representation: Adjoint

We define the charge conjugate of a spinor Ψ by

$$\Psi_C = C\bar{\Psi}^T = C\gamma^{0T}\Psi^* = i\gamma^2\Psi^* \tag{74}$$

where

$$C = i\gamma^2\gamma^0 \tag{75}$$

denotes the charge conjugation matrix. A theory with quarks in the adjoint representation has the Lagrangian density

$$\begin{aligned}\mathcal{L} &= \mathrm{tr}_c\left(\overline{q}_{Li}i\gamma^\mu D_\mu q_{Li}\right) + \mathrm{tr}_c\left(\overline{q}_{Ri}i\gamma^\mu D_\mu q_{Ri}\right) + \mathrm{tr}_c\left(\overline{q}_{Li}\gamma^\mu l_{\mu ij}q_{Lj}\right) + \mathrm{tr}_c\left(\overline{q}_{Ri}\gamma^\mu r_{\mu ij}q_{Rj}\right) \\ &\quad -\mathrm{tr}_c\left(\overline{q}_{Ri}\mathcal{M}_{ij}q_{Lj}\right) - \mathrm{tr}_c\left(\overline{q}_{Li}\mathcal{M}^\dagger_{ij}q_{Rj}\right)\,,\end{aligned} \tag{76}$$

The trace is to be performed over the gauge group indices (color). The covariant derivative is $D_\mu q = \partial_\mu q - iG_\mu q + iqG_\mu$, note that this implies also $D_\mu\overline{q} = \partial_\mu - iG_\mu\overline{q} + i\overline{q}G_\mu$ with $\overline{q} = q^\dagger\gamma^0$.[34] Using C from equation (75) above, we define

$$\tilde{q}_{Ri} \equiv C\overline{q}^T_{Li} \tag{77}$$

which transform under the gauge group like the $\tilde{q}_R$ (and are furthermore right-handed under the Lorentz group).[35] This property enlarges the global symmetry group to $SU(2N)$.[36] Explicitly, with the construction

$$\hat{q} = \begin{pmatrix} q_R \\ \tilde{q}_R \end{pmatrix}, \hat{V}_\mu = \begin{pmatrix} r_\mu & 0 \\ 0 & -l^T_\mu \end{pmatrix} \qquad \hat{\mathcal{M}} = \begin{pmatrix} 0 & \mathcal{M} \\ \mathcal{M}^T & 0 \end{pmatrix}, \tag{78}$$

the Lagrangian (76) reads

$$\mathcal{L} = \mathrm{tr}_c\left(\overline{\hat{q}}i\gamma^\mu D_\mu\hat{q}\right) + \mathrm{tr}_c\left(\overline{\hat{q}}\gamma^\mu\hat{V}_\mu\hat{q}_j\right) - \frac{1}{2}\mathrm{tr}_c\left(\overline{\hat{q}}C\hat{\mathcal{M}}\overline{\hat{q}}^T\right) - \frac{1}{2}\mathrm{tr}_c\left(\hat{q}^TC\hat{\mathcal{M}}^\dagger\hat{q}\right)\,, \tag{79}$$

allowing for transformations out of $SU(2N)$ according to

$$\hat{q} \to \hat{g}\hat{q}\,, \quad \hat{V}_\mu \to \hat{g}\hat{V}_\mu\hat{g}^\dagger + i\hat{g}\partial_\mu\hat{g}^\dagger\,, \quad \hat{\mathcal{M}} \to \hat{g}\hat{\mathcal{M}}\hat{g}^T\,. \tag{80}$$

[34] The Hermitian conjugate of the quark field transposes both Dirac and gauge indices.

[35] Here, in contrast to above, the transpose acts on Dirac (and later also flavour) indices, but not on the color.

[36] This statement specifically means that the $SU(N) \times SU(N)$ of QCD gets enlarged to a $SU(2N)$. Note that an enlarged symmetry group of odd dimension is also possible since a total odd number of helicity-reduced fermions can be achieved via including fields of the Majorana type. This is not possible for the symplectic case though, to be discussed in section 10.3. To improve readability of the introduction without restricting the applicability of the results, we choose $SU(2N)$ to denote the global symmetry group in the introduction whereas we use $SU(N)$ in paper IV, i.e. in the latter the breaking pattern will be $SU(N) \to SO(N)$.

Since the VEV $\langle \mathrm{tr}_c\,(\bar{q}q)\rangle$ can be written as $\langle \mathrm{tr}_c\left(\hat{q}^T C J_S \hat{q}\right)\rangle + \mathrm{h.c.}$, with

$$J_S = \begin{pmatrix} 0 & \mathrm{I} \\ \mathrm{I} & 0 \end{pmatrix} \tag{81}$$

and I the $N_F \times N_F$ unit matrix, we note its invariance under transformations obeying

$$g^T J_S g = J_S \tag{82}$$

which we identify as the $SO(2N)$ subgroup whose generators V_i are defined by

$$V_i^T J_S + J_S V_i = 0\,.^{37} \tag{83}$$

10.3 Pseudo-Real Representation: Two-Color QCD

The fundamental representation of $SU(2)$ is pseudo-real. The Lagrangian for a QCD-like theory with two colors reads

$$\begin{aligned} \mathcal{L} &= \overline{q}_{Li} i\gamma^\mu D_\mu q_{Li} + \overline{q}_{Ri} i\gamma^\mu D_\mu q_{Ri} + \overline{q}_{Li}\gamma^\mu l_{\mu ij} q_{Lj} + \overline{q}_{Ri}\gamma^\mu r_{\mu ij} q_{Rj} \\ &\quad -\overline{q}_{Ri}\mathcal{M}_{ij} q_{Lj} - \overline{q}_{Li}\mathcal{M}^\dagger_{ij} q_{Rj}\,. \end{aligned} \tag{84}$$

with $D_\mu q = \partial_\mu q - iG_\mu q$ as for QCD. The charge conjugate field

$$\tilde{q}_{R\alpha i} = \epsilon_{\alpha\beta} C \overline{q}^T_{L\beta i}\,, \tag{85}$$

now additionally needs application of the symplectic tensor $\epsilon_{12} = -\epsilon_{21} = 1$, $\epsilon_{11} = \epsilon_{22} = 0$ to obtain a right handed-handed fermion that indeed transforms as the fundamental representation of $SU(2)$. α, β denote gauge group indices. With

$$\hat{q} = \begin{pmatrix} q_R \\ \tilde{q}_R \end{pmatrix}, \hat{V}_\mu = \begin{pmatrix} r_\mu & 0 \\ 0 & -l_\mu^T \end{pmatrix} \qquad \hat{\mathcal{M}} = \begin{pmatrix} 0 & -\mathcal{M} \\ \mathcal{M}^T & 0 \end{pmatrix}, \tag{86}$$

the Lagrangian (84) becomes

$$\mathcal{L} = \overline{\hat{q}} i\gamma^\mu D_\mu \hat{q} + \overline{\hat{q}}\gamma^\mu \hat{V}_\mu \hat{q}_j - \frac{1}{2}\overline{\hat{q}}_\alpha C \epsilon_{\alpha\beta} \hat{\mathcal{M}} \overline{\hat{q}}^T_\beta - \frac{1}{2}\hat{q}_\alpha \epsilon_{\alpha\beta} C \hat{\mathcal{M}}^\dagger \hat{q}_\beta\,. \tag{87}$$

The symmetry is again extended to $SU(2N)$, with the fields transforming as

$$\hat{q} \to \hat{g}\hat{q}\,, \quad \hat{V}_\mu \to \hat{g}\hat{V}_\mu \hat{g}^\dagger + i\hat{g}\partial_\mu \hat{g}^\dagger\,, \quad \hat{\mathcal{M}} \to \hat{g}\hat{\mathcal{M}}\hat{g}^T\,. \tag{88}$$

[37] A common choice for the generators of a $SO(N)$ group are the purely imaginary $V_i = -V_i^T$. The resulting representation of the $SO(N)$ group are then really $SO(N)$ matrices, i. e. they are real. The reader shall have in mind that the latter condition is not a necessary criterion that also the generators of SO(2N) given in equation (83) do not immediately fulfill. A similarity transformation will of course succeed in changing between canonical generator basis and the one given here.

Since the VEV $\langle \bar{q}q \rangle$ can be written as $\langle \hat{q}_\alpha^T \epsilon_{\alpha\beta} C J_A \hat{q}_\beta \rangle + \text{h.c.}$, with

$$J_A = \begin{pmatrix} 0 & -\mathrm{I} \\ \mathrm{I} & 0 \end{pmatrix} \tag{89}$$

and I the $N_F \times N_F$ unit matrix, we note its invariance under transformations obeying

$$g^T J_A g = J_A \tag{90}$$

which we identify as the $Sp(2N)$ subgroup whose generators are defined by

$$V_i^T J_A + J_A V_i = 0\,. \tag{91}$$

10.4 Technical Remarks

As a matter of principle, all three calculations can be treated on equal footing.[38] In particular, we can choose a representation of the generators as $2N \times 2N$ matrices in all three cases. Here, we show both the generators for the invariant subgroup V_i and the broken generators X_a in block matrix notation.

$$V_i = \begin{pmatrix} A & B \\ B^\dagger & -A^T \end{pmatrix}, \qquad X_a = \begin{pmatrix} C & D \\ D^\dagger & C^T \end{pmatrix} \tag{92}$$

A, B, C, D are complex matrices of dimension $N \times N$. A is Hermitian, C is Hermitian and traceless in all three cases. For the SO case, B is antisymmetric and D is symmetric. For the Sp case, D is antisymmetric and B is symmetric. For the simpler SU case, B and D are simply zero.[39]

$$V_i = \begin{pmatrix} A & 0 \\ 0 & -A^T \end{pmatrix}, \qquad X_a = \begin{pmatrix} C & 0 \\ 0 & C^T \end{pmatrix} \tag{93}$$

As a side remark, equation (93) are the generators for the QCD case when treated on equal footing with the other two, i.e. using a field basis where the left-handed spinors have been traded for their charge conjugates, thus implying complex conjugation. In the standard basis (71) for QCD that uses left- and right-handed quark fields, the generators (93) instead become[40]

$$V_i = \begin{pmatrix} A & 0 \\ 0 & A \end{pmatrix}, \qquad X_a = \begin{pmatrix} C & 0 \\ 0 & -C \end{pmatrix}. \tag{94}$$

[38] It should be noted that the real and the pseudo-real cases extend both the full chiral symmetry group and the unbroken subgroup, compared to the QCD case, i. e. $SU(2N) \supset SU(N) \times SU(N)$, but also $SO(2N) \supset SU(N)$ and $Sp(2N) \supset SU(N)$. The latter two are in accordance with the Vafa-Witten theorem that states the conservation of vector symmetries under spontaneous breaking mechanisms [25, 26].

[39] To be precise, the resulting N^2 V_i and (N^2-1) X_a generate the full $SU(N)_L \times SU(N)_R \times U(1)_V$. The counting of generators obviously also works out in the other cases: In the Sp case, there are $N^2+N(N+1) = 2N^2 + N$ V_i and $(N^2-1) + N(N-1) = 2N^2 - N - 1$ X_a while there are $N^2 + N(N-1) = 2N^2 - N$ V_i and $(N^2-1) + N(N+1) = 2N^2 + N - 1$ X_a. In both cases, the sum equates to the desired $4N^2 - 1$

[40] Note also that the generator for $U(1)_V$, being traceless in equation (93), now corresponds to the trace. Loosely speaking, the matrices that generate $U(1)_V$ and $U(1)_A$ interchange.

element	G	C	P
U	$g_R U g_L^\dagger$	U^T	$U^\dagger$
$D_{\lambda_1}\cdots D_{\lambda_n}U$	$g_R D_{\lambda_1}\cdots D_{\lambda_n}U g_L^\dagger$	$(D_{\lambda_1}\cdots D_{\lambda_n}U)^T$	$(D^{\lambda_1}\cdots D^{\lambda_n}U)^\dagger$
χ	$g_R\chi g_L^\dagger$	χ^T	$\chi^\dagger$
$D_{\lambda_1}\cdots D_{\lambda_n}\chi$	$g_R D_{\lambda_1}\cdots D_{\lambda_n}\chi g_L^\dagger$	$(D_{\lambda_1}\cdots D_{\lambda_n}\chi)^T$	$(D^{\lambda_1}\cdots D^{\lambda_n}\chi)^\dagger$
r_μ	$g_R r_\mu g_R^\dagger + i g_R\partial_\mu g_R^\dagger$	$-l_\mu^T$	l^μ
l_μ	$g_L l_\mu g_L^\dagger + i g_L\partial_\mu g_L^\dagger$	$-r_\mu^T$	r^μ
$f_{\mu\nu}^R$	$g_R f_{\mu\nu}^R g_R^\dagger$	$-(f_{\mu\nu}^L)^T$	$f_L^{\mu\nu}$
$f_{\mu\nu}^L$	$g_L f_{\mu\nu}^L g_L^\dagger$	$-(f_{\mu\nu}^R)^T$	$f_R^{\mu\nu}$

Table 3: Transformation properties under the group (G), charge conjugation (C), and parity (P). The expressions for adjoint matrices are trivially obtained by taking the Hermitian conjugate of each entry. In the parity transformed expression it is understood that the argument is $(t, -\vec{x})$ and that partial derivatives ∂_μ act with respect to x and not with respect to the argument of the corresponding function. Table adapted from [8]

For the SU case, we have not employed this (unnecessary large, redundant) parametrization, but instead generalized the quarkflow calculation from section 9.2 to N_F flavours. Both the Sp and SO calculations have been done with the representation of the Lie algebra given in equation (92). The SO calculation has, as a cross-check for both the result and the method, furthermore been derived independently by a modification of the quarkflow calculation from section 9.2 that explicitly symmetrizes the fields in the flavour indices at all computational steps.

A Construction of the Chiral Lagrangian

The construction of the chiral NLO Lagrangian can be systematically achieved by a careful consideration of the transformation behaviour of the single elements under the symmetries of QCD and their successive combination into larger building blocks and finally invariants. Table 3 lists the transformation properties of the elements which lead to the general chiral Lagrangian (in the notation used throughout section 3).

The enumeration of the possible terms can also be done very elegantly in a slightly different notation. We introduce this new formalism first in order to then construct the chiral Lagrangian in the general flavour case, later specifying to $n_f = 2$ and $n_f = 3$. Starting from ChPT in the external field formulation with the canonical transformation behaviour

$$
\begin{aligned}
U &\to g_R\, U\, g_L^\dagger, \\
\chi \equiv 2\hat{B}\,(s+ip) &\to g_R\, \chi\, g_L^\dagger, \\
l_\mu \equiv v_\mu - a_\mu &\to g_L\, l_\mu\, g_L^\dagger - i\partial_\mu\, g_L\, g_L^\dagger, \\
r_\mu \equiv v_\mu + a_\mu &\to g_R\, r_\mu\, g_R^\dagger - i\partial_\mu\, g_R\, g_R^\dagger.
\end{aligned} \tag{95}
$$

we define

$$
u \equiv \exp\left(i\Phi/(\sqrt{2}F_0)\right)\,; \qquad U = u^2 \tag{96}
$$

to transform as

$$
u \to g_R u h^\dagger \equiv h u g_L^\dagger\,. \tag{97}
$$

This condition actually defines $h \in SU(n_F)_V$ and determines it uniquely.[41] We then construct the chiral Lagrangian by using objects X that transform under chiral symmetry as $X \to hXh^\dagger$. At the present order, these are u_μ, $f_\pm^{\mu\nu}$, $\chi_\pm$ and χ_-^μ defined by

$$
\begin{aligned}
u_\mu &= i\left[u^\dagger\left(\partial_\mu - ir_\mu\right)u - u\left(\partial_\mu - il_\mu\right)u^\dagger\right]\,, \qquad \chi = 2B\,(s+ip)\,, \\
\chi_\pm &= u^\dagger\chi u^\dagger \pm u\chi^\dagger u\,, \qquad\qquad \chi_-^\mu = u^\dagger D^\mu\chi u^\dagger - uD^\mu\chi^\dagger u\,, \\
f_\pm^{\mu\nu} &= uF_L^{\mu\nu}u^\dagger \pm u^\dagger F_R^{\mu\nu}u\,, \qquad\qquad D_\mu\chi = \partial_\mu\chi - ir_\mu\chi + i\chi l_\mu\,, \\
F_L^{\mu\nu} &= \partial^\mu l^\nu - \partial^\nu l^\mu - i\left[l^\mu, l^\nu\right]\,, \qquad F_R^{\mu\nu} = \partial^\mu r^\nu - \partial^\nu r^\mu - i\left[r^\mu, r^\nu\right]\,.
\end{aligned} \tag{98}
$$

The lowest order Lagrangian (5) is in this new notation simply given by

$$
\mathcal{L}_2 = \frac{F^2}{4}\left\langle u_\mu u^\mu + \chi_+\right\rangle \tag{99}
$$

The most general Lagrangian, after elimination of redundant terms via partial integration, for the general n_f flavour case reads

$$
\begin{aligned}
\mathcal{L}_4 \;=\; & \hat{L}_0\left\langle u^\mu u^\nu u_\mu u_\nu\right\rangle + \hat{L}_1\left\langle u^\mu u_\mu\right\rangle^2 + \hat{L}_2\left\langle u^\mu u^\nu\right\rangle\left\langle u_\mu u_\nu\right\rangle + \hat{L}_3\left\langle (u^\mu u_\mu)^2\right\rangle + \hat{L}_4\left\langle u^\mu u_\mu\right\rangle\left\langle\chi_+\right\rangle \\
& + \hat{L}_5\left\langle u^\mu u_\mu\chi_+\right\rangle + \hat{L}_6\left\langle\chi_+\right\rangle^2 + \hat{L}_7\left\langle\chi_-\right\rangle^2 + \frac{\hat{L}_8}{2}\left\langle\chi_+^2 + \chi_-^2\right\rangle - i\hat{L}_9\left\langle f_+^{\mu\nu}u_\mu u_\nu\right\rangle \\
& + \frac{\hat{L}_{10}}{4}\left\langle f_+^2 - f_-^2\right\rangle + i\hat{L}_{11}\left\langle\hat{\chi}_-\left(\nabla^\mu u_\mu - \frac{i}{2}\hat{\chi}_-\right)\right\rangle + \hat{L}_{12}\left\langle\left(\nabla^\mu u_\mu - \frac{i}{2}\hat{\chi}_-\right)^2\right\rangle \\
& + \hat{H}_1\left\langle F_L^2 + F_R^2\right\rangle + \hat{H}_2\left\langle\chi\chi^\dagger\right\rangle.
\end{aligned} \tag{100}
$$

Applying the lowest order equation of motion will eliminate $\hat{L}_{11}$ and $\hat{L}_{12}$, thus leaving 11 LECs besides the contact terms.

[41] Both of these statements are non-trivial, but can be shown using group theory. [27] Note that h depends on g_L, g_R and u in a non-linear manner.

Due to Cayley-Hamilton relations, we can achieve a further reduction by one in the SU(3) case or by four in the SU(2) case. In this way, for the SU(3) case, we eliminate $\hat{L}_0$ from equation (100) via

$$\langle u^\mu u^\nu u_\mu u_\nu \rangle = -2\langle u^\mu u_\mu u^\nu u_\nu \rangle + \frac{1}{2}\langle u_\mu u^\mu \rangle \langle u_\nu u^\nu \rangle + \langle u^\mu u^\nu \rangle \langle u_\mu u_\nu \rangle \,. \tag{101}$$

In the two-flavour case, we exploit different cases of the general relation

$$\{A, B\} = A\langle B\rangle + B\langle A\rangle + \langle AB\rangle - \langle A\rangle\langle B\rangle \tag{102}$$

valid for arbitrary 2×2 matrices. The Gasser-Leutwyler LECs in the SU(2) case are related to the general basis in equation (100) by

$$\begin{aligned}
l_1 &= -2\,\hat{L}_0 + 4\,\hat{L}_1 + 2\,\hat{L}_3\,, \\
l_2 &= 4\,\hat{L}_0 + 4\,\hat{L}_2\,, \\
l_3 &= -8\,\hat{L}_4 - 4\,\hat{L}_5 + 16\,\hat{L}_6 + 8\,\hat{L}_8\,, \\
l_4 &= 8\,\hat{L}_4 + 4\,\hat{L}_5\,, \\
l_5 &= \hat{L}_{10}\,, \\
l_6 &= -2\,\hat{L}_9\,, \\
l_7 &= -16\,\hat{L}_7 - 8\,\hat{L}_8\,.
\end{aligned} \tag{103}$$

To summarize, the SU(2) Lagrangian then reads in this notation[42] (cf. also equation (12) for other notation)

$$\begin{aligned}
\mathcal{L}_4^{n_f=2} &= \frac{l_1}{4}\left\langle u_\mu u^\mu \right\rangle \left\langle u_\nu u^\nu \right\rangle + \frac{l_2}{4}\left\langle u_\mu u_\nu \right\rangle \left\langle u^\mu u^\nu \right\rangle + \frac{l_3}{16}\left\langle \chi_+ \right\rangle^2 + \frac{il_4}{4}\left\langle u_\mu \chi_-^\mu \right\rangle \\
&\quad + \frac{l_5}{4}\left\langle f_+^2 - f_-^2 \right\rangle + \frac{il_6}{2}\left\langle f_{+\mu\nu} u^\mu u^\nu \right\rangle - \frac{l_7}{16}\left\langle \chi_- \right\rangle^2 \\
&\quad + \;\; 3 \text{ contact terms}
\end{aligned} \tag{104}$$

whereas the $n_f = 3$ Lagrangian is given by (cf. also equation (11) for other notation)

$$\begin{aligned}
\mathcal{L}_4^{n_f=3} &= L_1 \left\langle u_\mu u^\mu \right\rangle \left\langle u_\nu u^\nu \right\rangle + L_2 \left\langle u_\mu u_\nu \right\rangle \left\langle u^\mu u^\nu \right\rangle + L_3 \left\langle u_\mu u^\mu u_\nu u^\nu \right\rangle \\
&\quad + L_4 \left\langle u_\mu u^\mu \right\rangle \left\langle \chi_+ \right\rangle + L_5 \left\langle u_\mu u^\mu \chi_+ \right\rangle + L_6 \left\langle \chi_+ \right\rangle^2 + L_7 \left\langle \chi_- \right\rangle^2 \\
&\quad + \frac{L_8}{2}\left\langle \chi_+^2 + \chi_-^2 \right\rangle - iL_9 \left\langle f_{+\mu\nu} u^\mu u^\nu \right\rangle + \frac{L_{10}}{4}\left\langle f_+^2 - f_-^2 \right\rangle \\
&\quad + \;\; 2 \text{ contact terms}\,.
\end{aligned} \tag{105}$$

The classification and reduction of the general Lagrangian at $\mathcal{O}(p^6)$ can be performed according to similar principles, but it additionally complicated due to the large number of terms. This was done in [28] and refined in [29]. For a recent review regarding LECs and their numerical determination, see [30].

[42] The additional contact term $\det \chi$ is obviously of desired order in SU(2), but not in SU(3).

Table 4: Overview over relevant sets of LECs and used notation in the different cases of ChPT. The $i+j$ notation denotes the number of physically relevant (i) and contact (j) terms in the respective Lagrangians. At NLO, the latter ones are conventionally denoted h_i for $n_f = 2$ and H_i for $n_f = 3$. We also show the notation for partially quenched ChPT for completeness. The difficulty in obtaining a minimal set of operators can be seen from the fact that the number of independently physically relevant c_i in the two-flavour case was long thought to be 53 until it could be reduced to 52 due to an additional relation.

n_f	χPT 2	χPT 3	χPT n	PQχPT 2	PQχPT 3
LO	F, B	F_0, B_0	$\hat{F}_0, \hat{B}$	F, B	F_0, B_0
NLO $i+j$	l_i $7+3$	L_i $10+2$	$\hat{L}_i$ $11+2$	$L_i^{(2pq)}$ $11+2$	$L_i^{(3pq)}$ $11+2$
NNLO $i+j$	c_i $52+4$	C_i $90+4$	K_i $112+3$	$K_i^{(2pq)}$ $112+3$	$K_i^{(3pq)}$ $112+3$

B Numerical Evaluation Procedures for FV Integrals

Two different methods for the numerical evaluation of FV integrals have been suggested [13, 14, 15, 31]. The necessary cases emerging in our two-loop calculation including the sunsets have been worked out in [11]. Following section 8 and the Poisson summation theorem (49), it is readily apparent that the separation of IV and FV part of an integral leaves a sum of integrals as the structure to be calculated numerically. Depending on the preferred method, either the summation or the integration can be eliminated. The actual evaluation routines then have to solve only a summation over modified Bessel functions [13, 14, 15] or a numerical integration over Jacobi theta functions [31]. This is strictly true for the one-propagator cases, for two or more propagators additional numerical integrations over Feynman parameters might be necessary.

Strictly speaking, the Bessel function method does not only eliminate the integral, but reduces the three-dimensional sum over momenta to a one-dimensional sum. For two-propagator integrals then, the Bessel sum or the theta function integral are supplemented by an additional integration over a Feynman parameter. The sunset case is more complicated. As discussed in more detail in [11], the quantization of the sunset integral is decomposed according to

$$\langle\langle X\rangle\rangle^V \equiv \langle\langle X\rangle\rangle_r + \langle\langle X\rangle\rangle_s + \langle\langle X\rangle\rangle_t + \langle\langle X\rangle\rangle_{rs}, \tag{106}$$

into parts with one loop momentum quantized (one per propagator) $\langle\langle X\rangle\rangle_{r,s,t}$ and an addi-

tional part emerging from the quantization of both (independent) loop momenta $\langle\langle X\rangle\rangle_{rs}$. The $\langle\langle X\rangle\rangle_{r,s,t}$ come with a three-dimensional sum over momenta and three integrations. The Bessel method manages not only to reduce the three-dimensional sum to a one-dimensional one, but also eliminates one integration. The theta function method on the other hand eliminates the sum completely, but leaving all three integrations. The part $\langle\langle X\rangle\rangle_{rs}$ with both loop momenta quantized naturally comes with *two* three-dimensional sums in addition to the three integrations. Here, it should be noted that the Bessel method leaves three one-dimensional sums and two integrations whereas the theta function method can eliminate *both* summations completely, leaving only integrals over three parameters to be performed numerically.

It turns out that the Bessel function based method is to be preferred for large values of ML due to faster convergence whereas for small and medium ML rather the Jacobi method should be applied. For details, consider [11].

C Translation between Minkowski and Euclidean Space-Time

The required substitutions are

$$\begin{aligned}
\int \frac{d^q r}{(2\pi)^d} &\longleftrightarrow \frac{1}{i}\int \frac{d^q r}{(2\pi)^d}, \\
\delta_{\mu\nu} &\longleftrightarrow -g_{\mu\nu} \\
p\cdot q,\ p^2 &\longleftrightarrow -p\cdot q,\ \ -p^2 \\
t_{\mu\nu} &\longleftrightarrow -t_{\mu\nu} \\
\frac{1}{p^2+m^2} &\longleftrightarrow -\frac{1}{p^2-m^2},
\end{aligned} \tag{107}$$

with the Euclidean expressions on the left hand side and the corresponding Minkowski equivalent on the right. $t_{\mu\nu}$ corresponds to the spatial part of the metric $\delta_{\mu\nu}$ or $g_{\mu\nu}$ respectively, the latter is defined with signature $(+,-,-,-)$. Note that this implies that Passarino-Veltman type integral identities will look different in both space-time conventions, e. g. equation (61) in Minkowski space-time reads

$$dA_{22}(m^2) + 3A_{23}(m^2) - m^2 A(m^2) = 0\,. \tag{108}$$

References

[1] G. Colangelo and S. Durr, *Eur. Phys. J.* **C33** (2004) 543–553, arXiv:hep-lat/0311023 [hep-lat].

[2] G. Colangelo and C. Haefeli, *Phys. Lett.* **B590** (2004) 258–264, arXiv:hep-lat/0403025 [hep-lat].

[3] G. Colangelo, S. Durr, and C. Haefeli, *Nucl. Phys.* **B721** (2005) 136–174, arXiv:hep-lat/0503014 [hep-lat].

[4] G. Colangelo and C. Haefeli, *Nucl. Phys.* **B744** (2006) 14–33, arXiv:hep-lat/0602017 [hep-lat].

[5] S. Weinberg, *Physica* **A96** (1979) 327.

[6] J. Gasser and H. Leutwyler, *Annals Phys.* **158** (1984) 142.

[7] J. Gasser and H. Leutwyler, *Nucl.Phys.* **B250** (1985) 465.

[8] S. Scherer and M. R. Schindler, arXiv:hep-ph/0505265 [hep-ph].

[9] J. Bijnens, *Prog.Part.Nucl.Phys.* **58** (2007) 521–586, arXiv:hep-ph/0604043 [hep-ph].

[10] G. Amoros, J. Bijnens, and P. Talavera, *Nucl.Phys.* **B568** (2000) 319–363, arXiv:hep-ph/9907264 [hep-ph].

[11] J. Bijnens, E. Boström, and T. A. Lähde, *JHEP* **1401** (2014) 019, arXiv:1311.3531 [hep-lat].

[12] J. Vermaseren, arXiv:math-ph/0010025 [math-ph].

[13] J. Gasser and H. Leutwyler, *Phys.Lett.* **B184** (1987) 83.

[14] J. Gasser and H. Leutwyler, *Phys.Lett.* **B188** (1987) 477.

[15] J. Gasser and H. Leutwyler, *Nucl.Phys.* **B307** (1988) 763.

[16] C. W. Bernard and M. F. L. Golterman, *Phys. Rev.* **D49** (1994) 486–494, arXiv:hep-lat/9306005 [hep-lat].

[17] S. R. Sharpe and N. Shoresh, *Phys. Rev.* **D62** (2000) 094503, arXiv:hep-lat/0006017 [hep-lat].

[18] S. R. Sharpe and N. Shoresh, *Phys. Rev.* **D64** (2001) 114510, arXiv:hep-lat/0108003 [hep-lat].

[19] C. Bernard and M. Golterman, *Phys. Rev.* **D88** (2013) no. 1, 014004, arXiv:1304.1948 [hep-lat].

[20] P. H. Damgaard and K. Splittorff, *Phys. Rev.* **D62** (2000) 054509, arXiv:hep-lat/0003017 [hep-lat].

[21] S. R. Sharpe, *Phys. Rev.* **D46** (1992) 3146–3168, arXiv:hep-lat/9205020 [hep-lat].

[22] M. E. Peskin, *Nucl. Phys.* **B175** (1980) 197–233.

[23] J. B. Kogut, M. A. Stephanov, D. Toublan, J. J. M. Verbaarschot, and A. Zhitnitsky, *Nucl. Phys.* **B582** (2000) 477–513, arXiv:hep-ph/0001171 [hep-ph].

[24] J. Bijnens and J. Lu, *JHEP* **11** (2009) 116, arXiv:0910.5424 [hep-ph].

[25] C. Vafa and E. Witten, *Phys. Rev. Lett.* **53** (1984) 535.

[26] C. Vafa and E. Witten, *Nucl. Phys.* **B234** (1984) 173.

[27] S. R. Coleman, J. Wess, and B. Zumino, *Phys.Rev.* **177** (1969) 2239–2247.

[28] H. Fearing and S. Scherer, *Phys.Rev.* **D53** (1996) 315–348, arXiv:hep-ph/9408346 [hep-ph].

[29] J. Bijnens, G. Colangelo, and G. Ecker, *JHEP* **9902** (1999) 020, arXiv:hep-ph/9902437 [hep-ph].

[30] J. Bijnens and G. Ecker, arXiv:1405.6488 [hep-ph].

[31] D. Becirevic and G. Villadoro, *Phys.Rev.* **D69** (2004) 054010, arXiv:hep-lat/0311028 [hep-lat].

Paper I

Der Harfner

Wer nie sein Brot mit Thränen aß,
Wer nie die kummervollen Nächte
Auf seinem Bette weinend saß,
Der kennt euch nicht, ihr himmlischen Mächte.

Ihr schickt ins Leben uns hinein,
Ihr lasst den Armen schuldig werden,
Dann überlasst ihr ihn der Pein:
Denn alle Schuld rächt sich auf Erden.

Johan Wolfgang von Goethe

LU TP 12-24
June 2012

Closing the Window on Light Charged Higgs Bosons in the NMSSM

Johan Rathsman* and Thomas Rössler†

Department of Astronomy and Theoretical Physics,
Lund University, Sölvegatan 14A, SE-223 62 Lund, Sweden

Abstract

In the Next-to-Minimal SuperSymmetric Model (NMSSM) the lightest CP-odd Higgs bosons (a_1) can be very light. As a consequence, in addition to the standard charged Higgs boson ($h^\pm$) decays considered in the MSSM for a light charged Higgs ($m_{h^\pm} < m_t$), the branching fraction for $h^\pm \to a_1 W$ can be dominant. We investigate how this signal can be searched for in $t\bar{t}$ production at the Large Hadron Collider (LHC) in the case that ($m_{a_1} \gtrsim 2m_B$) with the a_1 giving rise to a single $b\bar{b}$–jet and discuss to what extent the LHC experiments are able to discover such a scenario with an integrated luminosity ~ 20 fb^{-1}. We also discuss the implications of the possible Higgs-signal observed at the LHC.

* Johan.Rathsman@thep.lu.se
† tr@thep.lu.se

I. INTRODUCTION

With the successful start-up of the LHC and the intriguing results from the first year of data-taking at the center of mass energy of 7 TeV and a integrated luminosity close to ≈ 5 fb^{-1} for each of the ATLAS and CMS experiments, the ongoing run in 2012 is set to be a milestone in particle physics. The possible signal for a Higgs boson around 125 GeV may or may not be confirmed and the search for physics Beyond the Standard Model (BSM) will continue. Contrary to the neutral Higgs boson, which if discovered may need to be analyzed in detail regarding its branching fraction into various channels in order to determine whether it is the Standard Model (SM) Higgs boson or not, the discovery of a charged Higgs boson would be an unmistakable sign of BSM physics.

The charged Higgs boson arises in theories with more than one Higgs doublet. The prime example is the MSSM [1, 2] which has two Higgs doublets, leading to two CP-even Higgs bosons (h, H) and one CP-odd (A) in the case of CP-conservation and two charged states $(H^{\pm})$ after electroweak symmetry breaking. In this case the two Higgs doublets are required by supersymmetry with one of the giving masses to the up-type fermions and one to the down-type ones. For a complete introduction to the Higgs sector in the MSSM we refer to [3].

The main reason for introducing supersymmetry (for a general introduction to supersymmetric theories we refer to [4]) is to solve the so called hierarchy problem, *i.e.* why the scale of the electroweak interaction is so much smaller than the cut-off of the SM, normally taken to be the Planck mass where gravity becomes the dominant force and the SM breaks down. With the Higgs boson being a scalar particle, the higher order corrections to its mass are proportional to this cut-off and with the SM only being an effective theory this cut-off dependence cannot be renormalized away. In a supersymmetric theory this problem is essentially solved by the introduction of the fermionic partners of the Higgs fields, which only get logarithmic corrections to their masses and thereby avoids fine-tuning. In turn this means that the Higgs boson masses are also protected from receiving quadratic corrections as long as supersymmetry is not broken or only softly broken.

In addition to solving the hierarchy problem supersymmetry also offers a candidate for cold dark matter [5, 6] in the case that R-symmetry is preserved, which in turn is introduced to avoid terms in the Lagrangian that otherwise would mediate proton decay. In this case the lightest supersymmetric particle (LSP) is stable and generically it has the right mass and cross-section to constitute the observed dark matter. Supersymmetry also improves the unification of gauge forces at an hypothesized grand unification scale although the unification is not exact and it does depend on the details of the spectrum of SUSY-particles.

As is well known, the MSSM by itself is not without problems. Leaving the question of the precise mechanism for supersymmetry breaking aside, the MSSM faces the so called μ-problem. This relates to the magnitude of the dimensionful μ-parameter which couples the two Higgs doublets to each other in the superpotential. In order to avoid large cancellations between this contribution to the Higgs masses and the soft supersymmetry breaking terms as well as having a phenomenologically viable supersymmetric theory (mainly having a large enough chargino mass), the magnitude of μ should be of order the electroweak or supersymmetry breaking scales. The problem is then that there is no a priori reason for this parameter to have any particular value, in principle it could be anything up to the Planck scale, so why is it similar to the electroweak or supersymmetry breaking scales?

In the NMSSM the μ-problem is solved by introducing an additional Higgs singlet into the theory. After supersymmetry breaking this field gets a vacuum expectation value (vev) that effectively acts as a μ-term. The original μ-term in the superpotential can then be set to zero without spoiling the viability of the theory. For a more detailed review of the NMSSM we refer

to [7, 8].

The additional Higgs singlet has important consequences for the phenomenology of the Higgs sector. In the MSSM, the masses of the heavy Higgs bosons $(H, A, H^\pm)$ are closely related to each other as they originate from the same (second) Higgs doublet if viewed in the Higgs basis where only one (the first) of the Higgs doublets has a vev. For example, at tree-level the masses of the CP-odd and charged Higgs bosons are related by $m^2_{H^\pm} = m^2_A + m^2_W$. As a consequence the decay $H^\pm \to AW$ is typically not open.

In the NMSSM the additional Higgs singlet means that there is one more CP-even and one more CP-odd field with a separate mass scale introduced into the Higgs sector. As a consequence, the by now three CP-even and two CP-odd electroweak states will mix into the respective mass eigenstates. Thus the mass-relations from the MSSM will be altered. This is particularly evident in the CP-odd sector where the lightest state a_1 may now be much lighter than the charged Higgs boson – even after taking experimental constraints into account as discussed below – opening up the possibility for the $h^\pm \to a_1 W$ decay to be dominant. In turn this means that the search for charged Higgs bosons, in t-quark decays for example, has to be widened also to include this decay channel.

The decay $h^\pm \to a_1 W$ has already been considered to different levels of detail [9–11] in the literature and there are constraints from the DELPHI experiment for $m_{a_1} > 12$ GeV [12], as well as the CDF experiment for the case $a_1 \to \tau^+\tau^-$ [13]. In this paper we want to focus on the region in parameter space where the a_1 mass is above the $b\bar{b}$ threshold but still so close to it that the two b-quarks will fragment into a single $b\bar{b}$–jet. The viability of scenarios with light a_1's have also been considered by [14–18].

Our paper is organized as follows. In the next section we give some basic properties of the Higgs sector in the NMSSM that are relevant to our discussion. We then discuss the constraints on the parameter space in section 3, including the latest results from LHC. In section 4 we illustrate how the signal $h^\pm \to a_1 W$ can be searched for in $t\bar{t}$-production taking into account the appropriate backgrounds. Section 5 contains a discussion of the implications of the possible Higgs signal from the ATLAS and CMS experiments and in section 6 we summarize and conclude.

II. BASIC PROPERTIES OF THE NMSSM

We consider the Z_3-symmetric version of the NMSSM with the superpotential given by

$$W_{\rm NMSSM} = W_{\rm MSSM} + \lambda \hat{S} \hat{H}_u \cdot \hat{H}_d + \kappa \hat{S}^3 \tag{1}$$

where $W_{\rm MSSM}$ is the superpotential of the MSSM with μ set to zero. The soft supersymmetry breaking potential relative to the MSSM is then given by

$$V^{\rm NMSSM}_{\rm soft} = V^{\rm MSSM}_{\rm soft} + m^2_S |S|^2 + \left(\lambda A_\lambda S H_u \cdot H_d + \frac{1}{3} \kappa A_\kappa S^3 + h.c. \right) \tag{2}$$

where the part of $V^{\rm MSSM}_{\rm soft}$ only depending on the Higgs fields is given by,

$$V^{\rm MSSM}_{\rm soft,higgs} = m^2_{H_u} |H_u|^2 + m^2_{H_d} |H_d|^2 \quad . \tag{3}$$

In addition $V^{\rm MSSM}_{\rm soft}$ contains all the dependence on the other soft supersymmetry breaking parameters: the gaugino masses M_1, M_2, M_3, the tri-linear couplings $\mathbf{a}_u, \mathbf{a}_d, \mathbf{a}_e$, the squark masses $\mathbf{M}_Q, \mathbf{M}_u, \mathbf{M}_d$, and finally the slepton masses $\mathbf{M}_L, \mathbf{M}_e$. In the following we will assume minimal flavour violation so that the sfermion mass matrices are diagonal and the tri-linear couplings are proportional to the corresponding Yukawa coupling matrices $\mathbf{a}_u = A_u \mathbf{y}_u$ etc.

After electroweak symmetry breaking, and assuming that CP is conserved, the Higgs sector will contain three CP-even Higgs bosons (h_1, h_2, h_3), two CP-odd (a_1, a_2) and one charged $(h^\pm)$, where the states are ordered in terms of increasing mass. In the same way as in the MSSM the minimization conditions for the Higgs potential allows one to trade the m_{H_u}, m_{H_d} parameters for the doublet vev $v \approx 174$ GeV and $\tan\beta = v_u/v_d$. Similarly m_S can be expressed in terms of the singlet vev v_s which in turn gives rise to the effective μ-parameter, $\mu = \lambda v_s$. All in all this leaves us with 6 unknown parameters describing the Higgs sector of NMSSM at tree-level: $\tan\beta, \mu, \lambda, \kappa, A_\lambda, A_\kappa$. Below we will trade the latter two parameters for the masses $m_{h^\pm}$ and m_{a_1}.

As already alluded to the mass-eigenstates are mixtures of the electroweak eigenstates. More specifically, writing $S^{\text{weak}} = (\text{Re}(H_u), \text{Re}(H_d), \text{Re}(S))$ we have $h_i = \mathbf{S}_{ij} S_j^{\text{weak}}$. (In the MSSM limit this means that $\mathbf{S}_{12} = -\sin\alpha$.) Similarly for the CP-odd states we have $a_i = \mathbf{A}_{ij} A_j^{\text{weak}}$ with $A^{\text{weak}} = (\text{Im}(\cos\beta H_u + \sin\beta H_d), \text{Im}(S))$. Here the mixing matrix is simply $\mathbf{A} = \begin{pmatrix} \cos\theta_A & \sin\theta_A \\ -\sin\theta_A & \cos\theta_A \end{pmatrix}$. Together with the ratio of the two doublet vevs (or equivalently the rotation angle needed to go to the Higgs basis where only one of the doublets have a vev) $\tan\beta$, the mixing matrices $\mathbf{S}$ and $\mathbf{A}$ specify the reduced couplings to fermions and gauge bosons as given in table I.

Vertex	NMSSM	MSSM	SM
h_1tt	$\frac{\mathbf{S}_{11}}{\sin\beta}$	$\frac{\cos\alpha}{\sin\beta}$	1
h_1bb	$\frac{\mathbf{S}_{12}}{\cos\beta}$	$\frac{\sin\alpha}{\cos\beta}$	1
h_2tt	$\frac{\mathbf{S}_{21}}{\sin\beta}$	$\frac{\sin\alpha}{\sin\beta}$	n.a.
h_2bb	$\frac{\mathbf{S}_{22}}{\cos\beta}$	$\frac{\cos\alpha}{\cos\beta}$	n.a.
a_1tt	$\cot\beta\,\cos\theta_A$	$\cot\beta$	n.a.
a_1bb	$\tan\beta\,\cos\theta_A$	$\tan\beta$	n.a.
h_1VV	$\sin\beta\,\mathbf{S}_{11} + \cos\beta\,\mathbf{S}_{12}$	$\sin(\beta-\alpha)$	1
h_2VV	$\sin\beta\,\mathbf{S}_{21} + \cos\beta\,\mathbf{S}_{22}$	$\cos(\beta-\alpha)$	n.a.
a_1h_1Z	$(\cos\beta\,\mathbf{S}_{11} - \sin\beta\,\mathbf{S}_{12})\cos\theta_A$	$\cos(\beta-\alpha)$	n.a.
a_1h_2Z	$(\cos\beta\,\mathbf{S}_{21} - \sin\beta\,\mathbf{S}_{22})\cos\theta_A$	$\sin(\beta-\alpha)$	n.a.
$h_1h^+W^-$	$\cos\beta\,\mathbf{S}_{11} - \sin\beta\,\mathbf{S}_{12}$	$\cos(\beta-\alpha)$	n.a.
$a_1h^+W^-$	$\cos\theta_A$	1	n.a.

TABLE I. Reduced Higgs couplings in the NMSSM compared to the MSSM and the SM (when applicable). Note that the reduced couplings to fermions are identical for all three generations, even if only the third generation is displayed here. The couplings to h_3 can be obtained from the h_1 ones by the replacements $\mathbf{S}_{11} \to \mathbf{S}_{31}$ and $\mathbf{S}_{12} \to \mathbf{S}_{32}$ wheras the couplings to a_2 can be obtained from the a_1 ones by the replacement $\cos\theta_A \to \sin\theta_A$.

III. EXPERIMENTAL CONSTRAINTS

In this section we will explore to what extent the process we are interested in is constrained by existing experimental data. Since we are interested in a light $h^\pm$ (with $m_{h^\pm} < m_t$) and a light a_1 there are constraints both from collider experiments as well as low-energy flavour experiments. However, before going in to the various constraints we will specify the scenarios that we have considered and then come back to the question of experimental constraints.

A. Specification of SUSY scenario considered

In the following we will consider a variant of the well motivated $m_h^{\max}$-scenario in the MSSM [19], similarly to what was done in [17]. Thus we will consider a universal scale $M_{\rm SUSY}$ for the sfermion masses at the supersymmetry breaking scale. In other words we assume, as already stated, that the sfermion mass matrices ($\mathbf{M}_Q$ etc) are diagonal, and furthermore we assume that all diagonal entries are equal to $M_{\rm SUSY}$ which we keep fixed at 1 TeV. In addition we assume that the gaugino masses are related as in the constrained MSSM, where supersymmetry breaking is assumed to be mediated by gravity, namely $M_1 = 100$ GeV, $M_2 = 200$ GeV, $M_3 = 800$ GeV. Finally we will assume that $A_t = A_b = A_\tau$ but contrary to what was done in [17] we will let them vary in the range $A_t \in [-5000, 5000]$ GeV so that the amount of mixing between the $\tilde{t}_L$ and $\tilde{t}_R$ is unconstrained.

For the Higgs sector we will let all six parameters vary freely. However, as was done in [17], we will trade the A_κ parameter for m_{a_1} and A_λ parameter for $m_{h^\pm}$ using an iterative procedure starting from the tree-level relations:

$$m_{h^\pm}^2 = \frac{2\mu}{\sin 2\beta}\left(A_\lambda + \frac{\kappa}{\lambda}\mu\right) + m_W^2 - \lambda^2 v^2 \tag{4}$$

$$\mathcal{M}_P^2 = \begin{pmatrix} \frac{2\mu}{\sin 2\beta}\left(A_\lambda + \frac{\kappa}{\lambda}\mu\right) & \lambda v\left(A_\lambda - 2\frac{\kappa}{\lambda}\mu\right) \\ \lambda v\left(A_\lambda - 2\frac{\kappa}{\lambda}\mu\right) & \frac{\lambda^2 v^2 \sin 2\beta}{2\mu}\left(A_\lambda + 4\frac{\kappa}{\lambda}\mu\right) - 3\frac{\kappa}{\lambda}A_\kappa\mu \end{pmatrix}, \tag{5}$$

where the latter gives the masses of the mass-eigenstates a_1, a_2 after diagonalisation. Thus the parameters we consider with their respective ranges are:

$$\begin{aligned} \tan\beta &\in [1, 60], \\ \lambda &\in [0, 0.7], \\ \kappa &\in [-0.7, 0.7], \\ \mu &\in [125, 1000]\ \text{GeV}, \\ m_{h^\pm} &\in [80, 170]\ \text{GeV}, \\ m_{a_1} &\in [4, 150]\ \text{GeV}. \end{aligned}$$

The limits for the various parameters has been chosen as follows: For $\tan\beta$, κ and λ we impose perturbativity up to the GUT scale which effectively means that any value out side the above regions are bound to fail. (In addition some points inside these regions also fail because of this requirement.) The lower limits on μ and $m_{h^\pm}$ are dictated by experimental constraints. The upper limit on μ is not a hard one but follows from the implicit assumption that μ should be of order the electroweak scale whereas the upper limit on $m_{h^\pm}$ is given by the condition that the decay $t \to bh^+$ should be open. The reason for letting μ vary freely is mainly that this decreases the correlations between the masses of the Higgs bosons as will be discussed more below. Finally the lower limit on m_{a_1} is chosen in order to have $a_1 \to \tau^+\tau^-$ open whereas the upper limit follows from having $m_{h^\pm} < 170$ GeV.

In order to calculate the resulting models from the inputs we use the package NMSSMTools version 3.2.0 [20, 21] with default settings. Among other thing this means that we impose perturbativity of the model up to the GUT scale. Finally, in all scans we generate ~ 1 M points (with flat priors in the parameters considered) which fulfill the theoretical constraints implemented in NMSSMTools.

B. Current experimental constraints

The most important constraints comes from the direct searches for Higgs bosons for which we use the package HiggsBounds version 3.7.0 [22, 23]. In addition there are also constraints from direct searches for supersymmetric particles, various flavour constraints and in principle also the anomalous magnetic moment of the muon as well as the relic density of dark matter. We have not applied the lattr two constraints for the following reasons. To investigate the amount of dark matter in the various models one would also need to vary the gaugino masses as was done in [24]. Since we keep these fixed we have not applied the dark matter constraints. On the same vain we have not applied the constraint from the anomalous magnetic moment of the muon, since this depends on the masses of the scalar partners of the muon and the neutrinos, apart from requiring μ to be positive.

When it comes to the flavour constraints the situation is more involved in that various constraints have different level of model dependence. On the one hand there are constraints from tree-level mediated processes such as $B_u \to \tau^+\nu_\tau$, which only depend on the Higgs sector and on the other hand there a constraints from loop-mediated processes such as $B_s \to \mu^+\mu^-$ and $b \to s\gamma$ which depend on details of the supersymmetric sector of the model. In the following we will limit ourselves to applying the most severe constraints from $B_u \to \tau^+\nu_\tau$, which limits the available parameter space in $[m_{h^\pm}, \tan\beta]$ and $B_s \to \mu^+\mu^-$ which puts limits on $[m_{a_1}, \tan\beta]$. The latter constraint is especially important since we will consider light a_1 which is very constrained by the data from LHCb and CMS [25, 26]. Finally we apply the direct constraints from searches for supersymmetric particles. For all constraints except the Higgs bosons we use NMSSMTools version 3.2.0.

The results from the scan are displayed in Fig. 1 with black points being viable models from a theory point of view but excluded by the direct searches for Higgs bosons and coloured points being allowed by the same constraint. Of primary interest are the allowed regions in $[m_{a_1}, m_{h^\pm}]$. As is clear from the figure there is a distinct region of points with $m_{a_1} \sim 2m_B \approx 10.6$ GeV allowed by all constraints (indicated by green colour) for essentially any value of $m_{h^\pm} \gtrsim 90$ GeV. The same is also true in the constrained $m_h^{\rm max}$ scenario where $\mu = 200$ GeV and $A_t = -\sqrt{6}M_{\rm SUSY} + \mu\cot\beta$ are fixed as was already noted in [17]. However, at difference to the constrained $m_h^{\rm max}$ scenario there are regions with larger m_{a_1} that are allowed also for $m_{h^\pm} \lesssim 120$ GeV.

Looking at the $[m_{h^\pm}, \tan\beta]$-plane one clearly sees the constraint from $B_u \to \tau^+\nu_\tau$ for intermediate $\tan\beta$ (show as blue points). For larger $\tan\beta$ there is a cancellation between the SM and $h^\pm$ contributions, which makes this region allowed by $B_u \to \tau^+\nu_\tau$, but instead the constraints from $B_s \to \mu^+\mu^-$ come into play (red points). It should be noted that the points excluded by $B_u \to \tau^+\nu_\tau$ are plotted on top of the constraints from $B_s \to \mu^+\mu^-$. Similarly the constraints from searches for supersymmetric particles are plotted (in yellow) on top of the constraints from B-decays, but with the cut $\mu > 125$ GeV there are hardly any points excluded by this constraint. Finally we note that for $\tan\beta \lesssim 15$ there are allowed points in parameter space for essentially any value of $m_{h^\pm} \gtrsim 90$ GeV.

Turning to the $[m_{a_1}, \tan\beta]$-plane we see that the region $m_{a_1} \sim 2m_B$ is allowed by all constraints up to $\tan\beta \lesssim 10$, whereas for larger $\tan\beta$ there are points allowed by direct Higgs boson searches but not allowed by $B_s \to \mu^+\mu^-$ and $B_u \to \tau^+\nu_\tau$. Given the uncertainties related to the indirect constraints from B-decays we conclude that there is a region in parameter space with $m_{a_1} \sim 2m_B$, $m_{h^\pm} \in [90, 170]$ GeV, and $\tan\beta \in [1, 60]$ that should be searched for by the ATLAS and CMS experiments. It should also be noted that values both above and below the threshold $m_{a_1} = 2m_B$ are allowed by the constraints.

Before turning to the signal of interest, *i.e.* $Br(h^\pm \to a_1 W)$, we also show in Fig. 1 the

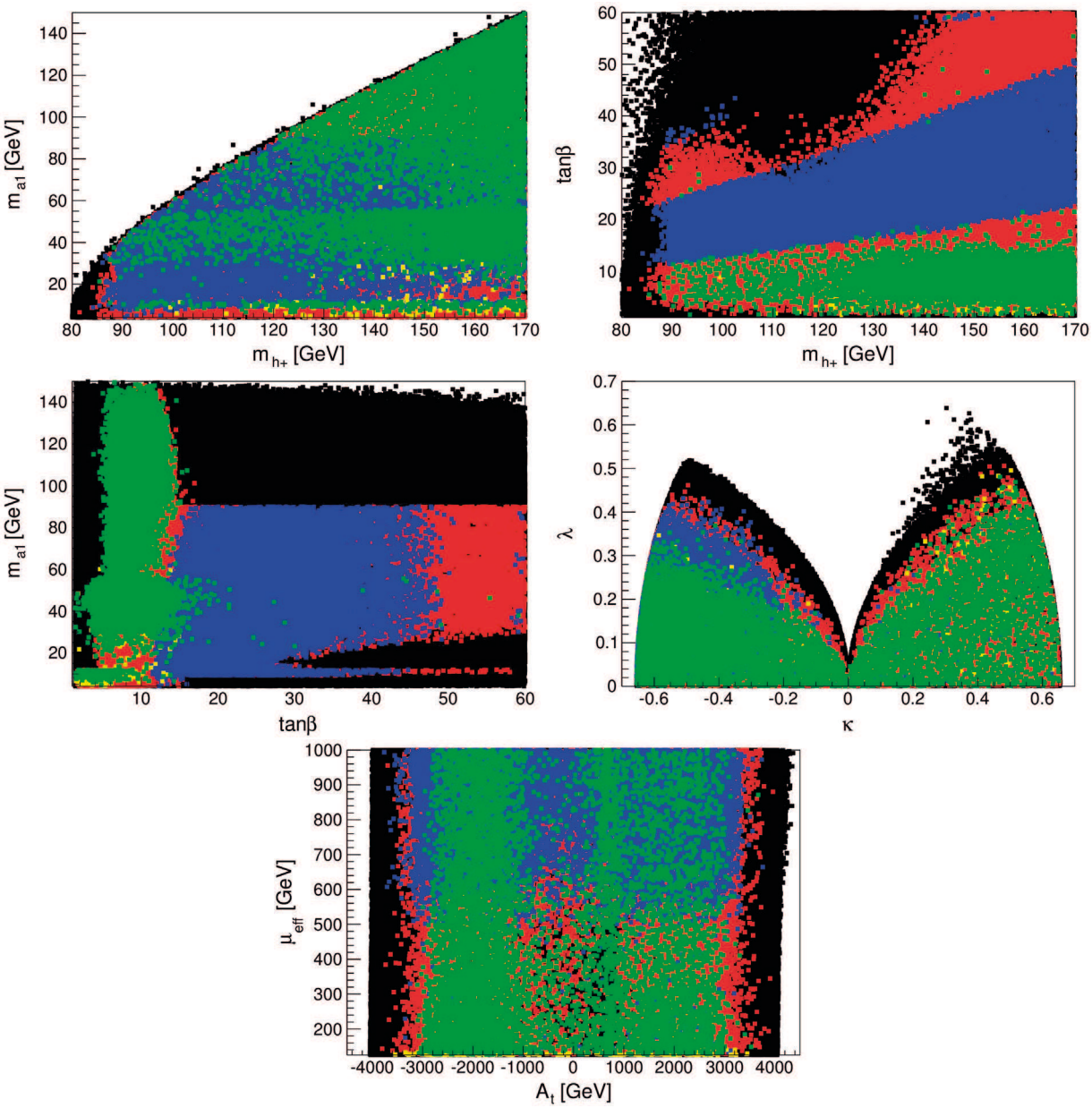

FIG. 1. Correlations between the parameters of the scan in the scenario under consideration (see text for details) with the various constraints applied as follows. All points in black are viable model points but are excluded by HiggsBounds. The coloured points are allowed by HiggsBounds and plotted in the following order: red points are excluded by $B_s \to \mu^+\mu^-$, blue points are excluded by $B_u \to \tau^+\nu_\tau$, yellow points are excluded by direct searches for supersymmetric particles, and finally green points are allowed by all constraints considered.

effects of the various constraints when projected onto the $[\kappa, \lambda]$ and $[A_t, \mu]$-planes. From the first of these plots one clearly sees the constraint $\sqrt{\kappa^2 + \lambda^2} \lesssim 0.7$ which arises from requiring perturbativity up to the GUT scale. From the second we see that the constraints imply $|A_t| \lesssim 3500$ GeV, which essentially follows from the radiative corrections to the lightest CP-even Higgs becoming small or even negative for large $|A_t|$ relative to the value $M_{\rm SUSY} = 1$ TeV that we are using. We also see that for μ there are hardly no experimental constraints in the region considered. On the other hand, if we would extend μ to values smaller than 125 GeV then all those points would be excluded by searches for supersymmetric particles.

As promised we turn now to the resulting branching ratios for the decay $h^\pm \to a_1 W$. From Fig. 2 we observe the following general feature, the branching ratio can be large as soon as

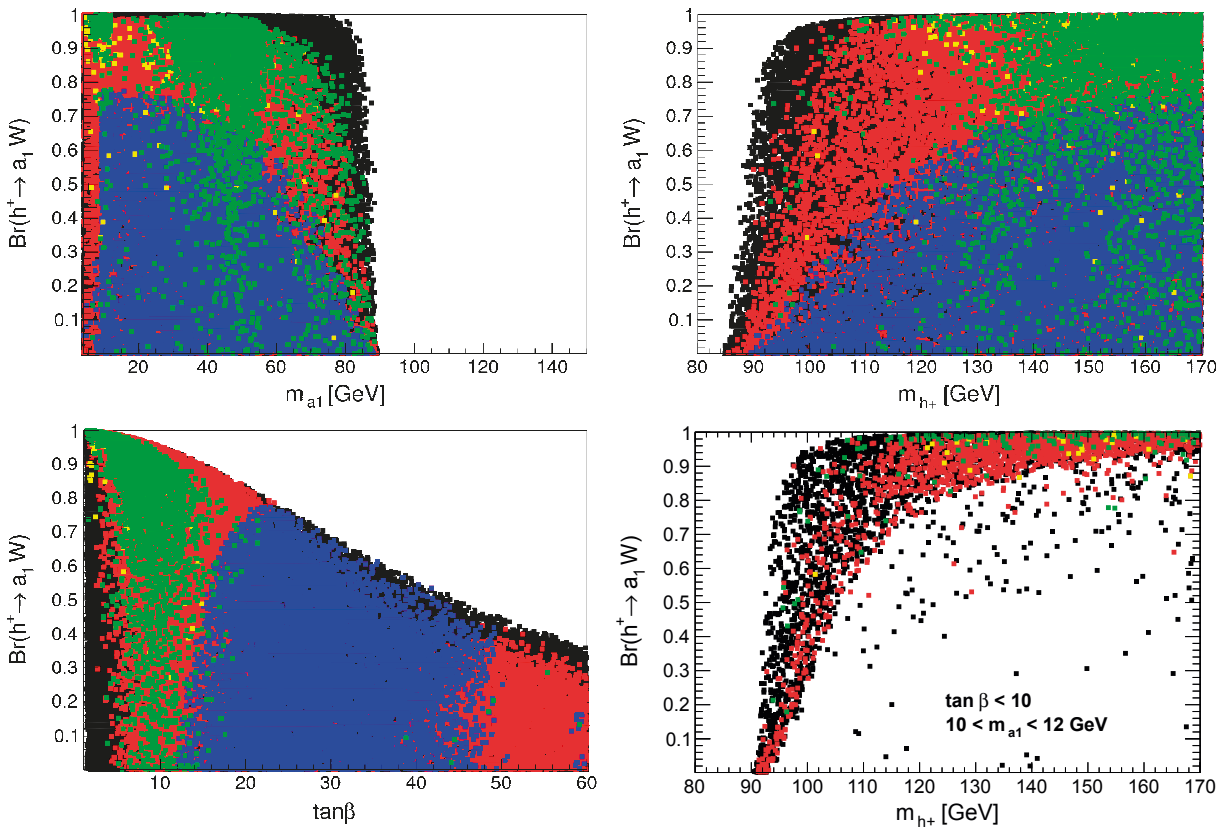

FIG. 2. The branching ratio for $h^\pm \to a_1 W$ when scanning over the parameters in the scenario under consideration (see text for details) with the various constraints applied. The colour coding is the same as in Fig. 1

the channel is open ($m_{a_1} < m_{h^\pm} - m_W$) except for large $\tan\beta$ where the decay $h^\pm \to \tau\nu_\tau$ becomes dominant. Concentrating on those points that pass all the constraints considered and the region $m_{a_1} \sim 2m_B$ we also see from the lower right plot that $Br(h^\pm \to a_1 W) \gtrsim 0.9$ as long as $\tan\beta \lesssim 10$ and $m_{h^\pm} \gtrsim 100$ GeV. Thus we can conclude that not only is the parameter space region $m_{a_1} \sim 2m_B$, $m_{h^\pm} \in [100, 170]$ GeV, and $\tan\beta \in [1, 10]$ allowed - in this region the decay $h^\pm \to a_1 W$ is also dominant. In the next section we will exemplify how the so far unexplored region of parameter space with $m_{a_1} \in [10, 12]$ GeV can be probed by searching for $h^\pm \to a_1 W$ with $a_1 \to b\bar{b}$ in $t\bar{t}$-production at the LHC.

Before ending this section we also show in Fig. 3 the branching rations for the decay chains of interest, *i.e.* $t \to bh^+$, $t \to bh^+ \to ba_1 W$, and $t \to bh^+ \to ba_1 W \to bb\bar{b}W$ as a function of $\tan\beta$ when restricting to parameter space points with $m_{h^\pm} < 160$ GeV. As can be seen from the figure, points with $Br(t \to bh^+)$ as large as 0.2 are still allowed when the decay $h^\pm \to a_1 W$ is included. This should be compared with the experimental constraints from ATLAS and CMS which so far have assumed that $Br(h^\pm \to \tau\nu_\tau) = 1$ giving a limit $Br(t \to bh^+) \lesssim$ few percent [27, 28].

IV. SEARCH STRATEGY

In the following section we will perform a signal-to-background analysis for three different charged Higgs masses: $m_{h^+} = 100$, 130 and 150 GeV respectively. For definiteness we have used $\tan\beta = 50$ when simulating the signal but the end results will not depend on this value. The mass of the a_1 is set to 11 GeV throughout as an example of a small a_1 mass that is just

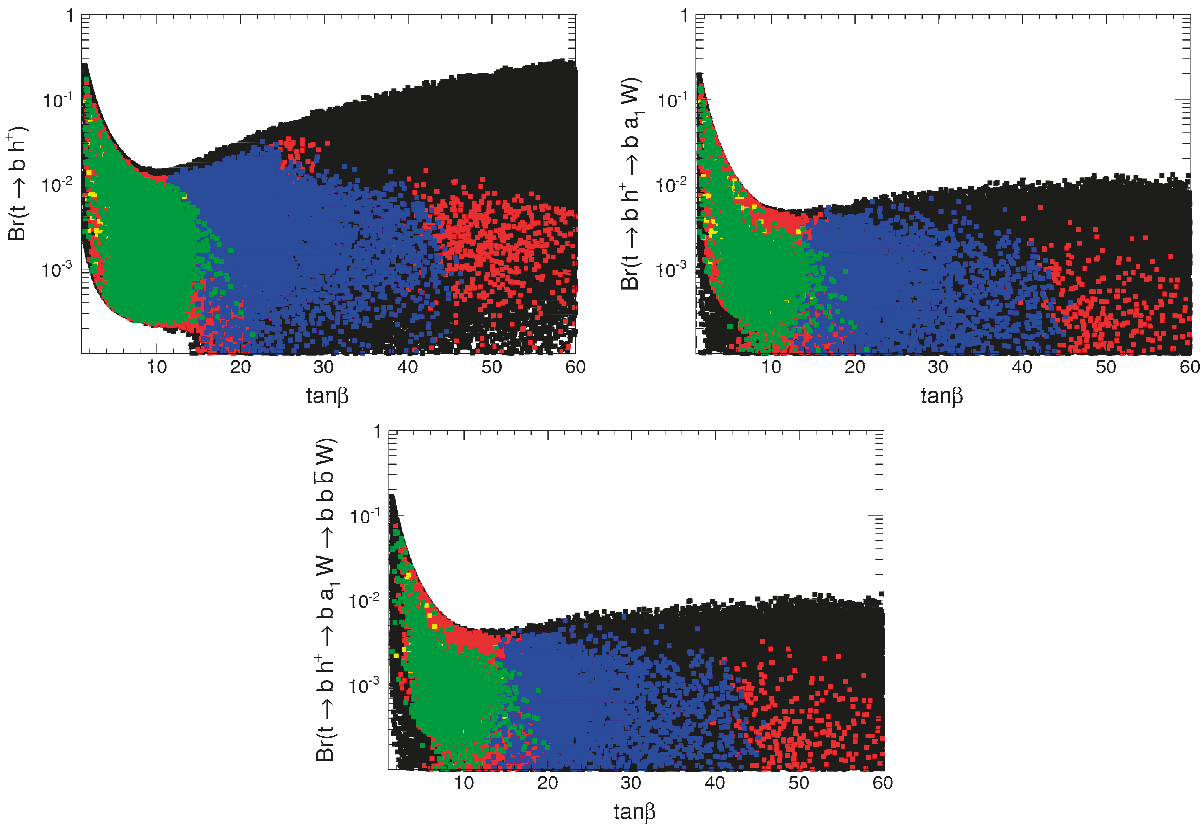

FIG. 3. The branching ratios for the decay chains $t \to bh^+$, $t \to bh^+ \to ba_1W$, and $t \to bh^+ \to ba_1W \to bb\bar{b}W$ respectively when scanning over the parameters in the scenario under consideration (see text for details) with the various constraints applied and only considering points with $m_{h^\pm} < 160$ GeV. The colour coding is the same as in Fig. 1

above $b\bar{b}$-threshold. The three charged Higgs masses are chosen to illustrate different kinematic properties: at $m_{h^\pm} = 150$ GeV the b-jet from the $t \to bh^+$ decay will be rather soft whereas the a_1 from the h^+ will be harder. For $m_{h^\pm} = 100$ GeV the situation will be the opposite, and in the intermediate case $m_{h^\pm} = 130$ GeV both jets can be relatively hard and in addition the available phase-space will be largest.

We aim to reconstruct the signal process where one of the t-quarks decays leptonically via $h^\pm \to a_1W$ with $W \to \ell\nu_\ell$ and the other hadronically via $W \to jj$ as illustrated in Fig. 4. All cross-sections have been corrected for these enforced W decays as well as a factor of 2 for taking account of the process also with interchanged roles between the t and the $\bar{t}$. Because the a_1 is supposed to decay close to threshold to $b\bar{b}$, we aim for a reconstruction where the two b's from the a_1 are clustered together to give a single $b\bar{b}$-jet.

As backgrounds to the process we consider the irreducible $t\bar{t}b\bar{b}$ as well as, because of its higher magnitude, $t\bar{t}$ with one jet being accidentally b-tagged (weighted with a mis-tagging probability, assumed to be 0.01 [29, 30]). In order to include also the single top contributions to the background we have simulated the processes $\bar{t}bW^+b\bar{b}$ and $\bar{t}bW^+$ respectively, but in the following we will denote them as $t\bar{t}b\bar{b}$ and $t\bar{t}$ for simplicity. For other reducible backgrounds, such as $W + b$ jets, we assume that similar procedures can be applied as in the $t\bar{t}$ cross-section determination. For example, requiring two b-tagged jets reduces the $W + b$jets background to $t\bar{t}$ production to about 10% [31]. Several cuts are applied to strengthen the signal and to suppress the background as will be discussed in the following.

A center-of-mass energy of 8 TeV at the Large Hadron Collider is assumed throughout the whole analysis. For the generation of the hard matrix elements, we use MadGraph 5 [32] with a

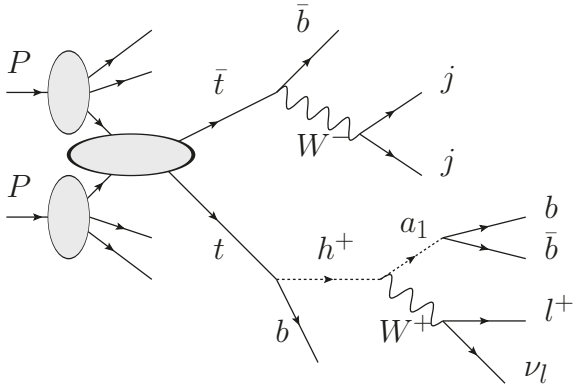

FIG. 4. Illustrations of $t\bar{t}$ production in proton-proton collisions with the subsequent decay chain considered in this paper.

fixed renormalization and factorization scale (set as default to the Z mass) and the 'CTEQ6L1' parton distribution functions. To supply MadGraph with the proper parameters of the signal we have for simplicity used a simple two Higgs Doublet Model with the masses given above as implemented in the Two Higgs Doublet Model Calculator 2HDMC [33]. The only important difference to the NMSSM then arises from the $h^\pm \to a_1 W$ decay giving and extra factor $\cos^2\theta_A$ (cf. Table I). All other steps to generate complete events, such as radiation, underlying events and hadronization, are carried out using Pythia 8. We start from bare samples of 100000 events for the different signals as well as the $t\bar{t}b\bar{b}$ background whereas for the $t\bar{t}$ background we have 50 times higher statistics to start with. There is no detector simulation included in this exploratory analysis but we have simulated b-tagging in a simplified way as detailed below.

For all processes we use the leading order cross-sections obtained from MadGraph. On the one hand this means that there is an overall scale factor which is more or less the same for both signal and background. On the other hand the rates will be lower than what would have been result if higher order cross-sections had been used. All in all this means that the signal over background rates we find will be underestimated in this respect. For example we get a LO cross-section for $pp \to t\bar{t}$ process in the SM of 138 pb to be compared with the NNLL resummed result of 232 pb [34].

A. Reconstruction of the leptonic W

To reconstruct the leptonic W, we first need to identify the charged lepton (e or μ) associated to the hard process. The transverse momentum ($p_\perp$) and pseudo-rapidity (η)-distributions are shown in Fig. 5. After applying cuts on the lepton kinematics ($p_\perp > 20$ GeV, $|\eta| < 2.5$), we require the summed $p_\perp$ of the surrounding particles in an (η, ϕ)-cone of size $\Delta R = \sqrt{\Delta\eta^2 + \Delta\phi^2} = 0.3$ around the lepton to be less than 10 GeV to call it isolated [1]. On the whole event then, we require to have precisely one isolated lepton in the final state.

The next step in reconstructing the leptonic W is to identify the missing energy (MET)/missing $\vec{p}_\perp$ of the event with the transverse momentum of the neutrino. Assuming the W to be on mass-shell and using a mass-less neutrino then leaves two possible solutions for the longitudinal

[1] The numerical values for the $p_\perp$ cut and the cone size have been optimized by observation of the changes in efficiency and purity when varying the cuts

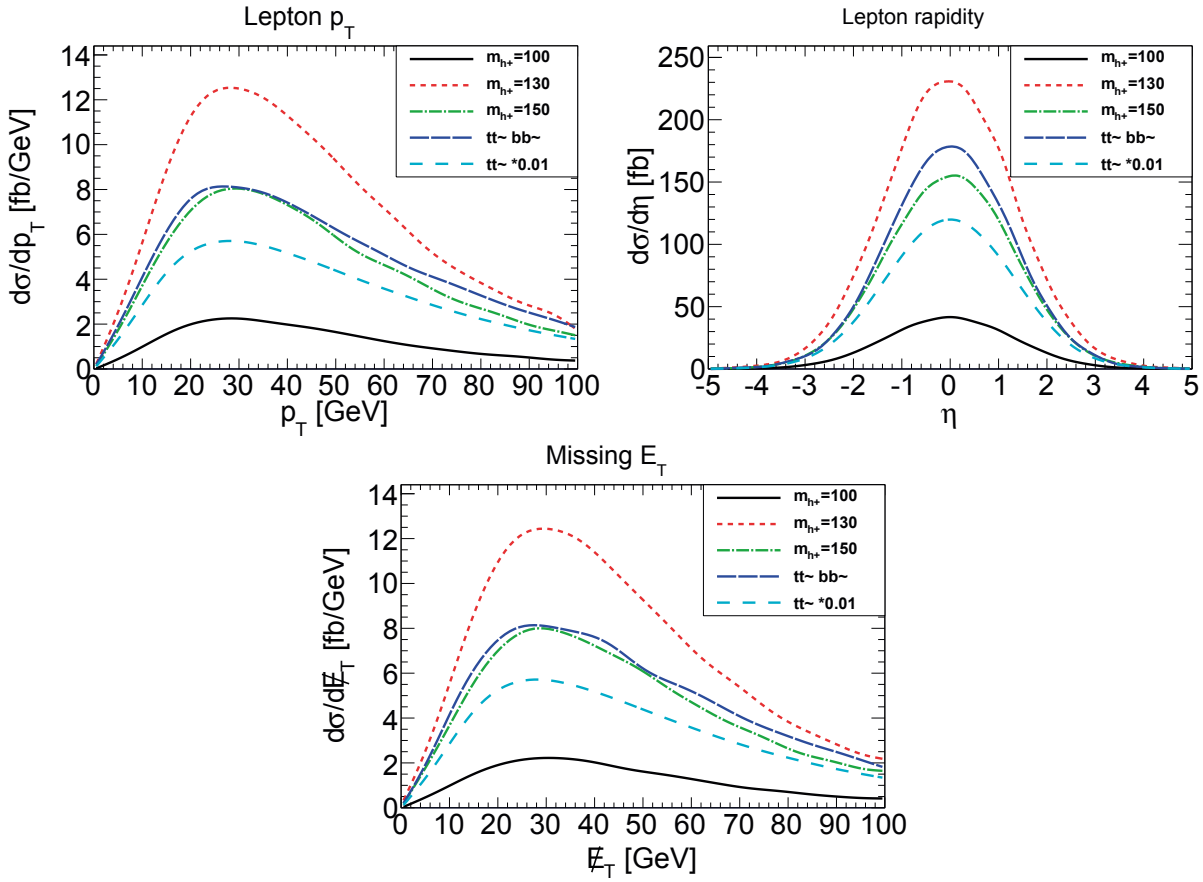

FIG. 5. Transverse momentum and pseudo-rapidity of the charged lepton from the W decay and missing transverse energy (MET) before applying cuts.

momentum of the neutrino $p_{\nu z} = A \pm \sqrt{D}$ with

$$A = \frac{m_W^2 p_{lz} + 2p_{lz}(\vec{p}_{\nu\perp}\vec{p}_{l\perp})}{2m_{\perp l}^2}\,, \tag{6}$$

$$D = \frac{E_l^2}{m_{\perp l}^4}\left(\frac{m_W^4}{4} - (\vec{p}_{\nu\perp})^2(\vec{p}_{l\perp})^2 + (\vec{p}_{\nu\perp}\vec{p}_{l\perp})^2 + (\vec{p}_{\nu\perp}\vec{p}_{l\perp})m_W^2\right). \tag{7}$$

In order to have a more accurate reconstruction of $p_{\nu z}$ we have applied a cut $\not{E}_\perp > 30$ GeV. In addition, different selection criteria for the choice of the sign have been examined, e.g. the invariant mass of the reconstructed $h^\pm$. Among these, the most viable one turned out to be a simple selection of the smaller $|p_{\nu z}|$, which is correct in roughly three quarters of the signal events.

B. Jet reconstruction and tagging

For the reconstruction of the hadronic part of the event, we consider different jet clustering schemes (anti-kT [35], Cambridge/Aachen [36], kT [37, 38]) as well as cone-sizes. All particles, except neutrinos and the isolated lepton, in the rapidity range $|\eta| < 4.9$ are fed into FastJet [39, 40]. The resulting clustered jets are required to have $p_\perp > 20$ GeV. Afterwards, a simplified b-tagging is simulated for all jets in the region $|\eta| < 2.5$ by comparing the (η, ϕ) of the jets to the b-quarks of the hard process. All jets within $\Delta R = 0.4$ are then classified as b-jets.

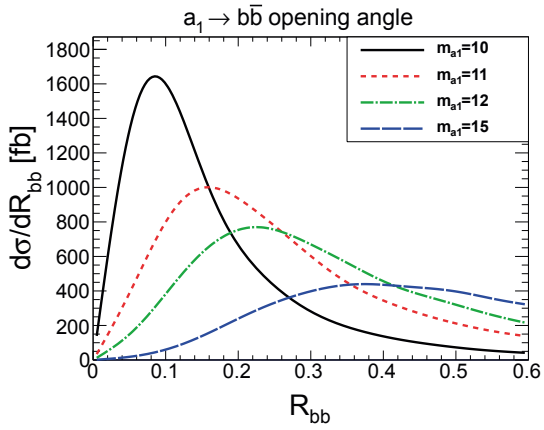

FIG. 6. The distance between the two b-quarks coming from the a_1-decay on parton level for the signal with $m_{h^\pm} = 130$ GeV.

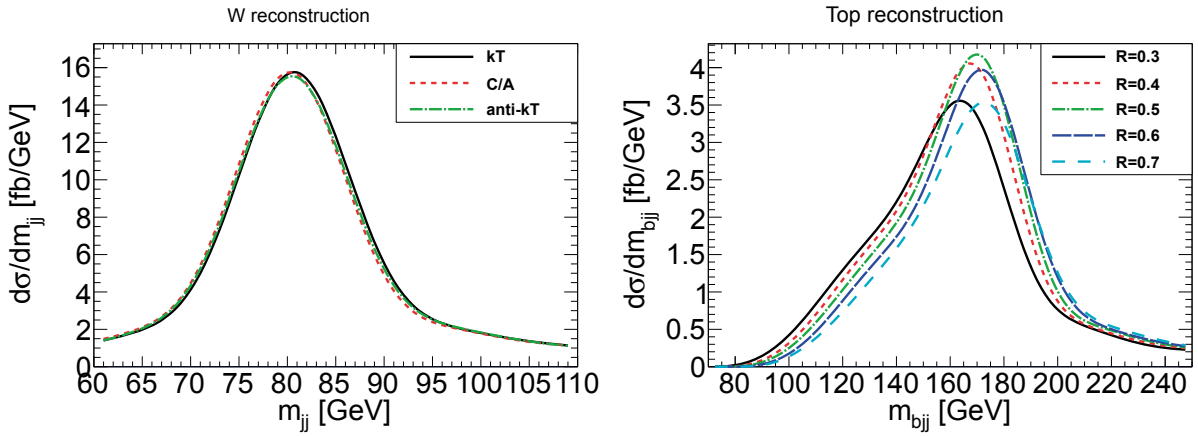

FIG. 7. Mass reconstruction of the hadronically decaying W (left) and t-quark (right) for the signal with $m_{h^\pm} = 130$ GeV when $R = 0.5$ (left) and using the anti-kT algorithm (right).

The jet-algorithms requires to specify the distance measure R used when calculating the jet measure. Since we want to cluster the $b\bar{b}$ pair from the a_1 into one jet, it is crucial that the distance between the two subjets is not too large. Fig. 6 shows the distance measure between the two b-quarks on parton level for different a_1 masses. As can be seen from the figure, for reasonable clustering cone sizes (around 0.4 to 0.6) and with m_{a_1} in the region of interest for this analysis, the two b-quarks will most likely be clustered together as a single jet.

As an ideal reconstruction will now give rise to three b-jets, the correct reconstruction of the $h^\pm$ will be enhanced by the identification of the "wrong" b-jet which comes from the $\bar{t}$ together with the hadronically decaying W^-. The strategy to achieve this here is to first find the pair of untagged jets that is closest to the W mass and then combine this pair with the b-jet that gives a mass closest to the t mass. This b-jet will then be excluded in the $h^\pm$ reconstruction, reducing the number of b-jets which have to be considered (in an event with a so far correct clustering in the desired way) to two. In addition to this, we put cuts on the quality of the reconstruction by requiring the reconstructed masses shown in Fig. 7 to be in the regions $m_W \pm 20$ GeV or $m_t \pm 30$ GeV respectively. We have checked that the reconstruction of the W and t masses are quite independent of the choice of jet clustering scheme and cone-size as is also shown in Fig. 7. Only the 0.3 cone size gives a slightly inferior top reconstruction, but then the a_1 will also not give rise to a single b-jet. If not mentioned differently, we thus use the anti-kT algorithm with $R = 0.5$ in the following.

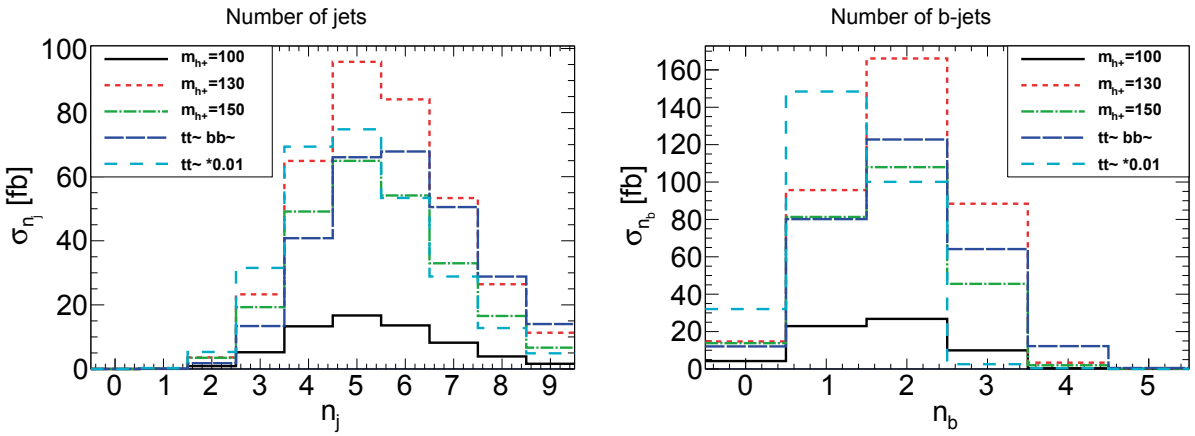

FIG. 8. Jet (left) and b-jet (right) multiplicity for the signal and backgrounds when using the anti-kT algorithm with $R = 0.5$.

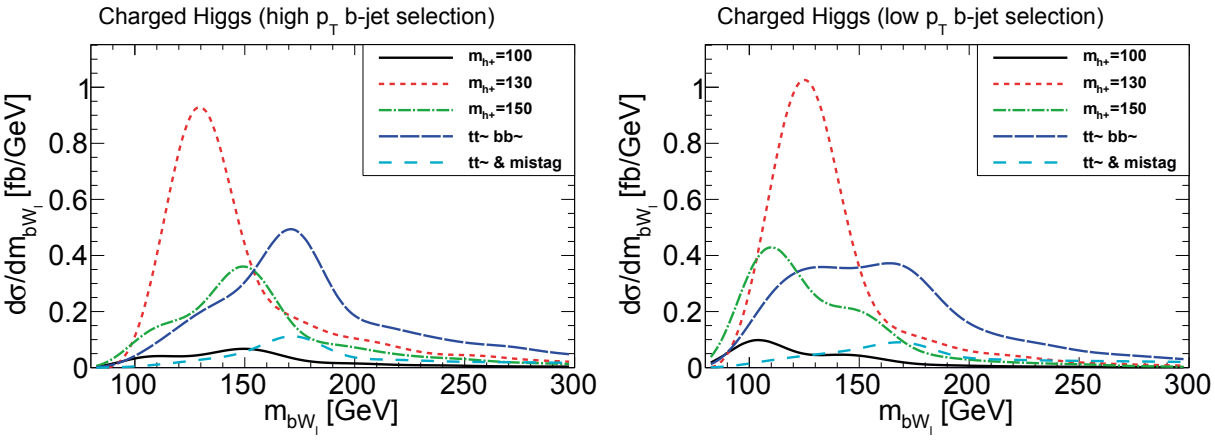

FIG. 9. Reconstructed charged Higgs masses, using either the higher-$p_\perp$ (left) or the lower-$p_\perp$ (right) b-jet combined with the leptonically decaying W.

Using the jet-reconstruction outlined above we obtain the jet and b-jet multiplicity respectively shown in Fig. 8. As is clear from the figure, the number of jets peaks around the expected five and the number of b-jets is a typically smaller than ideal which is due to the limited b-tagging region enforced. Also note the large decrease in b-jet multiplicity for the $t\bar{t}$ sample from 2 to 3. Here the 3 b-jet sample arises from gluon splitting into $b\bar{b}$ and we do not take it into account below since that would amount to double counting with the $t\bar{t}b\bar{b}$ background.

Given the large background from $t\bar{t}$ for the two b-jet sample we resort to requiring at least three b-jets. Assuming that one of the b-jets has been identified as coming from the t-quark this leaves two b-jets that may originate from the $h^\pm$. Due to the strong dependence of the hardness of the b-jet from the $t \to h^+ b$ decay on the $h^\pm$ mass, we consider both of these remaining solutions in general as possible candidates for the $h^\pm$ reconstruction. The resulting distributions when combining with the leptonically decaying W are shown in Fig. 9. In the $h^\pm$ reconstruction, we thus require 3 b-jets for the signals and the $t\bar{t}b\bar{b}$ background, while we require 2 b-jets in the $t\bar{t}$ sample. For the latter we then assume that any of the non b-jets inside the b-tagger region ($|\eta| < 2.5$) can be mis-tagged with a probability of 0.01 per jet [29, 30].

C. Signal significance and reach

To estimate the signal reach as well as its significance, we choose a common window of 90 to 160 GeV to integrate the signal as well as the backgrounds. We correct for b-tagging efficiencies which we assume to be 0.6 per b-jet. The resulting cross-sections are shown in Table II.

	σ_{peak} [fb]					
signal/background	100 GeV	130 GeV	150 GeV	$t\bar{t}b\bar{b}$	$t\bar{t}$	Σ BG
High $p_\perp$ channel	0.78	7.9	3.7	3.0	0.9	3.9
Low $p_\perp$ channel	0.97	9.2	4.7	4.8	1.2	6.0

TABLE II. Integrated signal cross-sections (cf figure 9) for the three different charged Higgs masses as well as the two backgrounds. The integration region is 90 to 160 GeV

$S/\sqrt{B}$ ratios for the three different mass cases are then calculated for an integrated luminosity of 20 fb^{-1} and summarized in Table III. The table also shows the branching ratios at the simulated parameter points, as well as the extrapolations to branching ratios necessary for a 5σ discovery. From the table it is clear that for $m_{h^\pm} \sim 130$ GeV, the discovery reach is maximal. For smaller or larger $m_{h^\pm}$, the limitations in phase space will reduce the branching ratio for $h^\pm \to a_1 W$ and $t \to h^\pm b$ respectively. In the former case this means that the standard decay channel $h^\pm \to \tau\nu_\tau$ will also be significant.

$m_{h^\pm}$	100 GeV		130 GeV		150 GeV	
b-jet selection	high $p_\perp$	low $p_\perp$	high $p_\perp$	low $p_\perp$	high $p_\perp$	low $p_\perp$
$S/\sqrt{B}$	1.77	1.76	18.0	16.7	8.5	8.5
BR($t \to bh^+ \to ba_1W \to bb\bar{b}W$)	0.0051		0.022		0.015	
BR$_{crit}$	0.014	0.014	0.0060	0.0065	0.0085	0.0085

TABLE III. The $S/\sqrt{B}$ ratios obtained for an integrated luminosity of 20 fb^{-1} for the different signals considered together with the branching ratios for the total decay chain $t \to bh^+ \to ba_1W \to bb\bar{b}W$ of the respective parameter points and a linear extrapolation to the critical branching ratio necessary for a 5σ discovery.

Before ending this section we note that similarly to the standard decay modes of the charged Higgs boson it should be possible to use the spin-correlations between the decay products of the two top quarks as a way of enhancing the signal [41–43].

V. COMPATIBILITY WITH POSSIBLE HIGGS SIGNAL

Recently the ATLAS and CMS experiments announced the combined results of the SM Higgs (ϕ) searches using ≈ 5 fb^{-1} of data from 2011 [44, 45]. In short they can be summarized as follows: the CMS experiment has ruled out the region $m_\phi \in [129, 600]$ GeV at the 95 % confidence level as expected whereas in the region [118,129] GeV they have not been able to make any exclusion at all even though they expected to be able to do so at the 95 % confidence level, the ATLAS experiment has similarly ruled out the regions $m_\phi \in [112.9, 115.5]$ GeV, $m_\phi \in [131, 238]$ GeV, and $m_\phi \in [251, 466]$ GeV at the 95 % confidence level whereas they had expected to rule out the region $[125, 519]$ GeV.

Instead, both experiments have found an excess of events in the regions $m_\phi \sim 126$ GeV and $m_\phi \sim 124$ GeV for ATLAS and CMS respectively, which when corrected for the so called look-elsewhere-effect and combining the different channels has a statistical significance of about 2σ for each of the two experiments. Although not statistically significant these results have stirred a lot of excitement in the high-energy physics community [24, 46–54]. It will most likely not be possible to draw any final conclusions about whether this is a true signal or not before the end of the run in 2012 which will give another ~ 20 fb^{-1} of data.

One of the most important properties of the possible signal at the LHC is that the $\phi \to \gamma\gamma$ channel is similar to what is expected from the SM. Therefore we start by considering the would be signal from the h_1 as well as the h_2 compared to what is expected in the SM for a Higgs boson (ϕ) with the same mass. Assuming that gluon-gluon fusion dominates the production, which we have verified is always the case in the scenarios we consider, this ratio is given by

$$R^{h_i}_{gg\gamma\gamma} = \frac{\sigma(gg \to h_i)_{\rm NMSSM}}{\sigma(gg \to \phi)_{\rm SM}} \frac{Br(h_i \to \gamma\gamma)_{\rm NMSSM}}{Br(\phi \to \gamma\gamma)_{\rm SM}} \simeq \frac{\Gamma(h_i \to gg)_{\rm NMSSM}}{\Gamma(\phi \to gg)_{\rm SM}} \frac{Br(h_i \to \gamma\gamma)_{\rm NMSSM}}{Br(\phi \to \gamma\gamma)_{\rm SM}} \quad (8)$$

where in the second equality, following for example [51, 53], we have made the implicit assumption that the difference in radiative corrections for the production and decay processes are canceled in the ratio.

The results obtained for this quantity when using the same scan as in section III are displayed in Fig. 10. From the figure it is clear that if the possible signal seen at the LHC is the h_1 then we would have to have $m_{a_1} \gtrsim 60$ GeV. Even so $R^{h_1}_{gg\gamma\gamma}$ does not become larger than ~ 0.5 for $m_{h_1} \gtrsim 120$ GeV in our scan and there appears to be an upper bound $m_{h_1} \lesssim 122$ GeV. However, the difference in mass compared to the possible observation is so small that it should be considered to be within the theoretical uncertainty [2]. In any case it is clear that it is hardly possible to have a light a_1 if it is the h_1 that has been seen at the LHC.

Next we turn to the possibility that it is the h_2 that has been seen by the LHC experiments. The results of the scan are also shown in Fig. 10. As can be seen from the figure the results are more promising in this case. There are points with $R^{h_2}_{gg\gamma\gamma} \gtrsim 0.1$ also for small m_{a_1} and intermediate $m_{h^\pm}$ that have m_{h_2} in the region indicated by the LHC experiments.

In order to explore this possibility more closely we show in Fig. 11 the results when fixing the a_1 mass to 11 GeV as was done in section IV for the three cases $m_{h^\pm} = 100, 130, 160$ GeV. As can be seen from the figure, for the intermediate charged Higgs mass it is possible to reach $R^{h_2}_{gg\gamma\gamma} \sim 0.15$. However it should be noted that in this case, as also shown in the figure, the branching fraction for $h^\pm \to a_1 W$ is quite small meaning that the standard decay channel $h^\pm \to \tau\nu_\tau$ can be used even though with a slightly reduced branching fraction.

The last logical possibility would be that it is the h_3 that has been observed by the CERN experiments. However, in the scenarios we consider it turns out that $R^{h_3}_{gg\gamma\gamma}$ is always small.

The trends seen in Fig. 11 can be understood on more general grounds from the difficulties of having a light a_1 with mass $m_{a_1} < m_{h_i}/2$ and at the same time have a large $R^{h_i}_{gg\gamma\gamma}$. The first problem is that unless the triple Higgs coupling $g_{h_i a_1 a_1}$ is small the decay $h_i \to a_1 a_1$ will become dominant. Looking at the structures of $g_{h_i a_1 a_1}$, which for example can be found in [8], this means that both λ and κ typically have to be small. Secondly the decay $h_i \to a_1 Z$ will also dominate if $m_{a_1} < m_{h_i} - m_Z$ unless the corresponding reduced coupling given in table I is small. In other words we need $(\cos\beta \mathbf{S}_{i1} - \sin\beta \mathbf{S}_{i2}) \cos\theta_A$ to be small. There are essentially three ways to achieve this. If $\cos\theta_A$ is small then a_1 will be mainly singlet like and decouple. However, then $h^\pm \to a_1 W$ will also be small. The second possibility is that $\mathbf{S}_{i1}$ and $\mathbf{S}_{i2}$ are

[2] For example, including the full one-loop corrections and the two-loop ones from the t and b Yukawa couplings could push the h_1 mass bit higher in compliance with the possible signal. Similarly increasing $M_{\rm SUSY}$ would also increase m_{h_1}.

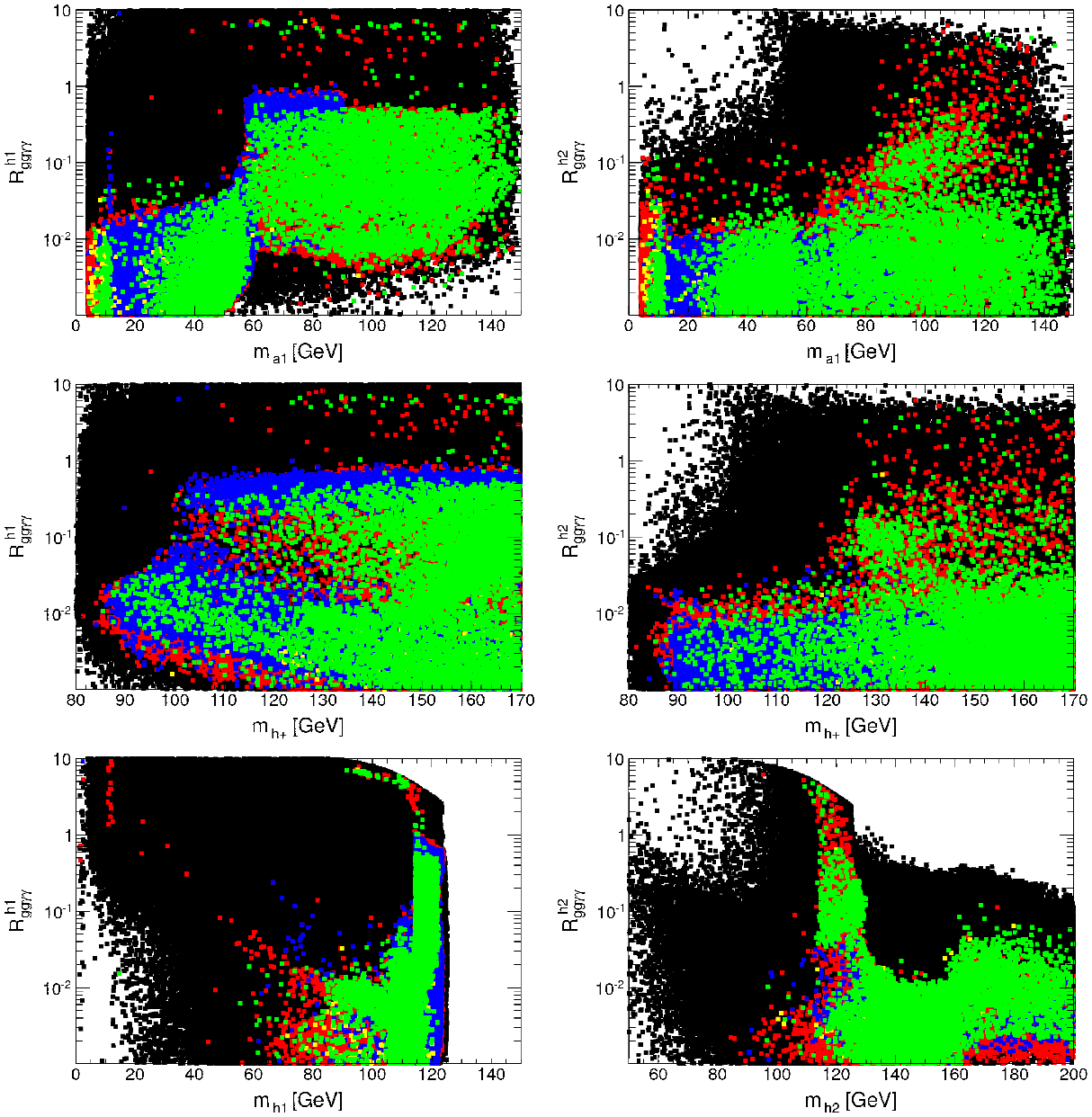

FIG. 10. The signal for $h_1 \to \gamma\gamma$ (left) and $h_2 \to \gamma\gamma$ (right) relative to the standard model when scanning over the parameters in the scenario under consideration (see text for details) with the various constraints applied. The colour coding is the same as in Fig. 1

small, but then the would-be-signal would be mainly singlet-like and not produced in the first place, so $\mathbf{S}_{i3}$ has to be small. Finally then, the combination $(\cos\beta\mathbf{S}_{i1} - \sin\beta\mathbf{S}_{i2})$ could be small but then the complementary combination $(\sin\beta\mathbf{S}_{i1} + \cos\beta\mathbf{S}_{i2})$ would have to be large giving an increased coupling $h_i \to VV$. All in all this means that is difficult to have a light a_1 that is not decoupled and still have a large $R^{h_i}_{gg\gamma\gamma}$, although it cannot be completely ruled out.

VI. SUMMARY AND CONCLUSIONS

We have considered a well motivated class of supersymmetric extensions of the standard model with non-minimal Higgs sector – namely the CP-conserving NMSSM. In these types of models the additional Higgs singlet can modify the phenomenology of the Higgs sector in many different ways. In this paper we have specifically addressed the possibility of having a

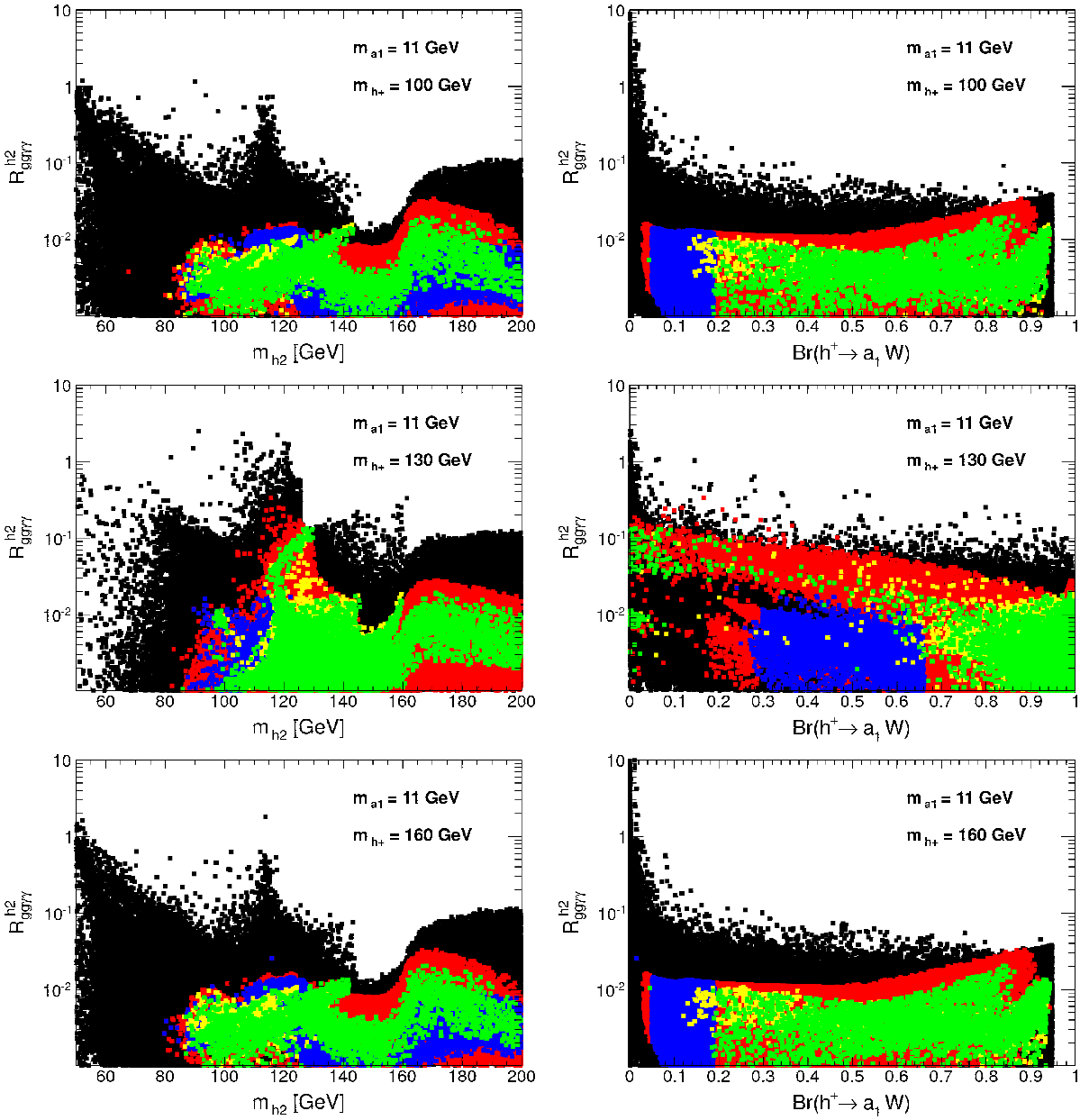

FIG. 11. The signal for $h_2 \to \gamma\gamma$ relative to the standard model (left) and the branching fraction for $h^\pm \to a_1 W$ (right) in a scan with $m_{a_1} = 11$ GeV and $m_{h^\pm}$ fixed at 100 (top), 130 (middle), and 160 (bottom) GeV respectively. The colour coding for the various constraints is the same as in Fig. 1

light CP-odd Higgs boson close to, but still above the $b\bar{b}$ threshold. This in turn means that the light charged Higgs boson, with mass $m_{h^\pm} < m_t$, can decay into $a_1 W$ in addition to the standard decays $h^\pm \to \tau\nu_\tau$, thus invalidating the interpretations made of charged Higgs bosons searches assuming that $Br(h^\pm \to \tau\nu_\tau) = 1$.

When investigating the viability of these types of scenarios we have found that the experimental constraints from direct searches are quite weak even when taking the latest constraints from LHC into account. The constraints from indirect searches in B-decays are more constraining but also more model dependent. Even when including the results from the most important ones, namely $B_u \to \tau\nu_\tau$ and $B_s \to \mu^+\mu^-$, we still find a region of parameter space that is allowed with $\tan\beta \in [1, 10]$. This is precisely the same region as the one where the decay $h^\pm \to a_1 W$ can be dominant.

The phenomenology of these types of scenarios is special in that, due to its low mass, the

a_1 will decay into a single $b\bar{b}$ jet. Even so we have shown that it is possible to reconstruct the decay $h^\pm \to a_1 W$ using standard jet finding algorithms when the W decays leptonically. This requires to use the missing transverse momentum to calculate the four momentum of the W, which can then be combined with the a_1-jet to give a mass peak at $m_{h^\pm}$. The other t quark is assumed to decay hadronically according to $t \to bjj$ giving an additional handle to identify the events of interest. The most important background is thus the irreducible one from $t\bar{t}b\bar{b}$ production but we have also taken into account the $t\bar{t}$ background by considering the possibility of mis-tagging ordinary jets as b-jets.

Based on our study we find that with an integrated luminosity of 20 fb^{-1} it should be possible to discover a charged Higgs bosons in these types of scenarios as long as the combined branching fraction for the decay chain $t \to bh^+ \to ba_1 W \to bb\bar{b}W$ is larger than ≈ 0.01.

Finally we have also investigated the phenomenological consequences of the possible Higgs signal seen at the LHC on the types of scenarios we consider. We find that it is difficult to have a light a_1 that is not decoupled and at the same time have a combined production and decay into $\gamma\gamma$ for one of the CP-even Higgs bosons with mass ~ 125 GeV. As a consequence we have not been able to find regions of parameter space where the $h^\pm \to a_1 W$ decay dominates and at the same time are compatible with the possible Higgs signal. This means that irrespectively of whether the possible Higgs signal is substantiated or not, the LHC experiments should be able to either discover or put very tight constraints on a light charged Higgs bosons also in the NMSSM.

Note added:
On July 4, 2012 the ATLAS and CMS experiments announced the discovery of a new Higgs-like particle in the same mass region as the previous observations already cited in the text.

ACKNOWLEDGMENTS

We thank Oscar Stål for helpful communications. Furthermore, we would like to thank Stefan Prestel for his kind advice and help, especially regarding the technical realization. This work is supported in part by the Swedish Research Council grant 621-2011-5333.

[1] H. P. Nilles, Phys.Rept., **110**, 1 (1984).
[2] H. E. Haber and G. L. Kane, Phys.Rept., **117**, 75 (1985).
[3] A. Djouadi, Phys.Rept., **459**, 1 (2008), arXiv:hep-ph/0503173 [hep-ph].
[4] S. P. Martin, (1997), arXiv:hep-ph/9709356 [hep-ph].
[5] H. Goldberg, Phys.Rev.Lett., **50**, 1419 (1983).
[6] J. R. Ellis, J. Hagelin, D. V. Nanopoulos, K. A. Olive, and M. Srednicki, Nucl.Phys., **B238**, 453 (1984).
[7] M. Maniatis, Int.J.Mod.Phys., **A25**, 3505 (2010), arXiv:0906.0777 [hep-ph].
[8] U. Ellwanger, C. Hugonie, and A. M. Teixeira, Phys.Rept., **496**, 1 (2010), arXiv:0910.1785 [hep-ph].
[9] M. Drees, E. Ma, P. Pandita, D. Roy, and S. K. Vempati, Phys.Lett., **B433**, 346 (1998), arXiv:hep-ph/9805242 [hep-ph].
[10] M. Drees, M. Guchait, and D. Roy, Phys.Lett., **B471**, 39 (1999), arXiv:hep-ph/9909266 [hep-ph].
[11] A. Akeroyd, A. Arhrib, and Q.-S. Yan, Eur.Phys.J., **C55**, 653 (2008), arXiv:0712.3933 [hep-ph].
[12] J. Abdallah *et al.* (DELPHI Collaboration), Eur.Phys.J., **C34**, 399 (2004), arXiv:hep-ex/0404012 [hep-ex].

[13] R. Erbacher, A. Ivanov, and W. Johnson (CDF collaboration), CDF note 10104 (2010).
[14] R. Dermisek and J. F. Gunion, Phys.Rev., **D79**, 055014 (2009), arXiv:0811.3537 [hep-ph].
[15] R. Dermisek and J. F. Gunion, Phys.Rev., **D81**, 055001 (2010), arXiv:0911.2460 [hep-ph].
[16] R. Dermisek and J. F. Gunion, Phys.Rev., **D81**, 075003 (2010), arXiv:1002.1971 [hep-ph].
[17] F. Mahmoudi, J. Rathsman, O. Stal, and L. Zeune, Eur.Phys.J., **C71**, 1608 (2011), arXiv:1012.4490 [hep-ph].
[18] O. Stal and G. Weiglein, JHEP, **1201**, 071 (2012), arXiv:1108.0595 [hep-ph].
[19] M. S. Carena, S. Heinemeyer, C. E. M. Wagner, and G. Weiglein, Eur. Phys. J., **C26**, 601 (2003), arXiv:hep-ph/0202167.
[20] U. Ellwanger, J. F. Gunion, and C. Hugonie, JHEP, **02**, 066 (2005), arXiv:hep-ph/0406215.
[21] U. Ellwanger and C. Hugonie, Comput. Phys. Commun., **175**, 290 (2006), arXiv:hep-ph/0508022.
[22] P. Bechtle, O. Brein, S. Heinemeyer, G. Weiglein, and K. E. Williams, Comput.Phys.Commun., **181**, 138 (2010), arXiv:0811.4169 [hep-ph].
[23] P. Bechtle, O. Brein, S. Heinemeyer, G. Weiglein, and K. E. Williams, Comput.Phys.Commun., **182**, 2605 (2011), arXiv:1102.1898 [hep-ph].
[24] D. A. Vasquez, G. Belanger, C. Boehm, J. Da Silva, P. Richardson, *et al.*, (2012), arXiv:1203.3446 [hep-ph].
[25] R. Aaij *et al.* (LHCb collaboration), (2012), arXiv:1203.4493 [hep-ex].
[26] S. Chatrchyan *et al.* (CMS Collaboration), JHEP, **1204**, 033 (2012), arXiv:1203.3976 [hep-ex].
[27] G. Aad *et al.* (ATLAS Collaboration), (2012), arXiv:1204.2760 [hep-ex].
[28] S. Chatrchyan *et al.* (CMS Collaboration), (2012), arXiv:1205.5736 [hep-ex].
[29] *b-Jet Identification in the CMS Experiment*, Tech. Rep. CMS-PAS-BTV-11-004 (2012).
[30] *Measurement of the Mistag Rate with 5 fb*^{1} *of Data Collected by the ATLAS Detector*, Tech. Rep. ATLAS-CONF-2012-040 (CERN, Geneva, 2012).
[31] S. Chatrchyan *et al.* (CMS Collaboration), Phys. Rev. D, **84**, 092004. 39 p (2011).
[32] J. Alwall, M. Herquet, F. Maltoni, O. Mattelaer, and T. Stelzer, JHEP, **1106**, 128 (2011), arXiv:1106.0522 [hep-ph].
[33] D. Eriksson, J. Rathsman, and O. Stal, Comput.Phys.Commun., **181**, 189 (2010), arXiv:0902.0851 [hep-ph].
[34] M. Beneke, P. Falgari, S. Klein, and C. Schwinn, Nucl.Phys., **B855**, 695 (2012), arXiv:1109.1536 [hep-ph].
[35] M. Cacciari, G. P. Salam, and G. Soyez, JHEP, **0804**, 063 (2008), arXiv:0802.1189 [hep-ph].
[36] Y. L. Dokshitzer, G. Leder, S. Moretti, and B. Webber, JHEP, **9708**, 001 (1997), arXiv:hep-ph/9707323 [hep-ph].
[37] S. Catani, Y. L. Dokshitzer, M. Seymour, and B. Webber, Nucl.Phys., **B406**, 187 (1993).
[38] S. D. Ellis and D. E. Soper, Phys.Rev., **D48**, 3160 (1993), arXiv:hep-ph/9305266 [hep-ph].
[39] M. Cacciari and G. P. Salam, Phys.Lett., **B641**, 57 (2006), arXiv:hep-ph/0512210 [hep-ph].
[40] M. Cacciari, G. P. Salam, and G. Soyez, Eur.Phys.J., **C72**, 1896 (2012), arXiv:1111.6097 [hep-ph].
[41] D. Eriksson, G. Ingelman, J. Rathsman, and O. Stal, JHEP, **0801**, 024 (2008), arXiv:0710.5906 [hep-ph].
[42] W. Bernreuther, J.Phys.G, **G35**, 083001 (2008), arXiv:0805.1333 [hep-ph].
[43] R. M. Godbole, L. Hartgring, I. Niessen, and C. D. White, JHEP, **1201**, 011 (2012), arXiv:1111.0759 [hep-ph].
[44] G. Aad *et al.* (ATLAS Collaboration), Phys.Lett., **B710**, 49 (2012), arXiv:1202.1408 [hep-ex].
[45] S. Chatrchyan *et al.* (CMS Collaboration), Phys.Lett., **B710**, 26 (2012), arXiv:1202.1488 [hep-ex].
[46] L. J. Hall, D. Pinner, and J. T. Ruderman, JHEP, **1204**, 131 (2012), arXiv:1112.2703 [hep-ph].
[47] S. Heinemeyer, O. Stal, and G. Weiglein, Phys.Lett., **B710**, 201 (2012), arXiv:1112.3026 [hep-ph].
[48] A. Arbey, M. Battaglia, A. Djouadi, F. Mahmoudi, and J. Quevillon, Phys.Lett., **B708**, 162 (2012), arXiv:1112.3028 [hep-ph].

[49] M. Carena, S. Gori, N. R. Shah, and C. E. Wagner, JHEP, **1203**, 014 (2012), arXiv:1112.3336 [hep-ph].
[50] M. Kadastik, K. Kannike, A. Racioppi, and M. Raidal, JHEP, **1205**, 061 (2012), arXiv:1112.3647 [hep-ph].
[51] U. Ellwanger, JHEP, **1203**, 044 (2012), arXiv:1112.3548 [hep-ph].
[52] J. Cao, Z. Heng, D. Li, and J. M. Yang, Phys.Lett., **B710**, 665 (2012), arXiv:1112.4391 [hep-ph].
[53] J. Cao, Z. Heng, J. M. Yang, Y. Zhang, and J. Zhu, JHEP, **1203**, 086 (2012), arXiv:1202.5821 [hep-ph].
[54] U. Ellwanger and C. Hugonie, (2012), arXiv:1203.5048 [hep-ph].

Paper II

Das Grab im Busento

Nächtlich am Busento lispeln
bei Cosenza dumpfe Lieder.
Aus den Wassern schallt es Antwort,
in den Wirbeln klingt es wider.

Und den Fluss hinauf, hinunter
zieh'n die Schatten tapfrer Goten,
Die den Alarich beweinen,
ihres Volkes besten Toten.

Allzu früh und fern der Heimat
mussten sie ihn hier begraben,
Während noch die Jugendlocken
seine Schultern blond umgaben.

Und am Ufer des Busento
reihten sie sich um die Wette.
Um die Strömung abzuleiten
gruben sie ein frisches Bette.

In der wogenleeren Höhlung
wühlten sie empor die Erde,
Senkten tief hinein den Leichnam
mit der Rüstung, auf dem Pferde.

Deckten dann mit Erde wieder
ihn und seine stolze Habe,
Dass die hohen Stromgewächse
wüchsen aus dem Heldengrabe.

Abgelenkt zum zweiten Male,
ward der Fluss herbeigezogen.
Mächtig in ihr altes Bette
schäumten die Busentowogen.

Und es sang ein Chor von Männern
"Schlaf in deinen Heldenehren!
Keines Römers schnöde Habsucht
soll dir je dein Grab versehren!"

Sangen's, und die Lobgesänge
tönten fort im Gotenheere.
Wälze sie, Busentowelle,
wälze sie von Meer zu Meere!

August Graf von Platen

LU TP 14-38
arXiv:1411.6384 [hep-lat]
Revised January 2015

Finite Volume at Two-loops in Chiral Perturbation Theory

Johan Bijnens and Thomas Rössler

Department of Astronomy and Theoretical Physics, Lund University,
Sölvegatan 14A, SE 223-62 Lund, Sweden

Abstract

We calculate the finite volume corrections to meson masses and decay constants in two and three flavour Chiral Perturbation Theory to two-loop order. The analytical results are compared with the existing result for the pion mass in two-flavour ChPT and the partial results for the other quantities. We present numerical results for all quantities.

1 Introduction

Lattice QCD now provides good calculations of a number of quantities relevant for low-energy particle physics as reviewed in [1]. These need several extrapolations, in the quark masses, in the lattice spacing, in the lattice size and in lattice artefacts. Chiral Perturbation Theory (ChPT) [2, 3, 4] provides guidance for all of these extrapolations. In particular, it can be used to estimate the corrections due to the finite lattice size. This was introduced by Gasser and Leutwyler in [5, 6, 7]. This is an alternative method compared to the one introduced by Lüscher [8] where the leading finite size corrections can be derived using the scattering amplitude.

In this paper we will restrict ourselves to the p-regime with $m_\pi L >> 1$. We will not do the all order integration over the zero mode as is necessary in the so-called ϵ-regime [5, 6, 7]. The finite volume corrections to the mass and decay constant in the equal mass case to one-loop order were calculated in these original papers. Since then, there have been many studies of finite size effects at one-loop order in ChPT, in particular the masses and decay constants to that order were derived in [9] and [10].

In infinite volume the ChPT expressions for masses and decay constants are known for all relevant cases and including a number of extensions as e.g. partially quenched ChPT to two-loop order. This is reviewed in [11]. There exist a few two-loop calculations at finite volume in ChPT. The mass in two-flavour ChPT was studied in [12] and the quark-anti quark vacuum expectation value in three-flavour ChPT in [13], the latter can be extended to the ϵ-regime [14].

The main purpose of this paper is to provide the two-loop finite volume expressions in two and three-flavour ChPT for the masses and decay constants. The extension to partially quenched ChPT is planned for future work. The main reason this was not done earlier is the complexity of the sunset integral at finite volume. The needed integrals have been recently worked out in [15]. We will use their expressions extensively. Our expressions are valid in the frame with $\vec{p} = 0$, often called the center-of-mass frame. In the so-called moving frames or with twisted boundary conditions there will be additional terms.

Some preliminary numerical results were reported in [16]. We find the typical $e^{-m_\pi L}$ behaviour for most quantities as expected. The corrections for the pion mass and decay constant are significant at the present lattice size and precision in lattice QCD calculations. The corrections for the kaon decay constant are needed but are not quite as large. The kaon mass has corrections below 1% and the corrections for the eta mass and decay constant turn out to be negligible at present precision. These results are in qualitative agreement with the earlier work.

We give a short list of references for ChPT and discuss some small points in Sect. 2. The definitions of the integrals we use and how they relate to the results in [15] is given in Sect. 3. The next section contains our first major results. The full finite volume correction to the pion mass and decay constant to two-loop order in ChPT. Sect. 5 contains the results for the three-flavour case for pion, kaon and eta for both the mass and decay constant but the large two-loop order formulas are collected in the appendices. The detailed numerical discussion of our results is in Sect. 6.

2 Chiral Perturbation Theory

An introduction to ChPT can be found in [17] and in the two-loop review [11]. The lowest order and p^4-Lagrangian can be found in [3] and [4] for the two and three flavour case respectively. The order p^6 Lagrangian is given in [18]. We use the standard renormalization scheme in ChPT. The needed part for the finite volume integrals is discussed in Sect. 3. An extensive discussion of the scheme can be found in [19] and [20]. An important comment is that the LECs do not depend on the volume [7].

We prefer to designate orders by the p-counting order at which the diagram appears. Thus we refer to order p^2, order p^4 or one-loop order and order p^6 or two-loop order and include in the terminology one- or two-loop order also the diagrams with fewer loops but the same order in p-counting.

We present the formulas here in terms of the physical *infinite* volume masses and decay constants.

3 Comments on the finite volume integrals

The loop integrals at finite volume at one-loop are well known. The difference with infinite volume is that there is a sum over discrete momenta in every direction with a finite size rather than a continuous integral. The use of the Poisson summation formula allows to identify the infinite volume part and the finite volume corrections. The remainder can be done in two ways. For one-loop tadpole integrals the first one was introduced in the original work [5, 6, 7] and one remains with a sum over Bessel functions, that for large ML converges fast. The other method can be found in [9] and one remains with an integral over a Jacobi theta function, this method can be used for small and medium ML as well. The extensions to other one-loop integrals can be done in both cases by combining propagators with Feynman parameters. The first method was extended to the equal mass two-loop sunset integral in [12]. The general mass case was then done in both methods in [15]. The methods are explained in detail in [15] for both the one and two-loop case. Note that here we use Minkowski notation for the integrals.

The tadpole integrals A and $A_{\mu\nu}$ are defined via

$$\left\{A(m^2), A_{\mu\nu}(m^2)\right\} = \frac{1}{i}\int_V \frac{d^d r}{(2\pi)^d}\frac{\{1, r_\mu r_\nu\}}{(r^2-m^2)}\,. \tag{1}$$

The B^0 tadpole integrals are defined similarly with a doubled propagator, alternatively as the derivative w.r.t. m^2 of the A-tadpoles. The subscript V on the integral indicates that the integral is a discrete sum over the three spatial components and an integral over the remainder. At finite volume, there are more Lorentz-structures possible. We define the tensor $t_{\mu\nu}$ as the spatial part of the Minkowski metric $g_{\mu\nu}$, to express these. For the center-of-mass (cms) case this is sufficient. The needed functions for $A_{\mu\nu}$ are

$$A_{\mu\nu}(m^2) = g_{\mu\nu}A_{22}(m^2) + t_{\mu\nu}A_{23}(m^2)\,. \tag{2}$$

In infinite volume A_{22} can be rewritten in terms of A. At finite volume, the relation is

$$dA_{22}(m^2) + 3A_{23}(m^2) = m^2 A(m^2)\,. \tag{3}$$

This is used to remove A_{22} from our expressions. In addition we do an expansion in ϵ with $d = 4 - 2\epsilon$ via

$$A(m^2) = \lambda_0 \frac{m^2}{16\pi^2} + \overline{A}(m^2) + A^V(m^2) + \epsilon\left(A^\epsilon(m^2) + A^{V\epsilon}(m^2)\right) + \cdots\,. \tag{4}$$

with $\lambda_0 = \frac{1}{\epsilon} + \log(4\pi) + 1 - \gamma$ and similarly for the other one-loop integrals. λ_0 corresponds to the usual $\overline{MS}$ variant used in ChPT. Doing the renormalization introduces a subtraction point dependence which corresponds to using for $\overline{A}(m^2)$ and $\overline{B}^0(m^2)$

$$\overline{A}(m^2) = \frac{-m^2}{16\pi^2}\log\frac{m^2}{\mu^2}\,, \quad \overline{B}^0(m^2) = \frac{-1}{16\pi^2}\left(\log\frac{m^2}{\mu^2} + 1\right)\,. \tag{5}$$

The sunset integrals are defined as

$$\begin{aligned}\left\{H, H_\mu, H^s_\mu, H_{\mu\nu}, H^{rs}_{\mu\nu}, H^{ss}_{\mu\nu}\right\}(m_1^2, m_2^2, m_3^2, p) = \\ \frac{1}{i^2}\int_V \frac{d^d r}{(2\pi)^d}\frac{d^d s}{(2\pi)^d}\frac{\{1, r_\mu, s_\mu, r_\mu r_\nu, r_\mu s_\nu, s_\mu s_\nu\}}{(r^2 - m_1^2)\,(s^2 - m_2^2)\,((r+s-p)^2 - m_3^2)}\,.\end{aligned} \tag{6}$$

The subscript V again indicates that the spatial dimensions are a discrete sum rather than an integral. The conventions correspond to those in infinite volume of [21]. The interchange $r, m_1^2 \leftrightarrow s, m_2^2$ shows that $H^s_\mu, H^{ss}_{\mu\nu}$ are related directly to $H^r_\mu, H^{rr}_{\mu\nu}$. $H^{rs}_{\mu\nu}$ can also be related to $H_{\mu\nu}$ using the trick shown in [21] which remains valid at finite volume in the cms frame [15].

In the cms frame we define the functions[1]

$$\begin{aligned} H_\mu &= p_\mu H_1 \\ H_{\mu\nu} &= p_\mu p_\nu H_{21} + g_{\mu\nu} H_{22} + t_{\mu\nu} H_{27}\,. \end{aligned} \tag{7}$$

The arguments of all functions in the cms frame are $(m_1^2, m_2^2, m_3^2, p^2)$. These functions satisfy the relations, valid in finite volume [15],

$$\begin{aligned} H_1(m_1^2, m_2^2, m_3^2, p^2) + H_1(m_2^2, m_3^2, m_1^2, p^2) + H_1(m_3^2, m_1^2, m_2^2, p^2) &= H(m_1^2, m_2^2, m_3^2, p^2)\,, \\ p^2 H_{21} + d H_{22} + 3H_{27} - m_1^2 H &= A(m_2^2)A(m_3^2)\,. \end{aligned} \tag{8}$$

The arguments of the sunset functions in the second relation are all $(m_1^2, m_2^2, m_3^2, p^2)$. These relations have been used to remove H_{22} from the final result and simplify the expressions somewhat.

[1] In the cms frame we have that $t_{\mu\nu} = g_{\mu\nu} - p_\mu p_\nu / p^2$ but the given separation appears naturally in the calculation [15]. It also avoids singularities in the limit $p \to 0$.

We now split the functions in an infinite volume part $\tilde{H}_i$ and a finite volume correction $\tilde{H}_i^V$ with $H_i = \tilde{H}_i + \tilde{H}_i^V$. The infinite volume part was derived in [21]. For the finite volume parts we define

$$\begin{aligned}
\tilde{H}^V &= \frac{\lambda_0}{16\pi^2}\left(A^V(m_1^2)+A^V(m_2^2)+A^V(m_3^2)\right)+\frac{1}{16\pi^2}\left(A^{V\epsilon}(m_1^2)+A^{V\epsilon}(m_2^2)+A^{V\epsilon}(m_3^2)\right) \\
&\quad +H^V\,, \\
\tilde{H}_1^V &= \frac{\lambda_0}{16\pi^2}\frac{1}{2}\left(A^V(m_2^2)+A^V(m_3^2)\right)+\frac{1}{16\pi^2}\frac{1}{2}\left(A^{V\epsilon}(m_2^2)+A^{V\epsilon}(m_3^2)\right)+H_1^V\,, \\
\tilde{H}_{21}^V &= \frac{\lambda_0}{16\pi^2}\frac{1}{3}\left(A^V(m_2^2)+A^V(m_3^2)\right)+\frac{1}{16\pi^2}\frac{1}{3}\left(A^{V\epsilon}(m_2^2)+A^{V\epsilon}(m_3^2)\right)+H_{21}^V\,, \\
\tilde{H}_{27}^V &= \frac{\lambda_0}{16\pi^2}\left(A_{23}^V(m_1^2)+\frac{1}{3}A_{23}(m_2^2)+\frac{1}{3}A_{23}^V(m_3^2)\right) \\
&\quad +\frac{1}{16\pi^2}\left(A_{23}^{V\epsilon}(m_1^2)+\frac{1}{3}A_{23}^{V\epsilon}(m_2^2)+\frac{1}{3}A_{23}^{V\epsilon}(m_3^2)\right)+H_{27}^V\,, \qquad (9)
\end{aligned}$$

Note that the finite parts are defined slightly different compared to the infinite volume definition in [21]. Here we have pulled out the extra parts with $A^{V\epsilon}$. These functions cancel in the final result. We will also use the derivatives w.r.t. p^2 of the sunset integrals. These we denote with an extra prime, $H_i^{V\prime} \equiv (\partial/\partial p^2) H_i^V$.

The functions H_i^V can be computed with the methods of [15]. They correspond to adding the parts labeled with G and H in Sect. 4.3 and the part of Sect. 4.4 in [15]. We have in addition added the derivatives w.r.t. p^2 for all the integrals and checked the analytical results with numerical differentiation.

For all cases discussed we have done checks that both methods, via Bessel or Jacobi theta functions, give the same results.

4 Two-flavour results

The diagrams needed to obtain the mass are shown in Fig. 1. We write the result for the mass at finite volume in the form

$$m_\pi^{V2} = m_\pi^2 + \Delta^V m_\pi^2\,, \quad \Delta^V m_\pi^2 = \Delta^V m_\pi^{2(4)} + \Delta^V m_\pi^{2(6)}\,. \qquad (10)$$

m_π^2 and F_π denote the infinite volume physical pion mass and decay constant. We have reproduced the expression for the infinite volume mass derived in [22, 23, 24]. The extra parts due to the finite volume are

$$\begin{aligned}
F_\pi^2 \Delta^V m_\pi^{2(4)} &= -\frac{1}{2} m_\pi^2 A^V(m_\pi^2)\,, \\
F_\pi^4 \Delta^V m_\pi^{2(6)} &= m_\pi^4 A^V(m_\pi^2)\left(-l_4^r+5\,l_3^r+8\,l_2^r+14\,l_1^r\right)+m_\pi^2 A_{23}^V(m_\pi^2)\left(-12\,l_2^r-6\,l_1^r\right) \\
&\quad +A^V(m_\pi^2)\left(13/12\,\frac{1}{16\pi^2}\,m_\pi^4-7/4\,\overline{A}(m_\pi^2)\,m_\pi^2\right)+A^V(m_\pi^2)^2\left(-3/8\,m_\pi^2\right) \\
&\quad +A^V(m_\pi^2)\,B^{0V}(m_\pi^2)\left(1/4\,m_\pi^4\right)+H^V(m_\pi^2,m_\pi^2,m_\pi^2,m_\pi^2)\left(5/6\,m_\pi^4\right) \\
&\quad +H_{21}^V(m_\pi^2,m_\pi^2,m_\pi^2,m_\pi^2)\left(3\,m_\pi^4\right)+H_{27}^V(m_\pi^2,m_\pi^2,m_\pi^2,m_\pi^2)\left(-3\,m_\pi^2\right). \qquad (11)
\end{aligned}$$

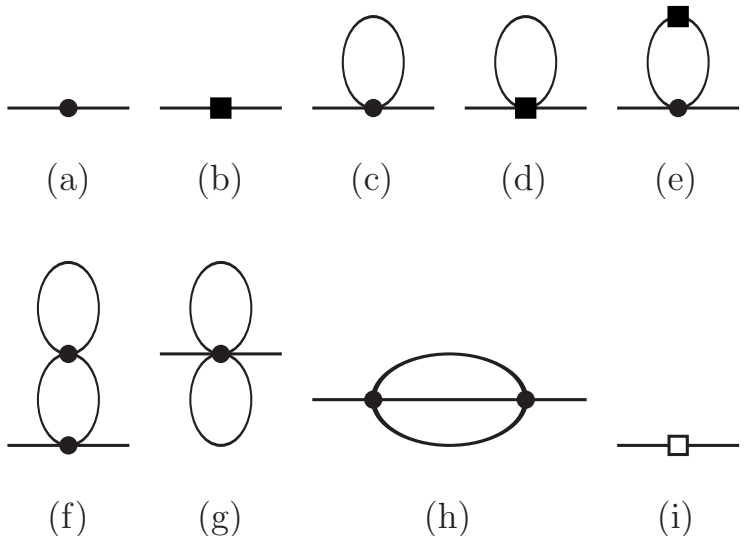

Figure 1: The Feynman diagrams needed for the mass calculation. A dot indicates a vertex of order p^2, a filled box of order p^4 and an open box of order p^6.

$\Delta^V m_\pi^{2(4)}$ agrees with the results of [5]. The comparison of $\Delta^V m_\pi^{2(6)}$ with the result in [12] is not quite so simple. The reason is that the splitting in parts has been done very differently there and here. However, we agree on the sunset part, (44) in [12] and on the part that has l_i^r multiplying finite volume integrals in (38) in [12]. The latter was first derived in [25]. Both their and our result are independent of the subtraction scale.

The pion decay constant is defined by

$$\langle 0|\bar{u}\gamma_\mu\gamma_5 d|\pi^-(p)\rangle = \sqrt{2}iF_\pi p_\mu\,. \tag{12}$$

It can be computed by the diagrams of Fig. 1 where the outgoing meson is replaced by an insertion of the axial current. The diagrams needed for wave-function renormalization are the same as those for the mass. The calculation proceeds along the same lines as above. We reproduce the known infinite volume results of [22, 23, 24]. The decay constant at finite volume we write as

$$F_\pi^V = F_\pi + \Delta^V F_\pi\,, \quad \Delta^V F_\pi = \Delta^V F_\pi^{(4)} + \Delta^V F_\pi^{(6)}\,. \tag{13}$$

The results are:

$$\begin{aligned}
F_\pi \Delta^V F_\pi^{(4)} &= A^V(m_\pi^2)\,, \\
F_\pi^3 \Delta^V F_\pi^{(6)} &= +A^V(m_\pi^2) m_\pi^2 \left(3/2\, l_4^r - 4\, l_2^r - 7\, l_1^r\right) + A_{23}^V(m_\pi^2)\left(6\, l_2^r + 3\, l_1^r\right) \\
&\quad +A^V(m_\pi^2)\left(-1/3\,\frac{1}{16\pi^2}\, m_\pi^2 + 1/2\,\overline{A}(m_\pi^2)\right) + A^V(m_\pi^2)\, B^{0V}(m_\pi^2)\left(-1/2\, m_\pi^2\right) \\
&\quad +H^V(m_\pi^2, m_\pi^2, m_\pi^2, m_\pi^2)\left(-1/2\, m_\pi^2\right) + H_{27}^V(m_\pi^2, m_\pi^2, m_\pi^2, m_\pi^2)\left(3/2\right)
\end{aligned}$$

$$+H^{V\prime}(m_\pi^2,m_\pi^2,m_\pi^2,m_\pi^2)\left(5/12\,m_\pi^4\right)+H_{21}^{V\prime}(m_\pi^2,m_\pi^2,m_\pi^2,m_\pi^2)\left(3/2\,m_\pi^4\right)$$
$$+H_{27}^{V\prime}(m_\pi^2,m_\pi^2,m_\pi^2,m_\pi^2)\left(-3/2\,m_\pi^2\right). \qquad (14)$$

$\Delta^V F_\pi^{(4)}$ agrees with the results of [5]. Here there exists no full two-loop calculation but an evaluation for the case with at most one propagator at finite volume [26]. We agree with their result for the terms containing l_i^r if the term multiplying B^2 in (54) in that paper is divided by 2. Comparing with the remainder is difficult due to the very different treatment of the loop integrals.

5 Three-flavour results

The principle of the calculation is exactly the same as before. The diagrams needed for the mass are shown in Fig. 1. However, we now need to use the three-flavour Lagrangians and include the kaons and eta as well. As a result the expressions become much more cumbersome. Here we use as symbols, m_π, m_K and m_η as the physical volume pion, kaon and eta mass at infinite volume. We have rewritten all expressions as an expansion in these masses and in the physical pion decay constant at infinite volume. Given that the eta mass to lowest order is given by the Gell-Mann–Okubo relation, there is an inherent ambiguity in precisely how one writes the result in the combination of kaon and eta masses. The form of the p^6 result given here is to be used together with the form for the p^4 expressions given here as well.

The pion, kaon and eta masses at two-loop order in infinite volume are known, [21], we have reproduced that result. The finite volume corrections for the masses are given by

$$m_i^{V2}=m_i^2+\Delta^V m_i^2\,,\quad \Delta^V m_i^2=\Delta^V m_i^{2(4)}+\Delta^V m_i^{2(6)}\,, \qquad (15)$$

for $i=\pi,K,\eta$. The p^4 results are:

$$\begin{aligned}
F_\pi^2\Delta^V m_\pi^{2(4)} &= A^V(m_\pi^2)\left(-1/2\,m_\pi^2\right)+A^V(m_\eta^2)\left(1/6\,m_\pi^2\right),\\
F_\pi^2\Delta^V m_K^{2(4)} &= A^V(m_\eta^2)\left(-1/4\,m_\eta^2-1/12\,m_\pi^2\right),\\
F_\pi^2\Delta^V m_\eta^{2(4)} &= A^V(m_\pi^2)\left(1/2\,m_\pi^2\right)+A^V(m_K^2)\left(-m_\eta^2-1/3\,m_\pi^2\right)\\
&\quad +A^V(m_\eta^2)\left(8/9\,m_K^2-7/18\,m_\pi^2\right). \qquad (16)
\end{aligned}$$

These agree with the expressions in [9, 10, 27]. The way in which the corrections are written is to be in agreement with the way the infinite volume result was written in [21]. The order p^6 expressions are rather large, they can be found in App. A. The contributions with at most one pion propagator at finite volume were calculated in [27] for the kaon and eta in three flavour ChPT, the expression for the pion was done in two-flavour ChPT and discussed above. We agree with the L_i^r times finite volume part there. The remainder is difficult to compare due to the different treatment of the integrals.

The decay constants for the mesons are defined similarly to (12) via

$$\begin{aligned}
\langle 0|\bar{u}\gamma_\mu\gamma_5 d|\pi^-(p)\rangle &= \sqrt{2}iF_\pi p_\mu\,, \\
\langle 0|\bar{u}\gamma_\mu\gamma_5 s|K^-(p)\rangle &= \sqrt{2}iF_K p_\mu\,, \\
\langle 0|\frac{1}{\sqrt{6}}\left(\bar{u}\gamma_\mu\gamma_5 u + \bar{d}\gamma_\mu\gamma_5 d - 2\bar{s}\gamma_\mu\gamma_5 s\right)|\eta(p)\rangle &= \sqrt{2}iF_\eta p_\mu\,. \qquad (17)
\end{aligned}$$

Note that since we work in the isospin limit, we use the octet axial current to define the eta decay constant.

We define

$$F_i^V = F_i + \Delta^V F_i\,, \quad \Delta^V F_i = \Delta^V F_i^{(4)} + \Delta^V F_i^{(6)}\,, \qquad (18)$$

for $i = \pi, K, \eta$. The pion, kaon and eta decay constants at two-loop order in infinite volume are known, [21], we have reproduced that result. Note that we give the corrections to the decay constants here, not divided by the chiral limit decay constant as in [21]. Note the correction for the expressions for the infinite volume decay constants described in the erratum of [28]. The correct expressions can be downloaded from [29]

The order p^4 results are

$$\begin{aligned}
F_\pi\Delta^V F_\pi^{(4)} &= A^V(m_\pi^2) + A^V(m_K^2)\left(1/2\right), \\
F_\pi\Delta^V F_K^{(4)} &= A^V(m_\pi^2)\left(3/8\right) + A^V(m_K^2)\left(3/4\right) + A^V(m_\eta^2)\left(3/8\right), \\
F_\pi\Delta^V F_\eta^{(4)} &= A^V(m_K^2)\left(3/2\right). \qquad (19)
\end{aligned}$$

These agree with [9, 10, 27]. The p^6 expressions are again rather long and are given in App. B. The contributions with at most one-pion propagator at finite volume were calculated in [27] for the kaon in three flavour ChPT, the expression for the pion was done in two-flavour ChPT and discussed above. We agree with the L_i^r dependent part if we multiply the contribution from the term with B^2 in (57) in by 1/2. This is the same factor we needed to get agreement for the two-flavour pion decay constant.

6 Numerical results

For numerical input we use $F_\pi = 92.2$ MeV, $m_\pi = m_{\pi^0} = 134.9764$ MeV, the average m_K with electromagnetic effects removed with the estimate of [30], $m_K = 494.53$ MeV, and $m_\eta = 547.30$ MeV. The values of the low-energy constants, we take from the last review [31]. We always use a subtraction scale $\mu = 770$ MeV.

6.1 Two-flavour results

The l_i^r we use we define via the usual $\bar{l}_i$ defined at the scale of the charged pion mass. The actual values we use are $\bar{l}_1 = -0.4, \bar{l}_2 = 4.3, \bar{l}_3 = 3.0, \bar{l}_4 = 4.3$. The relative finite volume corrections to m_π^2 are shown in Fig. 2(a) as a function of $m_\pi L$. We have checked that

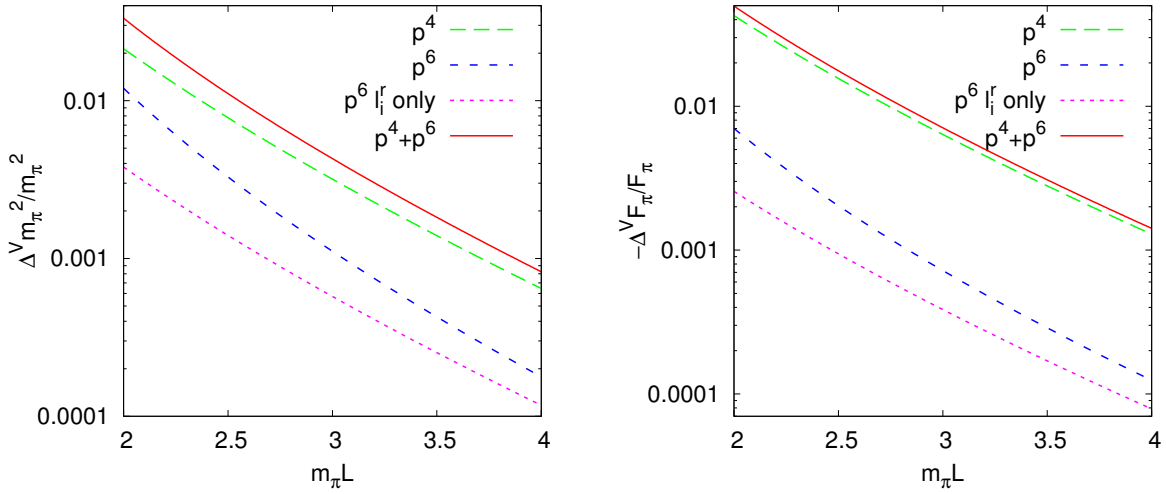

(a) (b)

Figure 2: The relative finite volume corrections for the mass squared and decay constant of the pion in two-flavour ChPT at a fixed infinite volume pion mass $m_\pi = m_{\pi^0}$. Shown are the one-loop or p^4 corrections, the full p^6 result and the part only dependent on the l_i^r, $p^6 l_i^r$, and the sum of the p^4 and p^6 result. $m_\pi L = 2, 4$ correspond to $L \approx 2.9, 5.8$ fm. (a) The pion mass, plotted is $(m_\pi^{V2} - m_\pi^2)/m_\pi^2$. (b) The pion decay constant. Plotted is $-(F_\pi^V - F_\pi)/F_\pi$.

changing the scale to $\mu = 500$ MeV does not change the result, but it does increase the l_i^r part. The equivalent plot for the relative correction to F_π is shown in Fig. 2(b).

We can also perform a study of the corrections at other values of m_π or as a function of m_π. One of the problems here is what to with the value of F_π that should be used. If we use the infinite volume formulas to two-loop order of [24] which are expressed in the form $F_\pi/F = f(F_\pi, m_\pi)$ for another pion mass $\tilde{m}_\pi$ we determine the associated value of the decay constant, $\tilde{F}_\pi$ by solving $\tilde{F}_\pi/F_\pi = f(\tilde{F}_\pi, \tilde{m}_\pi)/f(F_\pi, m_\pi)$ numerically. The contribution from the p^6 LECs c_i^r we have put to zero. This procedure might differ from the values of $\tilde{F}_\pi$ used in [12]. To compare with their numerical results we have plotted in Fig. 3 the equivalent of their Fig. 5. Namely $R_{m_\pi} = m_\pi^V/m_\pi - 1$ where we have numerically calculated $R_{m_\pi} = \sqrt{(m_\pi^2 + \Delta^V m_\pi^2)/m_\pi^2} - 1$. The calculated values of F_π are $90.1, 103.2, 113.8$ for $m_\pi = 100, 300, 500$ MeV. The resulting values of R_{m_π} as shown in Fig. 3(a) are in reasonable agreement with Fig. 5 in [12]. There is already a difference at order p^4, so we suspect it is simply due to somewhat different values of F_π. The one-loop result for R_{F_π} agrees with Fig. 2 in [26] with small differences probably due to the difference in F_π and the difference in the l_i^r-dependent part. Our result for the p^6 result is somewhat larger.

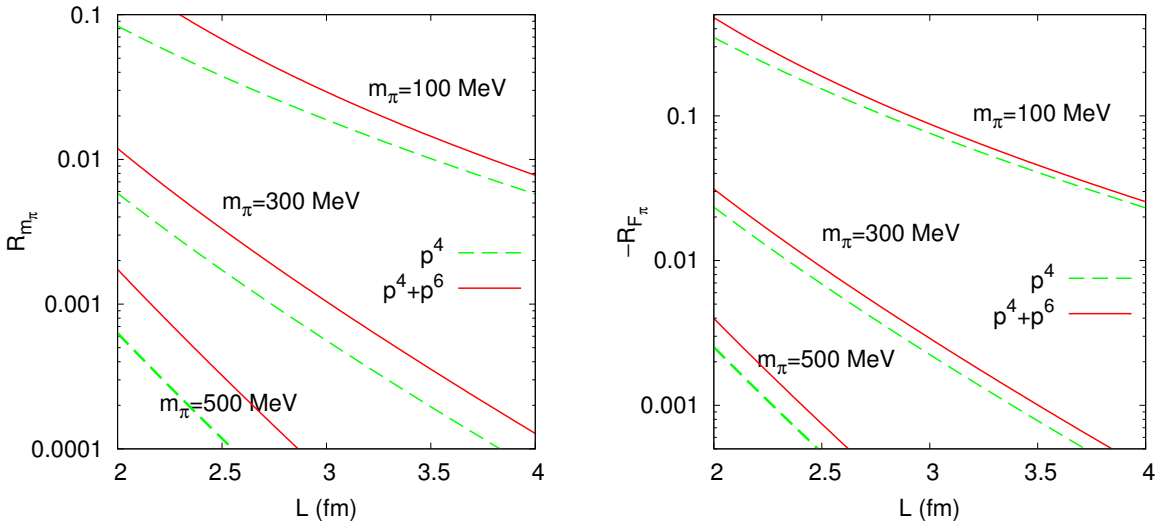

Figure 3: The relative finite volume corrections for the mass and decay constant of the pion in two-flavour ChPT at three values of the infinite volume pion mass. (a) $R_{m_\pi} = m_\pi^V/m_\pi - 1$. (b) $R_{F_\pi} = F_\pi^V/F_\pi - 1$, plotted is $-R_{F_\pi}$.

6.2 Three-flavour results: masses

The values of the low-energy constants, L_i^r and C_i^r, we take from the review [31], in particular the set labeled BE14 there. In addition, the formulas require the infinite volume physical masses for the pion, kaon and eta mass as well as the pion decay constant. The masses and F_π we use for the physical isospin averaged case are listed at the start of this section. For changed values of the infinite volume pion and kaon mass, $\tilde{m}_\pi, \tilde{m}_K$, we proceed similarly to F_π for the two-flavour case. We solve self-consistently the set of equations for $\tilde{m}_\eta$, $\tilde{F}_\pi$, $\tilde{F}_K/\tilde{F}_\pi$ and $\tilde{F}_\eta/\tilde{F}_\pi$. For the latter ratios we use the expanded version, similar to what was done in [31], see Eq. (45) in there. The results for a number of input cases is shown in Tab. 1. The top line is the physical case. The resulting output is within the expected quality of the fit in [31]. The next two lines have the kaon mass tuned to keep the same value of m_s. The value of F_π can be compared with the result for the two-flavour case given above.

Let us have a look at the pion mass finite volume corrections for the physical case. The comparison of the two- and three-flavour results are plotted in Fig. 4(a). The one-loop result differs only by a very small kaon and eta loop. The difference is not visible in the figure. The two-loop results are also in very good agreement. The convergence is quite reasonable.

The equivalent results for the kaon and eta are plotted in Fig. 5. The one-loop result for the kaon mass has only an eta loop as can be seen from (16). As a result, that part is very small. The total result is thus essentially coming only from two-loop order. The eta mass has a negative one-loop finite volume contribution. The pure loop part and the

m_π	m_K	m_η	F_π	F_K/F_π	F_η/F_π	$\hat{m}/\hat{m}_{\rm phys}$	$m_s/m_{s\rm phys}$	$m_s/\hat{m}$
134.9764*	494.53*	545.9	92.2*	1.199	1.306	1*	1*	27.3
100	487.14	540.46	90.4	1.219	1.337	0.547	1.000	49.9
300	549.6	593.73	101.4	1.099	1.154	5.025	1.000	5.43
100	400	446.53	87.3	1.199	1.293	0.518	0.644	33.9
100	495	549.07	90.7	1.219	1.340	0.550	1.037	51.4
300	495	533.00	100.3	1.094	1.138	4.867	0.778	4.36
495	495	495.00	108.0	1	1	12.70	0.465	1

Table 1: The self consistent solution for the infinite volume values of m_η, F_π, F_K, F_η and the output quark mass ratios compared with the physical one. Units for dimensional quantities are in MeV. The input values for the physical case are starred.

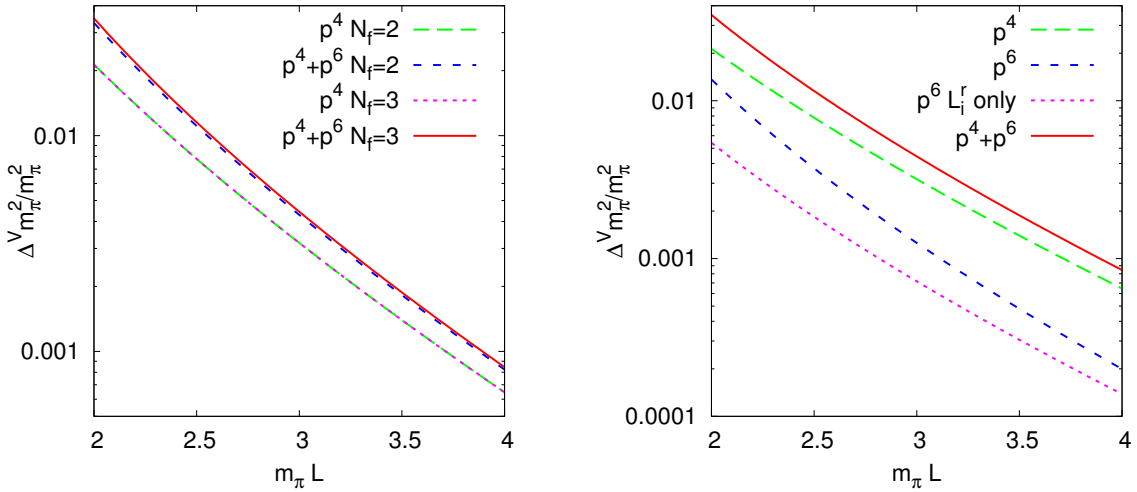

(a) (b)

Figure 4: The finite volume corrections to the pion mass squared at $m_\pi = m_{\pi^0}$. All other inputs are given in the text. Plotted is the quantity $(m_\pi^{V2} - m_\pi^2)/m_\pi^2$. (a) Comparison of the two- and three-flavour ChPT results. (b) The corrections for the three-flavour case also showing the L_i^r dependent part.

L_i^r-dependent part of the p^6 contribution are of the expected size. However, there is a very strong cancellation between the two parts leaving a very small positive correction. The total finite volume correction for the eta mass is negative.

We can also check how the finite volume correction depends on the different masses. In Fig. 6 we have plotted the corrections to the pion mass squared for a number of different scenarios. In Fig. 6(a) we look at three cases. The bottom two lines are the physical case labeled with $m_\pi = m_{\pi^0}$ while the top four lines are with $m_\pi = 100$ MeV. There we have plotted two cases, $m_K = 400$ and 495 MeV. The effect of the change in the pion mass is quite large while the effect due to the kaon mass change is smaller. The effect of changing

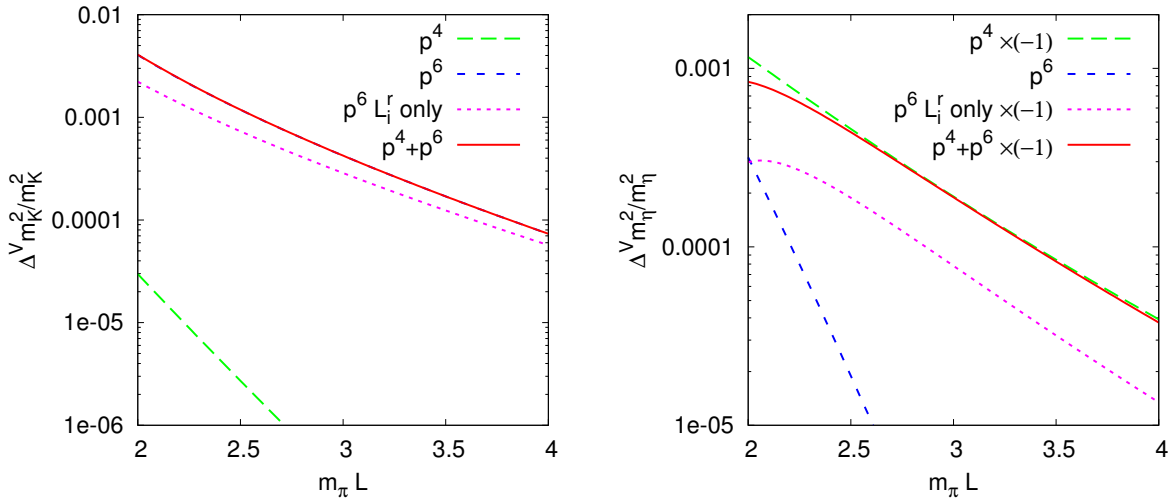

(a) (b)

Figure 5: The corrections to the kaon and eta mass squared for the physical case. Plotted is the quantity $(m_i^{V2} - m_i^2)/m_i^2$ for $i = K, \eta$. Shown are the one-loop, the two-loop, the sum and the two-loop L_i^r dependent part. (a) Kaon, the p^4 is so small that p^6 and $p^4 + p^6$ are indistinguishable. (b) Eta, note the signs, some parts are negative.

the pion mass can be better seen in Fig. 6(b) where we kept the kaon mass at 495 MeV while varying the pion mass. The L dependence is given as a function of $m_{\pi^0} L$ with the physical π^0 mass.

We have plotted the same cases for the finite volume corrections to the kaon mass squared in Fig. 7. The one-loop correction for the physical case and $m_\pi, m_K = 100, 495$ MeV is virtually identical. The $p^4 + p^6$ is a bit more different for the three cases as can be seen in Fig. 7(a). In Fig. 7(b) we have shown the corrections for a fixed kaon mass but three different pion masses. The bottom three lines are the one-loop result while the top three lines are the full result. Note that, as it should be, the case where the pion mass and kaon mass are the same, the finite volume corrections to the kaon are the same as for the pion in Fig. 6(b). This is another small check on our result.

We have plotted the same cases once more for the finite volume corrections to the eta mass squared in Fig. 8. Here the result is rather variable due to cancellations. In Fig. 8(a) the one-loop corrections increase going from the physical case via $m_\pi, m_K = 100, 495$ MeV to $m_\pi, m_K = 100, 400$ MeV. The two-loop corrections are rather small in the first two cases, due to the cancellations between the pure two-loop and the L_i^r dependent part. The one-loop correction for the physical case and $m_\pi, m_K = 100, 495$ MeV is virtually identical. The $p^4 + p^6$ is a bit more different for the three cases. In Fig. 8(b) we have shown the corrections for a fixed kaon mass but three different pion masses. The bottom lines are the case with $m_\pi, m_K = 495$ MeV. It agrees with the pion and kaon corrections for this case. For $m_\pi = 300$ MeV the correction is negative but goes through zero for small L due

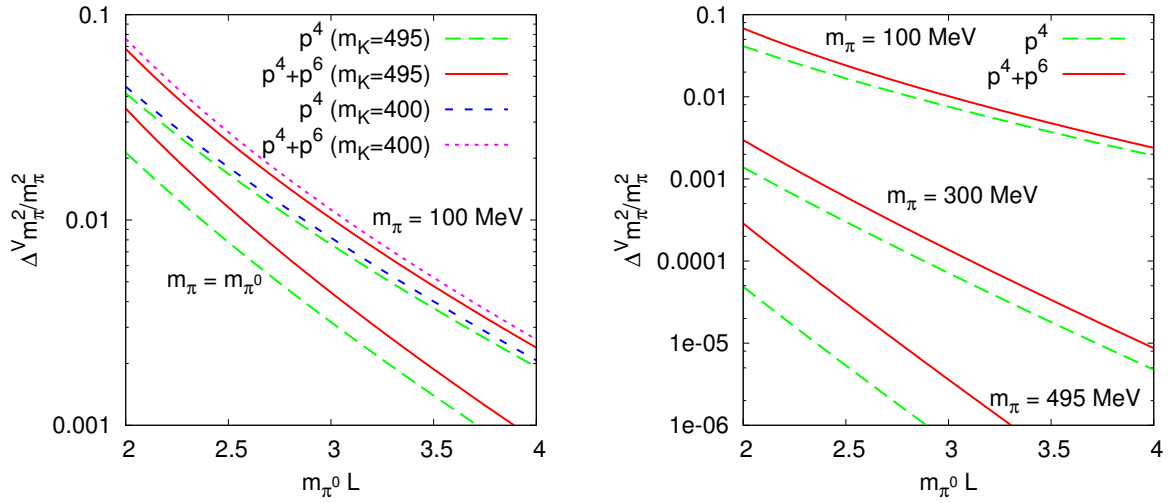

(a) (b)

Figure 6: The finite volume corrections to the pion mass squared for a number of cases listed in Tab. 1. Plotted is the quantity $(m_\pi^{V2} - m_\pi^2)/m_\pi^2$. (a) Physical case, bottom two lines, $(m_\pi, m_K) = (100, 495)$ and $(100, 400)$ MeV. (b) $m_K = 495$ MeV and $m_\pi = 100, 300, 495$ MeV. The size L is given in units of the physical π^0 mass.

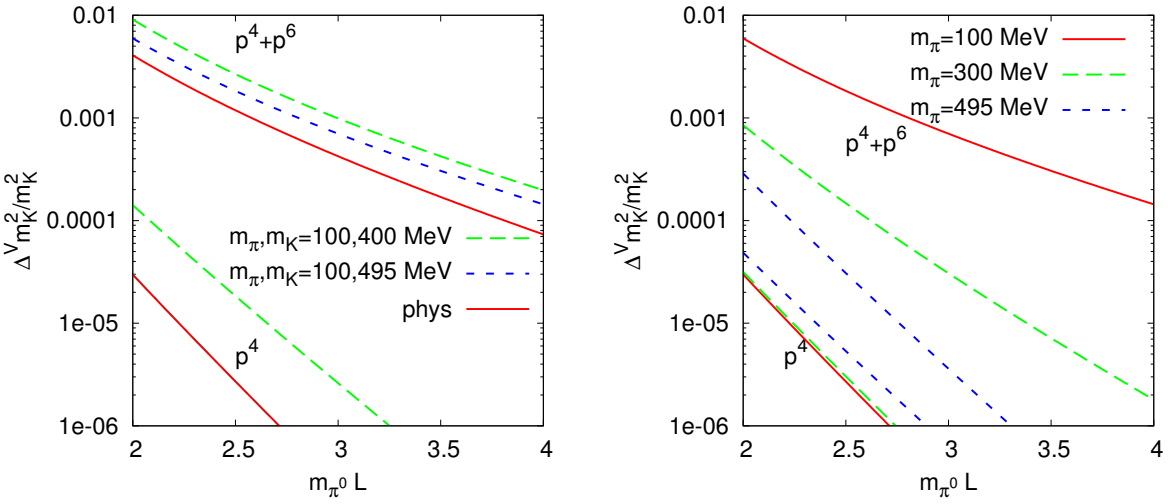

(a) (b)

Figure 7: The finite volume corrections to the kaon mass squared for a number of cases listed in Tab. 1.for the physical case. Plotted is the quantity $(m_K^{V2} - m_K^2)/m_K^2$. (a) Physical case and $(m_\pi, m_K) = (100, 495)$ and $(100, 400)$ MeV. (b) $m_K = 495$ MeV and $m_\pi = 100, 300, 495$ MeV. The size L is given in units of the physical π^0 mass.

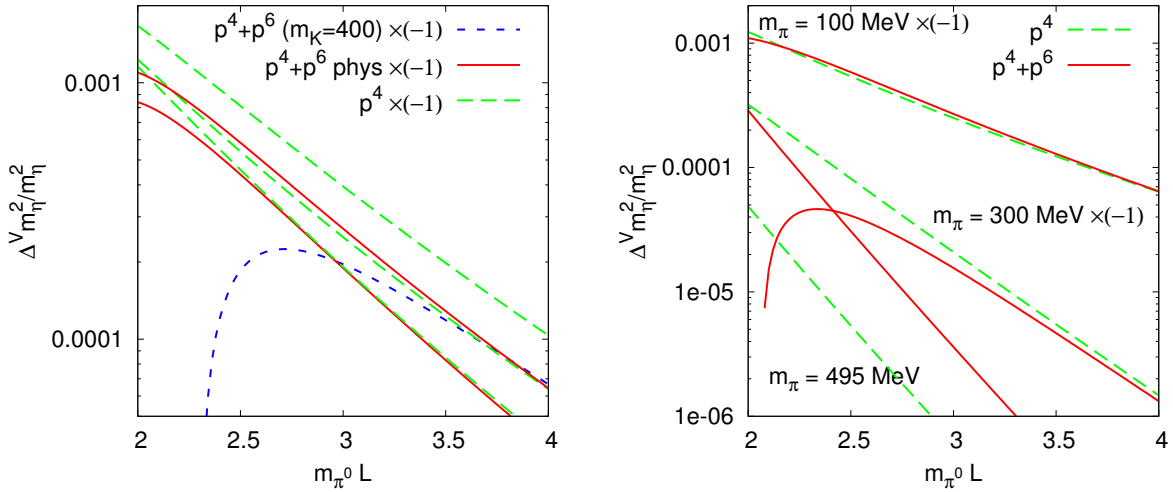

(a) (b)

Figure 8: The finite volume corrections to the eta mass squared for a number of cases listed in Tab. 1.for the physical case. Plotted is the quantity $(m_\eta^{V2} - m_\eta^2)/m_\eta^2$. (a) Physical case and $(m_\pi, m_K) = (100, 495)$ and $(100, 400)$ MeV. Lines are for the one-loop result at the right bottom physical case, middle $(m_\pi, m_K) = (100, 495)$, top $(m_\pi, m_K) = (100, 400)$. The first two have only a small change due to p^6, while for the last case there is a large cancellation between one and two-loops. (b) $m_K = 495$ MeV and $m_\pi = 100, 300, 495$ MeV. The size L is given in units of the physical π^0 mass.

to a cancellation between one-and two-loop results. The p^6 correction for $m_\pi = 100$ MeV is very small, we again have a large cancellation between the pure two-loop and the L_i^r dependent part.

We did not compare with the numerical results in [27], since there was a small mistake in the relevant figures [32].

6.3 Three-flavour results: decay constants

We will use exactly the same input values as in the previous subsection now but for the decay constants. Note that here in most cases the finite volume correction is negative.

The comparison of the two- and three-flavour results for the pion decay constant is plotted in Fig. 9(a). The one-loop result differs only by a very small kaon and eta loop. The difference is not visible in the figure. The two-loop results are also essentially indistinguishable. The convergence is quite reasonable. The bottom line and top line(s) are respectively the one-loop and the sum of one- and two-loops. Note that in agreement with the earlier estimates there is a sizable correction at finite volume even at $m_\pi L = 2$.

The equivalent results for the kaon and eta are plotted in Fig. 10. The kaon decay constant corrections are somewhat smaller than for the pion, but still important for precision studies. The one-loop result for the eta decay constant has only a kaon loop as can be

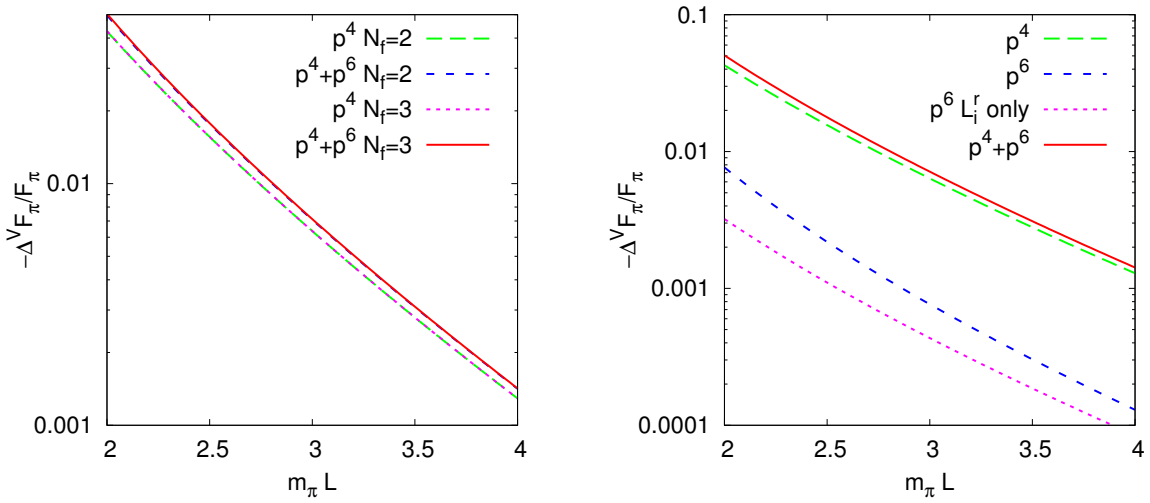

(a) (b)

Figure 9: The finite volume corrections to the pion decay constant at $m_\pi = m_{\pi^0}$. All other inputs are given in the text. Plotted is the quantity $-(F_\pi^V - F_\pi)/F_\pi$. (a) Comparison of the two- and three-flavour ChPT results. (b) The corrections for the three-flavour case also showing the L_i^r dependent part.

seen from (16). As a result, that part is very small. The total result comes mainly from two-loop order. The eta mass has a negative one-loop finite volume contribution. The pure loop part and the L_i^r-dependent part of the p^6 contribution are of the expected size. However, there is a very strong cancellation between the two parts leaving a very small positive correction. The total finite volume correction for the eta decay constant is quite small.

We can also check how the finite volume correction depends on the different masses. In Fig. 11 we have plotted the corrections to the pion decay constant for several scenarios. In Fig. 11(a) we look at three cases. The bottom two lines are the physical case labeled with $m_\pi = m_{\pi^0}$ while the top four lines are with $m_\pi = 100$ MeV. There we have plotted two cases, $m_K = 400$ and 495 MeV. The effect of the change in the pion mass is quite large while the effect due to the kaon mass change is smaller. In Fig. 11(b) we can see the effect of only varying the pion mass.

We have plotted the same cases for the finite volume corrections to the kaon decay constant in Fig. 12. In Fig. 12(a), the bottom two-lines are the physical case. The four top lines are with $m_\pi = 100$ MeV, where the smaller kaon mass gives a somewhat larger correction. In Fig. 12(b) we have shown the corrections for a fixed kaon mass but three different pion masses. The bottom three lines are the one-loop result while the top three lines are the full result. Note that, as it should be, for the case where the pion mass and kaon mass are the same, the finite volume corrections to the kaon are the same as for the pion in Fig. 11(b). This is another small check on our result.

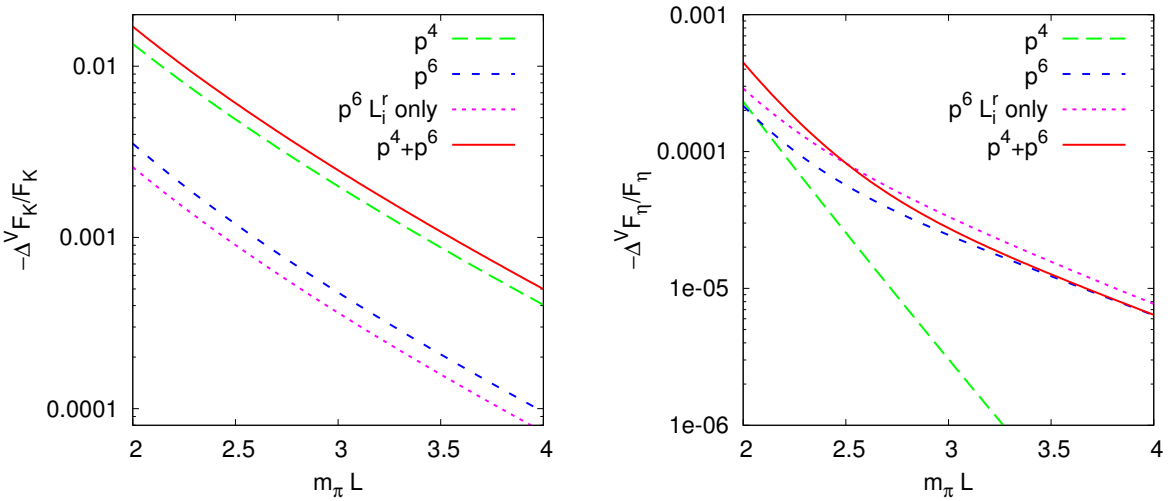

(a) (b)

Figure 10: The corrections to the kaon and eta decay constant for the physical case. Plotted is the quantity $-(F_i^V - F_i)/F_i$ for $i = K, \eta$. Shown are the one-loop, the two-loop, the sum and the two-loop L_i^r dependent part. (a) Kaon. (b) Eta.

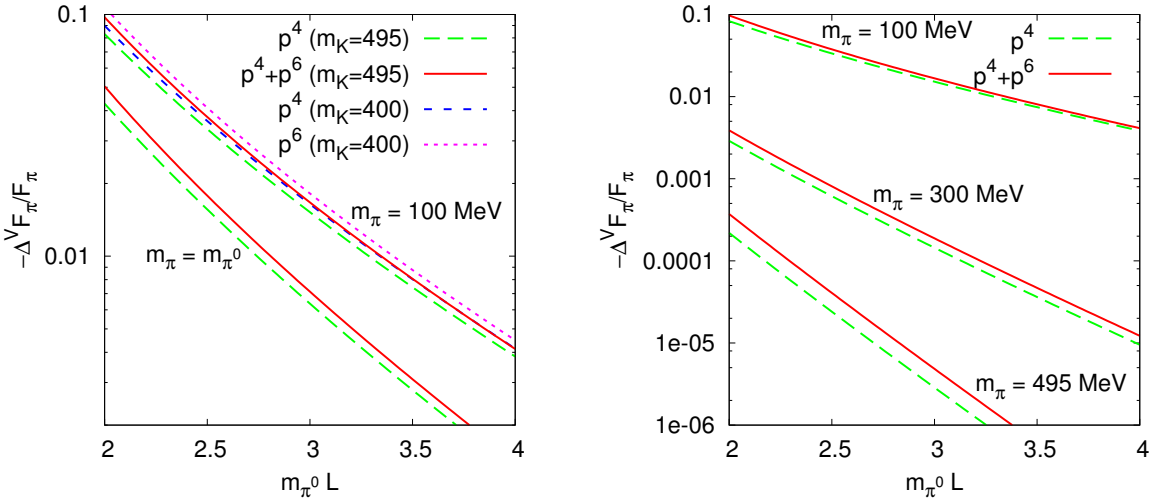

(a) (b)

Figure 11: The finite volume corrections to the pion decay constant for a number of cases listed in Tab. 1. Plotted is the quantity $-(F_\pi^V - F_\pi)/F_\pi$. (a) Physical case and $(m_\pi, m_K) = (100, 495)$ and $(100, 400)$ MeV. (b) $m_K = 495$ MeV and $m_\pi = 100, 300, 495$ MeV. The size L is given in units of the physical π^0 mass.

We have plotted the same cases once more for the finite volume corrections to the eta decay constant squared in Fig. 13. In Fig. 13(a) the one-loop corrections for the

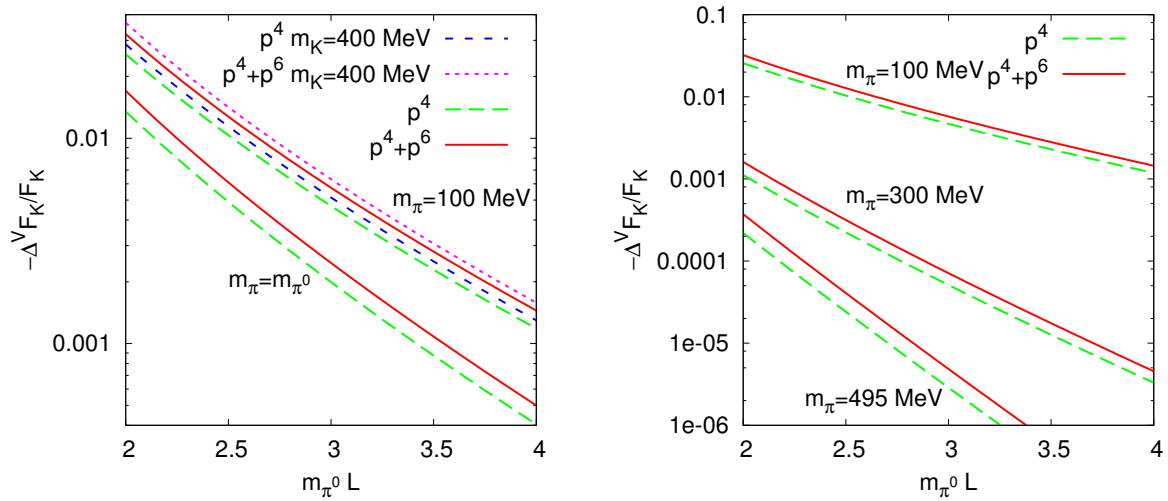

(a) (b)

Figure 12: The finite volume corrections to the kaon decay constant for a number of cases listed in Tab. 1. Plotted is the quantity $-(F_K^V - F_K)/F_K$. (a) Physical case and $(m_\pi, m_K) = (100, 495)$ and $(100, 400)$ MeV. (b) $m_K = 495$ MeV and $m_\pi = 100, 300, 495$ MeV. The size L is given in units of the physical π^0 mass.

physical case and $m_\pi, m_K = 100, 495$ MeV are extremely close, since it only depends on the kaon mass. The p^6 corrections for both cases are quite different though. Finally, for $m_\pi, m_K = 100, 400$ MeV both the one- and two-loop corrections are larger but the total correction remains fairly small. In Fig. 13(b) we have shown the corrections for a fixed kaon mass but three different pion masses. The p^4 correction is thus identical for the three cases. The correction for $m_\pi, m_K = 495$ MeV agrees with the pion and kaon corrections for this case. The total correction remains small for all cases.

We did not compare with the numerical results in [27], since there was a small mistake in the relevant figures [32].

7 Conclusions

In this paper we calculated the finite volume corrections to two-loop order in ChPT. The pion mass and decay constant we calculated both in two and three-flavour ChPT. The kaon and eta mass and decay constant we obtained in three-flavour ChPT. These expressions in the main text and the appendices are the main result of this work.

We have compared as far as possible with existing work, where we are in agreement with the known one-loop results and have some disagreements with the existing results at two-loop order. What we agree on and differ on is discussed in Sects. 4 and 5. Note that a full comparison at the analytical level was not possible due to the large differences in the loop integral treatments.

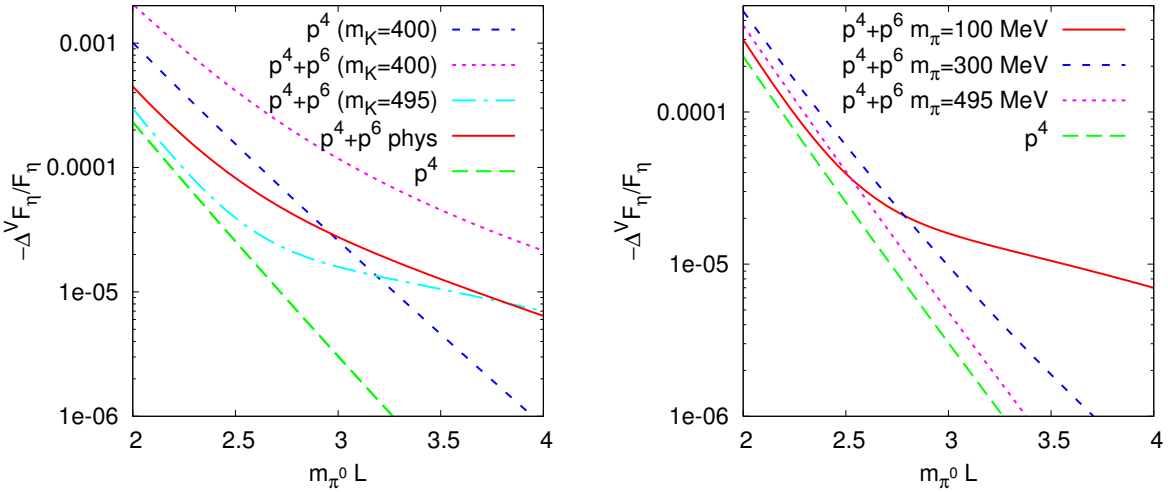

(a) (b)

Figure 13: The finite volume corrections to the eta decay constant for a number of cases listed in Tab. 1. Plotted is the quantity $-(F_\eta^V - F_\eta)/F_\eta$. (a) Physical case and $(m_\pi, m_K) = (100, 495)$ and $(100, 400)$ MeV. The bottom line is the one-loop result for the physical case and $(m_\pi, m_K) = (100, 495)$. Others as labeled. (b) $m_K = 495$ MeV and $m_\pi = 100, 300, 495$ MeV. The size L is given in units of the physical π^0 mass.

We have presented numerical results for a number of representative cases. In all cases the exponential decay $e^{-m_\pi/L}$ is clearly visible and as expected the numbers are dominated by the finite volume pion loops. The corrections at order p^6 are sometimes large, especially when the order p^4 result did not contain pion loops. We find that the finite volume corrections are necessary for the pion mass and decay constant as well as the kaon decay constant. The kaon mass receives corrections at a somewhat lower level while finite volume corrections for the eta mass and decay constant are at present negligible.

The numerical work has been done using C++. The programs will be made available together with the infinite volume results in [33]. The analytical work relied heavily on FORM [34].

Acknowledgements

We thank Gilberto Colangelo for discussions. This work is supported in part by the European Community-Research Infrastructure Integrating Activity "Study of Strongly Interacting Matter" (HadronPhysics3, Grant Agreement No. 283286) and the Swedish Research Council grants 621-2011-5080 and 621-2013-4287.

A Three flavour p^6 expressions for the masses

This appendix lists the order p^6 result for the three-flavour ChPT finite volume corrections to the masses squared at order p^6.

$$
\begin{aligned}
F_\pi^4\Delta^V m_\pi^{2(6)} &= A^V(m_\pi^2)m_\pi^4\left(40\,L_8^r+80\,L_6^r-24\,L_5^r-48\,L_4^r+28\,L_3^r+32\,L_2^r+56\,L_1^r\right)\\
&+A^V(m_K^2)m_\pi^2\,m_K^2\left(32\,L_8^r+64\,L_6^r-16\,L_5^r-64\,L_4^r+20\,L_3^r+16\,L_2^r+64\,L_1^r\right)\\
&+A^V(m_\eta^2)m_\pi^2\left(8\,L_8^r m_\pi^2-64/3\,L_7^r\,m_K^2+64/3\,L_7^r m_\pi^2+64/3\,L_6^r\,m_K^2-16/3\,L_6^r m_\pi^2\right.\\
&-32/9\,L_5^r m_K^2+8/9\,L_5^r m_\pi^2-64/3\,L_4^r m_K^2+16/3\,L_4^r m_\pi^2+16/3\,L_3^r m_K^2-4/3\,L_3^r\\
&\left.m_\pi^2+16/3\,L_2^r m_K^2-4/3\,L_2^r m_\pi^2+64/3\,L_1^r m_K^2-16/3\,L_1^r m_\pi^2\right)\\
&+A_{23}^V(m_\pi^2)m_\pi^2\left(-12\,L_3^r-48\,L_2^r-24\,L_1^r\right)+A_{23}^V(m_K^2)m_\pi^2\left(-12\,L_3^r-48\,L_2^r\right)\\
&+A_{23}^V(m_\eta^2)m_\pi^2\left(-4\,L_3^r-12\,L_2^r\right)\\
&+A^V(m_\pi^2)m_\pi^2\left(\frac{1}{16\pi^2}\,m_K^2+3/4\,\frac{1}{16\pi^2}\,m_\pi^2-7/4\,\overline{A}(m_\pi^2)-\overline{A}(m_K^2)+1/12\,\overline{B}^0(m_\eta^2)\,m_\pi^2\right)\\
&+A^V(m_\pi^2)^2\left(-3/8\,m_\pi^2\right)+A^V(m_\pi^2)\,A^V(m_K^2)\left(-1/2\,m_\pi^2\right)\\
&+A^V(m_\pi^2)\,A^V(m_\eta^2)\left(-1/12\,m_\pi^2\right)+A^V(m_\pi^2)\,B^{0V}(m_\pi^2)\left(1/4\,m_\pi^4\right)\\
&+A^V(m_\pi^2)\,B^{0V}(m_\eta^2)\left(1/12\,m_\pi^4\right)\\
&+A^V(m_K^2)m_\pi^2\left(\frac{1}{16\pi^2}m_K^2-1/2\,\overline{A}(m_\pi^2)-1/2\,\overline{A}(m_K^2)-1/2\,\overline{A}(m_\eta^2)-2/9\,\overline{B}^0(m_\eta^2)\,m_K^2\right)\\
&+A^V(m_K^2)^2\left(-1/4\,m_\pi^2\right)+A^V(m_K^2)\,A^V(m_\eta^2)\left(-1/2\,m_\pi^2\right)+A^V(m_K^2)\,B^{0V}(m_\eta^2)\left(-2/9\,m_\pi^2\,m_K^2\right)\\
&+A^V(m_\eta^2)m_\pi^2\left(1/12\,\frac{1}{16\pi^2}\,m_\pi^2+1/4\,\overline{A}(m_\pi^2)-1/3\,\overline{A}(m_K^2)+\overline{B}^0(m_\eta^2)\left(4/27\,m_K^2-7/108\,m_\pi^2\right)\right)\\
&+A^V(m_\eta^2)^2\left(1/72\,m_\pi^2\right)+A^V(m_\eta^2)\,B^{0V}(m_\pi^2)\left(-1/12\,m_\pi^4\right)\\
&+A^V(m_\eta^2)\,B^{0V}(m_\eta^2)\left(4/27\,m_\pi^2\,m_K^2-7/108\,m_\pi^4\right)\\
&+H^V(m_\pi^2,m_\pi^2,m_\pi^2,m_\pi^2)\left(5/6\,m_\pi^4\right)+H^V(m_\pi^2,m_K^2,m_K^2,m_\pi^2)\left(m_\pi^2\,m_K^2-5/8\,m_\pi^4\right)\\
&+H^V(m_\pi^2,m_\eta^2,m_\eta^2,m_\pi^2)\left(1/18\,m_\pi^4\right)+H^V(m_K^2,m_K^2,m_\eta^2,m_\pi^2)\left(1/2\,m_\pi^2\,m_K^2+1/24\,m_\pi^4\right)\\
&+H_1^V(m_\pi^2,m_K^2,m_K^2,m_\pi^2)\left(m_\pi^4\right)+H_1^V(m_\eta^2,m_K^2,m_K^2,m_\pi^2)\left(-m_\pi^4\right)\\
&+H_{21}^V(m_\pi^2,m_\pi^2,m_\pi^2,m_\pi^2)\left(3\,m_\pi^4\right)+H_{21}^V(m_\pi^2,m_K^2,m_K^2,m_\pi^2)\left(-3/8\,m_\pi^4\right)\\
&+H_{21}^V(m_K^2,m_\pi^2,m_K^2,m_\pi^2)\left(3\,m_\pi^4\right)+H_{21}^V(m_\eta^2,m_K^2,m_K^2,m_\pi^2)\left(9/8\,m_\pi^4\right)\\
&+H_{27}^V(m_\pi^2,m_\pi^2,m_\pi^2,m_\pi^2)\left(-3\,m_\pi^2\right)+H_{27}^V(m_\pi^2,m_K^2,m_K^2,m_\pi^2)\left(3/8\,m_\pi^2\right)\\
&+H_{27}^V(m_K^2,m_\pi^2,m_K^2,m_\pi^2)\left(-3\,m_\pi^2\right)+H_{27}^V(m_\eta^2,m_K^2,m_K^2,m_\pi^2)\left(-9/8\,m_\pi^2\right). \qquad (20)
\end{aligned}
$$

$$
F_\pi^4\Delta^V m_K^{2(6)} = A^V(m_\pi^2)\left(24\,L_8^r m_\pi^2\,m_K^2+48\,L_6^r m_\pi^2\,m_K^2-12\,L_5^r m_\pi^2\,m_K^2-48\,L_4^r m_\pi^2\,m_K^2\right.
$$

$$
\begin{aligned}
&+15\,L_3^r m_\pi^2\,m_K^2+12\,L_2^r m_\pi^2\,m_K^2+48\,L_1^r m_\pi^2\,m_K^2\Big)\\
&+A^V(m_K^2)\,\Big(48\,L_8^r m_K^4+96\,L_6^r m_K^4-24\,L_5^r m_K^4-64\,L_4^r\,m_K^4+30\,L_3^r m_K^4+36\,L_2^r m_K^4+72\,L_1^r m_K^4\Big)\\
&+A^V(m_\eta^2)\,\Big(64/3\,L_8^r m_K^4-56/3\,L_8^r m_\pi^2\,m_K^2+16/3\,L_8^r m_\pi^4+64/3\,L_7^r m_K^4-32\,L_7^r m_\pi^2\,m_K^2\\
&+32/3\,L_7^r m_\pi^4+64/3\,L_6^r m_K^4-16/3\,L_6^r m_\pi^2\,m_K^2-64/9\,L_5^r m_K^4+4/3\,L_5^r m_\pi^2\,m_K^2-8/9\,L_5^r m_\pi^4\\
&-64/3\,L_4^r m_K^4+16/3\,L_4^r m_\pi^2\,m_K^2+28/3\,L_3^r m_K^4-7/3\,L_3^r m_\pi^2\,m_K^2+16/3\,L_2^r m_K^4\\
&-4/3\,L_2^r m_\pi^2\,m_K^2+64/3\,L_1^r m_K^4-16/3\,L_1^r m_\pi^2\,m_K^2\Big)\\
&+A_{23}^V(m_\pi^2)\,\Big(-9\,L_3^r m_K^2-36\,L_2^r m_K^2\Big)+A_{23}^V(m_K^2)\,\Big(-18\,L_3^r m_K^2-60\,L_2^r m_K^2-24\,L_1^r m_K^2\Big)\\
&+A_{23}^V(m_\eta^2)\,\Big(-L_3^r m_K^2-12\,L_2^r m_K^2\Big)\\
&+A^V(m_\pi^2)\,\Big(3/4\,\frac{1}{16\pi^2}\,m_K^4-3/16\,\overline{A}(m_\pi^2)\,m_K^2-3/4\,\overline{A}(m_K^2)\,m_K^2-3/16\,\overline{A}(m_\eta^2)\,m_K^2\\
&-1/6\,\overline{B}^0(m_\eta^2)\,m_\pi^2\,m_K^2\Big)\\
&+A^V(m_\pi^2)^2\,\Big(-3/32\,m_K^2\Big)+A^V(m_\pi^2)\,A^V(m_K^2)\,\Big(-3/4\,m_K^2\Big)+A^V(m_\pi^2)\,A^V(m_\eta^2)\,\Big(-3/16\,m_K^2\Big)\\
&+A^V(m_\pi^2)\,B^{0V}(m_\eta^2)\,\Big(-1/6\,m_\pi^2\,m_K^2\Big)\\
&+A^V(m_K^2)\,\Big(3/4\,\frac{1}{16\pi^2}\,m_K^4+3/4\,\frac{1}{16\pi^2}\,m_\pi^2\,m_K^2-3/4\,\overline{A}(m_\pi^2)\,m_K^2-3/2\,\overline{A}(m_K^2)\,m_K^2\\
&+4/9\,\overline{B}^0(m_\eta^2)\,m_K^4\Big)\\
&+A^V(m_K^2)^2\,\Big(-3/4\,m_K^2\Big)+A^V(m_K^2)\,B^{0V}(m_\eta^2)\,\Big(4/9\,m_K^4\Big)\\
&+A^V(m_\eta^2)\,\Big(1/2\,\frac{1}{16\pi^2}\,m_K^4+1/4\,\frac{1}{16\pi^2}\,m_\pi^2\,m_K^2-41/48\,\overline{A}(m_\pi^2)\,m_K^2+1/12\,\overline{A}(m_\pi^2)\,m_\pi^2\\
&-2/3\,\overline{A}(m_K^2)\,m_K^2+19/48\,\overline{A}(m_\eta^2)\,m_K^2-1/12\,\overline{A}(m_\eta^2)\,m_\pi^2-8/27\,\overline{B}^0(m_\eta^2)\,m_K^4\\
&+7/54\,\overline{B}^0(m_\eta^2)\,m_\pi^2\,m_K^2\Big)\\
&+A^V(m_\eta^2)^2\,\Big(25/288\,m_K^2\Big)+A^V(m_\eta^2)\,B^{0V}(m_\eta^2)\,\Big(-8/27\,m_K^4+7/54\,m_\pi^2\,m_K^2\Big)\\
&+H^V(m_\pi^2,m_\pi^2,m_K^2,m_K^2)\,\Big(-15/32\,m_K^4+3/4\,m_\pi^2\,m_K^2\Big)\\
&+H^V(m_\pi^2,m_K^2,m_\eta^2,m_K^2)\,\Big(13/16\,m_K^4\Big)+H^V(m_K^2,m_K^2,m_K^2,m_K^2)\,\Big(3/4\,m_K^4\Big)\\
&+H^V(m_K^2,m_\eta^2,m_\eta^2,m_K^2)\,\Big(181/288\,m_K^4\Big)+H_1^V(m_K^2,m_\pi^2,m_\pi^2,m_K^2)\,\Big(3/4\,m_K^4\Big)\\
&+H_1^V(m_K^2,m_\pi^2,m_\eta^2,m_K^2)\,\Big(-3/2\,m_K^4\Big)+H_1^V(m_K^2,m_\eta^2,m_\eta^2,m_K^2)\,\Big(-5/4\,m_K^4\Big)\\
&+H_{21}^V(m_\pi^2,m_\pi^2,m_K^2,m_K^2)\,\Big(9/4\,m_K^4\Big)+H_{21}^V(m_K^2,m_\pi^2,m_\pi^2,m_K^2)\,\Big(-9/32\,m_K^4\Big)\\
&+H_{21}^V(m_K^2,m_\pi^2,m_\eta^2,m_K^2)\,\Big(27/16\,m_K^4\Big)+H_{21}^V(m_K^2,m_K^2,m_K^2,m_K^2)\,\Big(9/4\,m_K^4\Big)\\
&+H_{21}^V(m_K^2,m_\eta^2,m_\eta^2,m_K^2)\,\Big(27/32\,m_K^4\Big)+H_{27}^V(m_\pi^2,m_\pi^2,m_K^2,m_K^2)\,\Big(-9/4\,m_K^2\Big)\\
&+H_{27}^V(m_K^2,m_\pi^2,m_\pi^2,m_K^2)\,\Big(9/32\,m_K^2\Big)+H_{27}^V(m_K^2,m_\pi^2,m_\eta^2,m_K^2)\,\Big(-27/16\,m_K^2\Big)\\
&+H_{27}^V(m_K^2,m_K^2,m_K^2,m_K^2)\,\Big(-9/4\,m_K^2\Big)+H_{27}^V(m_K^2,m_\eta^2,m_\eta^2,m_K^2)\,\Big(-27/32\,m_K^2\Big)\,. \qquad (21)
\end{aligned}
$$

$$
\begin{aligned}
F_\pi^4 \Delta^V m_\eta^{2(6)} = {} & A^V(m_\pi^2) \Big(24\, L_8^r m_\pi^4 - 64\, L_7^r m_\pi^2\, m_K^2 + 64\, L_7^r m_\pi^4 + 64\, L_6^r m_\pi^2\, m_K^2 - 16\, L_6^r m_\pi^4 \\
& - 32/3\, L_5^r m_\pi^2\, m_K^2 + 8/3\, L_5^r m_\pi^4 - 64\, L_4^r m_\pi^2\, m_K^2 + 16\, L_4^r m_\pi^4 + 16\, L_3^r m_\pi^2\, m_K^2 - 4\, L_3^r m_\pi^4 \\
& + 16\, L_2^r m_\pi^2\, m_K^2 - 4\, L_2^r m_\pi^4 + 64\, L_1^r m_\pi^2\, m_K^2 - 16\, L_1^r m_\pi^4 \Big) \\
& + A^V(m_K^2) \Big(256/3\, L_8^r m_K^4 - 224/3\, L_8^r m_\pi^2\, m_K^2 + 64/3\, L_8^r m_\pi^4 + 256/3\, L_7^r m_K^4 \\
& - 128\, L_7^r m_\pi^2\, m_K^2 + 128/3\, L_7^r m_\pi^4 + 256/3\, L_6^r m_K^4 - 64/3\, L_6^r m_\pi^2\, m_K^2 - 256/9\, L_5^r m_K^4 \\
& + 16/3\, L_5^r m_\pi^2\, m_K^2 - 32/9\, L_5^r m_\pi^4 - 256/3\, L_4^r m_K^4 + 64/3\, L_4^r m_\pi^2\, m_K^2 + 112/3\, L_3^r m_K^4 \\
& - 28/3\, L_3^r m_\pi^2\, m_K^2 + 64/3\, L_2^r m_K^4 - 16/3\, L_2^r m_\pi^2\, m_K^2 + 256/3\, L_1^r m_K^4 - 64/3\, L_1^r m_\pi^2\, m_K^2 \Big) \\
& + A^V(m_\eta^2) \Big(896/9\, L_8^r m_K^4 - 1024/9\, L_8^r m_\pi^2\, m_K^2 + 344/9\, L_8^r m_\pi^4 + 1024/9\, L_7^r m_K^4 \\
& - 1664/9\, L_7^r m_\pi^2\, m_K^2 + 640/9\, L_7^r m_\pi^4 + 256/3\, L_6^r m_K^4 - 128/3\, L_6^r m_\pi^2\, m_K^2 + 16/3\, L_6^r m_\pi^4 \\
& - 832/27\, L_5^r m_K^4 + 896/27\, L_5^r m_\pi^2\, m_K^2 - 280/27\, L_5^r m_\pi^4 - 256/9\, L_4^r m_K^4 + 128/9\, L_4^r m_\pi^2\, m_K^2 \\
& - 16/9\, L_4^r m_\pi^4 + 64/3\, L_3^r m_K^4 - 32/3\, L_3^r m_\pi^2\, m_K^2 + 4/3\, L_3^r m_\pi^4 + 128/3\, L_2^r m_K^4 \\
& - 64/3\, L_2^r m_\pi^2\, m_K^2 + 8/3\, L_2^r m_\pi^4 + 128/3\, L_1^r m_K^4 - 64/3\, L_1^r m_\pi^2\, m_K^2 + 8/3\, L_1^r m_\pi^4 \Big) \\
& + A_{23}^V(m_\pi^2) \Big(- 16\, L_3^r m_K^2 + 4\, L_3^r m_\pi^2 - 48\, L_2^r m_K^2 + 12\, L_2^r m_\pi^2 \Big) \\
& + A_{23}^V(m_K^2) \Big(- 16/3\, L_3^r m_K^2 + 4/3\, L_3^r m_\pi^2 - 64\, L_2^r m_K^2 + 16\, L_2^r m_\pi^2 \Big) \\
& + A_{23}^V(m_\eta^2) \Big(- 16\, L_3^r m_K^2 + 4\, L_3^r m_\pi^2 - 32\, L_2^r m_K^2 + 8\, L_2^r m_\pi^2 - 32\, L_1^r m_K^2 + 8\, L_1^r m_\pi^2 \Big) \\
& + A^V(m_\pi^2) \Big(1/4\, \frac{1}{16\pi^2}\, m_\pi^4 + 3/4\, \overline{A}(m_\pi^2)\, m_\pi^2 - \overline{A}(m_K^2)\, m_\pi^2 + 4/9\, \overline{B}^0(m_\eta^2)\, m_\pi^2\, m_K^2 \\
& - 7/36\, \overline{B}^0(m_\eta^2)\, m_\pi^4 \Big) \\
& + A^V(m_\pi^2)^2 \Big(- 1/8\, m_\pi^2 \Big) + A^V(m_\pi^2)\, A^V(m_K^2) \Big(- 3/2\, m_\pi^2 \Big) + A^V(m_\pi^2)\, A^V(m_\eta^2) \Big(1/12\, m_\pi^2 \Big) \\
& + A^V(m_\pi^2)\, B^{0V}(m_\pi^2) \Big(- 1/4\, m_\pi^4 \Big) + A^V(m_\pi^2)\, B^{0V}(m_\eta^2) \Big(4/9\, m_\pi^2\, m_K^2 - 7/36\, m_\pi^4 \Big) \\
& + A^V(m_K^2) \Big(8/3\, \frac{1}{16\pi^2}\, m_K^4 + 2/3\, \frac{1}{16\pi^2}\, m_\pi^2\, m_K^2 - 1/3\, \frac{1}{16\pi^2}\, m_\pi^4 - 8/3\, \overline{A}(m_\pi^2)\, m_K^2 \\
& - 7/6\, \overline{A}(m_\pi^2)\, m_\pi^2 - 2/3\, \overline{A}(m_K^2)\, m_K^2 + 3/2\, \overline{A}(m_K^2)\, m_\pi^2 - 8/3\, \overline{A}(m_\eta^2)\, m_K^2 + 7/6\, \overline{A}(m_\eta^2)\, m_\pi^2 \\
& - 32/27\, \overline{B}^0(m_\eta^2)\, m_K^4 + 14/27\, \overline{B}^0(m_\eta^2)\, m_\pi^2\, m_K^2 \Big) \\
& + A^V(m_K^2)^2 \Big(m_K^2 + 3/4\, m_\pi^2 \Big) + A^V(m_K^2)\, A^V(m_\eta^2) \Big(- 32/9\, m_K^2 + 3/2\, m_\pi^2 \Big) \\
& + A^V(m_K^2)\, B^{0V}(m_\eta^2) \Big(- 32/27\, m_K^4 + 14/27\, m_\pi^2\, m_K^2 \Big) \\
& + A^V(m_\eta^2) \Big(- 4/9\, \frac{1}{16\pi^2}\, m_K^4 - 1/12\, \frac{1}{16\pi^2}\, m_\pi^4 + 16/9\, \overline{A}(m_\pi^2)\, m_K^2 - 29/36\, \overline{A}(m_\pi^2)\, m_\pi^2 \\
& - 20/9\, \overline{A}(m_K^2)\, m_K^2 + 10/9\, \overline{A}(m_K^2)\, m_\pi^2 + 8/9\, \overline{A}(m_\eta^2)\, m_K^2 - 2/9\, \overline{A}(m_\eta^2)\, m_\pi^2 \\
& + 64/81\, \overline{B}^0(m_\eta^2)\, m_K^4 - 56/81\, \overline{B}^0(m_\eta^2)\, m_\pi^2\, m_K^2 + 49/324\, \overline{B}^0(m_\eta^2)\, m_\pi^4 \Big) \\
& + A^V(m_\eta^2)^2 \Big(8/27\, m_K^2 - 31/216\, m_\pi^2 \Big) + A^V(m_\eta^2)\, B^{0V}(m_\pi^2) \Big(1/12\, m_\pi^4 \Big)
\end{aligned}
$$

$$
\begin{aligned}
&+A^V(m_\eta^2)\,B^{0V}(m_K^2)\left(4/9\,m_K^4\right)\\
&+A^V(m_\eta^2)\,B^{0V}(m_\eta^2)\left(64/81\,m_K^4-56/81\,m_\pi^2\,m_K^2+49/324\,m_\pi^4\right)\\
&+H^V(m_\pi^2,m_\pi^2,m_\eta^2,m_\eta^2)\left(1/6\,m_\pi^4\right)+H^V(m_\pi^2,m_K^2,m_K^2,m_\eta^2)\left(3/2\,m_\pi^2\,m_K^2+1/8\,m_\pi^4\right)\\
&+H^V(m_K^2,m_K^2,m_\eta^2,m_\eta^2)\left(50/9\,m_K^4-11/3\,m_\pi^2\,m_K^2+5/8\,m_\pi^4\right)\\
&+H^V(m_\eta^2,m_\eta^2,m_\eta^2,m_\eta^2)\left(128/243\,m_K^4-112/243\,m_\pi^2\,m_K^2+49/486\,m_\pi^4\right)\\
&+H_1^V(m_\pi^2,m_K^2,m_K^2,m_\eta^2)\left(-4\,m_\pi^2\,m_K^2+m_\pi^4\right)\\
&+H_1^V(m_\eta^2,m_K^2,m_K^2,m_\eta^2)\left(-32/3\,m_K^4+20/3\,m_\pi^2\,m_K^2-m_\pi^4\right)\\
&+H_{21}^V(m_\pi^2,m_K^2,m_K^2,m_\eta^2)\left(6\,m_K^4-3\,m_\pi^2\,m_K^2+3/8\,m_\pi^4\right)\\
&+H_{21}^V(m_\eta^2,m_K^2,m_K^2,m_\eta^2)\left(6\,m_K^4-3\,m_\pi^2\,m_K^2+3/8\,m_\pi^4\right)\\
&+H_{27}^V(m_\pi^2,m_K^2,m_K^2,m_\eta^2)\left(-9/2\,m_K^2+9/8\,m_\pi^2\right)\\
&+H_{27}^V(m_\eta^2,m_K^2,m_K^2,m_\eta^2)\left(-9/2\,m_K^2+9/8\,m_\pi^2\right). \qquad (22)
\end{aligned}
$$

B Three flavour p^6 expressions for the decay constants

This appendix lists the order p^6 result for the three-flavour ChPT finite volume corrections to the decay constants at order p^6.

$$
\begin{aligned}
&F_\pi^3\Delta^V F_\pi^{(6)}=A^V(m_\pi^2)\left(6\,L_5^r m_\pi^2+12\,L_4^r m_\pi^2-14\,L_3^r m_\pi^2-16\,L_2^r m_\pi^2-28\,L_1^r m_\pi^2\right)\\
&+A^V(m_K^2)\left(4\,L_5^r m_\pi^2+16\,L_4^r m_K^2-10\,L_3^r m_K^2-8\,L_2^r m_K^2-32\,L_1^r m_K^2\right)\\
&+A^V(m_\eta^2)\left(2/3\,L_5^r m_\pi^2+16/3\,L_4^r m_K^2-4/3\,L_4^r m_\pi^2-8/3\,L_3^r m_K^2+2/3\,L_3^r m_\pi^2\right.\\
&\left.-8/3\,L_2^r m_K^2+2/3\,L_2^r m_\pi^2-32/3\,L_1^r m_K^2+8/3\,L_1^r m_\pi^2\right)\\
&+A_{23}^V(m_\pi^2)\left(6\,L_3^r+24\,L_2^r+12\,L_1^r\right)+A_{23}^V(m_K^2)\left(6\,L_3^r+24\,L_2^r\right)+A_{23}^V(m_\eta^2)\left(2\,L_3^r+6\,L_2^r\right)\\
&+A^V(m_\pi^2)\left(-1/2\,\frac{1}{16\pi^2}\,m_K^2-1/4\,\frac{1}{16\pi^2}\,m_\pi^2+1/2\,\overline{A}(m_\pi^2)+1/2\,\overline{A}(m_K^2)\right)\\
&+A^V(m_\pi^2)\,B^{0V}(m_\pi^2)\left(-1/2\,m_\pi^2\right)\\
&+A^V(m_K^2)\left(-1/2\,\frac{1}{16\pi^2}\,m_K^2-1/8\,\frac{1}{16\pi^2}\,m_\pi^2+1/2\,\overline{A}(m_\pi^2)+1/4\,\overline{A}(m_K^2)\right)\\
&+A^V(m_\eta^2)\left(1/6\,\frac{1}{16\pi^2}\,m_K^2-1/6\,\frac{1}{16\pi^2}\,m_\pi^2+1/6\,\overline{A}(m_\pi^2)-1/6\,\overline{A}(m_K^2)\right)\\
&+A^V(m_\eta^2)\,B^{0V}(m_\pi^2)\left(1/6\,m_\pi^2\right)+A^V(m_\eta^2)\,B^{0V}(m_K^2)\left(-1/6\,m_K^2\right)\\
&+H^V(m_\pi^2,m_\pi^2,m_\pi^2,m_\pi^2)\left(-1/2\,m_\pi^2\right)+H^V(m_\pi^2,m_K^2,m_K^2,m_\pi^2)\left(-1/2\,m_K^2+1/16\,m_\pi^2\right)\\
&+H^V(m_K^2,m_K^2,m_\eta^2,m_\pi^2)\left(-1/4\,m_K^2+1/16\,m_\pi^2\right)+H_{27}^V(m_\pi^2,m_\pi^2,m_\pi^2,m_\pi^2)\left(3/2\right)
\end{aligned}
$$

$$
\begin{aligned}
&+H_{27}^{V}(m_\pi^2,m_K^2,m_K^2,m_\pi^2)\,\Big(-3/16\Big)+H_{27}^{V}(m_K^2,m_\pi^2,m_K^2,m_\pi^2)\,\Big(3/2\Big)\\
&+H_{27}^{V}(m_\eta^2,m_K^2,m_K^2,m_\pi^2)\,\Big(9/16\Big)+H^{V\prime}(m_\pi^2,m_\pi^2,m_\pi^2,m_\pi^2)\,\Big(5/12\,m_\pi^4\Big)\\
&+H^{V\prime}(m_\pi^2,m_K^2,m_K^2,m_\pi^2)\,\Big(1/2\,m_\pi^2\,m_K^2-5/16\,m_\pi^4\Big)+H^{V\prime}(m_\pi^2,m_\eta^2,m_\eta^2,m_\pi^2)\,\Big(1/36\,m_\pi^4\Big)\\
&+H^{V\prime}(m_K^2,m_K^2,m_\eta^2,m_\pi^2)\,\Big(1/4\,m_\pi^2\,m_K^2+1/48\,m_\pi^4\Big)+H_1^{V\prime}(m_\pi^2,m_K^2,m_K^2,m_\pi^2)\,\Big(1/2\,m_\pi^4\Big)\\
&+H_1^{V\prime}(m_\eta^2,m_K^2,m_K^2,m_\pi^2)\,\Big(-1/2\,m_\pi^4\Big)+H_{21}^{V\prime}(m_\pi^2,m_\pi^2,m_\pi^2,m_\pi^2)\,\Big(3/2\,m_\pi^4\Big)\\
&+H_{21}^{V\prime}(m_\pi^2,m_K^2,m_K^2,m_\pi^2)\,\Big(-3/16\,m_\pi^4\Big)+H_{21}^{V\prime}(m_K^2,m_\pi^2,m_K^2,m_\pi^2)\,\Big(3/2\,m_\pi^4\Big)\\
&+H_{21}^{V\prime}(m_\eta^2,m_K^2,m_K^2,m_\pi^2)\,\Big(9/16\,m_\pi^4\Big)+H_{27}^{V\prime}(m_\pi^2,m_\pi^2,m_\pi^2,m_\pi^2)\,\Big(-3/2\,m_\pi^2\Big)\\
&+H_{27}^{V\prime}(m_\pi^2,m_K^2,m_K^2,m_\pi^2)\,\Big(3/16\,m_\pi^2\Big)+H_{27}^{V\prime}(m_K^2,m_\pi^2,m_K^2,m_\pi^2)\,\Big(-3/2\,m_\pi^2\Big)\\
&+H_{27}^{V\prime}(m_\eta^2,m_K^2,m_K^2,m_\pi^2)\,\Big(-9/16\,m_\pi^2\Big)\,. \qquad (23)
\end{aligned}
$$

$$
\begin{aligned}
F_\pi^3\Delta^V F_K^{(6)} &= A^V(m_\pi^2)\,\Big(3/2\,L_5^r m_K^2+3/2\,L_5^r m_\pi^2+12\,L_4^r m_\pi^2-15/2\,L_3^r m_\pi^2-6\,L_2^r m_\pi^2\\
&-24\,L_1^r m_\pi^2\Big)\\
&+A^V(m_K^2)\,\Big(3\,L_5^r m_K^2+3\,L_5^r m_\pi^2+16\,L_4^r m_K^2-15\,L_3^r m_K^2-18\,L_2^r m_K^2-36\,L_1^r m_K^2\Big)\\
&+A^V(m_\eta^2)\,\Big(1/6\,L_5^r m_K^2+3/2\,L_5^r m_\pi^2+16/3\,L_4^r m_K^2-4/3\,L_4^r m_\pi^2-14/3\,L_3^r m_K^2\\
&+7/6\,L_3^r m_\pi^2-8/3\,L_2^r m_K^2+2/3\,L_2^r m_\pi^2-32/3\,L_1^r m_K^2+8/3\,L_1^r m_\pi^2\Big)\\
&+A_{23}^V(m_\pi^2)\,\Big(9/2\,L_3^r+18\,L_2^r\Big)+A_{23}^V(m_K^2)\,\Big(9\,L_3^r+30\,L_2^r+12\,L_1^r\Big)\\
&+A_{23}^V(m_\eta^2)\,\Big(1/2\,L_3^r+6\,L_2^r\Big)\\
&+A^V(m_\pi^2)\,\Big(-15/32\,\frac{1}{16\pi^2}\,m_K^2+3/16\,\frac{1}{16\pi^2}\,m_\pi^2-3/64\,\overline{A}(m_\pi^2)+9/32\,\overline{A}(m_K^2)\\
&+9/64\,\overline{A}(m_\eta^2)+3/16\,\overline{B}^0(m_\eta^2)\,m_\pi^2\Big)\\
&+A^V(m_\pi^2)^2\,\Big(-15/128\Big)+A^V(m_\pi^2)\,A^V(m_K^2)\,\Big(3/32\Big)+A^V(m_\pi^2)\,A^V(m_\eta^2)\,\Big(9/64\Big)\\
&+A^V(m_\pi^2)\,B^{0V}(m_\pi^2)\,\Big(-3/16\,m_\pi^2\Big)+A^V(m_\pi^2)\,B^{0V}(m_\eta^2)\,\Big(3/16\,m_\pi^2\Big)\\
&+A^V(m_K^2)\,\Big(-9/16\,\frac{1}{16\pi^2}\,m_K^2-3/8\,\frac{1}{16\pi^2}\,m_\pi^2+27/32\,\overline{A}(m_\pi^2)+9/16\,\overline{A}(m_K^2)\\
&-9/32\,\overline{A}(m_\eta^2)-1/2\,\overline{B}^0(m_\eta^2)\,m_K^2\Big)\\
&+A^V(m_K^2)^2\,\Big(3/32\Big)+A^V(m_K^2)\,A^V(m_\eta^2)\,\Big(-9/32\Big)+A^V(m_K^2)\,B^{0V}(m_\eta^2)\,\Big(-1/2\,m_K^2\Big)\\
&+A^V(m_\eta^2)\,\Big(-3/32\,\frac{1}{16\pi^2}\,m_K^2-3/16\,\frac{1}{16\pi^2}\,m_\pi^2+37/64\,\overline{A}(m_\pi^2)-11/32\,\overline{A}(m_K^2)\\
&+9/64\,\overline{A}(m_\eta^2)+1/3\,\overline{B}^0(m_\eta^2)\,m_K^2-7/48\,\overline{B}^0(m_\eta^2)\,m_\pi^2\Big)\\
&+A^V(m_\eta^2)^2\,\Big(9/128\Big)+A^V(m_\eta^2)\,B^{0V}(m_\pi^2)\,\Big(1/16\,m_\pi^2\Big)+A^V(m_\eta^2)\,B^{0V}(m_K^2)\,\Big(-1/4\,m_K^2\Big)\\
&+A^V(m_\eta^2)\,B^{0V}(m_\eta^2)\,\Big(1/3\,m_K^2-7/48\,m_\pi^2\Big)
\end{aligned}
$$

$$
\begin{aligned}
&+H^V(m_\pi^2,m_\pi^2,m_K^2,m_K^2)\left(3/64\,m_K^2-3/8\,m_\pi^2\right)+H^V(m_\pi^2,m_K^2,m_\eta^2,m_K^2)\left(-9/32\,m_K^2\right)\\
&+H^V(m_K^2,m_K^2,m_K^2,m_K^2)\left(-3/8\,m_K^2\right)+H^V(m_K^2,m_\eta^2,m_\eta^2,m_K^2)\left(-9/64\,m_K^2\right)\\
&+H_{27}^V(m_\pi^2,m_\pi^2,m_K^2,m_K^2)\left(9/8\right)+H_{27}^V(m_K^2,m_\pi^2,m_\pi^2,m_K^2)\left(-9/64\right)\\
&+H_{27}^V(m_K^2,m_\pi^2,m_\eta^2,m_K^2)\left(27/32\right)+H_{27}^V(m_K^2,m_K^2,m_K^2,m_K^2)\left(9/8\right)\\
&+H_{27}^V(m_K^2,m_\eta^2,m_\eta^2,m_K^2)\left(27/64\right)+H^{V\prime}(m_\pi^2,m_\pi^2,m_K^2,m_K^2)\left(-15/64\,m_K^4+3/8\,m_\pi^2\,m_K^2\right)\\
&+H^{V\prime}(m_\pi^2,m_K^2,m_\eta^2,m_K^2)\left(13/32\,m_K^4\right)+H^{V\prime}(m_K^2,m_K^2,m_K^2,m_K^2)\left(3/8\,m_K^4\right)\\
&+H^{V\prime}(m_K^2,m_\eta^2,m_\eta^2,m_K^2)\left(181/576\,m_K^4\right)+H_1^{V\prime}(m_K^2,m_\pi^2,m_\pi^2,m_K^2)\left(3/8\,m_K^4\right)\\
&+H_1^{V\prime}(m_K^2,m_\pi^2,m_\eta^2,m_K^2)\left(-3/4\,m_K^4\right)+H_1^{V\prime}(m_K^2,m_\eta^2,m_\eta^2,m_K^2)\left(-5/8\,m_K^4\right)\\
&+H_{21}^{V\prime}(m_\pi^2,m_\pi^2,m_K^2,m_K^2)\left(9/8\,m_K^4\right)+H_{21}^{V\prime}(m_K^2,m_\pi^2,m_\pi^2,m_K^2)\left(-9/64\,m_K^4\right)\\
&+H_{21}^{V\prime}(m_K^2,m_\pi^2,m_\eta^2,m_K^2)\left(27/32\,m_K^4\right)+H_{21}^{V\prime}(m_K^2,m_K^2,m_K^2,m_K^2)\left(9/8\,m_K^4\right)\\
&+H_{21}^{V\prime}(m_K^2,m_\eta^2,m_\eta^2,m_K^2)\left(27/64\,m_K^4\right)+H_{27}^{V\prime}(m_\pi^2,m_\pi^2,m_K^2,m_K^2)\left(-9/8\,m_K^2\right)\\
&+H_{27}^{V\prime}(m_K^2,m_\pi^2,m_\pi^2,m_K^2)\left(9/64\,m_K^2\right)+H_{27}^{V\prime}(m_K^2,m_\pi^2,m_\eta^2,m_K^2)\left(-27/32\,m_K^2\right)\\
&+H_{27}^{V\prime}(m_K^2,m_K^2,m_K^2,m_K^2)\left(-9/8\,m_K^2\right)+H_{27}^{V\prime}(m_K^2,m_\eta^2,m_\eta^2,m_K^2)\left(-27/64\,m_K^2\right). \qquad (24)
\end{aligned}
$$

$$
\begin{aligned}
F_\pi^3\Delta^V F_\eta^{(6)} &= A^V(m_\pi^2)\left(2\,L_5^r m_\pi^2+12\,L_4^r m_\pi^2-6\,L_3^r m_\pi^2-6\,L_2^r m_\pi^2-24\,L_1^r m_\pi^2\right)\\
&+A^V(m_K^2)\left(8/3\,L_5^r m_K^2+4\,L_5^r m_\pi^2+16\,L_4^r m_K^2-14\,L_3^r m_K^2-8\,L_2^r m_K^2-32\,L_1^r m_K^2\right)\\
&+A^V(m_\eta^2)\left(32/9\,L_5^r m_K^2-14/9\,L_5^r m_\pi^2+16/3\,L_4^r m_K^2-4/3\,L_4^r m_\pi^2-8\,L_3^r m_K^2+2\,L_3^r m_\pi^2\right.\\
&\left.-16\,L_2^r m_K^2+4\,L_2^r m_\pi^2-16\,L_1^r m_K^2+4\,L_1^r m_\pi^2\right)\\
&+A_{23}^V(m_\pi^2)\left(6\,L_3^r+18\,L_2^r\right)+A_{23}^V(m_K^2)\left(2\,L_3^r+24\,L_2^r\right)+A_{23}^V(m_\eta^2)\left(6\,L_3^r+12\,L_2^r+12\,L_1^r\right)\\
&+A^V(m_K^2)\left(-3/2\,\frac{1}{16\pi^2}\,m_K^2-3/8\,\frac{1}{16\pi^2}\,m_\pi^2+3/2\,\overline{A}(m_\pi^2)+3/4\,\overline{A}(m_K^2)\right)\\
&+A^V(m_\eta^2)\left(1/2\,\frac{1}{16\pi^2}\,m_K^2-1/2\,\overline{A}(m_K^2)\right)+A^V(m_\eta^2)\,B^{0V}(m_K^2)\left(-1/2\,m_K^2\right)\\
&+H^V(m_\pi^2,m_K^2,m_K^2,m_\eta^2)\left(-9/16\,m_\pi^2\right)+H^V(m_K^2,m_K^2,m_\eta^2,m_\eta^2)\left(-3/4\,m_K^2+3/16\,m_\pi^2\right)\\
&+H_{27}^V(m_\pi^2,m_K^2,m_K^2,m_\eta^2)\left(27/16\right)+H_{27}^V(m_\eta^2,m_K^2,m_K^2,m_\eta^2)\left(27/16\right)\\
&+H^{V\prime}(m_\pi^2,m_\pi^2,m_\eta^2,m_\eta^2)\left(1/12\,m_\pi^4\right)+H^{V\prime}(m_\pi^2,m_K^2,m_K^2,m_\eta^2)\left(3/4\,m_\pi^2\,m_K^2+1/16\,m_\pi^4\right)\\
&+H^{V\prime}(m_K^2,m_K^2,m_\eta^2,m_\eta^2)\left(25/9\,m_K^4-11/6\,m_\pi^2\,m_K^2+5/16\,m_\pi^4\right)\\
&+H^{V\prime}(m_\eta^2,m_\eta^2,m_\eta^2,m_\eta^2)\left(64/243\,m_K^4-56/243\,m_\pi^2\,m_K^2+49/972\,m_\pi^4\right)\\
&+H_1^{V\prime}(m_\pi^2,m_K^2,m_K^2,m_\eta^2)\left(-2\,m_\pi^2\,m_K^2+1/2\,m_\pi^4\right)\\
&+H_1^{V\prime}(m_\eta^2,m_K^2,m_K^2,m_\eta^2)\left(-16/3\,m_K^4+10/3\,m_\pi^2\,m_K^2-1/2\,m_\pi^4\right)
\end{aligned}
$$

$$
\begin{aligned}
&+H_{21}^{V\prime}(m_\pi^2, m_K^2, m_K^2, m_\eta^2)\left(3\,m_K^4 - 3/2\,m_\pi^2\,m_K^2 + 3/16\,m_\pi^4\right)\\
&+H_{21}^{V\prime}(m_\eta^2, m_K^2, m_K^2, m_\eta^2)\left(3\,m_K^4 - 3/2\,m_\pi^2\,m_K^2 + 3/16\,m_\pi^4\right)\\
&+H_{27}^{V\prime}(m_\pi^2, m_K^2, m_K^2, m_\eta^2)\left(-9/4\,m_K^2 + 9/16\,m_\pi^2\right)\\
&+H_{27}^{V\prime}(m_\eta^2, m_K^2, m_K^2, m_\eta^2)\left(-9/4\,m_K^2 + 9/16\,m_\pi^2\right). \qquad (25)
\end{aligned}
$$

References

[1] S. Aoki *et al.*, Eur. Phys. J. C **74** (2014) 2890 [arXiv:1310.8555 [hep-lat]].

[2] S. Weinberg, Physica A **96** (1979) 327.

[3] J. Gasser and H. Leutwyler, Annals Phys. **158** (1984) 142.

[4] J. Gasser and H. Leutwyler, Nucl. Phys. B **250** (1985) 465.

[5] J. Gasser and H. Leutwyler, Phys. Lett. B **184** (1987) 83.

[6] J. Gasser and H. Leutwyler, Phys. Lett. B **188** (1987) 477.

[7] J. Gasser and H. Leutwyler, Nucl. Phys. B **307** (1988) 763.

[8] M. Luscher, Commun. Math. Phys. **104** (1986) 177.

[9] D. Becirevic and G. Villadoro, Phys. Rev. D **69** (2004) 054010 [hep-lat/0311028].

[10] S. Descotes-Genon, Eur. Phys. J. C **40** (2005) 81 [hep-ph/0410233].

[11] J. Bijnens, Prog. Part. Nucl. Phys. **58** (2007) 521 [hep-ph/0604043].

[12] G. Colangelo and C. Haefeli, Nucl. Phys. B **744** (2006) 14 [hep-lat/0602017].

[13] J. Bijnens and K. Ghorbani, Phys. Lett. B **636** (2006) 51 [hep-lat/0602019].

[14] P. H. Damgaard and H. Fukaya, JHEP **0901** (2009) 052 [arXiv:0812.2797 [hep-lat]].

[15] J. Bijnens, E. Boström and T. A. Lähde, JHEP **1401** (2014) 019 [arXiv:1311.3531 [hep-lat]].

[16] J. Bijnens, talk in Quark Confinement and the hadron spectrum, St. Petersburg, 8-12 September 2014.

[17] S. Scherer and M. R. Schindler, Lect. Notes Phys. **830** (2012) 1; hep-ph/0505265.

[18] J. Bijnens, G. Colangelo and G. Ecker, JHEP **9902** (1999) 020 [hep-ph/9902437].

[19] J. Bijnens, G. Colangelo, G. Ecker, J. Gasser and M. E. Sainio, Nucl. Phys. B **508** (1997) 263 [Erratum-ibid. B **517** (1998) 639] [hep-ph/9707291].

[20] J. Bijnens, G. Colangelo and G. Ecker, Annals Phys. **280** (2000) 100 [hep-ph/9907333].

[21] G. Amorós, J. Bijnens and P. Talavera, Nucl. Phys. B **568** (2000) 319 [hep-ph/9907264].

[22] U. Burgi, Nucl. Phys. B **479** (1996) 392 [hep-ph/9602429].

[23] J. Bijnens, G. Colangelo, G. Ecker, J. Gasser and M. E. Sainio, Phys. Lett. B **374** (1996) 210 [hep-ph/9511397].

[24] J. Bijnens, G. Colangelo and P. Talavera, JHEP **9805** (1998) 014 [hep-ph/9805389].

[25] G. Colangelo and S. Durr, Eur. Phys. J. C **33** (2004) 543 [hep-lat/0311023].

[26] G. Colangelo and C. Haefeli, Phys. Lett. B **590** (2004) 258 [hep-lat/0403025].

[27] G. Colangelo, S. Durr and C. Haefeli, Nucl. Phys. B **721** (2005) 136 [hep-lat/0503014].

[28] G. Amorós, J. Bijnens and P. Talavera, Nucl. Phys. B **585** (2000) 293 [Erratum-ibid. B **598** (2001) 665] [hep-ph/0003258].

[29] `http://www.thep.lu.se/~bijnens/chpt/`

[30] J. Bijnens and J. Prades, Nucl. Phys. B **490** (1997) 239 [hep-ph/9610360].

[31] J. Bijnens and G. Ecker, arXiv:1405.6488 [hep-ph].

[32] G. Colangelo, private communication.

[33] J. Bijnens, "CHIRON: a package for ChPT numerical results at two loops," arXiv:1412.0887 [hep-ph], to be published in Eur. Phys. J. C.

[34] J. A. M. Vermaseren, "New features of FORM," math-ph/0010025.

Paper III

LU TP 15-29
arXiv:1508.07238 [hep-lat]
August 2015

Finite Volume for Three-Flavour Partially Quenched Chiral Perturbation Theory through NNLO in the Meson Sector

Johan Bijnens and Thomas Rössler

Department of Astronomy and Theoretical Physics, Lund University,
Sölvegatan 14A, SE 223-62 Lund, Sweden

Abstract

We present a calculation of the finite volume corrections to meson masses and decay constants in three flavour Partially Quenched Chiral Perturbation Theory (PQChPT) through two-loop order in the chiral expansion for the flavour-charged (or off-diagonal) pseudoscalar mesons. The analytical results are obtained for three sea quark flavours with one, two or three different masses. We reproduce the known infinite volume results and the finite volume results in the unquenched case. The calculation has been performed using the supersymmetric formulation of PQChPT as well as with a quark-flow technique.

Partial analytical results can be found in the appendices. Some examples of cases relevant to lattice QCD are studied numerically. Numerical programs for all results are available as part of the CHIRON package.

1 Introduction

Quantum chromodynamics (QCD) is nowadays accepted to be the theory describing the strong force. The smallness of the coupling constant at high energies makes it possible to test and confirm the theory in highly energetic scattering. It also provides – at least in principle – a way to obtain various low-energy hadronic observables, such as masses and decay constants, but it has hitherto been impossible to derive such quantities of interest in terms of analytical expressions by means of ab initio calculations. A numerical approach that can circumvent the problem is lattice QCD. A review of the applications to flavour and low-energy hadron physics is [1]. To calculate observables, one uses a numerical evaluation of the QCD path integral in a Monte Carlo approach. A number of restrictions follow from the nature of the calculation. Since it is carried out on a space-time lattice in a finite volume, it is of high interest to have the effect of the finite volume under good control. Furthermore, although lattice computations in meson physics are now feasible when using physical parameters for the light quark masses, a lot of calculations still use unphysically high masses for the quarks. It is also useful to vary quark masses to study a number of phenomena. A common solution to study quark mass dependence with lower computational needs is given by partial quenching. In partially quenched QCD (PQQCD), one associates different masses (usually larger ones) to the sea quarks and the valence quarks. Valence quarks are those connected to the external operators while sea quarks are those in the fermion determinant or equivalently in closed loops. Sea quarks are only connected to external states via gluons.

The preferable way to correct for unphysical quark masses is by means of Chiral Perturbation Theory (ChPT) [2, 3, 4]. Finite volume effects for ChPT have been introduced in [5, 6, 7]. The corresponding effective theory for PQQCD is given by Partially Quenched Chiral Perturbation Theory (PQChPT) [8]. The arguments underlying this are elaborated in [9].

The proper matching of calculations in PQChPT to results from Partially Quenched Lattice QCD allows a whole new landscape of possibilities, such as improved validation and extrapolation of lattice results, or a more accurate determination of the chiral low-energy constants (LECs), see e.g. [10]. It should be stressed that, as opposed to fully quenched calculations, partially quenched calculations are connected to their corresponding unquenched scenarios by a *continuous* change in variables, making it possible to immediately extract physical results from otherwise unphysical simulations.

In this paper, we address the finite volume corrections through two-loop order in the PQChPT framework, specifically for the flavour-charged or off-diagonal mesons. The infinite volume (IV) results in PQChPT to this order are known for three [11, 12, 13] and two [14] sea quark flavours. The finite volume (FV) corrections in (unquenched) ChPT at two-loop order have been addressed in our earlier study [15]. The needed integrals have been worked out in [16]. Our expressions are valid in the frame with vanishing spatial momentum, $\vec{p} = 0$, often called the center-of-mass frame. In the so-called moving frames or with twisted boundary conditions there will be additional terms. We have chosen to present our result in terms of lowest order masses given the ambiguity in expressing the

results in terms of the large number of possible different physical masses.

Earlier work on finite volume corrections at NNLO are besides our own work [15], the pion mass in two-flavour ChPT [17] and the vacuum expectation value in three flavour ChPT [18]. Extensions of the latter work to partially quenched are in [19]. We did not find published results for the finite volume corrections at one-loop order in the partially quenched case. They are however implicit in the expressions given for the staggered partially quenched case in [20, 21].

We give a short list of references for ChPT and discuss some small points in Sect. 2. The definitions of the integrals we use and how they relate to the results in [16] is given in Sect. 3. The next section describes our major result which is the full finite volume correction to the pion mass and decay constant to two-loop order in ChPT. Sect. 4 contains the results for the three-flavour case for pion, kaon and eta for both the mass and decay constant. The large two-loop order formulas are collected for one case in the appendices and all of them can be downloaded from [22]. A numerical discussion of our results is in Sect. 5.

2 Partially Quenched Chiral Perturbation Theory

This section is very similar to the description of PQChPT given in [13] since our work is the extension to finite volume of that paper.

An introduction to ChPT can be found in [23] and in the two-loop review [24]. The lowest order and p^4-Lagrangian can be found in [4]. The order p^6 Lagrangian is given in [25]. We use the standard renormalization scheme in ChPT. An extensive discussion of the renormalization scheme can be found in [26] and [27]. Important for our work is that the LECs do not depend on the volume [7]. An introduction with applications to lattice QCD is [28]. References to more introductory literature can be found on [22].

The expansion in ChPT is in momenta p and quark-masses. We count the latter as two powers of p. This counting is referred to as p-counting. We prefer to designate orders by the p-counting order at which the diagram appears. Thus we refer to lowest order (LO) as order p^2, next-to-leading order (NLO) as order p^4 or one-loop order and next-to-next-to-leading order (NNLO) as order p^6 or two-loop order and include in the terminology one- or two-loop order also the diagrams with fewer loops but the same order in p-counting.

2.1 The Lagrangian

Three massless quark flavours QCD has a chiral symmetry

$$G = SU(n_f)_L \times SU(n_f)_R \,. \tag{1}$$

which is spontaneously broken to the diagonal subgroup $SU(3)_V$. The Goldstone bosons following from this spontaneous breakdown are described by the meson octet matrix

$$\phi(x) \;=\; \begin{pmatrix} \frac{1}{\sqrt{2}}\pi^0 + \frac{1}{\sqrt{6}}\eta & \pi^+ & K^+ \\ \pi^- & -\frac{1}{\sqrt{2}}\pi^0 + \frac{1}{\sqrt{6}}\eta & K^0 \\ K^- & \bar{K}^0 & -\frac{1}{\sqrt{3}}\eta \end{pmatrix}, \tag{2}$$

The flavour-singlet component has been integrated out since it is heavy due to the $U(1)_A$ anomaly. The spontaneous symmetry breaking is the basis of ChPT.

In partially quenched QCD one distinguishes between valence and sea quarks. Valence quarks are connected to the external states (or operators) while the sea-quarks are those contributing in closed loops only connected via gluons to external states. These can be given different masses in lattice QCD calculations. The ChPT for this partial quenching can be done by studying the quark flow generalizing the quenched case studied in [29]. One can then treat the sea and valence lines differently. Alternatively, one can make use of the supersymmetric formulation of PQChPT [8]. In the latter, three corresponding sets of quarks are introduced instead of only two: In addition to the valence and sea sector, a set of so-called ghost quarks is added. These are "bosonic" in the sense that they are treated as commuting variables. With their masses fixed to the same numerical values as present in the valence sector, they will cancel exactly the contribution coming from closed valence quark loops. Most of the remainder of this section will be concerned with the supersymmetric formulation. The changes needed to use a quark flow technique are discussed at the end.

The chiral symmetry group is formally extended to the graded[1]

$$G = SU(n_{\rm val} + n_{\rm sea}|n_{\rm val})_L \times SU(n_{\rm val} + n_{\rm sea}|n_{\rm val})_R \,, \tag{3}$$

for the case of $n_{\rm val}$ valence and $n_{\rm sea}$ quarks. The chiral group G is spontaneously broken to the diagonal subgroup $SU(n_{\rm val} + n_{\rm sea}|n_{\rm val})_V$. We will work in the flavour basis rather than in the meson basis. We will thus use fields ϕ_{ab} corresponding to the flavour content of $q_a\bar{q}_b$. The mixing of the neutral eigenstates and the integrating out of the singlet degree of freedom is taken care of by using a more complicated propagator[2].

The corresponding Goldstone degrees of freedom are put in a matrix with the generic structure

$$\Phi = \begin{pmatrix} \left[\ q_V\bar{q}_V\ \right] & \left[\ q_V\bar{q}_S\ \right] & \left[\ q_V\bar{q}_B\ \right] \\ \left[\ q_S\bar{q}_V\ \right] & \left[\ q_S\bar{q}_S\ \right] & \left[\ q_S\bar{q}_B\ \right] \\ \left[\ q_B\bar{q}_V\ \right] & \left[\ q_B\bar{q}_S\ \right] & \left[\ q_B\bar{q}_B\ \right] \end{pmatrix} . \tag{4}$$

V denotes valence, S denotes sea and B denotes the bosonic ghost quarks. Note that the meson fields containing one single ghost quark only will themselves obey fermionic, i. e. anticommuting, statistics.

The structure of the Lagrangian is similar to standard ChPT for a generic number of flavours. The lowest order Lagrangian is

$$\mathcal{L}_2 = \frac{F_0^2}{4}\langle u_\mu u^\mu + \chi_+ \rangle \,. \tag{5}$$

[1]The precise structure of the symmetry group is somewhat different, but the one given here is sufficient for both the present discussion as well as for practical calculations. The "approximate" symmetry group reproduces the right Ward identities [10, 30].

[2]This is described in detail in [30]. It is possible to use the same method also in standard ChPT.

At one-loop, it is given by

$$\begin{aligned}\mathcal{L}_4 &= \hat{L}_0 \langle u^\mu u^\nu u_\mu u_\nu \rangle + \hat{L}_1 \langle u^\mu u_\mu \rangle^2 + \hat{L}_2 \langle u^\mu u^\nu \rangle \langle u_\mu u_\nu \rangle + \hat{L}_3 \langle (u^\mu u_\mu)^2 \rangle \\ &+ \hat{L}_4 \langle u^\mu u_\mu \rangle \langle \chi_+ \rangle + \hat{L}_5 \langle u^\mu u_\mu \chi_+ \rangle + \hat{L}_6 \langle \chi_+ \rangle^2 + \hat{L}_7 \langle \chi_- \rangle^2 + \frac{\hat{L}_8}{2} \langle \chi_+^2 + \chi_-^2 \rangle + \dots \quad (6)\end{aligned}$$

We show only the terms relevant for our work.

The generalized Goldstone manifold is parametrized by

$$u \equiv \exp\left(i\Phi/(\sqrt{2}\hat{F})\right) \quad (7)$$

similar to the exponential representation in standard ChPT. It is a 9×9 matrix with fermionic parts. We have furthermore introduced

$$\begin{aligned}u_\mu &= i\left\{u^\dagger(\partial_\mu - ir_\mu)\, u - u\,(\partial_\mu - il_\mu)\, u^\dagger\right\}, \\ \chi_\pm &= u^\dagger \chi\, u^\dagger \pm u\, \chi^\dagger\, u\,. \quad (8)\end{aligned}$$

The matrix χ is for this work restricted to

$$\chi = 2B_0\, \mathrm{diag}(m_1, \dots, m_9) \quad (9)$$

with m_i the quark mass of quark i and B_0 a LEC. We have here $m_1 = m_7, m_2 = m_8, m_3 = m_9$ as the valence masses and m_4, m_5, m_6 as the sea quark masses. Ordinary traces have been replaced by supertraces, denoted by $\langle\ \rangle$, defined in terms of the ordinary ones by

$$\mathrm{Str}\begin{pmatrix} A & B \\ C & D \end{pmatrix} = \mathrm{Tr}\, A - \mathrm{Tr}\, D\,. \quad (10)$$

B and C denote the fermionic blocks in the matrix. The supersinglet Φ_0, generalizing the η', is integrated out to account for the axial anomaly as in standard ChPT, implying the additional condition

$$\langle \Phi \rangle = \mathrm{Str}\,(\Phi) = 0\,. \quad (11)$$

However, as mentioned above, we will work in the flavour basis enforcing the constraint (11) via the propagator.

A calculation in PQChPT has to be performed using a larger set of operators since no further reduction by means of Cayley-Hamilton relations can be performed. The three-flavour PQChPT Lagrangian (equation (6)) thus has 11 LECs for PQChPT.

The LECs for standard three flavour ChPT are related to those of three flavour PQChPT via

$$L_1^r = \hat{L}_1^r + \hat{L}_0^r/2, \qquad L_2^r = \hat{L}_2^r + \hat{L}_0^r, \qquad L_3^r = \hat{L}_3^r - 2\,\hat{L}_0^r, \quad (12)$$

and $L_i^r = \hat{L}_i^r$ for the others. Note that a numerical value for $\hat{L}_0$ cannot be obtained by experiment, but can be determined only via PQQCD lattice simulations or modelling.

An additional comment is that the divergences for PQChPT are directly related to those for n_{sea}-flavour ChPT [27] when all traces are replaced by supertraces. This can be argued using the formal equivalence of the equations of motion used or via the replica trick [31].

2.2 The propagator and notation for masses and residues

The variant of PQChPT, considered in this paper, comes with three valence quarks, with masses m_1, m_2, m_3 and three sea quarks with masses m_4, m_5, m_6. The additional ghost quarks emerging only in the supersymmetric formulation have masses m_7, m_8, m_9. They do not appear explicitly since they are fixed to the ones in the valence sector, i.e. $m_7 = m_1$, $m_8 = m_2$, $m_9 = m_3$.

We use the numbers d_{val} and d_{sea} to denote the number of non-degenerate quark masses in each sector. In the case of two non-degenerate mass scales for one sector, it is the two masses with the lowest indices that we set degenerate, which will in turn both be represented by the mass scale with the lowest index, e.g. in the case $d_{sea} = 2$ we have $m_4 = m_5 \neq m_6$ and expressions will be explicitly dependent on m_4 and m_6 only.

In fact we will always absorb a factor $2B_0$ in the notation and we use

$$\chi_i \equiv 2B_0 m_i \,, \qquad \chi_{ij} \equiv \frac{1}{2}\left(\chi_i + \chi_j\right) \,. \tag{13}$$

The lowest order masses for off-diagonal mesons with flavour content $q_i\bar{q}_j$ are given by χ_{ij} and we will use χ_i rather then χ_{ii} for equal masses. Dealing with masses for the diagonal valence mesons in PQChPT is not trivial. This is discussed in detail in [30] and extended to NNLO in [32]. The diagonal sea quark sector has two masses associated with it, corresponding to the neutral pion and eta masses. These we denote by χ_π and χ_η. They are defined as the solutions to the equations

$$\begin{aligned} \chi_\pi + \chi_\eta &= \frac{2}{3}\left(\chi_4 + \chi_5 + \chi_6\right), \\ \chi_\pi \chi_\eta &= \frac{1}{3}\left(\chi_4\chi_5 + \chi_5\chi_6 + \chi_4\chi_6\right). \end{aligned} \tag{14}$$

They are non-polynomial in the sea masses χ_j for three non-degenerate quark masses, i.e. $d_{sea} = 3$. For $d_{sea} = 2$ one has instead $\chi_\pi = \chi_4$ and $\chi_\eta = (1/3)(\chi_4 + 2\chi_6)$.

The flavour-charged propagator, connecting ϕ_{ij} with ϕ_{ji}, is given by [8, 10, 30]

$$-i\,G^c_{ij}(k) \;=\; \frac{\epsilon_j}{k^2 - \chi_{ij} + i\varepsilon} \quad (i \neq j)\,. \tag{15}$$

with $\chi_{ij} \equiv (\chi_i + \chi_j)/2$, the lowest order meson mass, and the signature ϵ_j is defined as $+1$ for the flavor indices of the $n_{\rm val} + n_{\rm sea}$ fermionic quarks, and as -1 for the flavor indices of the $n_{\rm val}$ bosonic ghost quarks. In the present calculation, with the number of valence and sea quarks as given above, ϵ_j thus takes the values

$$\epsilon_j = \begin{cases} +1 & \text{for} \quad j = 1, \ldots, 6 \\ -1 & \text{for} \quad j = 7, 8, 9\,. \end{cases} \tag{16}$$

The flavour-neutral propagator, connecting a flavour field ϕ_{ii} to ϕ_{jj}, on the other hand suffers from additional contributions emerging from the elimination of the Φ_0 and the partial quenching [8, 10, 30]. We write it as

$$G^n_{ij}(k) \;=\; G^c_{ij}(k)\,\delta_{ij} - G^q_{ij}(k)/n_{\rm sea}. \tag{17}$$

The additional terms are either

$$\begin{aligned} -i\,G^q_{ij}(k) &= \frac{R^i_{j\pi\eta}}{k^2-\chi_i+i\varepsilon}+\frac{R^j_{i\pi\eta}}{k^2-\chi_j+i\varepsilon} \\ &+ \frac{R^\pi_{\eta ij}}{k^2-\chi_\pi+i\varepsilon}+\frac{R^\eta_{\pi ij}}{k^2-\chi_\eta+i\varepsilon}, \end{aligned} \tag{18}$$

for the case with $i \neq j$ and $\chi_i \neq \chi_j$, or

$$\begin{aligned} -i\,G^q_{ij}(k) &= \frac{R^d_i}{(k^2-\chi_i+i\varepsilon)^2}+\frac{R^c_i}{k^2-\chi_i+i\varepsilon} \\ &+ \frac{R^\pi_{\eta ii}}{k^2-\chi_\pi+i\varepsilon}+\frac{R^\eta_{\pi ii}}{k^2-\chi_\eta+i\varepsilon}, \end{aligned} \tag{19}$$

for the case with $\chi_i = \chi_j$ which clearly includes $i = j$. In the second case, the sum of single poles is supplemented with an unphysical double pole. Since double poles emerge due to the partial quenching in the valence sector, they disappear by taking the appropriate unquenched limit.

Using the ratios of products of differences of masses

$$\begin{aligned} R^z_{ab} &= \chi_a-\chi_b, \\ R^z_{abc} &= \frac{\chi_a-\chi_b}{\chi_a-\chi_c}, \\ R^z_{abcd} &= \frac{(\chi_a-\chi_b)(\chi_a-\chi_c)}{\chi_a-\chi_d}, \\ R^z_{abcdefg} &= \frac{(\chi_a-\chi_b)(\chi_a-\chi_c)(\chi_a-\chi_d)}{(\chi_a-\chi_e)(\chi_a-\chi_f)(\chi_a-\chi_g)}, \end{aligned} \tag{20}$$

the residues R of the neutral meson propagator in equations (18) and (19) are (for $d_{sea} = 3$)

$$R^i_{jkl} = R^z_{i456jkl}, \quad R^d_i = R^z_{i456\pi\eta}, \quad R^c_i = R^i_{4\pi\eta}+R^i_{5\pi\eta}+R^i_{6\pi\eta}-R^i_{\pi\eta\eta}-R^i_{\pi\pi\eta}. \tag{21}$$

Note that many of these quantities vanish when i takes the value of a sea quark index. The sea-quark propagators thus do not contribute any double poles as expected since these originate from the quenching in the valence sector.

For $d_{sea} = 2$ or $\chi_\pi = \chi_5 = \chi_4$. The needed residues simplify to

$$R^i_{jk} = R^z_{i46jk}, \quad R^d_i = R^z_{i46\eta}, \quad R^c_i = R^i_{4\eta}+R^i_{6\eta}-R^i_{\eta\eta}. \tag{22}$$

The corresponding propagator can be obtained by removing all pion indices as well as the pion mass pole from equations (18) and (19).

The physically less interesting case $d_{sea} = 1$ immediately yields $\chi_\pi = \chi_\eta = \chi_6 = \chi_5 = \chi_4$. All residues from the sea quark sector are reduced to numbers, only

$$R^i_j = R^z_{i4j}, R^d_i = R^z_{i4}\,, \tag{23}$$

appear.

2.3 The quark flow case

We have performed the calculation using the supersymmetric method described above but also with the quark flow method [29]. We use the same Lagrangians as in (5) and (6) but with normal traces everywhere. The matrix Φ is now written in terms of generic fields ϕ_{ij} and all indices are kept symbolic implying summations.

Connecting propagators of a field ϕ_{ij} to ϕ_{kl} should be done by using

$$G_{ijkl}(k) = G^c_{ij}(k)\delta_{il}\delta_{jk} - \delta_{ij}\delta_{kl}G^q_{ik}(k)/n_{\rm sea}\,. \tag{24}$$

The propagators $G^c_{ij}(k), G^q_{ij}(k)$ remain the same but we can now disregard the factors ϵ_j since with this method there are no bosonic ghost quarks.

After constructing the Feynman diagrams using the above, the quark flow is visible following the symbolic flavour indices. Next, one replaces the index lines that connect to external fields or operators by their appropriate valence value. The remaining index lines are now sea indices and are summed over with the sea quark indices.

The results obtained with the quark flow method agreed in all cases with those of the supersymmetric method.

3 The finite volume integrals

The loop integrals at finite volume at one-loop are well known. There is a sum over discrete momenta in every direction with a finite size rather than a continuous integral. The Poisson summation formula allows to identify the infinite volume part and the finite volume corrections. The remainder can be done with two different methods. For one-loop tadpole integrals the first method was introduced by [5, 6, 7] and a sum over Bessel functions, that for large ML converges fast, remains to be done. With the other method one remains instead with an integral over a Jacobi theta function, this method can be used for small and medium ML as well. It can be found in [33]. The extensions to other one-loop integrals is done in both cases by combining propagators with Feynman parameters. The first method was extended to the equal mass two-loop sunset integral [17] and later to the more general mass case in [16]. The latter extended the Jacobi theta function method as well to the sunset case. Details and further references can be found in [16]. In this paper we use Minkowski notation for the integrals.

For the one-loop integrals needed here, we use a notation that does a first classification according to the sum of the powers of the propagators with different masses, $m_1, m_2, ..., m_{max}$. We label the integrals A, B, C, D for a total power of propagators of $n = 1, 2, 3, 4$ respectively, since total powers of up to 4 can appear in the calculation as follows from the discussion of double poles in Sec. 2.2. The different mass scales are given as consecutive arguments of the integral. Alternatively, if only one mass scale in total is present, we omit its repetition as a shorthand notation. For the present calculation at most two different scales can appear.

Both scalar and tensor integrals will occur, e. g. in the simplest case of one single propagator raised to single power

$$\left\{A(m^2), A_{\mu\nu}(m^2)\right\} = \frac{1}{i}\int_V \frac{d^dr}{(2\pi)^d}\frac{\{1, r_\mu r_\nu\}}{(r^2-m^2)}\,. \tag{25}$$

We used the subscript V to indicate it is a finite volume sum and integral.

More Lorentz structures are possible than in the infinite volume case. We define the tensor $t_{\mu\nu}$ as the spatial part of the Minkowski metric $g_{\mu\nu}$, to express these. For the center-of-mass (cms) case this is sufficient. The needed functions for the above example are

$$A_{\mu\nu}(m^2) = g_{\mu\nu}A_{22}(m^2) + t_{\mu\nu}A_{23}(m^2)\,. \tag{26}$$

We then use Passarino-Veltman identities in order to further simplify the result. In infinite volume the relation obtained by considering $g^{\mu\nu}A_{\mu\nu}(m^2)$ can be used to remove A_{22}. In finite volume, we again remove the A_{22}-type integrals from the extended relation

$$dA_{22}(m^2) + 3A_{23}(m^2) = m^2A(m^2)\,. \tag{27}$$

Each integral is split into an infinite volume contribution and a finite volume correction by means of the Poisson summation formula, while simultaneously being expanded in ϵ up to the necessary order.

$$A(m^2) = \lambda_0\frac{m^2}{16\pi^2} + \overline{A}(m^2) + A^V(m^2) + \epsilon\left(A^\epsilon(m^2) + A^{V\epsilon}(m^2)\right) + \cdots\,. \tag{28}$$

Here, $\lambda_0 = \frac{1}{\epsilon} + \log(4\pi) + 1 - \gamma$. The same split is done for all one-loop integrals. The expressions can be obtained by using the relations

$$\begin{aligned}
B(m^2) &= \frac{\partial}{\partial m^2}A(m^2),\\
C(m^2) &= \frac{1}{2}\frac{\partial}{\partial m^2}B(m^2),\\
D(m^2) &= \frac{1}{3}\frac{\partial}{\partial m^2}C(m^2),\\
B(m_1^2, m_2^2) &= \frac{A(m_1^2) - A(m_2^2)}{m_1^2 - m_2^2}.
\end{aligned} \tag{29}$$

The sunset integrals, defined as

$$\begin{aligned}
&\left\{H, H_\mu, H^s_\mu, H_{\mu\nu}, H^{rs}_{\mu\nu}, H^{ss}_{\mu\nu}\right\}(n, m_1^2, m_2^2, m_3^2, p) =\\
&\quad\frac{1}{i^2}\int_V \frac{d^dr}{(2\pi)^d}\frac{d^ds}{(2\pi)^d}\frac{\{1, r_\mu, s_\mu, r_\mu r_\nu, r_\mu s_\nu, s_\mu s_\nu\}}{\left(r^2-m_1^2\right)^{n_1}\left(s^2-m_2^2\right)^{n_2}\left((r+s-p)^2-m_3^2\right)^{n_3}}\,,
\end{aligned} \tag{30}$$

now come with eight different pole configurations. We label these by the index n according to Tab. 1 analoguous to the infinite volume definitions of [11, 12, 13, 14].

	n_1	n_2	n_3
$n=1$	1	1	1
$n=2$	2	1	1
$n=3$	1	2	1
$(n=4)$	1	1	2
$n=5$	2	2	1
$(n=6)$	2	1	2
$n=7$	1	2	2
$n=8$	2	2	2

Table 1: Overview of the notation for the possible configurations of powers of propagators in the H functions in PQChPT. Redundant configurations are given in parentheses.

The interchange $(r, m_1^2, n_1) \leftrightarrow (s, m_2^2, n_2)$ allows to show that $H_\mu^s, H_{\mu\nu}^{ss}$ are related directly to $H_\mu^r, H_{\mu\nu}^{rr}$. $H_{\mu\nu}^{rs}$ can also be related to $H_{\mu\nu}$ using the trick shown in [34] and also used in [16], now taking the pole configurations into account properly. The resulting $H_{\mu\nu}$ and H_μ can then be reduced to six pole configurations only, cf. table 1, the bracketed ones can be eliminated via the interchange above. In the scalar case H, only four pole configurations are needed.

For the partially quenched calculation we thus generalized the sunset integrals used in our earlier work via

$$H(\chi_i, \chi_j, \chi_k; p^2) \to H(n, \chi_i, \chi_j, \chi_k; p^2), \tag{31}$$

introducing the new index n for the pole configurations as the first argument. Note on the side that all new pole configurations are related to the simplest one by differentiation with respect to the mass scales.

In the cms frame, we reduce the tensor structure of the sunsets as

$$\begin{aligned} H_\mu &= p_\mu H_1 \\ H_{\mu\nu} &= p_\mu p_\nu H_{21} + g_{\mu\nu} H_{22} + t_{\mu\nu} H_{27}\,. \end{aligned} \tag{32}$$

As in [15], we renormalize the FV sunsets by not only subtracting the infinite part but also an additional finite part containing $\mathcal{O}(\epsilon)$ contributions of one-loop integrals. In this way, the latter integrals will cancel out of the final result, and thus do not need to be computed. The splitting for $n = 1$

$$\tilde{H}^V = \frac{\lambda_0}{16\pi^2}\left(A^V(m_1^2) + A^V(m_2^2) + A^V(m_3^2)\right) + \frac{1}{16\pi^2}\left(A^{V\epsilon}(m_1^2) + A^{V\epsilon}(m_2^2) + A^{V\epsilon}(m_3^2)\right)$$

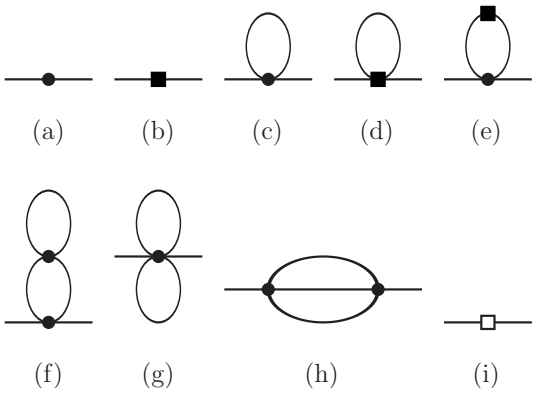

Figure 1: Diagrammatic contributions to the pseudoscalar self-energy, up to $\mathcal{O}(p^6)$. Circular vertices are of $\mathcal{O}(p^2)$, the filled boxes are of $\mathcal{O}(p^4)$, the open box is of $\mathcal{O}(p^6)$. The tree level diagrams (a,b,i) do not contribute to finite volume corrections.

$$
\begin{aligned}
& +H^V\,, \\
\tilde{H}_1^V &= \frac{\lambda_0}{16\pi^2}\frac{1}{2}\left(A^V(m_2^2)+A^V(m_3^2)\right)+\frac{1}{16\pi^2}\frac{1}{2}\left(A^{V\epsilon}(m_2^2)+A^{V\epsilon}(m_3^2)\right)+H_1^V\,, \\
\tilde{H}_{21}^V &= \frac{\lambda_0}{16\pi^2}\frac{1}{3}\left(A^V(m_2^2)+A^V(m_3^2)\right)+\frac{1}{16\pi^2}\frac{1}{3}\left(A^{V\epsilon}(m_2^2)+A^{V\epsilon}(m_3^2)\right)+H_{21}^V\,, \\
\tilde{H}_{27}^V &= \frac{\lambda_0}{16\pi^2}\left(A_{23}^V(m_1^2)+\frac{1}{3}A_{23}(m_2^2)+\frac{1}{3}A_{23}^V(m_3^2)\right) \\
& \quad +\frac{1}{16\pi^2}\left(A_{23}^{V\epsilon}(m_1^2)+\frac{1}{3}A_{23}^{V\epsilon}(m_2^2)+\frac{1}{3}A_{23}^{V\epsilon}(m_3^2)\right)+H_{27}^V\,, \qquad (33)
\end{aligned}
$$

has to be generalized for the other pole configurations by taking the appropriate derivatives w.r.t. the masses.

4 Analytical results

The calculation of the masses proceeds in the usual way from the Feynman diagrams for the self-energy shown in Fig. 1. We have performed the calculation for the off-diagonal mesons, i.e. consistening of a valence quark and a different valence anti-quark, and for the case of three flavours of sea quarks. The calculation has been done for all mass cases, equal and different valence quark-masses, $d_{val} = 1, 2$, and sea quark masses all equal, $d_{sea} = 1$, two equal and the third different, $d_{sea} = 2$ and all three different, $d_{sea} = 3$.

A large number of checks have been done on the calculations. They have been performed both in the supersymmetric formalism and using quark flow techniques. The infinite volume results are also in full agreement with [11, 12, 13]. The finite volume parts agree with our earlier results [15] when these are expressed in terms of lowest order masses and when the sea masses are put equal to the valence masses.

The formulas especially for the case of three different sea quark masses are very long. In App. A we list the case of equal valence masses and two sea quark masses. This corresponds to the charged pion mass in the isospin limit. The other cases can be downloaded from [22].

The masses are given as

$$m_{ij}^2 = \chi_{ij} + m_{ij}^{2(4)} + \Delta^V m_{ij}^{2(4)} + m_{ij}^{2(6)} + \Delta^V m_{ij}^{2(6)} \,. \tag{34}$$

In addition a superscript indicating $d_{val}d_{sea}$ is added. The infinite volume and the one-loop finite volume corrections were known before. The new parts are the two-loop finite volume corrections. These we split in addition in an L_i^r dependent part and a pure two-loop contribution

$$\Delta^V m_{ij}^{2(6)} = \Delta^V m_{ij}^{2(6L)} + \Delta^V m_{ij}^{2(6R)} \,. \tag{35}$$

The subscript ij is set to 12 for $d_{val} = 1$ and to 13 for $d_{val} = 2$ similar to the infinite volume work.

The decay constant is defined in the usual way as

$$\langle 0|\bar{q}_j \gamma_\mu \gamma_5 q_i|M_{ij}(p)\rangle = i\sqrt{2} F_{ij} p_\mu \,, \tag{36}$$

for the pseudoscalar meson M_{ij} with quark content $i \neq j$ and momentum p. The calculation needs the diagrams of Fig. 1 for the wave function renormalization and the same ones with one external meson leg replaced by an insertion of the axial current.

We split the result as

$$F_{ij} = F_0 + F_{ij}^{(4)} + \Delta^V F_{ij}^{(4)} + F_{ij}^{(6)} + \Delta^V F_{ij}^{(6)} \,. \tag{37}$$

The NNLO part is split again in

$$\Delta^V F_{ij}^{(6)} = \Delta^V F_{ij}^{(6L)} + \Delta^V F_{ij}^{2(6R)} \,. \tag{38}$$

The calculations have been done using the supersymmetric and the quark flow methods. The infinite volume and NLO results agree with the known expressions and the result reduces in the correct limit to the unquenched results of our earlier work [15]. The formulas are rather long, the case for equal valence masses and two different sea masses corresponding to the charged pion decay constant in the isospin limit is given in App. B. The expressions for the other cases can be downloaded from [22].

5 Numerical examples

The intention is that various lattice QCD collaborations can use our formulas. All cases discussed have been included in the package CHIRON [35] available from [36]. The numerical results shown in this section have been obtained with that implementation. The programs have been cross-checked with an independent version. It has been checked that

the results reduce in the appropriate limits to those of our earlier work [15]. For this purpose the expressions obtained in [15], but rewritten in terms of lowest order masses and decay constants, have been implemented and included in CHIRON [36]. In addition, a check has been done that the different mass cases reduce to each other numerically.

For input values we have chosen the recent global fit for the L_i^r [37]. We have set the extra LEC $L_0^r = 0$. We always use a scale of $\mu = 0.77$ GeV. For the size of the lattice we present results for a length L such that $ML = 2$ for $M = 0.13$ GeV. The lowest order pion decay constant we have chosen throughout as $F_0 = 87.7$ MeV.

The numerical results are presented via

$$\begin{aligned} \Delta_M^V &= \frac{m_{ij}^{2V} - m_{ij}^{2\infty}}{\chi_{ij}} \\ \Delta_F^V &= \frac{F_{ij}^V - F_{ij}^\infty}{F_0}\,. \end{aligned} \tag{39}$$

We thus plot the size of the finite volume corrections relative to the lowest order value of the quantity under consideration. Note that the results are for charged or off-diagonal mesons. They consist of a quark and a different anti-quark which might have equal mass.

5.1 $d_{\rm val} = d_{\rm sea} = 1$

Here we set all valence and all sea masses equal, $d_{\rm val} = d_{\rm sea} = 1$. The size of the finite volume corrections as a function of χ_1 and χ_4 is shown in Fig. 2. The corrections in this case are reasonable, at most a few %, except for very low masses and become very large for low valence and high sea quark mass.

5.2 The pion mass

In this subsection we look at the case where the lowest order mass is around the pion mass. We plot Δ_M^V with $\sqrt{\chi_{12}} = 0.13$ GeV. The strange sea quark mass we have always chosen such that the average lowest order kaon mass is 0.45 GeV. This corresponds to $\sqrt{\chi_6} = \sqrt{2(0.45)^2 - (0.13)^2}$ GeV ≈ 0.623 GeV. The other input parameters are chosen as given in the introduction of this section. We have restricted the sea up and down quark masses corresponding to a lowest order sea quark pion of 100 to 300 MeV.

The first case we look at is $d_{\rm val} = 1, d_{\rm sea} = 2$. This corresponds to taking the up and down quark masses equal in both the valence and sea quark sector and a different strange quark mass. This is the isospin limit. The result is shown in Fig. 3(a). There is a rather large cancellation between the p^4 and p^6 correction while the p^6 contribution coming from the L_i^r is fairly small.

We now include isospin breaking in the valence sector. We thus look at the case with $d_{\rm val} = 2, d_{\rm sea} = 2$. We fix the valence quark masses such that $\chi_1 + \chi_2 = 2\chi_{12}$ and $\chi_1/\chi_2 = 1/2$. There is a sizable isospin breaking visible in the finite volume corrections, as shown in Fig. 3(b).

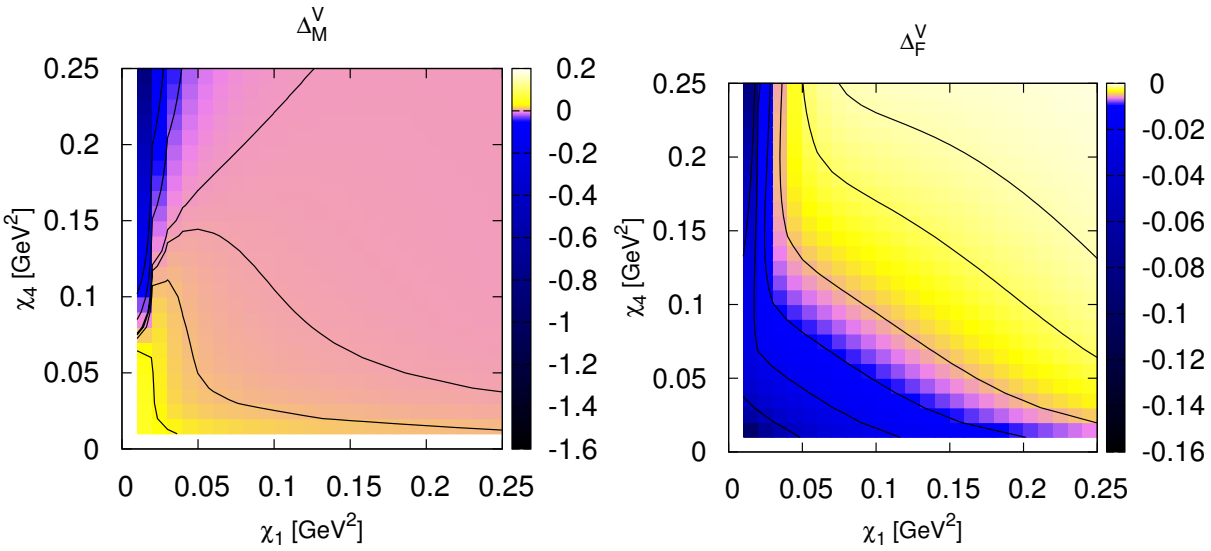

Figure 2: The finite volume corrections relative to the lowest order value as defined in (39) for the case with all valence masses equal and all sea masses equal. Left: Δ_M^V the correction to the mass-squared, contour lines are drawn at $0.03, 0.01, 0.003, 0, -0.03, -0.01$ starting from the bottom left and going counterclockwise. Right: The correction to the decay constant, contour lines are drawn at $-0.001, -0.002, -0.005, -0.01, -0.02, -0.05$ going from top-right to bottom-left.

The opposite case, isospin breaking in the sea sector, but not in the valence sector, leads to numerically similar but opposite sign corrections. Here we used $\chi_1 = \chi_2$, $\chi_4 = \chi_5/2$ and $\chi_4 + \chi_5 = 2\chi_{\rm av}$. The results are shown in Fig. 3(c).

Finally, we introduce isospin breaking in both the valence and sea quark sector with $\chi_1/\chi_2 = 1/2$, $\chi_4 = \chi_5/2$ and $\chi_4 + \chi_5 = 2\chi_{\rm av}$. The results are shown in Fig. 3(d). The total isospin corrections are rather small.

The numerical cancellation between the isospin breaking in the valence and sea quark case is accidental. The corrections due to valence and sea quark masses are all second order in isopin breaking. The same argument as in the unquenched case goes through both for the valence and sea quark masses. We have compared four scenarios in Fig. 4. We show the p^4 and the full $p^4 + p^6$ result first with no isospin breaking, then only in the valence sector or only in the sea sector and finally in both sectors. The curves are those shown in Fig. 3(a-d). We have checked numerically by using a different ratio for the isospin breaking that the corrections are indeed second order in isospin breaking.

5.3 The pion decay constant

In this subsection we look at the same cases as before. The lowest order mass is around the pion mass. We plot Δ_F^V with $\sqrt{\chi_{12}} = 0.13$ GeV. and as before $\sqrt{\chi_6} = \sqrt{2(0.45)^2 - (0.13)^2}$ GeV ≈ 0.623 GeV. The other input parameters are again chosen as given in introduction of this

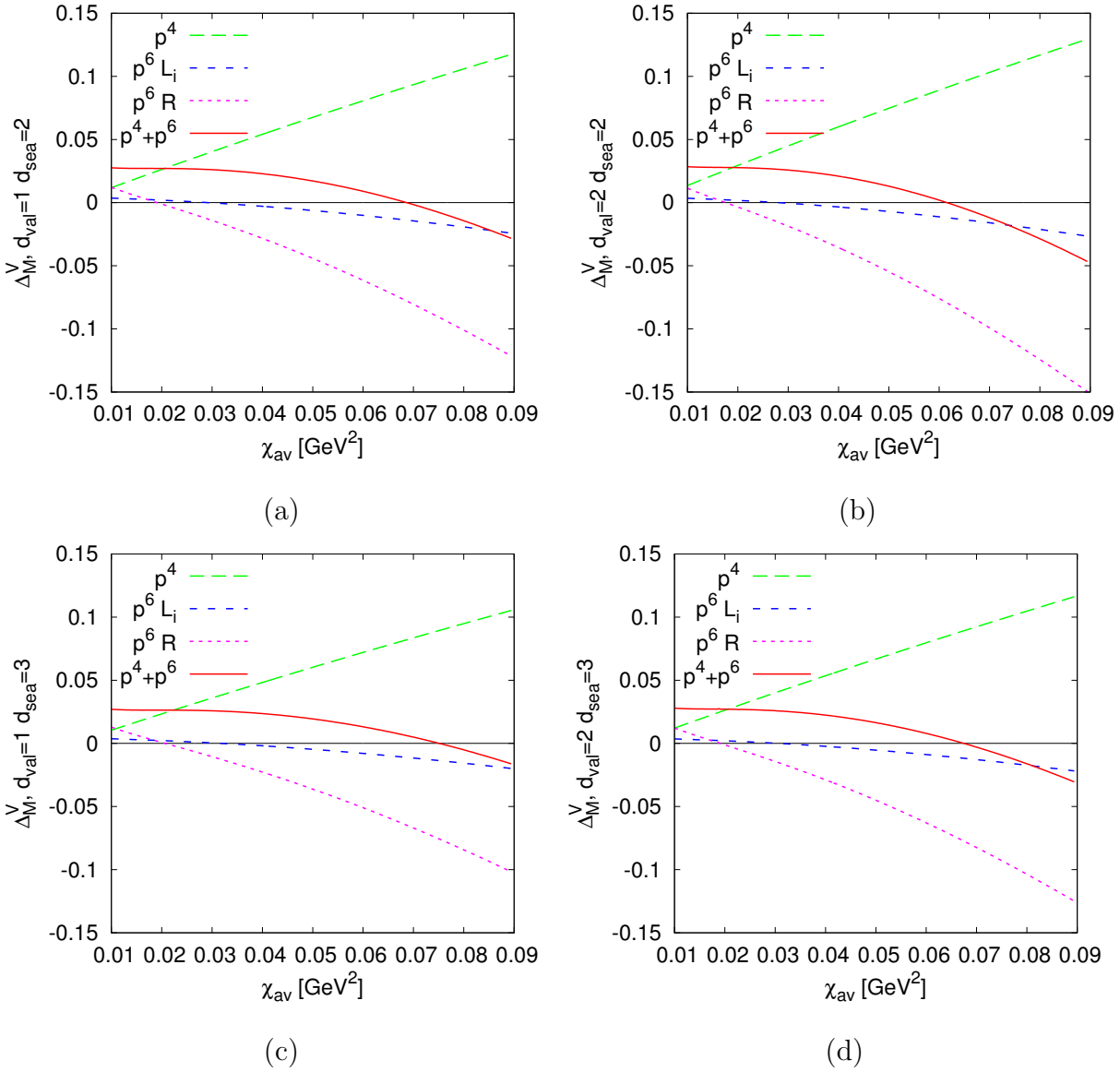

Figure 3: The corrections for the pion mass relative to the lowest order mass as a function of the average up and down sea quark mass via $\chi_{\rm av}$. (a) The isospin limit, $\chi_1 = \chi_2$, $\chi_4 = \chi_5 = \chi_{\rm av}$. (b) Isospin breaking in the valence sector, $\chi_1 = \chi_3/2$ and $\chi_4 = \chi_5 = \chi_{\rm av}$. (c) Isospin breaking in the sea sector, $\chi_1 = \chi_2$ and $\chi_4 = \chi_5/2$. (d) Isospin breaking in both sectors, $\chi_1 = \chi_3/2$ and $\chi_4 = \chi_5/2$.

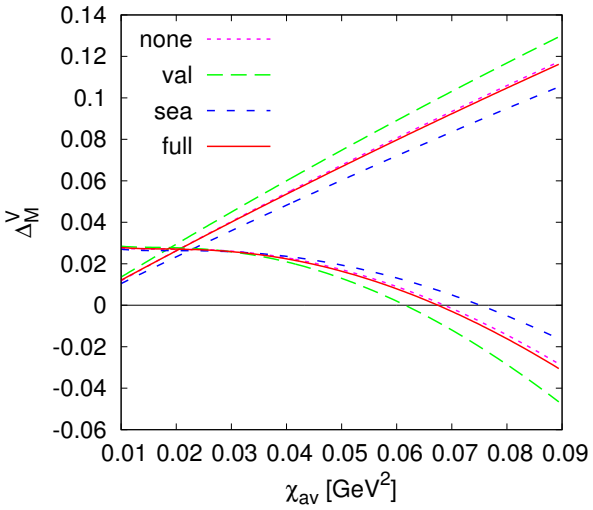

Figure 4: Comparing the finite volume correction for the meson masses for the cases with no isospin breaking (none), only in the valence sector (val), only in the sea sector (sea) and in both (full) for the meson mass squared. The upper curves are the p^4, the bottom the $p^4 + p^6$ results.

section. We have restricted the sea up and down quark masses corresponding to a lowest order sea quark pion of 100 to 300 MeV.

The first case we look at is $d_{\rm val} = 1, d_{\rm sea} = 2$. This corresponds to taking the up and down quark masses equal in both the valence and sea quark sector and a different strange quark mass, i.e. the isospin limit. The result is shown in Fig. 5(a). The total p^6 correction is fairly small.

We now include isospin breaking in the valence sector. We thus look at the case with $d_{\rm val} = 2, d_{\rm sea} = 2$. We fix the valence quark masses such that $\chi_1 + \chi_2 = 2\chi_{12}$ and $\chi_1/\chi_2 = 1/2$. There is a sizable isospin breaking visible in the finite volume corrections, as shown in Fig. 3(b).

The opposite case, isospin breaking in the sea sector but not in the valence sector leads to numerically much smaller effects. Here we used $\chi_1 = \chi_2$, $\chi_4 = \chi_5/2$ and $\chi_4 + \chi_5 = 2\chi_{\rm av}$. The results are shown in Fig. 3(c).

Finally, we introduce isospin breaking in both the valence and sea quark sector with $\chi_1/\chi_2 = 1/2$, $\chi_4 = \chi_5/2$ and $\chi_4 + \chi_5 = 2\chi_{\rm av}$. The results are shown in Fig. 3(d). The total isospin corrections are failry small.

The corrections due to valence and sea quark masses are all second order in isospin breaking. The same argument as in the unquenched case goes through both for the valence and sea quark masses. We compare the same four scenarios as for the pion mass, no isospin breaking, only in the valence sector, only in the sea sector and in both sectors. The curves are those shown in Fig. 5(a-d).

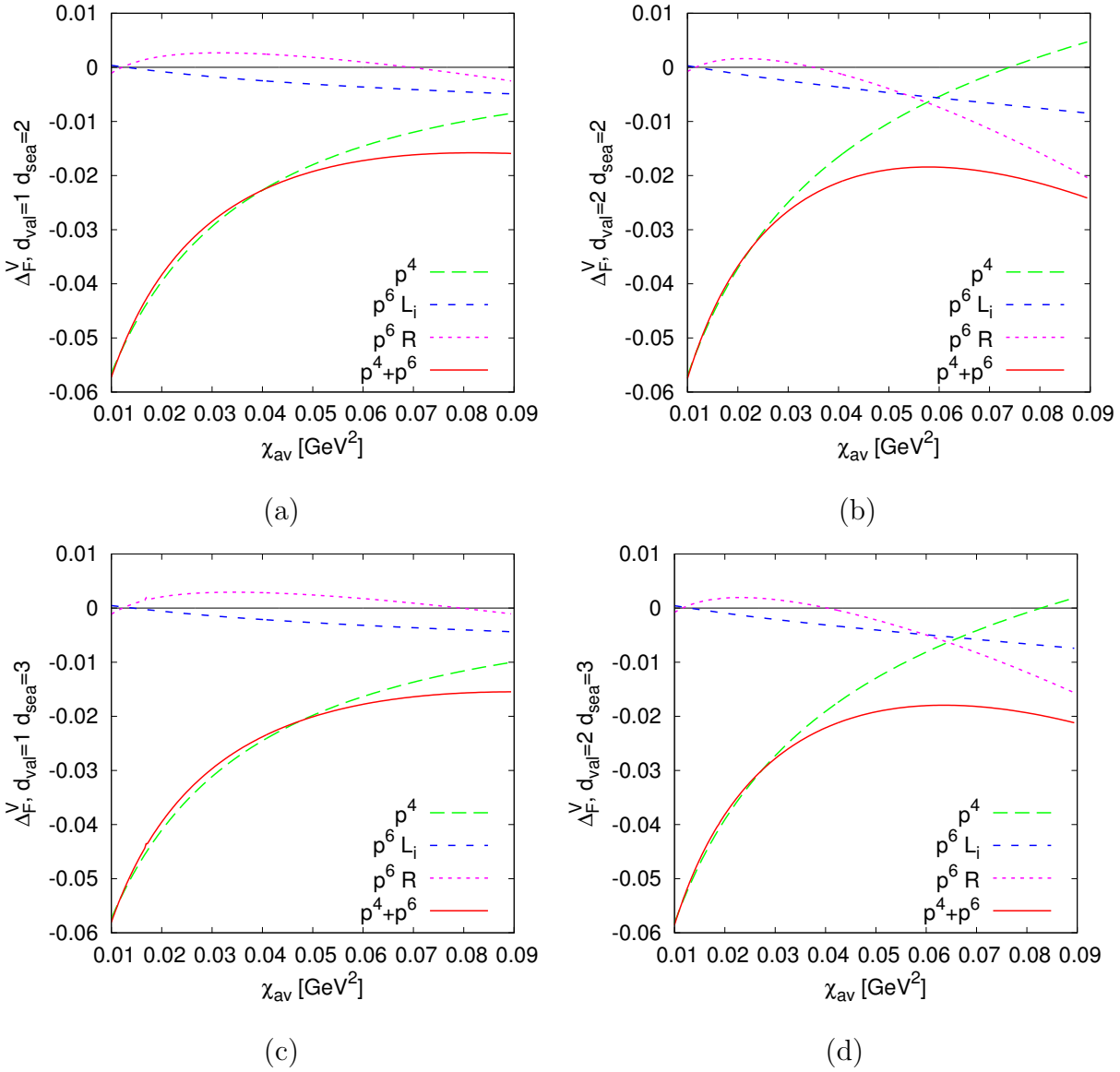

Figure 5: The corrections for the pion decay constant relative to its lowest order value as a function of the average up and down sea quark mass via $\chi_{\rm av}$. (a) The isospin limit, $\chi_1 = \chi_2$, $\chi_4 = \chi_5 = \chi_{\rm av}$. (b) Isospin breaking in the valence sector, $\chi_1 = \chi_3/2$ and $\chi_4 = \chi_5 = \chi_{\rm av}$. (c) Isospin breaking in the sea sector, $\chi_1 = \chi_2$ and $\chi_4 = \chi_5/2$. (d) Isospin breaking in both sectors, $\chi_1 = \chi_3/2$ and $\chi_4 = \chi_5/2$.

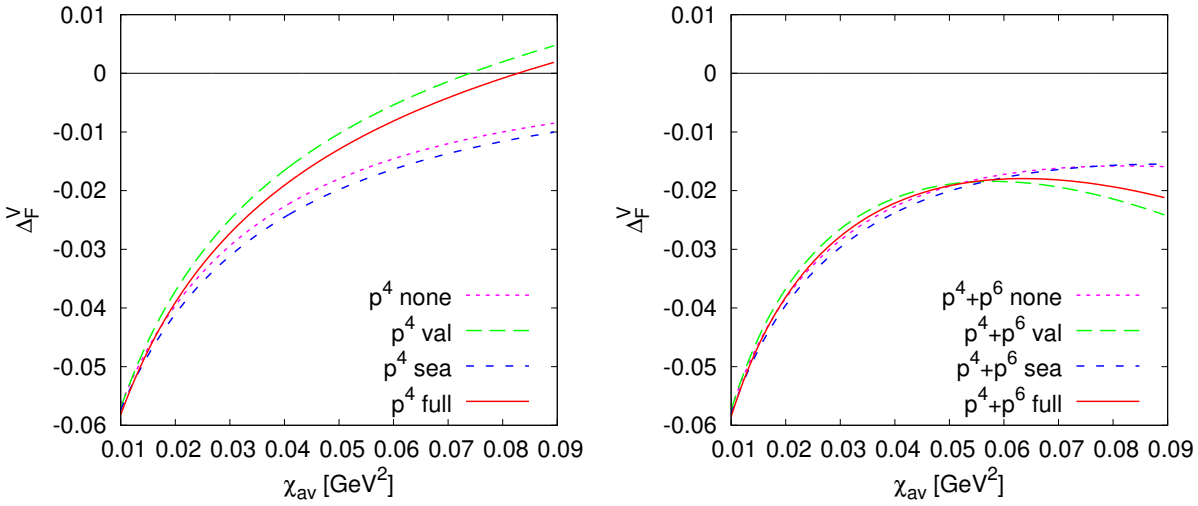

(a) (b)

Figure 6: Comparing the finite volume correction for the meson decay constant and masses for the cases with no isospin breaking (none), only in the valence sector (val), only in the sea sector (sea) and in both (full) for the meson mass squared. (a) p^4 (b) $p^4 + p^6$.

5.4 The kaon mass and decay constant

We now look only at the $d_{\rm val} = d_{\rm sea} = 2$ case but choose the valence masses such that we have a lowest order pion mass of 130 MeV and a lowest order kaon mass of 450 MeV. This corresponds to $\sqrt{\chi_1} = 130$ MeV and $\sqrt{\chi_3} \approx 623$ MeV. We plot the finite volume corrections relative to the lowest order value of the quantity in Fig. 7 as a function of $\chi_4 = \chi_5$. For the sea quark strange mass we use $\chi_6 = 1.02\chi_3$. The LECs are again the ones from [37] and L such that $ML = 2$ for M =130 MeV.

For the kaon we see that we reproduce the results of [15] that near the physical case the p^4 corrections are very small. The total finite volume corrections to the mass remain fairly small. The kaon decay constant has larger corrections but they remain in the few % region for the parameters considered.

6 Conclusions

We have computed the NNLO expressions for the masses and decay constants in three-flavour partially quenched ChPT for all possible mass cases. The calculation has been performed using two different formalisms, quark-flow and the supersymmetric method. The known infinite volume expressions have been reproduced. We quoted the expressions for the equal valence and two different sea quark masses in the appendices. The other cases can be obtained from [22].

The numerical work shows finite volume corrections of a similar size as those in the

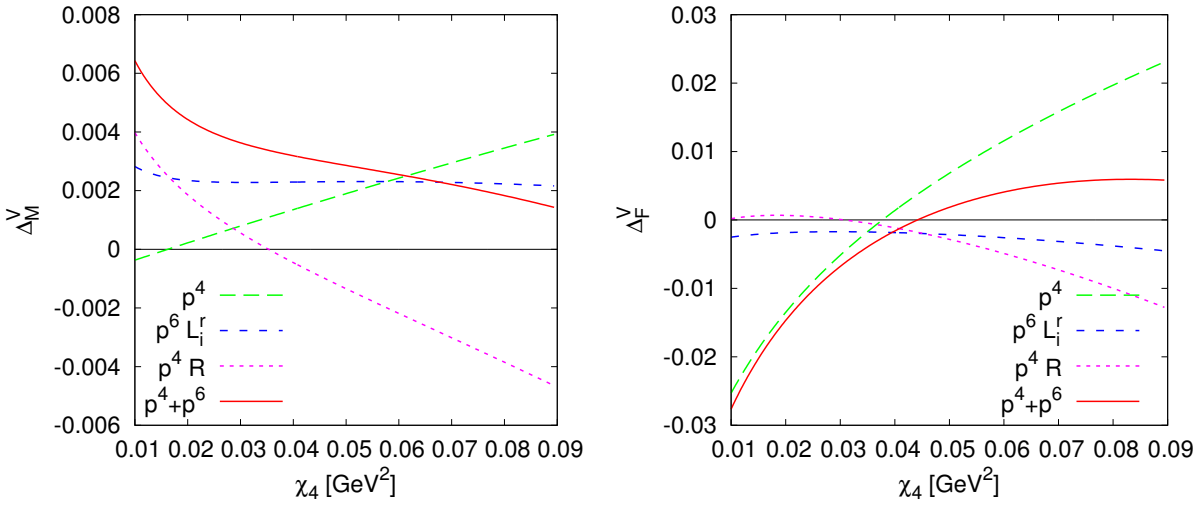

(a) (b)

Figure 7: The finite volume corrections for a valence mass close to the kaon mass relative to the lowest order value. (a) the kaon mass squared. (b) the kaon decay constant.

unquenched case [15]. We have presented some representative numerics. The numerical work has been done using C++. The programs are available together with the infinite volume results in [36]. The analytical work relied heavily on FORM [38].

Acknowledgements

This work is supported in part by the Swedish Research Council grants 621-2011-5080 and 621-2013-4287. JB thanks the Centro de Ciencias de Benasque Pedro Pascual, where part of this paper was written, for hospitality.

A Expressions for the mass

$$F_0^2\Delta^V m_{12}^{2(4)12} = +A^V(\chi_1)\left(-1/3\,\chi_1\,R^c_{146\eta}\right)+A^V(\chi_\eta)\left(2/3\,\chi_1\,{R^z_{\eta 61}}^2\right)+B^V(\chi_1)\left(-1/3\,\chi_1\,R^z_{146\eta}\right) \tag{40}$$

$$\begin{aligned}
F_0^4\Delta^V m_{12}^{2(6L)12} = {} & +A^V(\chi_1)\Big(-64/3\,\hat{L}^r_8\chi_1^2\,R^c_{146\eta}-32/3\,\hat{L}^r_7\chi_1\,\chi_6\,R^z_{14\eta}-64/3\,\hat{L}^r_7\chi_1\,\chi_4\,R^z_{16\eta}\\
& +32\,\hat{L}^r_7\chi_1^2+32\,\hat{L}^r_6\chi_1^2+8/3\,\hat{L}^r_5\chi_1\,R^z_{146\eta}-8/9\,\hat{L}^r_5\chi_1\,\chi_6\,{R^z_{14\eta}}^2-16/9\,\hat{L}^r_5\chi_1\,\chi_4\,{R^z_{16\eta}}^2\\
& +40/3\,\hat{L}^r_5\chi_1^2\,R^c_{146\eta}-8\,\hat{L}^r_3\chi_1\,R^z_{146\eta}-8\,\hat{L}^r_3\chi_1^2\,R^c_{146\eta}+20\,\hat{L}^r_2\chi_1^2+8\,\hat{L}^r_1\chi_1^2-8\,\hat{L}^r_0\chi_1\,R^z_{146\eta}\\
& -8\,\hat{L}^r_0\chi_1^2\,R^c_{146\eta}-16/3\,(\chi_6+2\,\chi_4)\,\hat{L}^r_6\chi_1\,R^c_{146\eta}-16/9\,(\chi_6+2\,\chi_4)\,\hat{L}^r_4\chi_1\,{R^z_{16\eta}}^2\\
& -8/9\,(\chi_6+2\,\chi_4)\,\hat{L}^r_4\chi_1\,{R^z_{14\eta}}^2+8\left(\chi_6+2\,\chi_4\right)\hat{L}^r_4\chi_1\,R^c_{146\eta}\Big)+A^V(\chi_{14})\left(32\,(\chi_4+\chi_1)\,\hat{L}^r_8\chi_1\right.
\end{aligned}$$

$$
\begin{aligned}
&-16\,(\chi_4+\chi_1)\,\hat{L}_5^r\chi_1+20\,(\chi_4+\chi_1)\,\hat{L}_3^r\chi_1+8\,(\chi_4+\chi_1)\,\hat{L}_0^r\chi_1\Big)+A^V(\chi_{16})\,\Big(16\,(\chi_6+\chi_1)\,\hat{L}_8^r\chi_1\\
&-8\,(\chi_6+\chi_1)\,\hat{L}_5^r\chi_1+10\,(\chi_6+\chi_1)\,\hat{L}_3^r\chi_1+4\,(\chi_6+\chi_1)\,\hat{L}_0^r\chi_1\Big)+A^V(\chi_4)\,\Big(48\,\hat{L}_6^r\chi_1\,\chi_4\\
&-48\,\hat{L}_4^r\chi_1\,\chi_4+12\,\hat{L}_2^r\chi_1\,\chi_4+48\,\hat{L}_1^r\chi_1\,\chi_4\Big)+A^V(\chi_{46})\,\Big(32\,(\chi_6+\chi_4)\,\hat{L}_6^r\chi_1-32\,(\chi_6+\chi_4)\,\hat{L}_4^r\chi_1\\
&+8\,(\chi_6+\chi_4)\,\hat{L}_2^r\chi_1+32\,(\chi_6+\chi_4)\,\hat{L}_1^r\chi_1\Big)+A^V(\chi_\eta)\,\Big(128/3\,\hat{L}_8^r\chi_1^2\,{R_{\eta61}^z}^2\\
&+32/9\,\hat{L}_5^r\chi_1\,\chi_6\,R_{14\eta}^z\,R_{\eta61}^z-32/9\,\hat{L}_5^r\chi_1\,\chi_4\,R_{16\eta}^z\,R_{\eta61}^z+16\,\hat{L}_3^r\chi_1\,\chi_\eta\,{R_{\eta61}^z}^2+4\,\hat{L}_2^r\chi_1\,\chi_\eta\\
&+16\,\hat{L}_1^r\chi_1\,\chi_\eta+16\,\hat{L}_0^r\chi_1\,\chi_\eta\,{R_{\eta61}^z}^2-8/3\,(3\,\chi_\eta+2\,\chi_6+\chi_4)\,\hat{L}_4^r\chi_1\\
&-16/9\,(3\,\chi_\eta+2\,\chi_6+\chi_4+12\,\chi_1)\,\hat{L}_5^r\chi_1\,{R_{\eta61}^z}^2+64/3\,(\chi_6-\chi_4)\,\hat{L}_7^r\chi_1\,R_{\eta61}^z\\
&+32/3\,(\chi_6+2\,\chi_4)\,\hat{L}_6^r\chi_1\,{R_{\eta61}^z}^2-64/3\,(\chi_6+2\,\chi_4)\,\hat{L}_4^r\chi_1\,{R_{\eta61}^z}^2\\
&-32/9\,(\chi_6+2\,\chi_4)\,\hat{L}_4^r\chi_1\,R_{16\eta}^z\,R_{\eta61}^z+32/9\,(\chi_6+2\,\chi_4)\,\hat{L}_4^r\chi_1\,R_{14\eta}^z\,R_{\eta61}^z+16/3\,(2\,\chi_6+\chi_4)\,\hat{L}_6^r\chi_1\Big)\\
&+B^V(\chi_1)\,\Big(16/9\,\hat{L}_8^r\chi_1\,\chi_6^2\,{R_{14\eta}^z}^2+32/9\,\hat{L}_8^r\chi_1\,\chi_4^2\,{R_{16\eta}^z}^2-64/3\,\hat{L}_8^r\chi_1^2\,R_{146\eta}^z-32/3\,\hat{L}_8^r\chi_1^3\,R_{146\eta}^c\\
&+16/9\,\hat{L}_7^r\chi_1\,\chi_6^2\,{R_{14\eta}^z}^2+64/9\,\hat{L}_7^r\chi_1\,\chi_4\,\chi_6\,R_{14\eta}^z\,R_{16\eta}^z+64/9\,\hat{L}_7^r\chi_1\,\chi_4^2\,{R_{16\eta}^z}^2-32/3\,\hat{L}_7^r\chi_1^2\,\chi_6\,R_{14\eta}^z\\
&-64/3\,\hat{L}_7^r\chi_1^2\,\chi_4\,R_{16\eta}^z+16\,\hat{L}_7^r\chi_1^3+40/3\,\hat{L}_5^r\chi_1^2\,R_{146\eta}^z-8/9\,\hat{L}_5^r\chi_1^2\,\chi_6\,{R_{14\eta}^z}^2-16/9\,\hat{L}_5^r\chi_1^2\,\chi_4\,{R_{16\eta}^z}^2\\
&+16/3\,\hat{L}_5^r\chi_1^3\,R_{146\eta}^c-8\,\hat{L}_3^r\chi_1^2\,R_{146\eta}^z-8\,\hat{L}_0^r\chi_1^2\,R_{146\eta}^z-16/3\,(\chi_6+2\,\chi_4)\,\hat{L}_6^r\chi_1\,R_{146\eta}^z\\
&+16/9\,(\chi_6+2\,\chi_4)\,\hat{L}_6^r\chi_1\,\chi_6\,{R_{14\eta}^z}^2+32/9\,(\chi_6+2\,\chi_4)\,\hat{L}_6^r\chi_1\,\chi_4\,{R_{16\eta}^z}^2\\
&-32/3\,(\chi_6+2\,\chi_4)\,\hat{L}_6^r\chi_1^2\,R_{146\eta}^c+8\,(\chi_6+2\,\chi_4)\,\hat{L}_4^r\chi_1\,R_{146\eta}^z-16/9\,(\chi_6+2\,\chi_4)\,\hat{L}_4^r\chi_1^2\,{R_{16\eta}^z}^2\\
&-8/9\,(\chi_6+2\,\chi_4)\,\hat{L}_4^r\chi_1^2\,{R_{14\eta}^z}^2+16/3\,(\chi_6+2\,\chi_4)\,\hat{L}_4^r\chi_1^2\,R_{146\eta}^c\Big)\\
&+B^V(\chi_1,\chi_\eta)\,\Big(-64/9\,\hat{L}_8^r\chi_1\,\chi_6^2\,R_{14\eta}^z\,R_{\eta61}^z+64/9\,\hat{L}_8^r\chi_1\,\chi_4^2\,R_{16\eta}^z\,R_{\eta61}^z+64/3\,\hat{L}_8^r\chi_1^3\,{R_{\eta61}^z}^2\\
&+32/9\,\hat{L}_5^r\chi_1^2\,\chi_6\,R_{14\eta}^z\,R_{\eta61}^z-32/9\,\hat{L}_5^r\chi_1^2\,\chi_4\,R_{16\eta}^z\,R_{\eta61}^z-32/3\,\hat{L}_5^r\chi_1^3\,{R_{\eta61}^z}^2\\
&-64/9\,(\chi_6-\chi_4)\,\hat{L}_7^r\chi_1\,\chi_6\,R_{14\eta}^z\,R_{\eta61}^z-128/9\,(\chi_6-\chi_4)\,\hat{L}_7^r\,\chi_1\,\chi_4\,R_{16\eta}^z\,R_{\eta61}^z\\
&+64/3\,(\chi_6-\chi_4)\,\hat{L}_7^r\chi_1^2\,R_{\eta61}^z-64/9\,(\chi_6+2\,\chi_4)\,\hat{L}_6^r\chi_1\,\chi_6\,R_{14\eta}^z\,R_{\eta61}^z\\
&+64/9\,(\chi_6+2\,\chi_4)\,\hat{L}_6^r\chi_1\,\chi_4\,R_{16\eta}^z\,R_{\eta61}^z+64/3\,(\chi_6+2\,\chi_4)\,\hat{L}_6^r\chi_1^2\,{R_{\eta61}^z}^2\\
&-32/3\,(\chi_6+2\,\chi_4)\,\hat{L}_4^r\chi_1^2\,{R_{\eta61}^z}^2-32/9\,(\chi_6+2\,\chi_4)\,\hat{L}_4^r\chi_1^2\,R_{16\eta}^z\,R_{\eta61}^z\\
&+32/9\,(\chi_6+2\,\chi_4)\,\hat{L}_4^r\chi_1^2\,R_{14\eta}^z\,R_{\eta61}^z\Big)+B^V(\chi_\eta)\,\Big(64/9\,(\chi_6-\chi_4)^2\,\hat{L}_7^r\chi_1\,{R_{\eta61}^z}^2\\
&-16/3\,(\chi_6+2\,\chi_4)\,\hat{L}_4^r\chi_1\,\chi_\eta\,{R_{\eta61}^z}^2+32/9\,(\chi_6+2\,\chi_4)\,(2\,\chi_6+\chi_4)\,\hat{L}_6^r\chi_1\,{R_{\eta61}^z}^2\\
&-16/9\,(2\,\chi_6+\chi_4)\,\hat{L}_5^r\chi_1\,\chi_\eta\,{R_{\eta61}^z}^2+32/9\,(2\,\chi_6^2+\chi_4^2)\,\hat{L}_8^r\chi_1\,{R_{\eta61}^z}^2\Big)\\
&+C^V(\chi_1)\,\Big(-32/3\,\hat{L}_8^r\chi_1^3\,R_{146\eta}^z+16/3\,\hat{L}_5^r\chi_1^3\,R_{146\eta}^z-32/3\,(\chi_6+2\,\chi_4)\,\hat{L}_6^r\chi_1^2\,R_{146\eta}^z\\
&+16/3\,(\chi_6+2\,\chi_4)\,\hat{L}_4^r\chi_1^2\,R_{146\eta}^z\Big)+A_{23}^V(\chi_1)\,\Big(8\,\hat{L}_3^r\chi_1\,R_{146\eta}^c-12\,\hat{L}_2^r\chi_1-24\,\hat{L}_1^r\chi_1+8\,\hat{L}_0^r\chi_1\,R_{146\eta}^c\Big)\\
&+A_{23}^V(\chi_{14})\,\Big(-24\,\hat{L}_3^r\chi_1-48\,\hat{L}_0^r\chi_1\Big)+A_{23}^V(\chi_{16})\,\Big(-12\,\hat{L}_3^r\chi_1-24\,\hat{L}_0^r\chi_1\Big)\\
&+A_{23}^V(\chi_4)\,\Big(-36\,\hat{L}_2^r\chi_1\Big)+A_{23}^V(\chi_{46})\,\Big(-48\,\hat{L}_2^r\chi_1\Big)+A_{23}^V(\chi_\eta)\,\Big(-16\,\hat{L}_3^r\chi_1\,{R_{\eta61}^z}^2-12\,\hat{L}_2^r\chi_1\\
&-16\,\hat{L}_0^r\chi_1\,{R_{\eta61}^z}^2\Big)+B_{23}^V(\chi_1)\,\Big(8\,\hat{L}_3^r\chi_1\,R_{146\eta}^z+8\,\hat{L}_0^r\chi_1\,R_{146\eta}^z\Big)
\end{aligned}
\tag{41}
$$

$$
\begin{aligned}
F_0^4 \Delta^V m_{12}^{2(6R)12} = & +\overline{A}(\chi_1)\, A^V(\chi_1) \left(\chi_1 + 1/9\, \chi_1\, {R^c_{146\eta}}^2\right) \\
& +\overline{A}(\chi_1)\, A^V(\chi_{14}) \left(4/45\, R^z_{146\eta} + 8/9\, \chi_1\, R^c_{146\eta} + 4/45\, (\chi_4 - 11\, \chi_1)\, R^z_{16\eta}\right) \\
& +\overline{A}(\chi_1)\, A^V(\chi_{16}) \left(2/45\, R^z_{146\eta} + 4/9\, \chi_1\, R^c_{146\eta} + 2/45\, (\chi_6 - 11\, \chi_1)\, R^z_{14\eta}\right) \\
& +\overline{A}(\chi_1)\, A^V(\chi_{46}) \left(- 2/27\, \chi_1\, {R^z_{16\eta}}^2 + 4/27\, \chi_1\, R^z_{14\eta}\, R^z_{16\eta} - 2/27\, \chi_1\, {R^z_{14\eta}}^2\right) \\
& +\overline{A}(\chi_1)\, A^V(\chi_\eta) \left(- 2/9\, \chi_1\, R^c_{146\eta}\, {R^z_{\eta 61}}^2\right) + \overline{A}(\chi_1)\, B^V(\chi_1) \left(1/9\, \chi_1\, R^z_{146\eta}\, R^c_{146\eta}\right. \\
& \left. +\chi_1^2 + 2/9\, \chi_1^2\, {R^c_{146\eta}}^2\right) + \overline{A}(\chi_1)\, B^V(\chi_1, \chi_\eta) \left(- 8/9\, \chi_1^2\, R^c_{146\eta}\, {R^z_{\eta 61}}^2\right) \\
& +\overline{A}(\chi_1)\, C^V(\chi_1) \left(2/9\, \chi_1^2\, R^z_{146\eta}\, R^c_{146\eta}\right) + \overline{A}(\chi_{14})\, A^V(\chi_1) \left(4/45\, R^z_{146\eta} + 8/9\, \chi_1\, R^c_{146\eta}\right. \\
& \left. +4/45\, (\chi_4 - 11\, \chi_1)\, R^z_{16\eta}\right) + \overline{A}(\chi_{14})\, A^V(\chi_{14}) \left(- 4/27\, R^z_{146\eta} + 10/27\, \chi_1\, R^z_{16\eta}\right. \\
& \left. +1/27\, (2\, \chi_\eta - 2\, \chi_4 - 47\, \chi_1) + 2/27\, (4\, \chi_\eta + 4\, \chi_4 + 9\, \chi_1)\, {R^z_{\eta 61}}^2 + 2/27\, (4\, \chi_\eta + \chi_1)\, R^z_{\eta 61}\right. \\
& \left. -1/27\, (4\, \chi_4 + 13\, \chi_1)\, R^c_{146\eta}\right) + \overline{A}(\chi_{14})\, A^V(\chi_{16}) \left(- \chi_1\right) + \overline{A}(\chi_{14})\, A^V(\chi_\eta) \left(- 2/45\, (\chi_\eta - \chi_4)\right. \\
& \left. -8/45\, (\chi_\eta + 9\, \chi_1)\, {R^z_{\eta 61}}^2 - 4/45\, (2\, \chi_\eta - \chi_4 + 9\, \chi_1)\, R^z_{\eta 61}\right) + \overline{A}(\chi_{14})\, B^V(\chi_1) \left(8/9\, \chi_1\, R^z_{146\eta}\right. \\
& \left. -4/9\, (\chi_4 + 2\, \chi_1)\, \chi_1\, R^z_{16\eta}\right) + \overline{A}(\chi_{14})\, B^V(\chi_1, \chi_\eta) \left(- 4/9\, (\chi_4 + 2\, \chi_1)\, \chi_1\, R^z_{\eta 61}\right) \\
& +\overline{A}(\chi_{16})\, A^V(\chi_1) \left(2/45\, R^z_{146\eta} + 4/9\, \chi_1\, R^c_{146\eta} + 2/45\, (\chi_6 - 11\, \chi_1)\, R^z_{14\eta}\right) \\
& +\overline{A}(\chi_{16})\, A^V(\chi_{14}) \left(- \chi_1\right) + \overline{A}(\chi_{16})\, A^V(\chi_{16}) \left(- 2/27\, R^z_{146\eta} + 5/27\, \chi_1\, R^z_{14\eta}\right. \\
& \left. +2/27\, (2\, \chi_\eta - 2\, \chi_6 - 5\, \chi_1) + 1/27\, (4\, \chi_\eta + 4\, \chi_6 + 9\, \chi_1)\, {R^z_{\eta 61}}^2 - 2/27\, (4\, \chi_\eta + \chi_1)\, R^z_{\eta 61}\right. \\
& \left. -1/54\, (4\, \chi_6 + 13\, \chi_1)\right) R^c_{146\eta}\Big) + \overline{A}(\chi_{16})\, A^V(\chi_\eta) \left(- 4/45\, (\chi_\eta - \chi_6)\right. \\
& \left. -4/45\, (\chi_\eta + 9\, \chi_1)\, {R^z_{\eta 61}}^2 + 4/45\, (2\, \chi_\eta - \chi_6 + 9\, \chi_1)\, R^z_{\eta 61}\right) + \overline{A}(\chi_{16})\, B^V(\chi_1) \left(4/9\, \chi_1\, R^z_{146\eta}\right. \\
& \left. -2/9\, (\chi_6 + 2\, \chi_1)\, \chi_1\, R^z_{14\eta}\right) + \overline{A}(\chi_{16})\, B^V(\chi_1, \chi_\eta) \left(4/9\, (\chi_6 + 2\, \chi_1)\, \chi_1\, R^z_{\eta 61}\right) \\
& +\overline{A}(\chi_4)\, B^V(\chi_1) \left(1/3\, \chi_1\, \chi_4\, {R^z_{16\eta}}^2\right) + \overline{A}(\chi_4)\, B^V(\chi_1, \chi_\eta) \left(2/3\, \chi_1\, \chi_4\, R^z_{16\eta}\, R^z_{\eta 61}\right) \\
& +\overline{A}(\chi_4)\, B^V(\chi_\eta) \left(1/3\, \chi_1\, \chi_4\, {R^z_{\eta 61}}^2\right) + \overline{A}(\chi_{46})\, A^V(\chi_1) \left(- 2/27\, \chi_1\, {R^z_{16\eta}}^2 + 4/27\, \chi_1\, R^z_{14\eta}\, R^z_{16\eta}\right. \\
& \left. -2/27\, \chi_1\, {R^z_{14\eta}}^2\right) + \overline{A}(\chi_{46})\, A^V(\chi_\eta) \left(- 2/3\, \chi_1\, {R^z_{\eta 61}}^2 - 4/9\, \chi_1\, R^z_{16\eta}\, R^z_{\eta 61} + 4/9\, \chi_1\, R^z_{14\eta}\, R^z_{\eta 61}\right) \\
& +\overline{A}(\chi_{46})\, B^V(\chi_1) \left(4/27\, (\chi_6 + \chi_4 + \chi_1)\, \chi_1\, R^z_{14\eta}\, R^z_{16\eta} + 2/27\, (\chi_6 - \chi_1)\, \chi_1\, {R^z_{14\eta}}^2\right. \\
& \left. +2/27\, (\chi_4 - \chi_1)\, \chi_1\, {R^z_{16\eta}}^2\right) + \overline{A}(\chi_{46})\, B^V(\chi_1, \chi_\eta) \left(- 4/27\, (\chi_6 - \chi_4 - 3\, \chi_1)\, \chi_1\, R^z_{14\eta}\, R^z_{\eta 61}\right. \\
& \left. -4/27\, (2\, \chi_6 + \chi_4 + 3\, \chi_1)\, \chi_1\, R^z_{16\eta}\, R^z_{\eta 61}\right) + \overline{A}(\chi_{46})\, B^V(\chi_\eta) \left(- 2/9\, (3\, \chi_\eta + \chi_4)\, \chi_1\, {R^z_{\eta 61}}^2\right) \\
& +\overline{A}(\chi_\eta)\, A^V(\chi_1) \left(- 2/9\, \chi_1\, R^c_{146\eta}\, {R^z_{\eta 61}}^2\right) + \overline{A}(\chi_\eta)\, A^V(\chi_{14}) \left(- 2/45\, (\chi_\eta - \chi_4)\right. \\
& \left. -8/45\, (\chi_\eta + 9\, \chi_1)\, {R^z_{\eta 61}}^2 - 4/45\, (2\, \chi_\eta - \chi_4 + 9\, \chi_1)\, R^z_{\eta 61}\right) + \overline{A}(\chi_\eta)\, A^V(\chi_{16}) \left(- 4/45\, (\chi_\eta - \chi_6)\right. \\
& \left. -4/45\, (\chi_\eta + 9\, \chi_1)\, {R^z_{\eta 61}}^2 + 4/45\, (2\, \chi_\eta - \chi_6 + 9\, \chi_1)\, R^z_{\eta 61}\right) + \overline{A}(\chi_\eta)\, A^V(\chi_{46}) \left(- 2/3\, \chi_1\, {R^z_{\eta 61}}^2\right. \\
& \left. -4/9\, \chi_1\, R^z_{16\eta}\, R^z_{\eta 61} + 4/9\, \chi_1\, R^z_{14\eta}\, R^z_{\eta 61}\right) + \overline{A}(\chi_\eta)\, A^V(\chi_\eta) \left(4/9\, \chi_1\, {R^z_{\eta 61}}^4\right)
\end{aligned}
$$

$$+\overline{A}(\chi_\eta)\,B^V(\chi_1)\,\Big(-2/9\,\chi_1\,R^z_{146\eta}\,{R^z_{\eta61}}^2+2/27\,\chi_1\,\chi_6\,{R^z_{14\eta}}^2+1/27\,\chi_1\,\chi_4\,{R^z_{16\eta}}^2$$
$$-4/9\,\chi_1^2\,R^c_{146\eta}\,{R^z_{\eta61}}^2\Big)+\overline{A}(\chi_\eta)\,B^V(\chi_1,\chi_\eta)\,\Big(-8/27\,\chi_1\,\chi_6\,R^z_{14\eta}\,R^z_{\eta61}+2/27\,\chi_1\,\chi_4\,R^z_{16\eta}\,R^z_{\eta61}$$
$$+8/9\,\chi_1^2\,{R^z_{\eta61}}^4+4/9\,\chi_1^2\,R^c_{146\eta}\,{R^z_{\eta61}}^2\Big)+\overline{A}(\chi_\eta)\,B^V(\chi_\eta)\,\Big(1/27\,(8\,\chi_6+\chi_4)\,\chi_1\,{R^z_{\eta61}}^2\Big)$$
$$+\overline{A}(\chi_\eta)\,C^V(\chi_1)\,\Big(-4/9\,\chi_1^2\,R^z_{146\eta}\,{R^z_{\eta61}}^2\Big)+\overline{B}(\chi_1)\,A^V(\chi_1)\,\Big(1/9\,\chi_1\,R^z_{146\eta}\,R^c_{146\eta}+\chi_1^2$$
$$+2/9\,\chi_1^2\,{R^c_{146\eta}}^2\Big)+\overline{B}(\chi_1)\,A^V(\chi_{14})\,\Big(8/9\,\chi_1\,R^z_{146\eta}-4/9\,(\chi_4+2\,\chi_1)\,\chi_1\,R^z_{16\eta}\Big)$$
$$+\overline{B}(\chi_1)\,A^V(\chi_{16})\,\Big(4/9\,\chi_1\,R^z_{146\eta}-2/9\,(\chi_6+2\,\chi_1)\,\chi_1\,R^z_{14\eta}\Big)+\overline{B}(\chi_1)\,A^V(\chi_4)\,\Big(1/3\,\chi_1\,\chi_4\,{R^z_{16\eta}}^2\Big)$$
$$+\overline{B}(\chi_1)\,A^V(\chi_{46})\,\Big(4/27\,(\chi_6+\chi_4+\chi_1)\,\chi_1\,R^z_{14\eta}\,R^z_{16\eta}+2/27\,(\chi_6-\chi_1)\,\chi_1\,{R^z_{14\eta}}^2$$
$$+2/27\,(\chi_4-\chi_1)\,\chi_1\,{R^z_{16\eta}}^2\Big)+\overline{B}(\chi_1)\,A^V(\chi_\eta)\,\Big(-2/9\,\chi_1\,R^z_{146\eta}\,{R^z_{\eta61}}^2+2/27\,\chi_1\,\chi_6\,{R^z_{14\eta}}^2$$
$$+1/27\,\chi_1\,\chi_4\,{R^z_{16\eta}}^2-4/9\,\chi_1^2\,R^c_{146\eta}\,{R^z_{\eta61}}^2\Big)+\overline{B}(\chi_1)\,B^V(\chi_1)\,\Big(1/9\,\chi_1\,{R^z_{146\eta}}^2+4/9\,\chi_1^2\,R^z_{146\eta}\,R^c_{146\eta}\Big)$$
$$+\overline{B}(\chi_1)\,B^V(\chi_1,\chi_\eta)\,\Big(-4/9\,\chi_1^2\,R^z_{146\eta}\,{R^z_{\eta61}}^2\Big)+\overline{B}(\chi_1)\,C^V(\chi_1)\,\Big(2/9\,\chi_1^2\,{R^z_{146\eta}}^2\Big)$$
$$+\overline{B}(\chi_1,\chi_\eta)\,A^V(\chi_{14})\,\Big(-4/9\,(\chi_4+2\,\chi_1)\,\chi_1\,R^z_{\eta61}\Big)+\overline{B}(\chi_1,\chi_\eta)\,A^V(\chi_{16})\,\Big(4/9\,(\chi_6$$
$$+2\,\chi_1)\,\chi_1\,R^z_{\eta61}\Big)+\overline{B}(\chi_1,\chi_\eta)\,A^V(\chi_4)\,\Big(2/3\,\chi_1\,\chi_4\,R^z_{16\eta}\,R^z_{\eta61}\Big)$$
$$+\overline{B}(\chi_1,\chi_\eta)\,A^V(\chi_{46})\,\Big(-4/27\,(\chi_6-\chi_4-3\,\chi_1)\,\chi_1\,R^z_{14\eta}\,R^z_{\eta61}-4/27\,(2\,\chi_6+\chi_4$$
$$+3\,\chi_1)\,\chi_1\,R^z_{16\eta}\,R^z_{\eta61}\Big)+\overline{B}(\chi_1,\chi_\eta)\,A^V(\chi_\eta)\,\Big(-8/27\,\chi_1\,\chi_6\,R^z_{14\eta}\,R^z_{\eta61}+2/27\,\chi_1\,\chi_4\,R^z_{16\eta}\,R^z_{\eta61}$$
$$+8/9\,\chi_1^2\,{R^z_{\eta61}}^4-4/9\,\chi_1^2\,R^c_{146\eta}\,{R^z_{\eta61}}^2\Big)+\overline{B}(\chi_1,\chi_\eta)\,B^V(\chi_1)\,\Big(-4/9\,\chi_1^2\,R^z_{146\eta}\,{R^z_{\eta61}}^2\Big)$$
$$+\overline{B}(\chi_\eta)\,A^V(\chi_4)\,\Big(1/3\,\chi_1\,\chi_4\,{R^z_{\eta61}}^2\Big)+\overline{B}(\chi_\eta)\,A^V(\chi_{46})\,\Big(-2/9\,(3\,\chi_\eta+\chi_4)\,\chi_1\,{R^z_{\eta61}}^2\Big)$$
$$+\overline{B}(\chi_\eta)\,A^V(\chi_\eta)\,\Big(1/27\,(8\,\chi_6+\chi_4)\,\chi_1\,{R^z_{\eta61}}^2\Big)+\overline{C}(\chi_1)\,A^V(\chi_1)\,\Big(2/9\,\chi_1^2\,R^z_{146\eta}\,R^c_{146\eta}\Big)$$
$$+\overline{C}(\chi_1)\,A^V(\chi_\eta)\,\Big(-4/9\,\chi_1^2\,R^z_{146\eta}\,{R^z_{\eta61}}^2\Big)+\overline{C}(\chi_1)\,B^V(\chi_1)\,\Big(2/9\,\chi_1^2\,{R^z_{146\eta}}^2\Big)$$
$$+A^V(\chi_1)\,\frac{1}{16\pi^2}\,\Big(-1/4\,\chi_1^2+1/6\,\chi_1^2\,R^z_{16\eta}+1/12\,\chi_1^2\,R^z_{14\eta}\Big)+A^V(\chi_1)^2\,\Big(1/2\,\chi_1+1/18\,\chi_1\,{R^c_{146\eta}}^2\Big)$$
$$+A^V(\chi_1)\,A^V(\chi_{14})\,\Big(4/45\,R^z_{146\eta}+8/9\,\chi_1\,R^c_{146\eta}+4/45\,(\chi_4-11\,\chi_1)\,R^z_{16\eta}\Big)$$
$$+A^V(\chi_1)\,A^V(\chi_{16})\,\Big(2/45\,R^z_{146\eta}+4/9\,\chi_1\,R^c_{146\eta}+2/45\,(\chi_6-11\,\chi_1)\,R^z_{14\eta}\Big)$$
$$+A^V(\chi_1)\,A^V(\chi_{46})\,\Big(-2/27\,\chi_1\,{R^z_{16\eta}}^2+4/27\,\chi_1\,R^z_{14\eta}\,R^z_{16\eta}-2/27\,\chi_1\,{R^z_{14\eta}}^2\Big)$$
$$+A^V(\chi_1)\,A^V(\chi_\eta)\,\Big(-2/9\,\chi_1\,R^c_{146\eta}\,{R^z_{\eta61}}^2\Big)+A^V(\chi_1)\,B^V(\chi_1)\,\Big(1/9\,\chi_1\,R^z_{146\eta}\,R^c_{146\eta}+\chi_1^2$$
$$+2/9\,\chi_1^2\,{R^c_{146\eta}}^2\Big)+A^V(\chi_1)\,B^V(\chi_1,\chi_\eta)\,\Big(-4/9\,\chi_1^2\,R^c_{146\eta}\,{R^z_{\eta61}}^2\Big)$$
$$+A^V(\chi_1)\,C^V(\chi_1)\,\Big(2/9\,\chi_1^2\,R^z_{146\eta}\,R^c_{146\eta}\Big)+A^V(\chi_{14})\,\frac{1}{16\pi^2}\,\Big(-1/6\,\chi_1\,R^z_{146\eta}+1/36\,(3\,\chi_\eta+18\,\chi_6$$
$$+42\,\chi_4-\chi_1)\,\chi_1+1/18\,\Big(6\,\chi_\eta+3\,\chi_4+\chi_1\Big)\,\chi_1\,R^z_{\eta61}+1/18\,(6\,\chi_\eta+3\,\chi_4+\chi_1)\,\chi_1\,{R^z_{\eta61}}^2$$
$$+1/18\,(3\,\chi_4+7\,\chi_1)\,\chi_1\,R^z_{16\eta}-1/36\,(3\,\chi_4+7\,\chi_1)\,\chi_1\,R^c_{146\eta}\Big)+A^V(\chi_{14})^2\,\Big(-2/27\,R^z_{146\eta}$$
$$+5/27\,\chi_1\,R^z_{16\eta}+1/54\,(2\,\chi_\eta-2\,\chi_4-47\,\chi_1)+1/27\,\Big(4\,\chi_\eta+4\,\chi_4+9\,\chi_1\Big)\,{R^z_{\eta61}}^2$$

$$+1/27\,(4\,\chi_\eta+\chi_1)\,R^z_{\eta61}-1/54\,(4\,\chi_4+13\,\chi_1)\,R^c_{146\eta}\Big)+A^V(\chi_{14})\,A^V(\chi_{16})\,\Big(-\chi_1\Big)$$
$$+A^V(\chi_{14})\,A^V(\chi_\eta)\,\Big(-2/45\,(\chi_\eta-\chi_4)-8/45\,(\chi_\eta+9\,\chi_1)\,{R^z_{\eta61}}^2-4/45\,(2\,\chi_\eta-\chi_4+9\,\chi_1)\,R^z_{\eta61}\Big)$$
$$+A^V(\chi_{14})\,B^V(\chi_1)\,\Big(8/9\,\chi_1\,R^z_{146\eta}-4/9\,(\chi_4+2\,\chi_1)\,\chi_1\,R^z_{16\eta}\Big)$$
$$+A^V(\chi_{14})\,B^V(\chi_1,\chi_\eta)\,\Big(-4/9\,(\chi_4+2\,\chi_1)\,\chi_1\,R^z_{\eta61}\Big)+A^V(\chi_{16})\,\frac{1}{16\pi^2}\,\Big(-1/12\,\chi_1\,R^z_{146\eta}$$
$$-1/18\,(6\,\chi_\eta+3\,\chi_6+\chi_1)\,\chi_1\,R^z_{\eta61}+1/36\,(6\,\chi_\eta+3\,\chi_6+\chi_1)\,\chi_1\,{R^z_{\eta61}}^2+1/72\,(12\,\chi_\eta+15\,\chi_6$$
$$+36\,\chi_4-\chi_1)\,\chi_1+1/36\,(3\,\chi_6+7\,\chi_1)\,\chi_1\,R^z_{14\eta}-1/72\,(3\,\chi_6+7\,\chi_1)\,\chi_1\,R^c_{146\eta}\Big)$$
$$+A^V(\chi_{16})^2\,\Big(-1/27\,R^z_{146\eta}+5/54\,\chi_1\,R^z_{14\eta}+1/27\,(2\,\chi_\eta-2\,\chi_6-5\,\chi_1)+1/54\,(4\,\chi_\eta+4\,\chi_6$$
$$+9\,\chi_1)\,{R^z_{\eta61}}^2-1/27\,(4\,\chi_\eta+\chi_1)\,R^z_{\eta61}-1/108\,(4\,\chi_6+13\,\chi_1)\,R^c_{146\eta}\Big)$$
$$+A^V(\chi_{16})\,A^V(\chi_\eta)\,\Big(-4/45\,(\chi_\eta-\chi_6)-4/45\,(\chi_\eta+9\,\chi_1)\,{R^z_{\eta61}}^2+4/45\,(2\,\chi_\eta-\chi_6+9\,\chi_1)\,R^z_{\eta61}\Big)$$
$$+A^V(\chi_{16})\,B^V(\chi_1)\,\Big(4/9\,\chi_1\,R^z_{146\eta}-2/9\,(\chi_6+2\,\chi_1)\,\chi_1\,R^z_{14\eta}\Big)+A^V(\chi_{16})\,B^V(\chi_1,\chi_\eta)\,\Big(4/9\,(\chi_6$$
$$+2\,\chi_1)\,\chi_1\,R^z_{\eta61}\Big)+A^V(\chi_4)\,B^V(\chi_1)\,\Big(1/3\,\chi_1\,\chi_4\,{R^z_{16\eta}}^2\Big)$$
$$+A^V(\chi_4)\,B^V(\chi_1,\chi_\eta)\,\Big(2/3\,\chi_1\,\chi_4\,R^z_{16\eta}\,R^z_{\eta61}\Big)+A^V(\chi_4)\,B^V(\chi_\eta)\,\Big(1/3\,\chi_1\,\chi_4\,{R^z_{\eta61}}^2\Big)$$
$$+A^V(\chi_{46})\,A^V(\chi_\eta)\,\Big(-2/3\,\chi_1\,{R^z_{\eta61}}^2-4/9\,\chi_1\,R^z_{16\eta}\,R^z_{\eta61}+4/9\,\chi_1\,R^z_{14\eta}\,R^z_{\eta61}\Big)$$
$$+A^V(\chi_{46})\,B^V(\chi_1)\,\Big(4/27\,(\chi_6+\chi_4+\chi_1)\,\chi_1\,R^z_{14\eta}\,R^z_{16\eta}+2/27\,(\chi_6-\chi_1)\,\chi_1\,{R^z_{14\eta}}^2$$
$$+2/27\,(\chi_4-\chi_1)\,\chi_1\,{R^z_{16\eta}}^2\Big)+A^V(\chi_{46})\,B^V(\chi_1,\chi_\eta)\,\Big(-4/27\,(\chi_6-\chi_4-3\,\chi_1)\,\chi_1\,R^z_{14\eta}\,R^z_{\eta61}$$
$$-4/27\,(2\,\chi_6+\chi_4+3\,\chi_1)\,\chi_1\,R^z_{16\eta}\,R^z_{\eta61}\Big)+A^V(\chi_{46})\,B^V(\chi_\eta)\,\Big(-2/9\,(3\,\chi_\eta+\chi_4)\,\chi_1\,{R^z_{\eta61}}^2\Big)$$
$$+A^V(\chi_\eta)^2\,\Big(2/9\,\chi_1\,{R^z_{\eta61}}^4\Big)+A^V(\chi_\eta)\,B^V(\chi_1)\,\Big(-2/9\,\chi_1\,R^z_{146\eta}\,{R^z_{\eta61}}^2+2/27\,\chi_1\,\chi_6\,{R^z_{14\eta}}^2$$
$$+1/27\,\chi_1\,\chi_4\,{R^z_{16\eta}}^2-4/9\,\chi_1^2\,R^c_{146\eta}\,{R^z_{\eta61}}^2\Big)+A^V(\chi_\eta)\,B^V(\chi_1,\chi_\eta)\,\Big(-8/27\,\chi_1\,\chi_6\,R^z_{14\eta}\,R^z_{\eta61}$$
$$+2/27\,\chi_1\,\chi_4\,R^z_{16\eta}\,R^z_{\eta61}+8/9\,\chi_1^2\,{R^z_{\eta61}}^4\Big)+A^V(\chi_\eta)\,B^V(\chi_\eta)\,\Big(1/27\,(8\,\chi_6+\chi_4)\,\chi_1\,{R^z_{\eta61}}^2\Big)$$
$$+A^V(\chi_\eta)\,C^V(\chi_1)\,\Big(-4/9\,\chi_1^2\,R^z_{146\eta}\,{R^z_{\eta61}}^2\Big)+B^V(\chi_1)^2\,\Big(1/18\,\chi_1\,{R^z_{146\eta}}^2+2/9\,\chi_1^2\,R^z_{146\eta}\,R^c_{146\eta}\Big)$$
$$+B^V(\chi_1)\,B^V(\chi_1,\chi_\eta)\,\Big(-4/9\,\chi_1^2\,R^z_{146\eta}\,{R^z_{\eta61}}^2\Big)+B^V(\chi_1)\,C^V(\chi_1)\,\Big(2/9\,\chi_1^2\,{R^z_{146\eta}}^2\Big)$$
$$+A^V_{23}(\chi_1)\,\frac{1}{16\pi^2}\,\Big(3/4\,\chi_1-1/2\,\chi_1\,R^z_{16\eta}-1/4\,\chi_1\,R^z_{14\eta}\Big)+A^V_{23}(\chi_{14})\,\frac{1}{16\pi^2}\,\Big(1/6\,\chi_1-1/3\,\chi_1\,R^z_{\eta61}$$
$$-1/3\,\chi_1\,{R^z_{\eta61}}^2-1/3\,\chi_1\,R^z_{16\eta}+1/6\,\chi_1\,R^c_{146\eta}\Big)+A^V_{23}(\chi_{16})\,\frac{1}{16\pi^2}\,\Big(1/12\,\chi_1+1/3\,\chi_1\,R^z_{\eta61}$$
$$-1/6\,\chi_1\,{R^z_{\eta61}}^2-1/6\,\chi_1\,R^z_{14\eta}+1/12\,\chi_1\,R^c_{146\eta}\Big)+H^V(1,\chi_1,\chi_1,\chi_1,\chi_1)\,\Big(1/3\,\chi_1^2+2/9\,\chi_1^2\,{R^c_{146\eta}}^2\Big)$$
$$+H^V(1,\chi_1,\chi_1,\chi_\eta,\chi_1)\,\Big(-8/9\,\chi_1^2\,R^c_{146\eta}\,{R^z_{\eta61}}^2\Big)+H^V(1,\chi_1,\chi_{14},\chi_{14},\chi_1)\,\Big(-11/18\,\chi_1\,R^z_{146\eta}$$
$$-5/6\,\chi_1^2\,R^c_{146\eta}-1/9\,(4\,\chi_4-7\,\chi_1)\,\chi_1\,R^z_{16\eta}\Big)+H^V(1,\chi_1,\chi_{16},\chi_{16},\chi_1)\,\Big(-11/36\,\chi_1\,R^z_{146\eta}$$
$$-5/12\,\chi_1^2\,R^c_{146\eta}-1/18\,(4\,\chi_6-7\,\chi_1\Big)\,\chi_1\,R^z_{14\eta}\Big)+H^V(1,\chi_1,\chi_\eta,\chi_\eta,\chi_1)\,\Big(8/9\,\chi_1^2\,{R^z_{\eta61}}^4\Big)$$

$$
\begin{aligned}
&+H^V(1,\chi_{14},\chi_{14},\chi_\eta,\chi_1)\left(1/27\,(\chi_\eta-\chi_4)\,(\chi_\eta-\chi_4-6\,\chi_1)+4/27\,(\chi_\eta+2\,\chi_1)\,(\chi_\eta-4\,\chi_1)\,{R^z_{\eta 61}}^2\right.\\
&\left.+4/27\,(\chi_\eta^2-\chi_4\,\chi_\eta-4\,\chi_1\,\chi_\eta+\chi_1\,\chi_4-6\,\chi_1^2)\,R^z_{\eta 61}\right)+H^V(1,\chi_{16},\chi_{16},\chi_\eta,\chi_1)\left(2/27\,(\chi_\eta\right.\\
&\left.-\chi_6)\,(\chi_\eta-\chi_6-6\,\chi_1)+2/27\,(\chi_\eta+2\,\chi_1)\,(\chi_\eta-4\,\chi_1)\,{R^z_{\eta 61}}^2-4/27\,(\chi_\eta^2-\chi_6\,\chi_\eta-4\,\chi_1\,\chi_\eta\right.\\
&\left.+\chi_1\,\chi_6-6\,\chi_1^2)\,R^z_{\eta 61}\right)+H^V(1,\chi_4,\chi_{14},\chi_{14},\chi_1)\left(3/4\,\chi_1\,\chi_4\right)+H^V(1,\chi_{46},\chi_{14},\chi_{16},\chi_1)\left(1/2\,(\chi_6\right.\\
&\left.+\chi_4)\,\chi_1\right)+H^V(1,\chi_\eta,\chi_{14},\chi_{14},\chi_1)\left(1/12\,\chi_1\,\chi_\eta+1/3\,\chi_1\,\chi_\eta\,R^z_{\eta 61}+1/3\,\chi_1\,\chi_\eta\,{R^z_{\eta 61}}^2\right)\\
&+H^V(1,\chi_\eta,\chi_{16},\chi_{16},\chi_1)\left(1/6\,\chi_1\,\chi_\eta-1/3\,\chi_1\,\chi_\eta\,R^z_{\eta 61}+1/6\,\chi_1\,\chi_\eta\,{R^z_{\eta 61}}^2\right)\\
&+H^V(2,\chi_1,\chi_1,\chi_1,\chi_1)\left(4/9\,\chi_1^2\,R^z_{146\eta}\,R^c_{146\eta}\right)+H^V(2,\chi_1,\chi_1,\chi_\eta,\chi_1)\left(-8/9\,\chi_1^2\,R^z_{146\eta}\,{R^z_{\eta 61}}^2\right)\\
&+H^V(2,\chi_1,\chi_{14},\chi_{14},\chi_1)\left(-5/6\,\chi_1^2\,R^z_{146\eta}\right)+H^V(2,\chi_1,\chi_{16},\chi_{16},\chi_1)\left(-5/12\,\chi_1^2\,R^z_{146\eta}\right)\\
&+H^V(5,\chi_1,\chi_1,\chi_1,\chi_1)\left(2/9\,\chi_1^2\,{R^z_{146\eta}}^2\right)+H_1^V(1,\chi_1,\chi_{14},\chi_{14},\chi_1)\left(4/9\,\chi_1\,R^z_{146\eta}+4/3\,\chi_1^2\,R^c_{146\eta}\right.\\
&\left.+4/9\,(\chi_4-4\,\chi_1)\,\chi_1\,R^z_{16\eta}\right)+H_1^V(1,\chi_1,\chi_{16},\chi_{16},\chi_1)\left(2/9\,\chi_1\,R^z_{146\eta}+2/3\,\chi_1^2\,R^c_{146\eta}\right.\\
&\left.+2/9\,(\chi_6-4\,\chi_1)\,\chi_1\,R^z_{14\eta}\right)+H_1^V(1,\chi_{14},\chi_{14},\chi_\eta,\chi_1)\left(4/9\,(\chi_\eta-\chi_4)\,\chi_1+16/9\,(\chi_\eta\right.\\
&\left.+2\,\chi_1)\,\chi_1\,{R^z_{\eta 61}}^2+8/9\,(2\,\chi_\eta-\chi_4+2\,\chi_1)\,\chi_1\,R^z_{\eta 61}\right)+H_1^V(1,\chi_{16},\chi_{16},\chi_\eta,\chi_1)\left(8/9\,(\chi_\eta-\chi_6)\,\chi_1\right.\\
&\left.+8/9\,(\chi_\eta+2\,\chi_1)\,\chi_1\,{R^z_{\eta 61}}^2-8/9\left(2\,\chi_\eta-\chi_6+2\,\chi_1\right)\chi_1\,R^z_{\eta 61}\right)\\
&+H_1^V(2,\chi_1,\chi_{14},\chi_{14},\chi_1)\left(4/3\,\chi_1^2\,R^z_{146\eta}\right)+H_1^V(2,\chi_1,\chi_{16},\chi_{16},\chi_1)\left(2/3\,\chi_1^2\,R^z_{146\eta}\right)\\
&+H_{21}^V(1,\chi_1,\chi_{14},\chi_{14},\chi_1)\left(\chi_1^2\,R^z_{16\eta}-1/2\,\chi_1^2\,R^c_{146\eta}\right)+H_{21}^V(1,\chi_1,\chi_{16},\chi_{16},\chi_1)\left(1/2\,\chi_1^2\,R^z_{14\eta}\right.\\
&\left.-1/4\,\chi_1^2\,R^c_{146\eta}\right)+H_{21}^V(1,\chi_4,\chi_{14},\chi_{14},\chi_1)\left(9/4\,\chi_1^2\right)+H_{21}^V(1,\chi_{46},\chi_{14},\chi_{16},\chi_1)\left(3\,\chi_1^2\right)\\
&+H_{21}^V(1,\chi_\eta,\chi_{14},\chi_{14},\chi_1)\left(1/4\,\chi_1^2+\chi_1^2\,R^z_{\eta 61}+\chi_1^2\,{R^z_{\eta 61}}^2\right)+H_{21}^V(1,\chi_\eta,\chi_{16},\chi_{16},\chi_1)\left(1/2\,\chi_1^2\right.\\
&\left.-\chi_1^2\,R^z_{\eta 61}+1/2\,\chi_1^2\,{R^z_{\eta 61}}^2\right)+H_{21}^V(2,\chi_1,\chi_{14},\chi_{14},\chi_1)\left(-1/2\,\chi_1^2\,R^z_{146\eta}\right)\\
&+H_{21}^V(2,\chi_1,\chi_{16},\chi_{16},\chi_1)\left(-1/4\,\chi_1^2\,R^z_{146\eta}\right)+H_{27}^V(1,\chi_1,\chi_{14},\chi_{14},\chi_1)\left(-\chi_1\,R^z_{16\eta}\right.\\
&\left.+1/2\,\chi_1\,R^c_{146\eta}\right)+H_{27}^V(1,\chi_1,\chi_{16},\chi_{16},\chi_1)\left(-1/2\,\chi_1\,R^z_{14\eta}+1/4\,\chi_1\,R^c_{146\eta}\right)\\
&+H_{27}^V(1,\chi_4,\chi_{14},\chi_{14},\chi_1)\left(-9/4\,\chi_1\right)+H_{27}^V(1,\chi_{46},\chi_{14},\chi_{16},\chi_1)\left(-3\,\chi_1\right)\\
&+H_{27}^V(1,\chi_\eta,\chi_{14},\chi_{14},\chi_1)\left(-1/4\,\chi_1-\chi_1\,R^z_{\eta 61}-\chi_1\,{R^z_{\eta 61}}^2\right)\\
&+H_{27}^V(1,\chi_\eta,\chi_{16},\chi_{16},\chi_1)\left(-1/2\,\chi_1+\chi_1\,R^z_{\eta 61}-1/2\,\chi_1\,{R^z_{\eta 61}}^2\right)\\
&+H_{27}^V(2,\chi_1,\chi_{14},\chi_{14},\chi_1)\left(1/2\,\chi_1\,R^z_{146\eta}\right)+H_{27}^V(2,\chi_1,\chi_{16},\chi_{16},\chi_1)\left(1/4\,\chi_1\,R^z_{146\eta}\right)
\end{aligned}
\tag{42}
$$

B Expressions for the decay constant

$$
F_0\Delta^V F_{12}^{2(4)12}=+A^V(\chi_{14})\left(1\right)+A^V(\chi_{16})\left(1/2\right)
\tag{43}
$$

$$
\begin{aligned}
F_0^3\Delta^V F_{12}^{2(6L)12}=&+A^V(\chi_1)\left(-4/3\,\hat{L}_5^r\,\chi_1\,R^c_{146\eta}+4\,\hat{L}_3^r\,R^z_{146\eta}+4\,\hat{L}_3^r\,\chi_1\,R^c_{146\eta}-10\,\hat{L}_2^r\,\chi_1-4\,\hat{L}_1^r\,\chi_1\right.
\end{aligned}
$$

$$
\begin{aligned}
&+4\,\hat{L}_0^r\,R_{146\eta}^z+4\,\hat{L}_0^r\,\chi_1\,R_{146\eta}^c\Big)+A^V(\chi_{14})\,\Big(4\,\hat{L}_5^r\,\chi_1-4\,(\chi_6+2\,\chi_4)\,\hat{L}_4^r-10\,(\chi_4+\chi_1)\,\hat{L}_3^r\\
&-4\,(\chi_4+\chi_1)\,\hat{L}_0^r\Big)+A^V(\chi_{16})\,\Big(2\,\hat{L}_5^r\,\chi_1-2\,(\chi_6+2\,\chi_4)\,\hat{L}_4^r-5\,(\chi_6+\chi_1)\,\hat{L}_3^r-2\,(\chi_6+\chi_1)\,\hat{L}_0^r\Big)\\
&+A^V(\chi_4)\,\Big(12\,\hat{L}_4^r\,\chi_4-6\,\hat{L}_2^r\,\chi_4-24\,\hat{L}_1^r\,\chi_4\Big)+A^V(\chi_{46})\,\Big(8\,(\chi_6+\chi_4)\,\hat{L}_4^r-4\,(\chi_6+\chi_4)\,\hat{L}_2^r\\
&-16\,(\chi_6+\chi_4)\,\hat{L}_1^r\Big)+A^V(\chi_\eta)\,\Big(8/3\,\hat{L}_5^r\,\chi_1\,{R_{\eta61}^z}^2-8\,\hat{L}_3^r\,\chi_\eta\,{R_{\eta61}^z}^2-2\,\hat{L}_2^r\,\chi_\eta-8\,\hat{L}_1^r\,\chi_\eta\\
&-8\,\hat{L}_0^r\,\chi_\eta\,{R_{\eta61}^z}^2+4/3\,(2\,\chi_6+\chi_4)\,\hat{L}_4^r\Big)+B^V(\chi_1)\,\Big(-4/3\,\hat{L}_5^r\,\chi_1\,R_{146\eta}^z+4\,\hat{L}_3^r\,\chi_1\,R_{146\eta}^z\\
&+4\,\hat{L}_0^r\,\chi_1\,R_{146\eta}^z\Big)+B^V(\chi_{14})\,\Big(8\,(\chi_4+\chi_1)\,(\chi_6+2\,\chi_4)\,\hat{L}_6^r-4\,(\chi_4+\chi_1)\,(\chi_6+2\,\chi_4)\,\hat{L}_4^r\\
&+4\,(\chi_4+\chi_1)^2\,\hat{L}_8^r-2\,(\chi_4+\chi_1)^2\,\hat{L}_5^r\Big)+B^V(\chi_{16})\,\Big(4\,(\chi_6+\chi_1)\,(\chi_6+2\,\chi_4)\,\hat{L}_6^r\\
&-2\,(\chi_6+\chi_1)\,(\chi_6+2\,\chi_4)\,\hat{L}_4^r+2\,(\chi_6+\chi_1)^2\,\hat{L}_8^r-\Big(\chi_6+\chi_1\Big)^2\,\hat{L}_5^r\Big)+A_{23}^V(\chi_1)\,\Big(-4\,\hat{L}_3^r\,R_{146\eta}^c\\
&+6\,\hat{L}_2^r+12\,\hat{L}_1^r-4\,\hat{L}_0^r\,R_{146\eta}^c\Big)+A_{23}^V(\chi_{14})\,\Big(12\,\hat{L}_3^r+24\,\hat{L}_0^r\Big)+A_{23}^V(\chi_{16})\,\Big(6\,\hat{L}_3^r+12\,\hat{L}_0^r\Big)\\
&+A_{23}^V(\chi_4)\,\Big(18\,\hat{L}_2^r\Big)+A_{23}^V(\chi_{46})\,\Big(24\,\hat{L}_2^r\Big)+A_{23}^V(\chi_\eta)\,\Big(8\,\hat{L}_3^r\,{R_{\eta61}^z}^2+6\,\hat{L}_2^r+8\,\hat{L}_0^r\,{R_{\eta61}^z}^2\Big)\\
&+B_{23}^V(\chi_1)\,\Big(-4\,\hat{L}_3^r\,R_{146\eta}^z-4\,\hat{L}_0^r\,R_{146\eta}^z\Big)
\end{aligned}
\tag{44}
$$

$$
\begin{aligned}
F_0^3\Delta^V F_{12}^{2(6R)12} &= +\overline{A}(\chi_1)\,B^V(\chi_{14})\,\Big(1/18\,R_{146\eta}^z-1/9\,(\chi_4+2\,\chi_1)\,R_{16\eta}^z\Big)\\
&+\overline{A}(\chi_1)\,B^V(\chi_{16})\,\Big(1/36\,R_{146\eta}^z-1/18\,(\chi_6+2\,\chi_1)\,R_{14\eta}^z\Big)\\
&+\overline{A}(\chi_{14})\,A^V(\chi_{14})\,\Big(5/54-5/27\,R_{\eta61}^z-5/27\,{R_{\eta61}^z}^2-5/27\,R_{16\eta}^z+5/54\,R_{146\eta}^c\Big)\\
&+\overline{A}(\chi_{16})\,A^V(\chi_{16})\,\Big(5/108+5/27\,R_{\eta61}^z-5/54\,{R_{\eta61}^z}^2-5/54\,R_{14\eta}^z+5/108\,R_{146\eta}^c\Big)\\
&+\overline{A}(\chi_\eta)\,B^V(\chi_{14})\,\Big(-1/36\,(\chi_\eta-\chi_4)-1/9\,(\chi_\eta+\chi_4+\chi_1)\,R_{\eta61}^z-1/9\,(\chi_\eta-\chi_1)\,{R_{\eta61}^z}^2\Big)\\
&+\overline{A}(\chi_\eta)\,B^V(\chi_{16})\,\Big(-1/18\,(\chi_\eta-\chi_6)+1/9\,(\chi_\eta+\chi_6+\chi_1)\,R_{\eta61}^z-1/18\,(\chi_\eta-\chi_1)\,{R_{\eta61}^z}^2\Big)\\
&+\overline{B}(\chi_{14})\,A^V(\chi_1)\,\Big(1/18\,R_{146\eta}^z-1/9\,(\chi_4+2\,\chi_1)\,R_{16\eta}^z\Big)+\overline{B}(\chi_{14})\,A^V(\chi_\eta)\,\Big(-1/36\,(\chi_\eta-\chi_4)\\
&-1/9\,(\chi_\eta+\chi_4+\chi_1)\,R_{\eta61}^z-1/9\,(\chi_\eta-\chi_1)\,{R_{\eta61}^z}^2\Big)+\overline{B}(\chi_{16})\,A^V(\chi_1)\,\Big(1/36\,R_{146\eta}^z\\
&-1/18\,(\chi_6+2\,\chi_1)\,R_{14\eta}^z\Big)+\overline{B}(\chi_{16})\,A^V(\chi_\eta)\,\Big(-1/18\,(\chi_\eta-\chi_6)+1/9\,(\chi_\eta+\chi_6+\chi_1)\,R_{\eta61}^z\\
&-1/18\,(\chi_\eta-\chi_1)\,{R_{\eta61}^z}^2\Big)+A^V(\chi_1)\,\frac{1}{16\pi^2}\,\Big(1/8\,\chi_1-1/12\,\chi_1\,R_{16\eta}^z-1/24\,\chi_1\,R_{14\eta}^z\Big)\\
&+A^V(\chi_1)\,B^V(\chi_{14})\,\Big(1/18\,R_{146\eta}^z-1/9\,(\chi_4+2\,\chi_1)\,R_{16\eta}^z\Big)+A^V(\chi_1)\,B^V(\chi_{16})\,\Big(1/36\,R_{146\eta}^z\\
&-1/18\,(\chi_6+2\,\chi_1)\,R_{14\eta}^z\Big)+A^V(\chi_{14})\,\frac{1}{16\pi^2}\,\Big(1/12\,R_{146\eta}^z-1/24\,(\chi_\eta+6\,\chi_6+14\,\chi_4+5\,\chi_1)\\
&-1/12\,(2\,\chi_\eta+\chi_4+\chi_1)\,R_{\eta61}^z-1/12\,(2\,\chi_\eta+\chi_4+\chi_1)\,{R_{\eta61}^z}^2-1/12\,(\chi_4+3\,\chi_1)\,R_{16\eta}^z\\
&+1/24\,(\chi_4+3\,\chi_1)\,R_{146\eta}^c\Big)+A^V(\chi_{14})^2\,\Big(5/108-5/54\,R_{\eta61}^z-5/54\,{R_{\eta61}^z}^2-5/54\,R_{16\eta}^z\\
&+5/108\,R_{146\eta}^c\Big)+A^V(\chi_{16})\,\frac{1}{16\pi^2}\,\Big(1/24\,R_{146\eta}^z+1/12\,(2\,\chi_\eta+\chi_6+\chi_1)\,R_{\eta61}^z\\
&-1/24\,(2\,\chi_\eta+\chi_6+\chi_1)\,{R_{\eta61}^z}^2-1/48\,\Big(4\,\chi_\eta+5\,\chi_6+12\,\chi_4+5\,\chi_1\Big)-1/24\,(\chi_6+3\,\chi_1)\,R_{14\eta}^z
\end{aligned}
$$

$$
\begin{aligned}
&+1/48\,(\chi_6+3\,\chi_1)\,R^c_{146\eta}\Big)+A^V(\chi_{16})^2\,\Big(5/216+5/54\,R^z_{\eta61}-5/108\,{R^z_{\eta61}}^2-5/108\,R^z_{14\eta}\\
&+5/216\,R^c_{146\eta}\Big)+A^V(\chi_\eta)\,B^V(\chi_{14})\,\Big(-1/36\,(\chi_\eta-\chi_4)-1/9\,(\chi_\eta+\chi_4+\chi_1)\,R^z_{\eta61}\\
&-1/9\,(\chi_\eta-\chi_1)\,{R^z_{\eta61}}^2\Big)+A^V(\chi_\eta)\,B^V(\chi_{16})\,\Big(-1/18\,(\chi_\eta-\chi_6)+1/9\,(\chi_\eta+\chi_6+\chi_1)\,R^z_{\eta61}\\
&-1/18\,(\chi_\eta-\chi_1)\,{R^z_{\eta61}}^2\Big)+A^V_{23}(\chi_1)\,\frac{1}{16\pi^2}\,\Big(-3/8+1/4\,R^z_{16\eta}+1/8\,R^z_{14\eta}\Big)\\
&+A^V_{23}(\chi_{14})\,\frac{1}{16\pi^2}\,\Big(-1/12+1/6\,R^z_{\eta61}+1/6\,{R^z_{\eta61}}^2+1/6\,R^z_{16\eta}-1/12\,R^c_{146\eta}\Big)\\
&+A^V_{23}(\chi_{16})\,\frac{1}{16\pi^2}\,\Big(-1/24-1/6\,R^z_{\eta61}+1/12\,{R^z_{\eta61}}^2+1/12\,R^z_{14\eta}-1/24\,R^c_{146\eta}\Big)\\
&+H^V(1,\chi_1,\chi_{14},\chi_{14},\chi_1)\,\Big(1/12\,R^z_{146\eta}-1/6\,\chi_1\,R^z_{16\eta}+1/12\,\chi_1\,R^c_{146\eta}\Big)\\
&+H^V(1,\chi_1,\chi_{16},\chi_{16},\chi_1)\,\Big(1/24\,R^z_{146\eta}-1/12\,\chi_1\,R^z_{14\eta}+1/24\,\chi_1\,R^c_{146\eta}\Big)\\
&+H^V(1,\chi_4,\chi_{14},\chi_{14},\chi_1)\,\Big(-3/8\,\chi_4\Big)+H^V(1,\chi_{46},\chi_{14},\chi_{16},\chi_1)\,\Big(-1/4\,(\chi_6+\chi_4)\Big)\\
&+H^V(1,\chi_\eta,\chi_{14},\chi_{14},\chi_1)\,\Big(-1/24\,\chi_\eta-1/6\,\chi_\eta\,R^z_{\eta61}-1/6\,\chi_\eta\,{R^z_{\eta61}}^2\Big)\\
&+H^V(1,\chi_\eta,\chi_{16},\chi_{16},\chi_1)\,\Big(-1/12\,\chi_\eta+1/6\,\chi_\eta\,R^z_{\eta61}-1/12\,\chi_\eta\,{R^z_{\eta61}}^2\Big)\\
&+H^V(2,\chi_1,\chi_{14},\chi_{14},\chi_1)\,\Big(5/54\,\chi_1\,R^z_{146\eta}\Big)+H^V(2,\chi_1,\chi_{16},\chi_{16},\chi_1)\,\Big(5/108\,\chi_1\,R^z_{146\eta}\Big)\\
&+H^V_1(2,\chi_1,\chi_{14},\chi_{14},\chi_1)\,\Big(-1/108\,\chi_1\,R^z_{146\eta}\Big)+H^V_1(2,\chi_1,\chi_{16},\chi_{16},\chi_1)\,\Big(-1/216\,\chi_1\,R^z_{146\eta}\Big)\\
&+H^V_1(3,\chi_{14},\chi_1,\chi_{14},\chi_1)\,\Big(-1/54\,\chi_1\,R^z_{146\eta}\Big)+H^V_1(3,\chi_{16},\chi_1,\chi_{16},\chi_1)\,\Big(-1/108\,\chi_1\,R^z_{146\eta}\Big)\\
&+H^V_{27}(1,\chi_1,\chi_{14},\chi_{14},\chi_1)\,\Big(1/2\,R^z_{16\eta}-1/4\,R^c_{146\eta}\Big)+H^V_{27}(1,\chi_1,\chi_{16},\chi_{16},\chi_1)\,\Big(1/4\,R^z_{14\eta}-1/8\,R^c_{146\eta}\Big)\\
&+H^V_{27}(1,\chi_4,\chi_{14},\chi_{14},\chi_1)\,\Big(9/8\Big)+H^V_{27}(1,\chi_{46},\chi_{14},\chi_{16},\chi_1)\,\Big(3/2\Big)\\
&+H^V_{27}(1,\chi_\eta,\chi_{14},\chi_{14},\chi_1)\,\Big(1/8+1/2\,R^z_{\eta61}+1/2\,{R^z_{\eta61}}^2\Big)\\
&+H^V_{27}(1,\chi_\eta,\chi_{16},\chi_{16},\chi_1)\,\Big(1/4-1/2\,R^z_{\eta61}+1/4\,{R^z_{\eta61}}^2\Big)\\
&+H^V_{27}(2,\chi_1,\chi_{14},\chi_{14},\chi_1)\,\Big(-1/4\,R^z_{146\eta}\Big)+H^V_{27}(2,\chi_1,\chi_{16},\chi_{16},\chi_1)\,\Big(-1/8\,R^z_{146\eta}\Big)\\
&+H'^V(1,\chi_1,\chi_1,\chi_1,\chi_1)\,\Big(1/6\,\chi_1^2+1/9\,\chi_1^2\,{R^c_{146\eta}}^2\Big)+H'^V(1,\chi_1,\chi_1,\chi_\eta,\chi_1)\,\Big(-4/9\,\chi_1^2\,R^c_{146\eta}\,{R^z_{\eta61}}^2\Big)\\
&+H'^V(1,\chi_1,\chi_{14},\chi_{14},\chi_1)\,\Big(-11/36\,\chi_1\,R^z_{146\eta}-5/12\,\chi_1^2\,R^c_{146\eta}-1/18\,(4\,\chi_4-7\,\chi_1)\,\chi_1\,R^z_{16\eta}\Big)\\
&+H'^V(1,\chi_1,\chi_{16},\chi_{16},\chi_1)\,\Big(-11/72\,\chi_1\,R^z_{146\eta}-5/24\,\chi_1^2\,R^c_{146\eta}-1/36\,(4\,\chi_6-7\,\chi_1)\,\chi_1\,R^z_{14\eta}\Big)\\
&+H'^V(1,\chi_1,\chi_\eta,\chi_\eta,\chi_1)\,\Big(4/9\,\chi_1^2\,{R^z_{\eta61}}^4\Big)+H'^V(1,\chi_{14},\chi_{14},\chi_\eta,\chi_1)\,\Big(1/54\,(\chi_\eta-\chi_4)\,(\chi_\eta-\chi_4\\
&-6\,\chi_1)+2/27\,(\chi_\eta+2\,\chi_1)\,(\chi_\eta-4\,\chi_1)\,{R^z_{\eta61}}^2+2/27\,(\chi_\eta^2-\chi_4\,\chi_\eta-4\,\chi_1\,\chi_\eta+\chi_1\,\chi_4-6\,\chi_1^2)\,R^z_{\eta61}\Big)\\
&+H'^V(1,\chi_{16},\chi_{16},\chi_\eta,\chi_1)\,\Big(1/27\,(\chi_\eta-\chi_6)\,(\chi_\eta-\chi_6-6\,\chi_1)+1/27\,(\chi_\eta+2\,\chi_1)\,(\chi_\eta-4\,\chi_1)\\
&{R^z_{\eta61}}^2-2/27\,(\chi_\eta^2-\chi_6\,\chi_\eta-4\,\chi_1\,\chi_\eta+\chi_1\,\chi_6-6\,\chi_1^2)\,R^z_{\eta61}\Big)+H'^V(1,\chi_4,\chi_{14},\chi_{14},\chi_1)\,\Big(3/8\,\chi_1\,\chi_4\Big)\\
&+H'^V(1,\chi_{46},\chi_{14},\chi_{16},\chi_1)\,\Big(1/4\,(\chi_6+\chi_4)\,\chi_1\Big)+H'^V(1,\chi_\eta,\chi_{14},\chi_{14},\chi_1)\,\Big(1/24\,\chi_1\,\chi_\eta
\end{aligned}
$$

$$
\begin{aligned}
&+1/6\,\chi_1\,\chi_\eta\,R^z_{\eta 61}+1/6\,\chi_1\,\chi_\eta\,{R^z_{\eta 61}}^2\Big)+H^{'V}(1,\chi_\eta,\chi_{16},\chi_{16},\chi_1)\Big(1/12\,\chi_1\,\chi_\eta-1/6\,\chi_1\,\chi_\eta\,R^z_{\eta 61}\\
&+1/12\,\chi_1\,\chi_\eta\,{R^z_{\eta 61}}^2\Big)+H^{'V}(2,\chi_1,\chi_1,\chi_1,\chi_1)\Big(2/9\,\chi_1^2\,R^z_{146\eta}\,R^c_{146\eta}\Big)\\
&+H^{'V}(2,\chi_1,\chi_1,\chi_\eta,\chi_1)\Big(-4/9\,\chi_1^2\,R^z_{146\eta}\,{R^z_{\eta 61}}^2\Big)+H^{'V}(2,\chi_1,\chi_{14},\chi_{14},\chi_1)\Big(-5/12\,\chi_1^2\,R^z_{146\eta}\Big)\\
&+H^{'V}(2,\chi_1,\chi_{16},\chi_{16},\chi_1)\Big(-5/24\,\chi_1^2\,R^z_{146\eta}\Big)+H^{'V}(5,\chi_1,\chi_1,\chi_1,\chi_1)\Big(1/9\,\chi_1^2\,{R^z_{146\eta}}^2\Big)\\
&+H_1^{'V}(1,\chi_1,\chi_{14},\chi_{14},\chi_1)\Big(2/9\,\chi_1\,R^z_{146\eta}+2/3\,\chi_1^2\,R^c_{146\eta}+2/9\,(\chi_4-4\,\chi_1)\,\chi_1\,R^z_{16\eta}\Big)\\
&+H_1^{'V}(1,\chi_1,\chi_{16},\chi_{16},\chi_1)\Big(1/9\,\chi_1\,R^z_{146\eta}+1/3\,\chi_1^2\,R^c_{146\eta}+1/9\,(\chi_6-4\,\chi_1)\,\chi_1\,R^z_{14\eta}\Big)\\
&+H_1^{'V}(1,\chi_{14},\chi_{14},\chi_\eta,\chi_1)\Big(2/9\,(\chi_\eta-\chi_4)\,\chi_1+8/9\,(\chi_\eta+2\,\chi_1)\,\chi_1\,{R^z_{\eta 61}}^2+4/9\,(2\,\chi_\eta-\chi_4\\
&+2\,\chi_1)\,\chi_1\,R^z_{\eta 61}\Big)+H_1^{'V}(1,\chi_{16},\chi_{16},\chi_\eta,\chi_1)\Big(4/9\,(\chi_\eta-\chi_6)\,\chi_1+4/9\,(\chi_\eta+2\,\chi_1)\,\chi_1\,{R^z_{\eta 61}}^2\\
&-4/9\,(2\,\chi_\eta-\chi_6+2\,\chi_1)\,\chi_1\,R^z_{\eta 61}\Big)+H_1^{'V}(2,\chi_1,\chi_{14},\chi_{14},\chi_1)\Big(2/3\,\chi_1^2\,R^z_{146\eta}\Big)\\
&+H_1^{'V}(2,\chi_1,\chi_{16},\chi_{16},\chi_1)\Big(1/3\,\chi_1^2\,R^z_{146\eta}\Big)+H_{21}^{'V}(1,\chi_1,\chi_{14},\chi_{14},\chi_1)\Big(1/2\,\chi_1^2\,R^z_{16\eta}-1/4\,\chi_1^2\,R^c_{146\eta}\Big)\\
&+H_{21}^{'V}(1,\chi_1,\chi_{16},\chi_{16},\chi_1)\Big(1/4\,\chi_1^2\,R^z_{14\eta}-1/8\,\chi_1^2\,R^c_{146\eta}\Big)+H_{21}^{'V}(1,\chi_4,\chi_{14},\chi_{14},\chi_1)\Big(9/8\,\chi_1^2\Big)\\
&+H_{21}^{'V}(1,\chi_{46},\chi_{14},\chi_{16},\chi_1)\Big(3/2\,\chi_1^2\Big)+H_{21}^{'V}(1,\chi_\eta,\chi_{14},\chi_{14},\chi_1)\Big(1/8\,\chi_1^2+1/2\,\chi_1^2\,R^z_{\eta 61}\\
&+1/2\,\chi_1^2\,{R^z_{\eta 61}}^2\Big)+H_{21}^{'V}(1,\chi_\eta,\chi_{16},\chi_{16},\chi_1)\Big(1/4\,\chi_1^2-1/2\,\chi_1^2\,R^z_{\eta 61}+1/4\,\chi_1^2\,{R^z_{\eta 61}}^2\Big)\\
&+H_{21}^{'V}(2,\chi_1,\chi_{14},\chi_{14},\chi_1)\Big(-1/4\,\chi_1^2\,R^z_{146\eta}\Big)+H_{21}^{'V}(2,\chi_1,\chi_{16},\chi_{16},\chi_1)\Big(-1/8\,\chi_1^2\,R^z_{146\eta}\Big)\\
&+H_{27}^{'V}(1,\chi_1,\chi_{14},\chi_{14},\chi_1)\Big(-1/2\,\chi_1\,R^z_{16\eta}+1/4\,\chi_1\,R^c_{146\eta}\Big)\\
&+H_{27}^{'V}(1,\chi_1,\chi_{16},\chi_{16},\chi_1)\Big(-1/4\,\chi_1\,R^z_{14\eta}+1/8\,\chi_1\,R^c_{146\eta}\Big)+H_{27}^{'V}(1,\chi_4,\chi_{14},\chi_{14},\chi_1)\Big(-9/8\,\chi_1\Big)\\
&+H_{27}^{'V}(1,\chi_{46},\chi_{14},\chi_{16},\chi_1)\Big(-3/2\,\chi_1\Big)+H_{27}^{'V}(1,\chi_\eta,\chi_{14},\chi_{14},\chi_1)\Big(-1/8\,\chi_1-1/2\,\chi_1\,R^z_{\eta 61}\\
&-1/2\,\chi_1\,{R^z_{\eta 61}}^2\Big)+H_{27}^{'V}(1,\chi_\eta,\chi_{16},\chi_{16},\chi_1)\Big(-1/4\,\chi_1+1/2\,\chi_1\,R^z_{\eta 61}-1/4\,\chi_1\,{R^z_{\eta 61}}^2\Big)\\
&+H_{27}^{'V}(2,\chi_1,\chi_{14},\chi_{14},\chi_1)\Big(1/4\,\chi_1\,R^z_{146\eta}\Big)+H_{27}^{'V}(2,\chi_1,\chi_{16},\chi_{16},\chi_1)\Big(1/8\,\chi_1\,R^z_{146\eta}\Big) \qquad (45)
\end{aligned}
$$

References

[1] S. Aoki *et al.*, Eur. Phys. J. C **74** (2014) 2890 [arXiv:1310.8555 [hep-lat]].

[2] S. Weinberg, Physica A **96** (1979) 327.

[3] J. Gasser and H. Leutwyler, Annals Phys. **158** (1984) 142.

[4] J. Gasser and H. Leutwyler, Nucl. Phys. B **250** (1985) 465.

[5] J. Gasser and H. Leutwyler, Phys. Lett. B **184** (1987) 83.

[6] J. Gasser and H. Leutwyler, Phys. Lett. B **188** (1987) 477.

[7] J. Gasser and H. Leutwyler, Nucl. Phys. B **307** (1988) 763.

[8] C. W. Bernard and M. F. L. Golterman, Phys. Rev. D **49** (1994) 486 [hep-lat/9306005].

[9] C. Bernard and M. Golterman, Phys. Rev. D **88** (2013) 1, 014004 [arXiv:1304.1948 [hep-lat]].

[10] S. R. Sharpe and N. Shoresh, Phys. Rev. D **62** (2000) 094503 [hep-lat/0006017].

[11] J. Bijnens, N. Danielsson and T. A. Lahde, Phys. Rev. D **70** (2004) 111503 [hep-lat/0406017].

[12] J. Bijnens and T. A. Lahde, Phys. Rev. D **71** (2005) 094502 [hep-lat/0501014].

[13] J. Bijnens, N. Danielsson and T. A. Lahde, Phys. Rev. D **73** (2006) 074509 [hep-lat/0602003].

[14] J. Bijnens and T. A. Lahde, Phys. Rev. D **72** (2005) 074502 [hep-lat/0506004].

[15] J. Bijnens and T. Rössler, JHEP **1501** (2015) 034 [arXiv:1411.6384 [hep-lat]].

[16] J. Bijnens, E. Boström and T. A. Lähde, JHEP **1401** (2014) 019 [arXiv:1311.3531 [hep-lat]].

[17] G. Colangelo and C. Haefeli, Nucl. Phys. B **744** (2006) 14 [hep-lat/0602017].

[18] J. Bijnens and K. Ghorbani, Phys. Lett. B **636** (2006) 51 [hep-lat/0602019].

[19] P. H. Damgaard and H. Fukaya, JHEP **0901** (2009) 052 [arXiv:0812.2797 [hep-lat]].

[20] C. Aubin and C. Bernard, Phys. Rev. D **68** (2003) 034014 [hep-lat/0304014].

[21] C. Aubin and C. Bernard, Phys. Rev. D **68** (2003) 074011 [hep-lat/0306026].

[22] http://www.thep.lu.se/~bijnens/chpt/

[23] S. Scherer and M. R. Schindler, Lect. Notes Phys. **830** (2012) 1; hep-ph/0505265.

[24] J. Bijnens, Prog. Part. Nucl. Phys. **58** (2007) 521 [hep-ph/0604043].

[25] J. Bijnens, G. Colangelo and G. Ecker, JHEP **9902** (1999) 020 [hep-ph/9902437].

[26] J. Bijnens, G. Colangelo, G. Ecker, J. Gasser and M. E. Sainio, Nucl. Phys. B **508** (1997) 263 [Erratum-ibid. B **517** (1998) 639] [hep-ph/9707291].

[27] J. Bijnens, G. Colangelo and G. Ecker, Annals Phys. **280** (2000) 100 [hep-ph/9907333].

[28] M. Golterman, arXiv:0912.4042 [hep-lat].

[29] S. R. Sharpe, Phys. Rev. D **46** (1992) 3146 [hep-lat/9205020].

[30] S. R. Sharpe and N. Shoresh, Phys. Rev. D **64** (2001) 114510 [hep-lat/0108003].

[31] P. H. Damgaard and K. Splittorff, Phys. Rev. D **62** (2000) 054509 [hep-lat/0003017].

[32] J. Bijnens and N. Danielsson, Phys. Rev. D **74** (2006) 054503 [hep-lat/0606017].

[33] D. Becirevic and G. Villadoro, Phys. Rev. D **69** (2004) 054010 [hep-lat/0311028].

[34] G. Amorós, J. Bijnens and P. Talavera, Nucl. Phys. B **568** (2000) 319 [hep-ph/9907264].

[35] J. Bijnens, Eur. Phys. J. C **75** (2015) 1, 27 [arXiv:1412.0887 [hep-ph]].

[36] http://www.thep.lu.se/~bijnens/chiron/

[37] J. Bijnens and G. Ecker, Ann. Rev. Nucl. Part. Sci. **64** (2014) 149 [arXiv:1405.6488 [hep-ph]].

[38] J. A. M. Vermaseren, "New features of FORM," math-ph/0010025.

Paper IV

LU TP 15-34
September 2015

Finite Volume and Partially Quenched QCD-like Effective Field Theories

Johan Bijnens and Thomas Rössler

Department of Astronomy and Theoretical Physics, Lund University,
Sölvegatan 14A, SE 223-62 Lund, Sweden

Abstract

We present a calculation of the meson masses, decay constants and quark-antiquark vacuum expectation value for the three generic QCD-like chiral symmetry breaking patterns $SU(N_F) \times SU(N_F) \to SU(N_F)_V$, $SU(N_F) \to SO(N_F)$ and $SU(2N_F) \to Sp(2N_F)$ in the effective field theory for these cases. We extend the previous two-loop work to include effects of partial quenching and finite volume.

The calculation has been performed using the quark flow technique. We reproduce the known infinite volume results in the unquenched case. The analytical results can be found in the supplementary material.

Some examples of numerical results are given. The numerical programs for all cases are included in version 0.54 of the CHIRON package.

The purpose of this work is the use in lattice extrapolations to zero mass for QCD-like and strongly interacting Higgs sector lattice calculations.

1 Introduction

Effective field theory is used extensively in the study of strongly interacting gauge theories. A recent review covering a number of different applications in addition to other methods is [1]. Besides general interest in understanding strongly interacting gauge theories, they might still be useful as an alternative for the Standard Model Higgs sector as well as for dark matter. These applications have been reviewed recently at the 2015 [2, 3] and 2013 [4] lattice conferences. A number of recent lattice studies is [5]. Reviews of technicolor and strongly interacting Higgs sectors are [6, 7, 8].

Lattice studies are always performed at a nonzero fermion mass. In order to obtain results in the massless limit extrapolations are needed. A main tool for this in the context of lattice QCD is Chiral Perturbation Theory (ChPT) [9, 10, 11].

In the case of equal mass fermions three main symmetry breaking patterns are possible [12, 13, 14]. For N_F Dirac fermions in a complex representation the global symmetry group is $SU(N_F)_L \times SU(N_F)_R$ and it breaks spontaneously to the diagonal subgroup $SU(N_F)_V$. For N_F Dirac fermions in a real representation the global symmetry group is $SU(2N_F)$ and it breaks spontaneously to $SO(2N_F)$. An alternative possibility is that we have N_F Majorana fermions in a real representation with a global symmetry group $SU(N_F)$ spontaneously broken to $SO(N_F)$. We show in this work that the EFT for the quantities we consider is really the same as for Dirac fermions. The final case is N_F Dirac fermions in a pseudo-real representation. The global symmetry group is again $SU(2N_F)$ but in this case it is expected to be broken spontaneously to $Sp(2N_F)$.

The effective field theory (EFT) for these cases is discussed at tree level or lowest order (LO) in [15]. At next-to-leading order (NLO) the first case is simply ChPT for N_F light quarks with a symmetry breaking pattern of $SU(N_F) \times SU(N_F) \to SU(N_F)$, a direct extension of the QCD case and was already done in [11]. The pseudo-real case was done at NLO by [16]. The $SU(2N_F) \to SO(2N_F)$ case was done in [17]. The extension for all three cases to next-to-next-to-leading order (NNLO) was done in earlier work by one of the authors [18]. More references to earlier work can be found there and in [19, 20].

This paper is an extension to the work of [18]. We add a short discussion showing that the calculations and the Lagrangian for the real case also covers the case of Majorana fermions in a real representation. The main part of the work concerns the extension of the calculations at NNLO order of the masses, decay constants and vacuum expectation values to include effects of partial quenching and finite volume.

Partial quenching was introduced in ChPT by [21]. A thorough discussion of the assumptions involved is in [22]. It allows to study a number of variations of input parameters at reduced cost, as discussed in e.g. [23]. We do not use the supersymmetric method introduced in [21] and extended (at NLO) to the cases discussed here in [17]. We only use the quark-flow technique introduced in [24]. Two-loop results in infinite volume partially quenched ChPT (PQChPT) for the masses and decay constants are in [25, 26, 27]. The definitions of the infinite volume integrals we use can be found there.

Finite volume effects in ChPT were introduced in ChPT in [28, 29, 30]. Early two-loop work is [31, 32]. The vacuum expectation value was discussed in more detail in [33].

After the proper evaluation of the finite volume two-loop sunsetintegrals using two different methods [34] the masses and decay constants were treated in both the unquenched [35] and partially quenched [36] case. In particular the integral notation at finite volume we use is defined in [36].

In Sect. 2 we recapitulate briefly the discussion from [18] at the quark level and add the case with Majorana fermions. Sect. 3 similarly recapitulates [18] at the effective field theory level and adds the Majorana fermion case. The cases with Dirac fermions and Majorana fermions are essentially identical from the EFT point of view for the quantities we consider. The underlying reason is an $U(2N_F)$ transformation that relates the two cases as discussed in Sect. 4. Partial quenching and the quark.flow techniques we have used for the different cases is discussed to some extent in Sect. 5. For a discussion on finite volume and the notation used there we refer to [36]. Our analytical results are described in Sect. 6, in particular we clarify the definitions of the decay constant and vacuum expectation value used in terms of quark fields. The numerical examples and checks are presented in Sect. 7. The analytical formulas are included in the supplementary file [37] and the numerical programs are available via CHIRON, [38, 39]. The last section briefly recapitulates the main points of our work.

2 Quark level

2.1 The three Dirac fermion cases

The discussion here is kept very short, longer versions can be found in [15] and [18]. This subsection is mainly included to show normalization conventions.

QCD or complex representation In the N_F equal mass Dirac fermions in a complex representation, we put the N_F fermions together in an N_F column matrix q. The global symmetry transformation by $g_L \times g_R \in SU(N_F)_L \times SU(N_F)_R$ is given by

$$q_L \to g_L q_L, \;\; q_R \to g_R q_R, l_\mu \to g_L l_\mu g_L^\dagger + i g_L \partial_\mu g_L^\dagger \,, \;\; r_\mu \to g_R l_\mu g_R^\dagger + i g_R \partial_\mu g_R^\dagger \,, \;\; \mathcal{M} \to g_R \mathcal{M} g_L^\dagger \,. \tag{1}$$

The matrix $\mathcal{M} = m_q \mathrm{I} + s + ip$ brings the quark mass term $m_q \mathrm{I}$ and the external scalar s and pseudo-scalar densities in the Lagrangian via $-\overline{q}_R \mathcal{M} q_L + \text{h.c.}$. The external fields l_μ, r_μ are in the Lagrangian via $\overline{q}_L \gamma^\mu l_\mu q_L + \overline{q}_R \gamma^\mu r_\mu q_R$. Taking derivatives w.r.t. the external fields allows to calculate relevant Green functions [10, 11]. In particular, deriving w.r.t. s_{11} allows us to obtain $\langle \overline{q}_{L1} q_{R1} + \overline{q}_{R1} q_{L1} \rangle$ and derivatives w.r.t. $a_{\mu 12}$ with $r_{\mu 12} = -l_{\mu 12} = a_{\mu 12}$ allows access to matrix-elements of $\overline{q}_2 \gamma^\mu \gamma^5 q_1$ The symmetry is spontaneously broken by a vacuum expectation value

$$\langle \overline{q}_{Lj} q_{Ri} \rangle = v_0 \delta_{ij} \,. \tag{2}$$

This leaves a global symmetry $SU(N_F)_V$ with $g_L = g_R$ unbroken.

Adjoint or real representation When the fermions are in a real representation, we can introduce besides the N_F right handed fermions q_{Ri} a second set of right handed fermions in the same gauge group representation, $\tilde{q}_{Ri} = C\overline{q}_{Li}^T$. These can be put together in a $2N_F$ column vector $\hat{q}$, $\hat{q}^T = (q_{R1} \dots q_{RN_F}\ \tilde{q}_{R1} \dots \tilde{q}_{RN_F})$. The global symmetry transformation with $g \in SU(2N_F)$ is now

$$\hat{q} \to g\hat{q}, \quad \hat{V}_\mu \to g\hat{V}_\mu g^\dagger, \quad \hat{\mathcal{M}} \to g\hat{\mathcal{M}}g^T. \tag{3}$$

We define the external densities and currents as in the QCD case with r_μ, l_μ and $\mathcal{M}$. We define $2N_F \times 2N_F$ matrices

$$\hat{\mathcal{M}} = \begin{pmatrix} 0 & \mathcal{M} \\ \mathcal{M}^T & 0 \end{pmatrix}, \quad \hat{V}_\mu = \begin{pmatrix} r_\mu & 0 \\ 0 & -l_\mu^T \end{pmatrix}. \tag{4}$$

Note that the global symmetry can change quark-antiquark currents to diquark currents. The fermions condense forming a vacuum expectation value

$$\frac{1}{2}\langle \hat{q}_j^T C \hat{q}_j \rangle = v_0 J_{Sij} \quad J_S = \begin{pmatrix} 0 & \mathrm{I} \\ \mathrm{I} & 0 \end{pmatrix}. \tag{5}$$

This leaves a global symmetry $SO(2N_F)$ with $gJ_S g^T = \mathrm{I}$.

$N_c = 2$ or pseudo-real representation When the fermions are in a pseudo-real representation, we can introduce besides the N_F right handed fermions q_{Ria} again a second set of right handed fermions in the same gauge group representation, $\tilde{q}_{Ria} = \epsilon_{ab} C\overline{q}_{Lib}^T$. a, b are gauge indices and the extra Levi-Civita tensor ϵ_{ab} is needed to have $\tilde{q}_{Ria}$ transform under the gauge group as q_{iRa}. The explicit formula is for the case of the fundamnetal representation with $N_c = 2$. q_{Ri} and $\tilde{q}_{Ri}$ can be put together in a $2N_F$ column vector $\hat{q}$, $\hat{q}^T = (q_{R1} \dots q_{RN_F}\ \tilde{q}_{R1} \dots \tilde{q}_{RN_F})$. The global symmetry transformation with $g \in SU(2N_F)$ is now

$$\hat{q} \to g\hat{q}, \quad \hat{V}_\mu \to g\hat{V}_\mu g^\dagger, \quad \hat{\mathcal{M}} \to g\hat{\mathcal{M}}g^T. \tag{6}$$

We define the external densities and currents as in the QCD case with r_μ, l_μ and $\mathcal{M}$. We then define

$$\hat{\mathcal{M}} = \begin{pmatrix} 0 & -\mathcal{M} \\ \mathcal{M}^T & 0 \end{pmatrix}, \quad \hat{V}_\mu = \begin{pmatrix} r_\mu & 0 \\ 0 & -l_\mu^T \end{pmatrix}. \tag{7}$$

Note that the global symmetry can again change quark-antiquark currents to diquark currents. The fermions condense forming a vacuum expectation value

$$\frac{1}{2}\langle \hat{q}_{ja}^T \epsilon_{ab} C \hat{q}_{jb} \rangle = v_0 J_{Aij} \quad J_A = \begin{pmatrix} 0 & -\mathrm{I} \\ \mathrm{I} & 0 \end{pmatrix}. \tag{8}$$

This leaves a global symmetry $Sp(2N_F)$ with $gJ_A g^T = \mathrm{I}$.

2.2 Majorana fermions in a real representation

In the earlier work [18] at infinite volume Dirac fermions and Dirac masses were assumed. It was then also asumed that the vacuum condensate was aligned with the Dirac fermion masses. There is in fact another possibility. Majorana fermions with a Majorana mass in a real representation of the gauge group. In this case the global symmetry is $SU(N_F)$. It is expected to be spontaneously broken down to $SO(N_F)$ which is aligned with the Majorana masses.

A Majorana spinor is a Dirac spinor that satisfies

$$\psi = C\overline{\psi}^T \quad \text{or} \quad \psi = \begin{pmatrix} \psi_M \\ -i\sigma^2\psi_M^* \end{pmatrix} . \tag{9}$$

The last equality are in the chiral representation for the Dirac matrices. The Lagrangian for a single free Majorana fermion is

$$\frac{1}{2}\overline{\psi}i\gamma^\mu\partial_\mu\psi - \frac{m}{2}\overline{\psi}\psi = \psi_M^\dagger C i\overline{\sigma}^\mu\partial_\mu\psi - \frac{im}{2}\left(\psi_M^T\sigma^2\psi + \psi_M^\dagger\sigma^2\psi^*\right) . \tag{10}$$

$\overline{\sigma}^0 = \mathrm{I}, \overline{\sigma}^i = -\sigma^i$. If we want to gauge this for $m \neq 0$ the mass term requires the fermions to be in a real representation of the gauge group.

For N_F Majorana fermions ψ_{Mi} in the adjoint representation with external fields $\hat{V}_\mu$ and $\hat{\mathcal{M}}$ the Lagrangian, put in a big column vector $\hat{q}^T = (\psi_1^T \dots \psi_{N_F}^T)$ is

$$\mathcal{L} = \frac{1}{2}\mathrm{tr}_c\left(\hat{q}^\dagger i\overline{\sigma}^\mu(iD_\mu + \hat{V}_\mu)\hat{q}\right) - \frac{1}{2}\mathrm{tr}_c\left(\hat{q}^T\sigma^2\hat{\mathcal{M}}^\dagger\hat{q} + \hat{q}^\dagger\sigma^2\hat{\mathcal{M}}\hat{q}^*\right) . \tag{11}$$

This Lagrangian has a global $SU(N_F)$ symmetry with $g \in SU(N_F)$ with

$$\hat{q} \to g\hat{q},, \quad \hat{V}_\mu \to g\hat{V}_\mu g^\dagger + ig\partial_\mu g^\dagger , \quad \hat{\mathcal{M}} \to g\hat{\mathcal{M}}g^T . \tag{12}$$

The maximal symmetry argument says that in this case the fermions will condense to the flavour neutral vacuum $\langle \mathrm{tr}_c\left(\hat{q}^T C\hat{q}\right)\rangle$. This is conserved by the part of the global group that satisfies $gg^T = \mathrm{I}$ or the conserved part of the global symmetry group is $SO(N_F)$.

Note that the form of the vacuum and the form of the mass term are the only differences as far as the global symmetry group and its breaking are concerned compared to the case with $N_F/2$ Dirac fermions in a real representation.

3 Effective field theory

3.1 The general LO and NLO Lagrangian

The ChPT Lagrangian for N_F flavours at LO and NLO has been derived in [11]. The Lagrangian for the other cases has the same form as has been shown in [15, 18] and other papers. The precise derivation can be found in [18] and the Majorana fermion case below in Sect. 3.3.

In terms of the quantities $u_\mu, f_{\pm\mu\nu}, \chi_\pm$ defined below for each case the lowest order Lagangian is

$$\mathcal{L}_2 = \frac{F^2}{4}\langle u_\mu u^\mu + \chi_+\rangle\,. \tag{13}$$

Here we use the notation $\langle A\rangle = \mathrm{tr}_F\,(A)$, denoting the trace over flavours. The NLO Lagrangian derived by [11] reads

$$\begin{aligned}\mathcal{L}_4 &= L_0\langle u^\mu u^\nu u_\mu u_\nu\rangle + L_1\langle u^\mu u_\mu\rangle\langle u^\nu u_\nu\rangle + L_2\langle u^\mu u^\nu\rangle\langle u_\mu u_\nu\rangle + L_3\langle u^\mu u_\mu u^\nu u_\nu\rangle \\ &\quad + L_4\langle u^\mu u_\mu\rangle\langle\chi_+\rangle + L_5\langle u^\mu u_\mu\chi_+\rangle + L_6\langle\chi_+\rangle^2 + L_7\langle\chi_-\rangle^2 + \frac{1}{2}L_8\langle\chi_+^2+\chi_-^2\rangle \\ &\quad - iL_9\langle f_{+\mu\nu}u^\mu u^\nu\rangle + \frac{1}{4}L_{10}\langle f_+^2 - f_-^2\rangle + \frac{1}{2}H_1\langle f_+^2+f_-^2\rangle + \frac{1}{4}H_2\langle\chi_+^2-\chi_-^2\rangle\,. \end{aligned}\tag{14}$$

The NNLO Lagrangian has been classified for the N_F-flavour case in [40]. The Lagrangian at NNLO for the other cases is not known, the direct equivalent of the results in [40] is definitely a complete Lagrangian but might not be minimal. For this reason we do not quote the dependence on the NNLO Lagrangian in the real and pseudo-real cases.

The divergences at NLO were derived for the QCD case in [11], for the others in [16, 18]. At NNLO only the QCD case is known [41].

3.2 The three Dirac fermion cases

A more extensive discussion can be found in [15, 18]. Here we simply quote the results.

When we have a global symmetry group G with generators T^a which is spontaneously broken down to a subgroup H with generators Q^a which form a subset of the T^a, the Goldstone bosons can be described by the coset G/H. This coset can be parametrized [42] via the broken generators X^a. Below we explain what is used for the different cases. We always work with generators normalized to 1, i.e. $\langle X^a X^b\rangle = \delta^{ab}$.

The quantities used from the quark level are given in Sect. 2.

QCD or complex representation The Goldstone boson manifold is in this case $SU(N_F)\times SU(N_F)/SU(N_F)$ which itself has the structure of an $SU(N_F)$ Note that the axial generators do not generate a subgroup of $SU(N_F)\times SU(N_F)$ even if G/H has the structure of a group in this case.

We choose as the broken generators X^a the generators of $SU(N_F) \approx G/H$. The quantities needed to construct the Lagrangian and their symmetry transformations are

$$\begin{aligned} u &= \exp\left(\frac{i}{\sqrt{2}F}\pi^a X^a\right) \to g_R u h^\dagger \equiv h u g_L^\dagger \\ u_\mu &= i\left(u^\dagger(\partial_\mu - ir_\mu)u - u(\partial_\mu - l_\mu)u^\dagger\right) \to h u_\mu h^\dagger\,, \\ \chi &= 2B_0\mathcal{M} \to g_R\chi g_L^\dagger \\ \chi_\pm &= u^\dagger\chi u^\dagger \pm u\chi^\dagger u \to h\chi_\pm h^\dagger\,, \end{aligned}$$

$$
\begin{aligned}
l_{\mu\nu} &= \partial_\mu l_\nu - \partial_\mu l_\nu - i l_\mu l_\mu + i l_\nu l_\mu \to g_L l_{\mu\nu} g_L^\dagger \\
r_{\mu\nu} &= \partial_\mu r_\nu - \partial_\mu r_\nu - i r_\mu r_\mu + i r_\nu r_\mu \to g_R r_{\mu\nu} g_R^\dagger \\
f_{\pm\mu\nu} &= u l_{\mu\nu} u^\dagger \pm u^\dagger r_{\mu\nu} u \to h f_{\pm\mu\nu} h^\dagger \,.
\end{aligned} \tag{15}
$$

The first line defines h [42].

Adjoint or real representation The Goldstone boson manifold is in this case $SU(2N_F)/SO(2N_F)$. The unbroken generators satisfy $Q^a J_S = -J_S Q^{aT}$ which follows from $g J_S g^T = J_S$. The broken generators satisfy $J_S X^a = X^{aT} J_S$.

The quantities needed to construct the Lagrangians are [18]

$$
\begin{aligned}
u &= \exp\left(\frac{i}{\sqrt{2}F}\pi^a X^a\right) \to g u h^\dagger \\
u_\mu &= i\left(u^\dagger(\partial_\mu - i\hat{V}_\mu)u - u(\partial_\mu + i J_S \hat{V}_\mu^T J_S)u^\dagger\right) , \\
\chi &= 2B_0 \hat{\mathcal{M}} \\
\chi_\pm &= u^\dagger \chi J_S u^\dagger \pm u J_S \chi^\dagger u \\
\hat{V}_{\mu\nu} &= \partial_\mu \hat{V}_\nu - \partial_\nu \hat{V}_\mu - i\left(\hat{V}_\mu \hat{V}_\nu - \hat{V}_\nu \hat{V}_\mu\right) \\
f_{\pm\mu\nu} &= J_S u \hat{V}_{\mu\nu} u^\dagger J_S \pm u \hat{V}_{\mu\nu} u^\dagger
\end{aligned} \tag{16}
$$

The first line defines h by requiring that $guh^\dagger$ is of the form $\exp(i\pi^a X^a/(\sqrt{2}F))$. Note that the derivation used $J_S u = u^T J_S$.

$N_c = 2$ or pseudo-real representation The Goldstone boson manifold is $SU(2N_F)/Sp(2N_F)$. The unbroken generators satisfy $Q^a J_A = -J_A Q^{aT}$ which follows from $g J_A g^T = J_A$. The broken generators satisfy $J_A X^a = X^{aT} J_A$.

The quantities needed are [18]

$$
\begin{aligned}
u &= \exp\left(\frac{i}{\sqrt{2}F}\pi^a X^a\right) \to g u h^\dagger \\
u_\mu &= i\left(u^\dagger(\partial_\mu - i\hat{V}_\mu)u - u(\partial_\mu + i J_A \hat{V}_\mu^T J_A^T)u^\dagger\right) , \\
\chi &= 2B_0 \hat{\mathcal{M}} \\
\chi_\pm &= u^\dagger \chi J_A^T u^\dagger \pm u J_A \chi^\dagger u \\
\hat{V}_{\mu\nu} &= \partial_\mu \hat{V}_\nu - \partial_\nu \hat{V}_\mu - i\left(\hat{V}_\mu \hat{V}_\nu - \hat{V}_\nu \hat{V}_\mu\right) \\
f_{\pm\mu\nu} &= J_A u \hat{V}_{\mu\nu} u^\dagger J_A^T \pm u \hat{V}_{\mu\nu} u^\dagger
\end{aligned} \tag{17}
$$

The first line defines h by requiring that $guh^\dagger$ is of the form $\exp(i\pi^a X^a/(\sqrt{2}F))$. Note that the derivation used $J_A u = u^T J_A$.

3.3 Majorana fermions in a real representation

The vacuum in this case is characterized by the condensate

$$\frac{1}{2}\langle \hat{q}_i^T C \hat{q}_j \rangle = \frac{1}{2}\langle \overline{q} q \rangle \delta_{ij} \,. \tag{18}$$

Under the symmetry group $g \in SU(N_F)$ this moves around as

$$\delta ij \to \left(g^T g \right)_{ij} \,. \tag{19}$$

The unbroken part of the group is given by the generators $\tilde{Q}^a$ and the broken part by the generators $\tilde{X}^a$ which satisfy

$$\tilde{Q}^a = -\tilde{Q}^{aT} \,, \qquad \tilde{X}^a = \tilde{X}^{aT} \,. \tag{20}$$

Just as in the cases discussed in [18] we can construct a rotated vacuum in general by using the broken part of the symmetry group on the vacuum. This leads to a matrix

$$U = uu^T \to gUg^T \qquad \text{with} \qquad u = \exp\left(\frac{i}{\sqrt{2}\,F} \pi^a X^a \right) \,. \tag{21}$$

The matrix u transforms as in the general $CCWZ$ case as

$$u \to guh^\dagger \,. \tag{22}$$

Some earlier work used the matrix U to describe the Lagrangian [15]. Here we will, as in [18] use the CCWZ scheme to obtain a notation that is formally identical to the QCD case. We add $N_F \times N_F$ matrices of external fields $\hat{V}_\mu$ and $\hat{\mathcal{M}}$. We need to obtain the u_μ, or broken generator, parts of $u^\dagger \left(\partial_\mu - i V_\mu \right) u$. Eq. (20) have as a consequence that u satisfies

$$u = u^T \,. \tag{23}$$

This leads using the same method as in [18] to

$$u_\mu \;\; = \;\; i \left(u^\dagger (\partial_\mu - i\hat{V}_\mu) u - u(\partial_\mu + i\hat{V}_\mu^T) u^\dagger \right) \,. \tag{24}$$

With this we can construct Lagrangians. The equivalent quantities to the field strengths are

$$f_{\pm \mu\nu} = u \hat{V}_{\mu\nu} u^\dagger \pm u \hat{V}_{\mu\nu} u^\dagger \tag{25}$$

with $\hat{V}_{\mu\nu} = \partial_\mu \hat{V}_\nu - \partial_\nu \hat{V}_\mu - i \left(\hat{V}_\mu \hat{V}_\nu - \hat{V}_\nu \hat{V}_\mu \right)$ and for the mass matrix

$$\chi_\pm = u^\dagger \chi u^{\dagger T} \pm u^T \chi^\dagger u \tag{26}$$

with $\chi = 2B_0 \hat{\mathcal{M}}$. The Lagrangians at LO and NLO have exactly the same form as given in (13) and (14) with u_μ, $\chi_\pm$ and $f_{\pm\mu\nu}$ as defined in (24), (25) and (26).

4 Relation Dirac and Majorana for the adjoint case

As discussed below, we have calculated the adjoint case using two methods. They were appropriate for the Dirac and the Majorana case respectively. After doing the trivial $2N_F \to N_F$ change the results agreed exactly. If we compare the two cases, we see that the main difference is really the choice of vacuum.

The Dirac and Majorana cases lead to a choice of vacuum

$$\langle \hat{q}_i^T C \hat{q}_j \rangle_D \propto J_{Sij}\,, \quad \langle \hat{q}_i^T C \hat{q}_j \rangle_D \propto \mathrm{I}_{ij}\,. \tag{27}$$

Is it possible to relate the two cases in a simple way? Under a global symmetry transformation the first one transforms as $J_S \to g J_S g^T$. If we could find a global transformation g_R that lead to $g_R J_S g_R^T = \mathrm{I}$ the two cases would be obviously the same.

It is not possible in general with a $SU(2N_F)$ rotation to accomplish this since $\det J_S = \pm 1$ (-1 for the $2N_F = 2$) while $\det \mathrm{I} = 1$. However it is possible with a $U(2N)$ transformation. An explicit choice for g_R, with a free phase α is

$$g_R = \frac{1}{\sqrt{2}} \begin{pmatrix} \mp i e^{i\alpha}\mathrm{I} & \pm i e^{-i\alpha}\mathrm{I} \\ e^{i\alpha}\mathrm{I} & e^{-i\alpha}\mathrm{I} \end{pmatrix}. \tag{28}$$

It can be checked that this transforms a Dirac mass term for N_F Dirac fermions into a Majorana mass term for $2N_F$ Majorana fermions.

Inspections of the effective Lagrangians needed lead to the immediate conclusion that the mass independent terms really are $U(2N_F)$ invariant, and the mass dependent terms for the two cases are turned into each other.

g_R can also be used to relate the two different embeddings of $SO(2N_F)$ in $SU(2N_F)$ to each other. For the Dirac case the $SO(2N)$ generators satisfied $Q^{aT} J_S = -J_S Q^a$ while for the Majorana case they satisfied $\tilde{Q}^{aT} = -\tilde{Q}^a$. The two sets of generators are related by

$$\tilde{Q}^a = g_R Q^a g_R^\dagger\,, \quad \tilde{X}^a = g_R X^a g_R^\dagger\,. \tag{29}$$

5 Partially quenching and the quark flow technique

A thorough discussion of PQChPT and in particular the derivation of the propagator used there is [43]. That discussion uses the supersymmetric method. Alternative methods of calculation are the replica trick [44] and the quark flow method [24]. The earliest partially quenched work for QCDlike theories used the supersymmetric method [17]. The replica trick has been used in [45]. We use the quark-flow method.

For this method we look at the matrix

$$\Phi = \pi^a X^a \tag{30}$$

for each of the cases.

For the QCD case, Φ is a traceless Hermitian matrix. We actually keep Φ in the flavour basis with elements ϕ_{ij} and i, j are flavour indices. The tracelessness condition is enforced

by the propagator. The indices are kept explicitly and the propagator connecting a field ϕ_{ij} to ϕ_{kl} is [43]

$$G_{ijkl}(k) = G^c_{ij}(k)\delta_{il}\delta_{jk} - \delta_{ij}\delta_{kl}G^q_{ik}(k)/n_{\rm sea}\,. \tag{31}$$

The number of sea quarks $n_{\rm sea}$ is what we call N_F. with $G^c_{ij} = i/(p^2 - \chi_{ij})$. The neutral part of the propagator, G^q_{ik}, can contain double poles. In particular for the mass cases we consider:

$$\begin{aligned} G^q_{vv'} &= i(\chi_1 - \chi_4)/(p^2 - \chi_1)^2 + i/(p^2 - \chi_1)\,, \\ G^q_{vs} &= i/(p^2 - \chi_1)\,, \\ G^q_{ss'} &= i/(p^2 - \chi_4)\,. \end{aligned} \tag{32}$$

v, s denote valence or sea quarks. The extra parts come from integrating out the Φ_0 [43] and enforec the condition that Φ must be traceless. When constructing the Feynman diagrams, we keep all flavour indices free. Those that connect to external states get replaced by the value of the external valence flavour index and the remaining ones are summed over the sea quark flavours. In the present calculation, with all sea quarks the same mass, that corresponds to a factor of N_F for each free flavour index.

For the Majorana, $SU(N_F) \to SO(N_F)$, case we have that $\Phi = \pi^a X^a$ with Φ Hermitian, traceless and symmetric. Hermitian and traceless follow from $SU(N_F)$ and symmetric from (20). Going to the flavour basis for the diagonal elements of Φ there is no change w.r.t. the QCD case, but the flavour charged or off-diagonal elements must be correctly symmetrized. This has to be done both for the propagator and the connection to the external states, keeping track of the needed normalization. Afterwards we set the flavour indices connected to external states to their valence values and sum ov the flavours for the free indices.

For the Dirac adjoint case, $SU(2N_F) \to SO(2N_F)$, case we have that $\Phi = \pi^a X^a$ with Φ Hermitian, traceless and satisfying $X^a J_S = J_S X^{aT}$ and the matrix Φ is $2N_F \times 2N_F$. Rewriting Φ with $N_F \times N_F$ matrices leads to the form

$$\Phi = \begin{pmatrix} \Phi_A & \Phi_C^\dagger \\ \Phi_C & \Phi_A^T \end{pmatrix}\,, \quad \text{with} \;\; \langle A\rangle = 0\,,\; \phi_C = \phi_C^T\,. \tag{33}$$

Φ_A is Hermitian. The elements in Φ_A correspond to quark-antiquark states, those in Φ_C to diquark states. Φ_A can be treated exactly as in the QCD case, both the diagonal and flavour charged or offdiagonal elements, since $\langle\Phi_A\rangle = 0$ replaces $\langle\Phi\rangle = 0$ in the QCD case. Φ_C can be treated as offdiagonal or flavour charged propagators but the needed symmetrizing should be taken care of both for external states and propagators. The normalization of all states must be done correctly as well. After constructing Feynman diagrams with both Φ_A and Φ_C degrees of freedom taken into account we sum free index lines over the N_F degrees of freedom, not $2N_F$. The results always agree with the calculations done with the previous, Majorana, method.

For the last case, $SU(2N_F) \to Sp(2N_F)$, pseudo-real, we have that $\Phi = \pi^a X^a$ with Φ Hermitian, traceless and satisfying $X^a J_A = J_A X^{aT}$ and the matrix Φ is $2N_F \times 2N_F$.

Rewriting Φ with $N_F \times N_F$ matrices leads to the form

$$\Phi = \begin{pmatrix} \Phi_A & \Phi_C^\dagger \\ \Phi_C & \Phi_A^T \end{pmatrix}, \quad \text{with} \quad \langle A \rangle = 0\,, \; \phi_C = -\phi_C^T\,. \tag{34}$$

Φ_A is Hermitian. The elements in Φ_A correspond to quark-antiquark states, those in Φ_C to diquark states. Φ_A can be treated exactly as in the QCD case, both the diagonal and flavour charged or offdiagonal elements, since $\langle \Phi_A \rangle = 0$ replaces $\langle \Phi \rangle = 0$ in the QCD case. Φ_C can be treated as offdiagonal or flavour charged propagators but the needed antisymmetrizing should be taken care of. The normalization of all states must be done correctly as well. After constructing Feynman diagrams with both Φ_A and Φ_C degrees of freedom taken into account we sum free index lines over the N_F degrees of freedom, not $2N_F$. In this case and the previous we can also compare calculations with Φ_A or Φ_C external states providing a check on our results.

6 Analytical results

We have calculated the masses, decay constants and vacuum expectation values to NNLO for the QCD-like theories with the symmetry breaking patterns discussed above. A number of checks have been performed on the analytical formulas. The infinite volume unquenched results were obtained earlier in [18] and we have reproduced those. The partially quenched and finite volume results in the QCD case are finite. The partially quenched expressions reduce to the unquenched results whenever we set the sea mass equal to the valence mass. In addition we reproduce the known results at NLO for the condensate [17] also for the partially quenched case. The finite volume expressions have been checked against the known NLO results and numerically with the earlier known NNLO results, as discussed in Sect. 7.

For the real and pseudo-real case we have the additional check that calculating the mass or decay constant of a quark-anti-quark or a diquark meson gives the same results. This corresponds to using a field from the A or the C sector in the matrices (33,34). For the real case we have the additional check that the results using the Dirac case and the Majorana case coincide.

The finite volume case is always done for three spatial dimensions of size L and an infinite temporal volume. In addition we work in the center of mass system, the momenta are such that the external states have zero spatial momentum.

The masses are the physical masses as defined as the pole of the full propagator. We consider here the case where all valence quarks have the same quark mass $m_1 = \hat{m}$ and the sea quarks all have the same mass $m_4 = m_S$. For the unquenced case obviously $m_4 = m_1$. The labeling is similar to those used in three flavour PQChPT [25, 26, 27, 36]. In the formulas we use instead the quantities

$$\chi_1 = 2B_0 m_1, \quad \chi_4 = 2B_0 \chi_4, \quad \chi_{14} = \frac{1}{2}\left(\chi_1 + \chi_4\right)\,. \tag{35}$$

These quantities are referred to in [37] as m11, m44 and m14 respectively.

The formulas are given for the cases $SU(N_F) \times SU(N_F) \to SU(N_F)$, $SU(N_F) \to SO(N_F)$ and $SU(2N_F) \to Sp(2N_F)$. Note the difference in convention for the second case compared to [18]. The three cases are referred to in the formulas with SUN, SON and SPN for the unquenced case and PQSUN,PQSON and PQSPN for the partially quenched case. In the latter case N_F referes to the number of sea quarks.

For the mass we consider a meson made of a different quark and anti-quark or a diquark state with two different quarks. These are always valence quarks. The physical mass at finite volume is given by

$$m^2_{\text{phys}} = \chi_1 + m^{(4)2} + \Delta^V m^{(4)2} + m^{(6)2} + \Delta^V m^{(6)2} \,. \tag{36}$$

The superscript (n) labels the order p^n correction and Δ^V indicates the finite volume corrections. In all cases the lowest order mass squared is given by χ_1. A further break up is done for the LEC dependent parts via the L_i^r (NLO) and K_i^r (NNLO) and the remainder via

$$\begin{aligned} m^{(4)2} &= m^{L(4)2} + m^{R(4)2} \\ m^{(6)2} &= m^{K(6)2} + m^{L(6)2} + m^{R(6)2} \\ \Delta^V m^{(6)2} &= \Delta^V m^{L(6)2} + \Delta^V m^{R(6)2} \end{aligned} \tag{37}$$

All quantities are given explicitly in [37].

The decay constant F_{phys} for the same mesons as above is expanded w.r.t. the lowest order as

$$F_{\text{phys}} = F_{LO} \left(1 + F^{(4)} + \Delta^V F^{(4)} + F^{(6)2} + \Delta^V F^{(6)}\right) , \tag{38}$$

with a similar split

$$\begin{aligned} F^{(4)} &= F^{L(4)} + F^{R(4)} \\ F^{(6)} &= F^{K(6)} + F^{L(6)} + F^{R(6)} \\ \Delta^V F^{(6)} &= \Delta^V F^{L(6)} + \Delta^V F^{R(6)} \end{aligned} \tag{39}$$

All quantities are given explicitly in [37].

The vacuum expectation value is expanded in exactly the same way

$$v_{\text{phys}} = v_{LO} \left(1 + v^{(4)} + \Delta^V v^{(4)} + v^{(6)2} + \Delta^V v^{(6)}\right) , \tag{40}$$

with a similar split

$$\begin{aligned} v^{(4)} &= v^{L(4)} + v^{R(4)} \\ v^{(6)} &= v^{K(6)} + v^{L(4)} + v^{R(4)} \\ \Delta^V v^{(6)} &= \Delta^V v^{L(6)} + \Delta^V v^{R(6)} \end{aligned} \tag{41}$$

All quantities are given explicitly in [37].

The quantities with K for the SON and SPN case have been set to zero. They are polynomials up to the needed degree in χ_1 and χ_4, with an overall factor of χ_1 for the mass.

The decay constant and the vacuum expectation value were defined implicitly in [18] using a generator X^a in the axial current normalized to one and an element in $\hat{\mathcal{M}}$ normalized to one. The consequence was that in [18] $F_{LO} = F$ and $v_{LO} = -B_0F^2$ for all cases. This is not exactly what was done in earlier work leading to differences in factors of 2 and $\sqrt{2}$. Below we explicitly specify all definitions in terms of the quark fields.

QCD or complex representation If we label the first Dirac (valence) quark by 1 and the second by 2 the decay constant and vacuum expectation value are defined as

$$\begin{aligned} \langle 0|\overline{q}_1\gamma_\mu\gamma_5 q_2|M(p)\rangle &= i\sqrt{2}F_{\rm phys}p_\mu \\ \langle \overline{q}_1 q_1\rangle &= \langle \overline{q}_{L1}q_{R1} + \overline{q}_{R1}q_{L1}\rangle = v_{\rm phys} \end{aligned} \tag{42}$$

M denotes a meson of that quark content with momentum p.

The resulting lowest orders are

$$F_{LO} = F \quad v_{LO} = -B_0F^2\,. \tag{43}$$

Adjoint or real representation Here we have to be careful how we define the physical decay constant. We can choose to do using generators normalized to one using Dirac Fermions or generators normalized to one using the $\hat{q}_i$ elements.

With a Dirac fermion definition, the first Dirac (valence) quark labeled by 1 and the second by 2, the definitions are

$$\begin{aligned} \langle 0|\overline{q}_1\gamma_\mu\gamma_5 q_2|M(p)\rangle &= i\sqrt{2}F_{\rm phys}p_\mu \\ \langle \overline{q}_1 q_1\rangle &= \langle \overline{q}_{L1}q_{R1} + \overline{q}_{R1}q_{L1}\rangle = v_{\rm phys} \end{aligned} \tag{44}$$

M denotes a meson of that quark content with momentum p. The resulting lowest orders are

$$F_{LO} = \sqrt{2}F \quad v_{LO} = -2B_0F^2\,. \tag{45}$$

If we instead choose to use the Majorana case, the natural definition of the decay constant and vacuum expectation value with the first (valence) Majorana fermion labeled as 1 and the second as 2 via

$$\begin{aligned} \frac{1}{2\sqrt{2}}\langle 0|\hat{q}_1^*\overline{\sigma}_\mu\hat{q}_2 + \hat{q}_2^*\overline{\sigma}_\mu\hat{q}_1|M(p)\rangle &= i\sqrt{2}F_{\rm phys}p_\mu \\ \frac{1}{2}\langle \hat{q}_1\sigma^2\hat{q}_1 + \hat{q}_1^*\sigma^2\hat{q}_1^*\rangle &= v_{\rm phys} \end{aligned} \tag{46}$$

The resulting lowest orders are

$$F_{LO} = F \quad v_{LO} = -B_0F^2\,. \tag{47}$$

$N_c = 2$ **or pseudo-real representation** Here we again need to be careful how we define the physical decay constant. We can choose to do using generators normalized to one using the original Dirac Fermions or generators normalized to one using the $\hat{q}_i$ elements.

With a Dirac fermion definition, the first Dirac (valence) quark labeled by 1 and the second by 2, the definitions are

$$\begin{aligned} \langle 0|\overline{q}_1\gamma_\mu\gamma_5 q_2|M(p)\rangle &= i\sqrt{2}F_{\rm phys}p_\mu \\ \langle \overline{q}_1 q_1\rangle &= \langle \overline{q}_{L1}q_{R1} + \overline{q}_{R1}q_{L1}\rangle = v_{\rm phys} \end{aligned} \tag{48}$$

M denotes a meson of that quark content with momentum p. The resulting lowest orders are

$$F_{LO} = \sqrt{2}F \quad v_{LO} = -2B_0F^2\,. \tag{49}$$

In terms of the $\hat{q}_i$ the definitions are

$$\begin{aligned} \langle 0|\overline{\hat{q}}_1\gamma_\mu\overline{\hat{q}}_2 + \overline{\hat{q}}_{1+N_F}\gamma_\mu\overline{\hat{q}}_{2+N_F}|M(p)\rangle &= i\sqrt{2}F_{\rm phys}p_\mu \\ \frac{1}{2}\langle \overline{\hat{q}}_{1+N_F,a}\epsilon_{ab}C\overline{\hat{q}}_{1,b} - \overline{\hat{q}}_{1,a}\epsilon_{ab}C\overline{\hat{q}}_{1+N_F,b} - \hat{q}_{1+N_F,a}\epsilon_{ab}C\hat{q}_{1,b} + \hat{q}_{1,a}\epsilon_{ab}C\hat{q}_{1+N_F,b} &= v_{\rm phys}\,. \end{aligned} \tag{50}$$

7 Numerical examples and checks

The main aim of this work is to provide the lattice work with the formulas and programs needed to do the extrapolation to zero mass. We therefore only present some representative numerical results. The numerical programs are included in the latest version of CHIRON, [38, 39].

For the numbers presented we always use $\chi_1 = 0.14^2$ GeV^2, if not varied explicitly, and $F = 0.0877$ GeV as well as a subtraction scale $\mu = 0.77$ GeV. The length L for the finite volume has been chosen such that $L \times 0.14$ GeV=3 or $L \approx 4.2$ fm.

The LECs at NLO we choose to be those of the recent determination of [46] with the extra LEC $L_0^r = 0$. The NNLO constants we have always put to zero.

A number of numerical checks for the QCD case have been done. The unquenched infinite volume results for three flavours agree with the three flavour results of [47, 48]. The partially quenched results for masses and decay constants at infinite volume agree with the case $d_{\rm sea} = 1, d_{\rm val} = 1$ of [25, 26, 27]. The unquenched results for masses and decay constants at finite volume agree with [35]. The partially quenched results for masses and decay constants at finite volume agree with the case $d_{\rm sea} = 1, d_{\rm val} = 1$ of [36] and finially the unquenched finite volume results for the vacuum expectation value agree with the results of [32].

In Fig. 1 we show the mass squared for the infinite volume for all cases we have considered for three values of N_F. In general, as was already noticed in [18] the corrections are larger for the larger values of N_F. The corrections are also larger for the $SU(2N_F) \to Sp(2N_F)$ case since this correspond to a twice as large number of fermions as the other cases. The partially quenched results shown in the right column are at a fixed value of χ_1. That explains why the corrections do not vanish for $\chi_4 = 0$.

The same types of results are shown for the decay constant in Fig. 2. The corrections are somewhat larger than for the masses but the convergence is typically somewhat better. The corrections for the vacuum expectation value shown in Fig. 3 are typically larger but with again a reasonable convergence from NLO to NNLO.

We can now make similar plots for the finite volume corrections. The overall size of them is as expected. The smallest mL is about two for the left hand sides of all plots. In the unquenched case the exponential falloff with the mass is clearly visible. The partially quenched cases contain a fixed mass scale χ_1 which is why the correction is more constant there, the stays at the $mL = 3$ point for the plots. The dips are caused by the finite volume corrections going through zero. The corrections to the mass are shown in Fig. 4, the decay constant in Fig. 5 and the vacuum expectation value in Fig 6.

8 Conclusions

We have calculated in the effective field theory for the three possible symmetry breaking patterns the NNLO order finite volume and partial quenching effects to NNLO in the expansion. The results satisfy a large number of checks agreeing analytically and numerically with earlier work that our results reduce to for some cases. The analytical part of this work relied heavily on FORM [49].

The analytical results are of reasonable length but given the total number of results we have included them as FORM output in a supplementary file. They can also be downloaded from [50].

The numerical programs have been included in CHIRON [38] version 0.54 which can downloaded from [39]. We have presented results in a number of cases with typical QCD values of the parameters. The results are of the expected sizes from earlier work in three flavour ChPT. We hope these results will be useful for lattice studies of these alternative symmetry breaking patterns.

Acknowledgements

This work is supported in part by the Swedish Research Council grants 621-2011-5080 and 621-2013-4287. JB thanks the Centro de Ciencias de Benasque Pedro Pascual, where part of this work was done, for hospitality.

References

[1] N. Brambilla *et al.*, Eur. Phys. J. C **74** (2014) 10, 2981 [arXiv:1404.3723 [hep-ph]].

[2] F. Sannino, plenary talk at Lattice2015.

[3] A. Hasenfratz, plenary talk at Lattice2015.

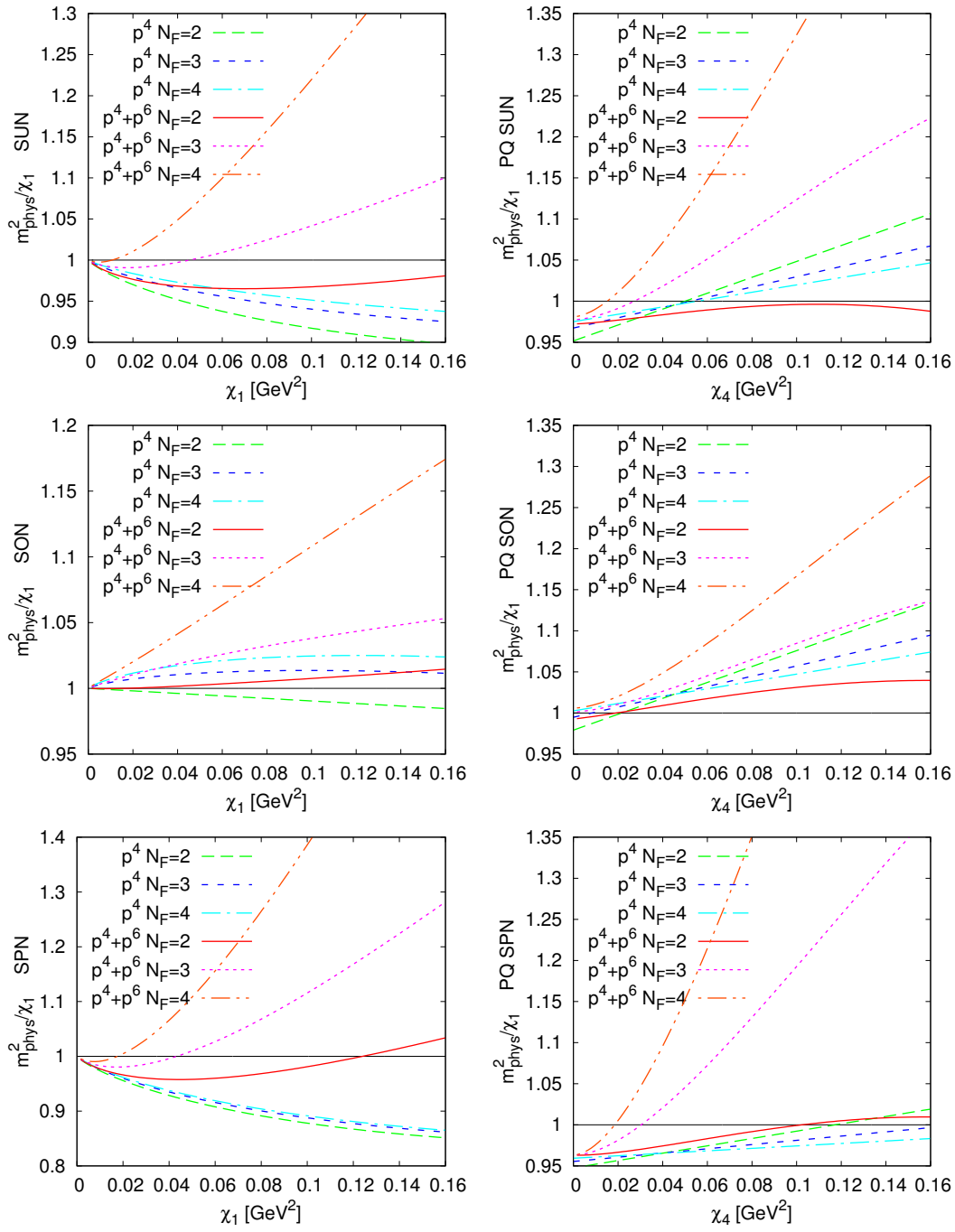

Figure 1: The physical mass squared divided by the lowest order mass squared for the unquenched (left) as a function of χ_1 and the partially quenched case (right) as a function of χ_4 with $\chi_1 = 0.14^2$ GeV^2. Other input as in the text. Shown are the NLO (p^4) and NNLO ($p^4 + p^6$) results for three values of N_F. Top line: $SU(N_F) \times SU(N_F) \to SU(N_F)$. Middle line: $SU(N_F) \to SO(N_F)$. Bottom line: $SU(2N_F) \to Sp(2N_F)$.

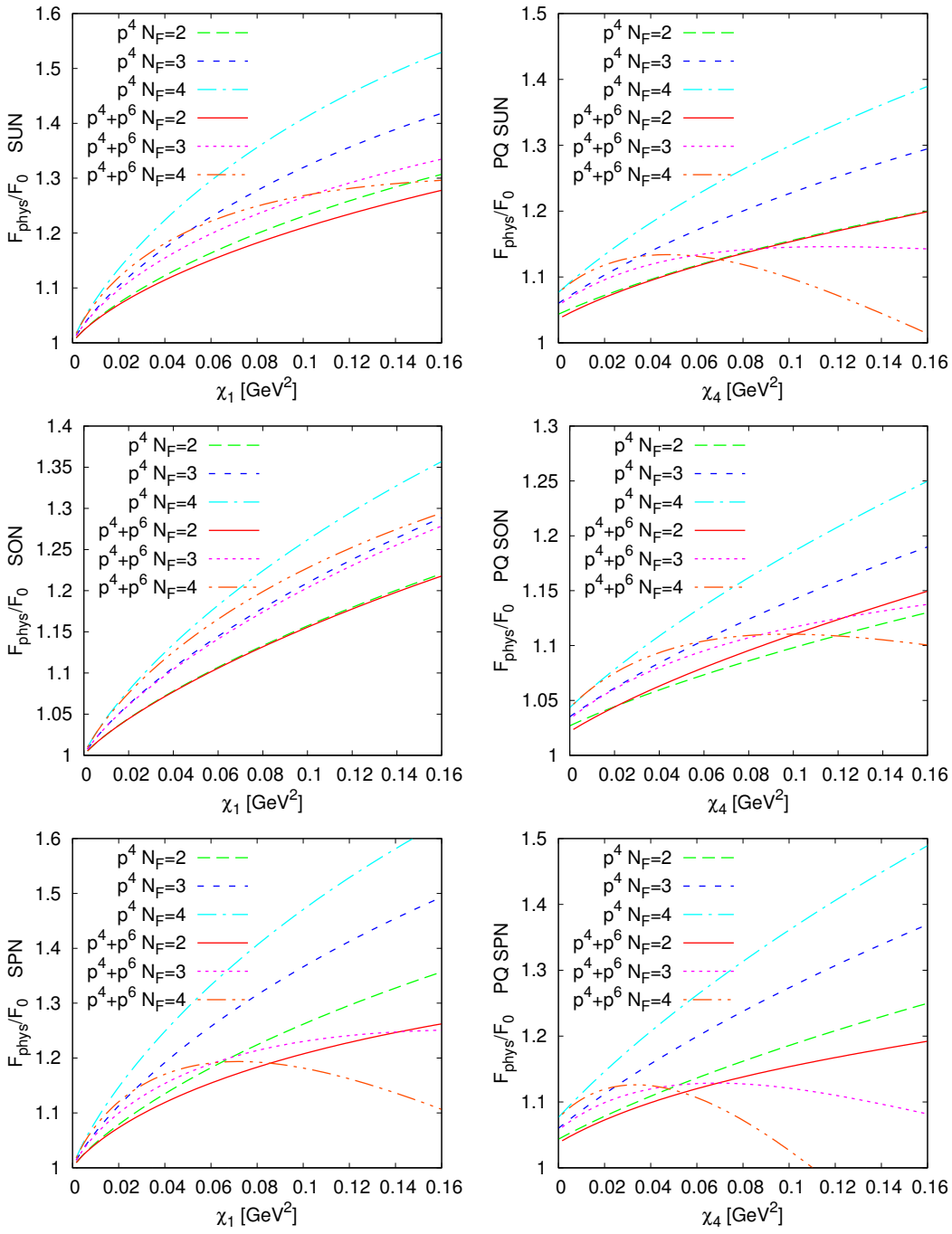

Figure 2: The decay constant divided by the lowest order value $F_0 = F_{LO}$ for the unquenched (left) as a function of χ_1 and the partially quenched case (right) as a function of χ_4 with $\chi_1 = 0.14^2$ GeV^2. Other input as in the text. Shown are the NLO (p^4) and NNLO ($p^4 + p^6$) results for three values of N_F. Top line: $SU(N_F) \times SU(N_F) \to SU(N_F)$. Middle line: $SU(N_F) \to SO(N_F)$. Bottom line: $SU(2N_F) \to Sp(2N_F)$.

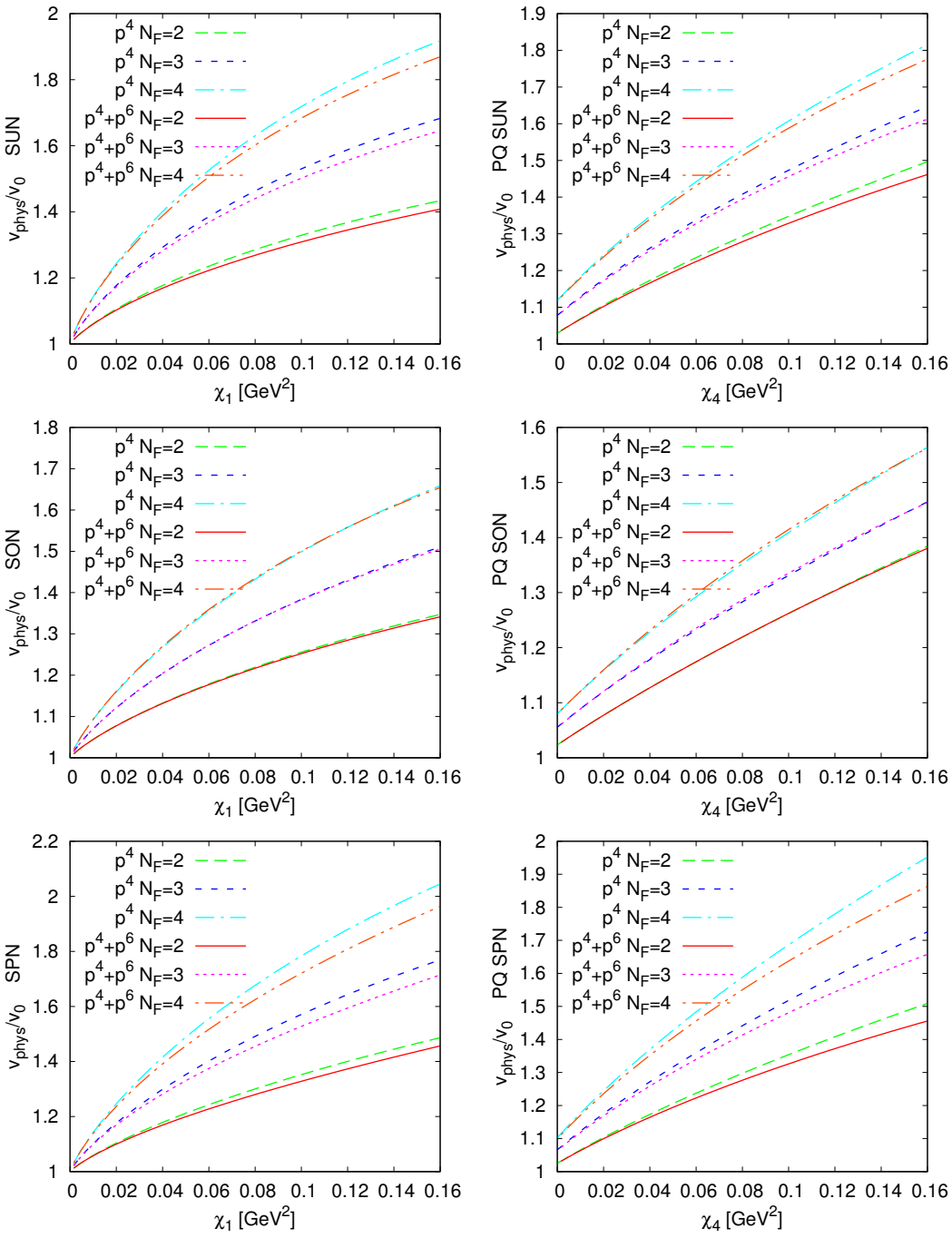

Figure 3: The vacuum expectation value divided by the lowest order value $v_0 = v_{LO}$ for the unquenched (left) as a function of χ_1 and the partially quenched case (right) as a function of χ_4 with $\chi_1 = 0.14^2$ GeV^2. Other input as in the text. Shown are the NLO (p^4) and NNLO ($p^4 + p^6$) results for three values of N_F. Top line: $SU(N_F) \times SU(N_F) \to SU(N_F)$. Middle line: $SU(N_F) \to SO(N_F)$. Bottom line: $SU(2N_F) \to Sp(2N_F)$.

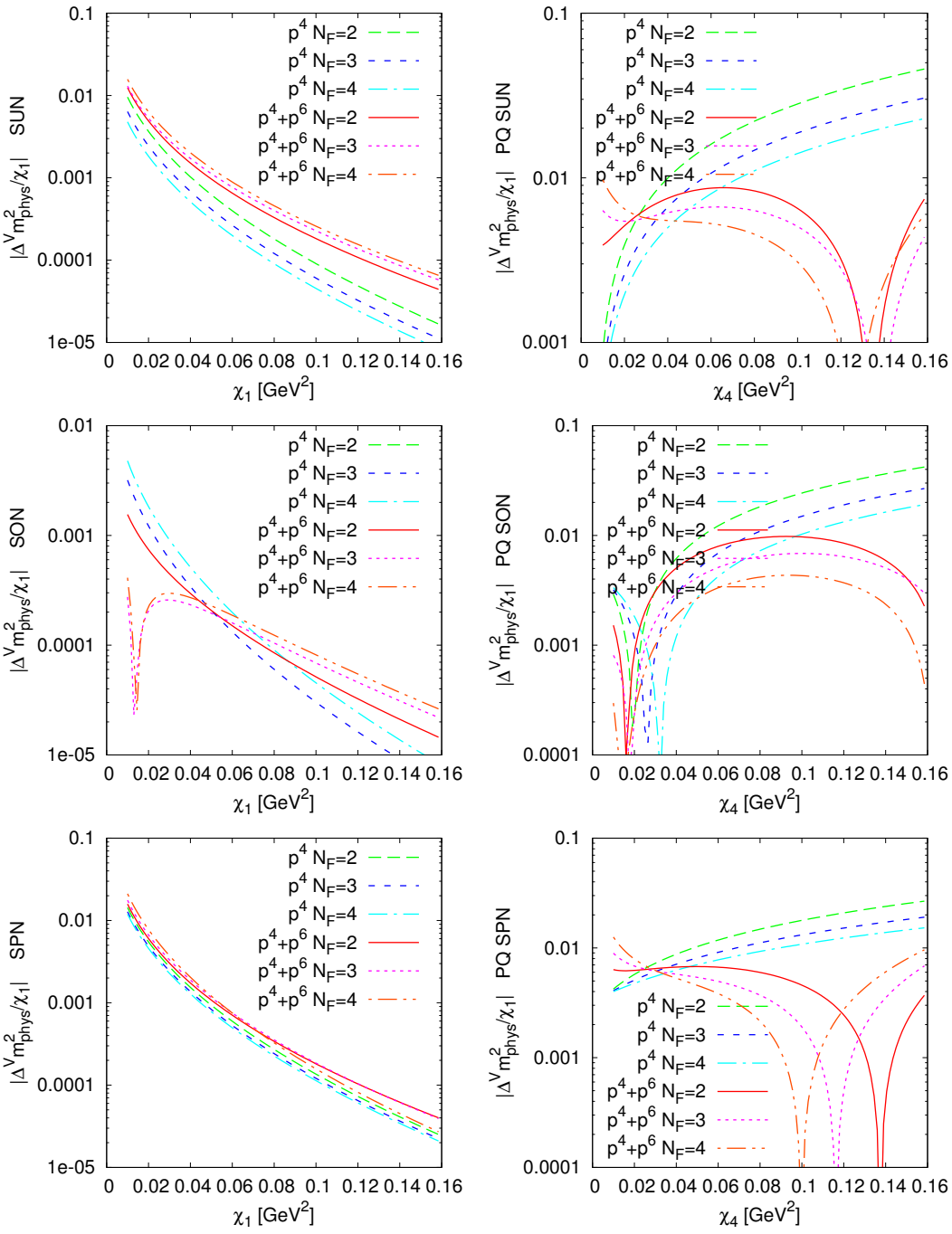

Figure 4: The absolute value of the finite volume correction to the physical mass squared divided by the lowest order mass squared for the unquenched (left) as a function of χ_1 and the partially quenched case (right) as a function of χ_4 with $\chi_1 = 0.14^2$ GeV^2. Shown are the NLO (p^4) and NNLO ($p^4 + p^6$) results for three values of N_F. Top line: $SU(N_F) \times SU(N_F) \to SU(N_F)$. Middle line: $SU(N_F) \to SO(N_F)$. Bottom line: $SU(2N_F) \to Sp(2N_F)$.

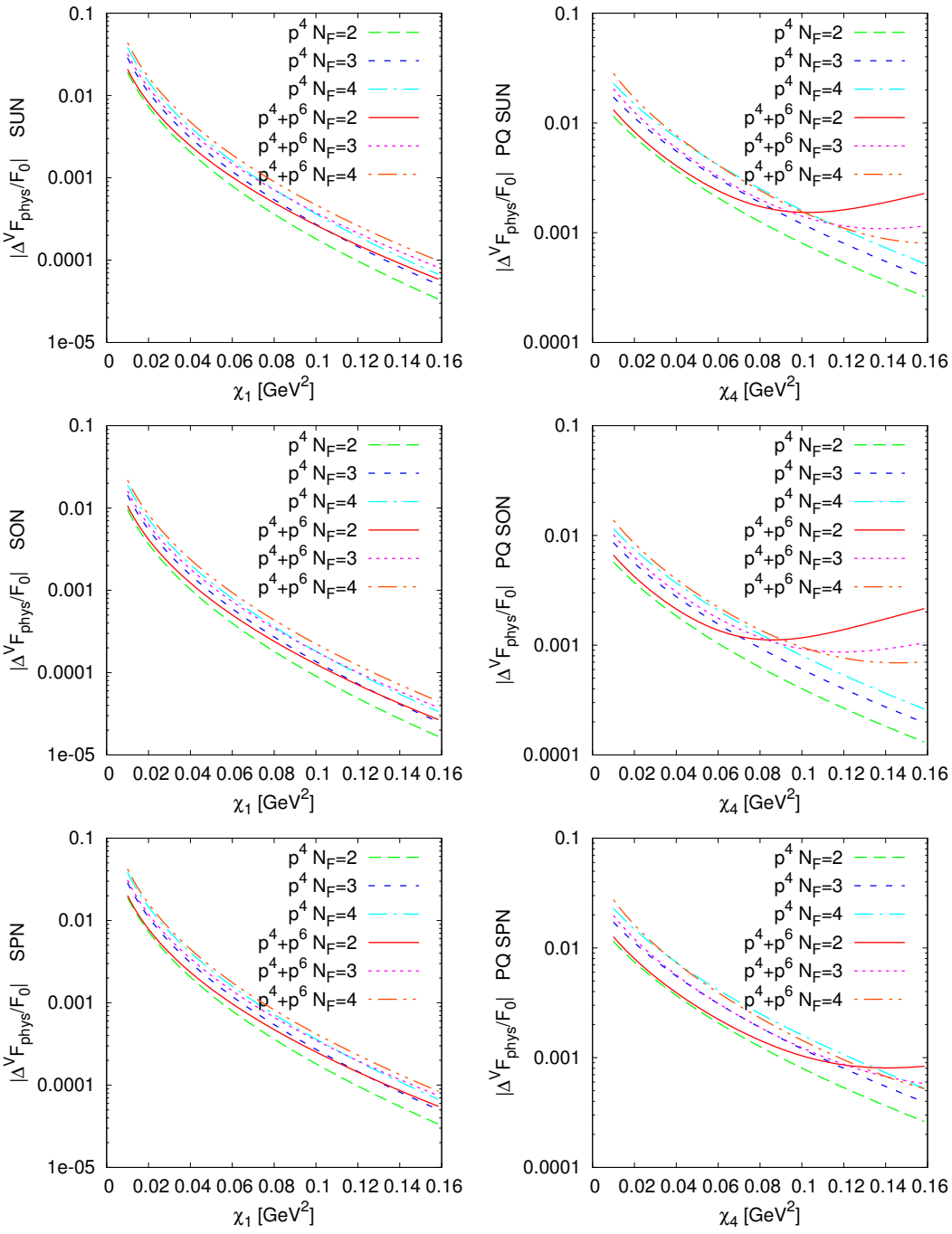

Figure 5: The absolute value of the finite volume correction to the decay constant divided by the lowest order value $F_0 = F_{LO}$ for the unquenched (left) as a function of χ_1 and the partially quenched case (right) as a function of χ_4 with $\chi_1 = 0.14^2$ GeV^2. Shown are the NLO (p^4) and NNLO ($p^4 + p^6$) results for three values of N_F. Top line: $SU(N_F) \times SU(N_F) \to SU(N_F)$. Middle line: $SU(N_F) \to SO(N_F)$. Bottom line: $SU(2N_F) \to Sp(2N_F)$.

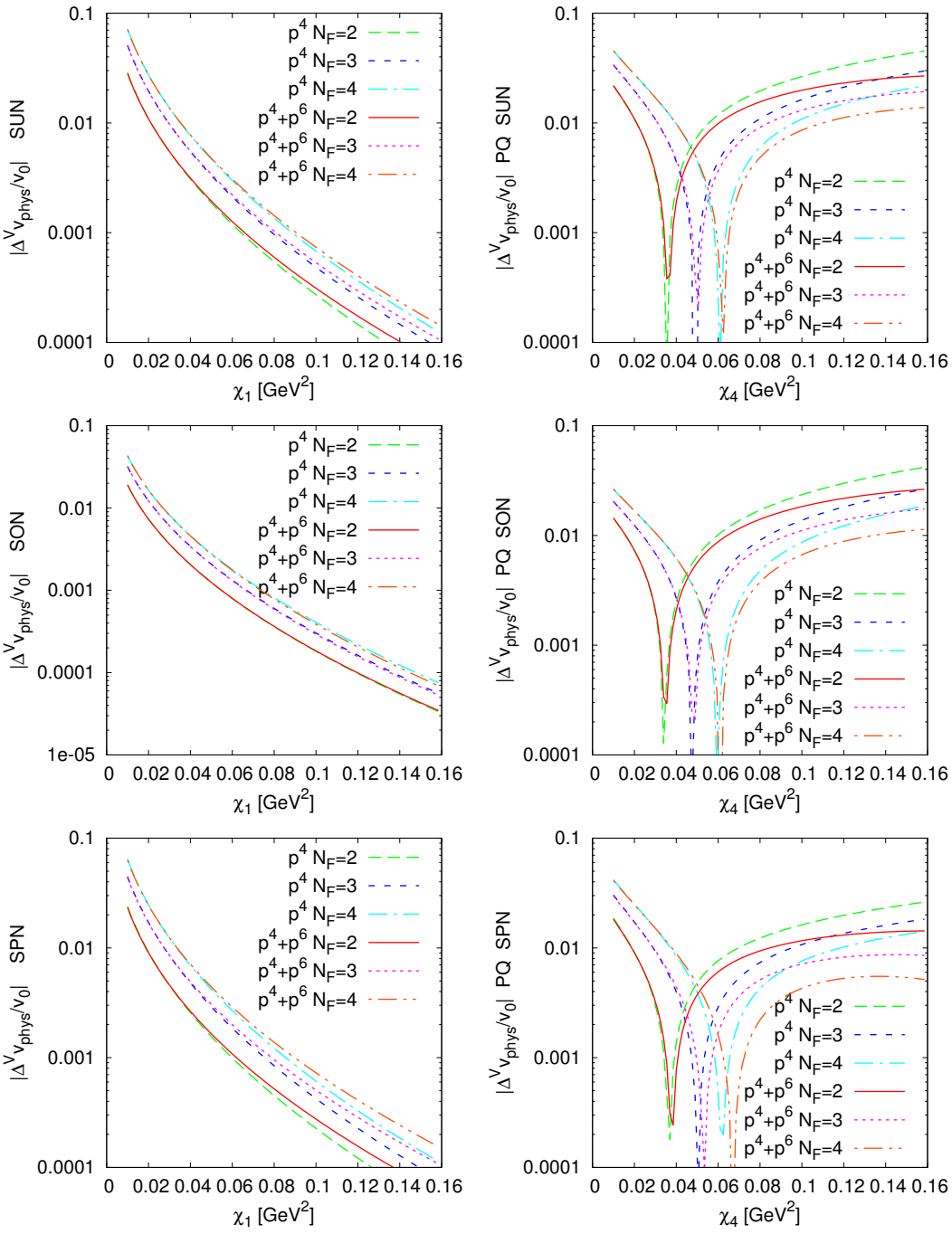

Figure 6: The absolute value of the finite volume correction to the vacuum expectation value divided by the lowest order value $v_0 = v_{LO}$ for the unquenched (left) as a function of χ_1 and the partially quenched case (right) as a function of χ_4 with $\chi_1 = 0.14^2$ GeV^2. Shown are the NLO (p^4) and NNLO ($p^4 + p^6$) results for three values of N_F. Top line: $SU(N_F) \times SU(N_F) \to SU(N_F)$. Middle line: $SU(N_F) \to SO(N_F)$. Bottom line: $SU(2N_F) \to Sp(2N_F)$.

[4] J. Kuti, PoS LATTICE **2013** (2014) 004.

[5] R. Lewis, C. Pica and F. Sannino, Phys. Rev. D **85** (2012) 014504 [arXiv:1109.3513 [hep-ph]].

A. Hietanen, R. Lewis, C. Pica and F. Sannino, JHEP **1407** (2014) 116 [arXiv:1404.2794 [hep-lat]].

D. Schaich *et al.* [LSD Collaboration], arXiv:1506.08791 [hep-lat].

T. N. da Silva, E. Pallante and L. Robroek, arXiv:1506.06396 [hep-th].

M. P. Lombardo, K. Miura, T. J. Nunes da Silva and E. Pallante, Int. J. Mod. Phys. A **29** (2014) 25, 1445007 [arXiv:1410.2036 [hep-lat]].

T. Appelquist *et al.*, Phys. Rev. D **85** (2012) 074505 [arXiv:1201.3977 [hep-lat]].

T. DeGrand, Y. Liu, E. T. Neil, Y. Shamir and B. Svetitsky, Phys. Rev. D **91** (2015) 114502 [arXiv:1501.05665 [hep-lat]].

[6] J. R. Andersen *et al.*, Eur. Phys. J. Plus **126** (2011) 81 [arXiv:1104.1255 [hep-ph]].

[7] F. Sannino, Acta Phys. Polon. B **40** (2009) 3533 [arXiv:0911.0931 [hep-ph]].

[8] C. T. Hill and E. H. Simmons, Phys. Rept. **381** (2003) 235 [Erratum-ibid. **390** (2004) 553] [arXiv:hep-ph/0203079].

[9] S. Weinberg, Physica A **96** (1979) 327.

[10] J. Gasser and H. Leutwyler, Annals Phys. **158** (1984) 142.

[11] J. Gasser and H. Leutwyler, Nucl. Phys. B **250** (1985) 465.

[12] M. E. Peskin, Nucl. Phys. B **175** (1980) 197.

[13] J. Preskill, Nucl. Phys. B **177**, 21 (1981).

[14] S. Dimopoulos, Nucl. Phys. B **168** (1980) 69.

[15] J. B. Kogut, M. A. Stephanov, D. Toublan, J. J. M. Verbaarschot and A. Zhitnitsky, Nucl. Phys. B **582** (2000) 477 [arXiv:hep-ph/0001171].

[16] K. Splittorff, D. Toublan and J. J. M. Verbaarschot, Nucl. Phys. B **620** (2002) 290 [arXiv:hep-ph/0108040].

[17] D. Toublan and J. J. M. Verbaarschot, Nucl. Phys. B **560** (1999) 259 [hep-th/9904199].

[18] J. Bijnens and J. Lu, JHEP **0911** (2009) 116 [arXiv:0910.5424 [hep-ph]].

[19] J. Bijnens and J. Lu, JHEP **1103** (2011) 028 [arXiv:1102.0172 [hep-ph]].

[20] J. Bijnens and J. Lu, JHEP **1201** (2012) 081 [arXiv:1111.1886 [hep-ph]].

[21] C. W. Bernard and M. F. L. Golterman, Phys. Rev. D **49** (1994) 486 [hep-lat/9306005].

[22] C. Bernard and M. Golterman, Phys. Rev. D **88** (2013) 1, 014004 [arXiv:1304.1948 [hep-lat]].

[23] S. R. Sharpe and N. Shoresh, Phys. Rev. D **62** (2000) 094503 [hep-lat/0006017].

[24] S. R. Sharpe, Phys. Rev. D **46** (1992) 3146 [hep-lat/9205020].

[25] J. Bijnens, N. Danielsson and T. A. Lahde, Phys. Rev. D **70** (2004) 111503 [hep-lat/0406017].

[26] J. Bijnens and T. A. Lahde, Phys. Rev. D **71** (2005) 094502 [hep-lat/0501014].

[27] J. Bijnens, N. Danielsson and T. A. Lahde, Phys. Rev. D **73** (2006) 074509 [hep-lat/0602003].

[28] J. Gasser and H. Leutwyler, Phys. Lett. B **184** (1987) 83.

[29] J. Gasser and H. Leutwyler, Phys. Lett. B **188** (1987) 477.

[30] J. Gasser and H. Leutwyler, Nucl. Phys. B **307** (1988) 763.

[31] G. Colangelo and C. Haefeli, Nucl. Phys. B **744** (2006) 14 [hep-lat/0602017].

[32] J. Bijnens and K. Ghorbani, Phys. Lett. B **636** (2006) 51 [hep-lat/0602019].

[33] P. H. Damgaard and H. Fukaya, JHEP **0901** (2009) 052 [arXiv:0812.2797 [hep-lat]].

[34] J. Bijnens, E. Boström and T. A. Lähde, JHEP **1401** (2014) 019 [arXiv:1311.3531 [hep-lat]].

[35] J. Bijnens and T. Rössler, JHEP **1501** (2015) 034 [arXiv:1411.6384 [hep-lat]].

[36] J. Bijnens and T. Rössler, arXiv:1508.07238 [hep-lat].

[37] See the supplementary file analyticalresults.txt. This can also be downloaaded from [50].

[38] J. Bijnens, Eur. Phys. J. C **75** (2015) 1, 27 [arXiv:1412.0887 [hep-ph]].

[39] http://www.thep.lu.se/~bijnens/chiron/

[40] J. Bijnens, G. Colangelo and G. Ecker, JHEP **9902** (1999) 020 [hep-ph/9902437].

[41] J. Bijnens, G. Colangelo and G. Ecker, Annals Phys. **280** (2000) 100 [hep-ph/9907333].

[42] S. R. Coleman, J. Wess and B. Zumino, Phys. Rev. **177** (1969) 2239; C. G. . Callan, S. R. Coleman, J. Wess and B. Zumino, Phys. Rev. **177** (1969) 2247.

[43] S. R. Sharpe and N. Shoresh, Phys. Rev. D **64** (2001) 114510 [hep-lat/0108003].

[44] P. H. Damgaard and K. Splittorff, Phys. Rev. D **62** (2000) 054509 [hep-lat/0003017].

[45] J. Levinsen, Phys. Rev. D **67** (2003) 125009 [hep-th/0301008].

[46] J. Bijnens and G. Ecker, Ann. Rev. Nucl. Part. Sci. **64** (2014) 149 [arXiv:1405.6488 [hep-ph]].

[47] G. Amorós, J. Bijnens and P. Talavera, Nucl. Phys. B **568** (2000) 319 [hep-ph/9907264].

[48] G. Amorós, J. Bijnens and P. Talavera, *Nucl. Phys.* B 585 (2000) 293 [Erratum-ibid. B 598 (2001) 665] [hep-ph/0003258].

[49] J. A. M. Vermaseren, arXiv:math-ph/0010025.

[50] http://www.thep.lu.se/˜bijnens/chpt/

Der Schmetterling

Zum Fest des Lebens feierlich geschmückt,
für einen Atemzug nur auf der Welt,
vom wilden Freudentaumel ganz verrückt,
ruht kurz ein Schmetterling im Rübenfeld.

Im Flammenkleid auf einem grünen Blatt,
mit allen Farben himmlischer Paletten,
zeigt hier ein Reicher alles, was er hat
und will's vergeuden, ganz und gar verwetten.

Für dieses Nu, das Gegenteil von Dauer,
hat er immense Schätze aufgeboten.
Ein Vogel steht vielleicht schon auf der Lauer,
ihn zu begleiten in das Reich der Toten.

Und wenn er dann im ahnungslosen Raum
weit über nie gekannten Grenzen schwebt,
dort wo kein Strauch, kein Hauch, kein Apfelbaum...
so weiss er doch, einmal hat er gelebt.

Leonard Ostendorf Terfloth